INNATE IMMUNE CELLS AND INFLAMMATORY MEDIATORS IN MUCOSAL PATHOLOGIES

EDITED BY: Elba Mónica Vermeulen, Maria Leite-de-Moraes and Marcello Chieppa

PUBLISHED IN: Frontiers in Immunology and Frontiers in Microbiology

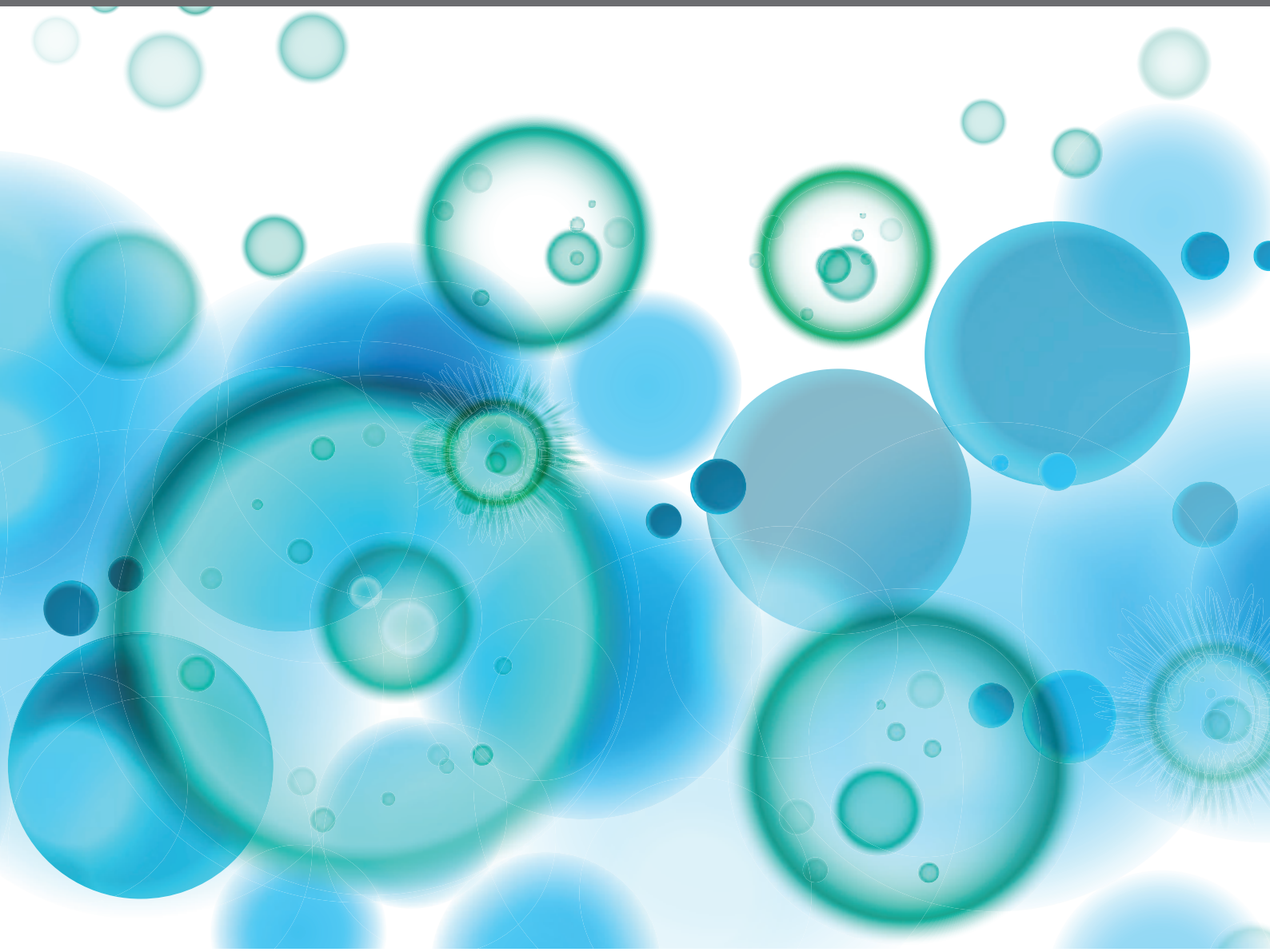

frontiers Research Topics

frontiers

ISSN 1664-8714
ISBN 978-2-88966-012-4
DOI 10.3389/978-2-88966-012-4

About Frontiers

Frontiers is more than just an open-access publisher of scholarly articles: it is a pioneering approach to the world of academia, radically improving the way scholarly research is managed. The grand vision of Frontiers is a world where all people have an equal opportunity to seek, share and generate knowledge. Frontiers provides immediate and permanent online open access to all its publications, but this alone is not enough to realize our grand goals.

Frontiers Journal Series

The Frontiers Journal Series is a multi-tier and interdisciplinary set of open-access, online journals, promising a paradigm shift from the current review, selection and dissemination processes in academic publishing. All Frontiers journals are driven by researchers for researchers; therefore, they constitute a service to the scholarly community. At the same time, the Frontiers Journal Series operates on a revolutionary invention, the tiered publishing system, initially addressing specific communities of scholars, and gradually climbing up to broader public understanding, thus serving the interests of the lay society, too.

Dedication to Quality

Each Frontiers article is a landmark of the highest quality, thanks to genuinely collaborative interactions between authors and review editors, who include some of the world's best academicians. Research must be certified by peers before entering a stream of knowledge that may eventually reach the public - and shape society; therefore, Frontiers only applies the most rigorous and unbiased reviews.
Frontiers revolutionizes research publishing by freely delivering the most outstanding research, evaluated with no bias from both the academic and social point of view. By applying the most advanced information technologies, Frontiers is catapulting scholarly publishing into a new generation.

What are Frontiers Research Topics?

Frontiers Research Topics are very popular trademarks of the Frontiers Journals Series: they are collections of at least ten articles, all centered on a particular subject. With their unique mix of varied contributions from Original Research to Review Articles, Frontiers Research Topics unify the most influential researchers, the latest key findings and historical advances in a hot research area! Find out more on how to host your own Frontiers Research Topic or contribute to one as an author by contacting the Frontiers Editorial Office: researchtopics@frontiersin.org

INNATE IMMUNE CELLS AND INFLAMMATORY MEDIATORS IN MUCOSAL PATHOLOGIES

Topic Editors:
Elba Mónica Vermeulen, Instituto de Medicina Experimental (IMEX)-CONICET. Academia Nacioanl de Medicina
Maria Leite-de-Moraes, Université Paris Descartes, France
Marcello Chieppa, European Biomedical Research Institute of Salerno (EBRIS), Italy

Citation: Vermeulen, E. M., Leite-de-Moraes, M., Chieppa, M., eds. (2020). Innate Immune Cells and Inflammatory Mediators in Mucosal Pathologies. Lausanne: Frontiers Media SA. doi: 10.3389/978-2-88966-012-4

Table of Contents

frontiers in Immunology

EDITORIAL
published: 28 July 2020
doi: 10.3389/fimmu.2020.01679

Editorial: Innate Immune Cells and Inflammatory Mediators in Mucosal Pathologies

Leite-de-Moraes Maria[1], *Chieppa Marcello*[2] *and Vermeulen Mònica*[3]*

[1] *Laboratory of Immunoregulation and Immunopathology, Institut Necker-Enfants Malades (INEM), CNRS UMR8253 and Inserm UMR1151, Paris, France,* [2] *National Institute of Gastroenterology "S. de Bellis", Research Hospital, Castellana Grotte, Italy,* [3] *Laboratorio de Células Presentadoras de Antígeno y Respuesta Inflamatoria, IMEX (Instituto de Medicina Experimental)-CONICET, Academia Nacional de Medicina, Buenos Aires, Argentina*

Keywords: inflammation, innate cells, mucosal pathology, mediators, homeostasis

Editorial on the Research Topic

Innate Immune Cells and Inflammatory Mediators in Mucosal Pathologies

Cells of the innate immune system play an essential role in early protection against pathogens and tissue damage. They are also in the front line for maintaining the fragile equilibrium between inflammatory responses and control of host body hemostasis. In this special issue you will find a number of original, complementary approaches aiming at a better understanding of how innate cells modulate inflammatory responses. Contributions focus mainly on mediators produced by these cells as well as mechanisms through which pathogens or allergens could modify their production.

The study by Jiao and Sun summarizes new advances in the understanding of bacterial manipulation of autophagic responses. The authors investigate the multiple levels at which microbial effectors interfere with this pathway to prevent pathogen recognition by the host. Improving the knowledge of these interactions will be a prerequisite for the development of more effective, specific therapies against several chronic pathologies.

One of the most frequent triggers of chronic inflammation is the disruption of the epithelial barrier. In line of evidence, Wei et al. demonstrate that the hybrid peptide cecropin-LL37 can prevent intestinal infection caused by enterohemorrhagic *Escherichia coli* by promoting an anti-inflammatory response, which reduced enterocyte apoptosis more effectively than previously developed compounds. In a similar perspective, Luo X. et al. propose a model of dextran sulfate sodium (DSS)-induced inflammatory bowel disease to evaluate the effects of obacunome, a natural citrus-derived compound. They found a marked suppression of the severe inflammatory response mediated through interference with toll-like receptor 4 (TLR4)/nuclear factor-kappa B (NF-κB) signaling. Furthermore, obacunone administration resulted in increased expression of proteins associated with the enterocytes' tight junctions and recovery of epithelial homeostasis.

The elegant work by Jang et al. investigates the mechanisms underlying IL-1β production by neutrophils in response to *Helicobacter pylori* infection. These gram-negative bacteria, which cause gastrointestinal diseases in humans, triggers massive production of IL-1β considered a key factor in inducing gastrointestinal malignancies. The authors report that neutrophils require NLRP3, ASC and caspase to secrete IL-1β in response to *H. pylori* suggesting an essential role for the NLRP3 inflammasome. TLR2, but not TLR4 and Nod2, also contributed to IL-1β secretion. On the other hand, *H. pylori* depends on both the bacterial-mediated type IV secretory system (T4SS) and motility to induce IL-1β production by neutrophils.

OPEN ACCESS

Edited and reviewed by:
Francesca Granucci,
University of Milano-Bicocca, Italy

***Correspondence:**
Vermeulen Mònica
mvermeulen@hematologia.anm.edu.ar

Specialty section:
This article was submitted to Molecular Innate Immunity, a section of the journal Frontiers in Immunology

Received: *08 June 2020*
Accepted: *23 June 2020*
Published: *28 July 2020*

Citation:
Maria L-d-M, Marcello C and Mònica V (2020) Editorial: Innate Immune Cells and Inflammatory Mediators in Mucosal Pathologies. Front. Immunol. 11:1679. doi: 10.3389/fimmu.2020.01679

Schulz-Kuhnt et al. addresses the role of $CCR6^+$ILC2 cells in patients with cystic fibrosis (CF). Having observed a substantial decrease in this population in patients' blood, the authors hypothesized that this might reflect pulmonary recruitment. To test this assumption, they used a new, sophisticated humanized mouse model with light-sheet fluorescence microscopic visualization, which enabled them to assess whether human ILC2 cells had accumulated in the lung following papain-induced airway inflammation. Upon adoptive transfer, $CCR6^+$ILC2 cells from healthy donors did effectively infiltrate the lung of these mice, enhanced local eosinophil and neutrophil accumulation and up-regulated type-VI collagen expression. These findings support the notion that in CF patients $CCR6^+$ILC2 cells might contribute to pulmonary damage once they have entered this tissue. Further analyses in lung biopsies of CF patients are required to confirm or infirm this assumption.

In their contribution Kindermann et al. likewise address the question of the involvement ILC2 cells in pulmonary infections using a model based on *Cryptococcus neoformans* injections. The authors observed an important increase in ILC2 cell counts in the lung of infected mice, accompanied by the induction of a type-2 immune response. Conversely, ILC2-deficient mice displayed increased type-1 immunity, classical macrophage activation, reduced lung inflammation and prolonged survival. These observations suggest that ILC2 cells could act as negative regulators of protective, type-1 anti-cryptococci immune responses.

Alberca-Custodio et al. propose a novel immunotherapy strategy against allergens, based on a liposomal formulation that contains the allergen at low doses associated with a TLR9 antagonist. In allergic asthma models using ovalbumine or mite extracts, the liposomal formulation containing co-encapsulated allergen plus CpG-ODN reversed an established allergic lung inflammation and provided long-term protection. It showed efficacy in reducing the inflammatory response by interacting with $CD11c^+$ cells via MyD88 signaling.

In allergies, the central role of mast cells as initiators of the symptoms associated with hypersensitivity reactions is widely accepted. However, little is known about the implication of connective tissue mast cells (MMCs) in allergic inflammatory responses. Lou Y. et al. offer researchers in this field a novel means of investigation, having developed genetically modified mice lacking this particular type of mast cells. Their model, obtained by crossing α-chymase-Cre transgenic with a strain bearing a floxed allele of the myeloid cell leukemia sequence 1 (Mcl-1), provides an innovative tool to learn more about the role of mast cells, especially MMCs, in the development of allergy and will likely contribute to the development of new therapeutic strategies.

Finally, the review of Sui and Berzofsky, focuses on the new concept of trained innate immunity. The authors discuss the "memory and specificity" of innate immune populations, such as myeloid and NK cells including the contribution of epigenetics, metabolism as well as a variety of agents, such as adjuvants, in the developments of trained immunity. They focus more particularly on trained innate immunity induced by vectors/adjuvants that have been used in AIDS vaccine studies and propose new ways of thinking about these additives.

The contributions to this special topic highlight recent advances in the understanding of the complex mechanisms leading to tissue damage following activation of the innate effectors and/or their mediators. They lend further support to the importance of this first line of defense to safeguard mucosal homeostasis, which has been increasingly consolidated during the last years. By identifying new therapeutic targets they pave the way for the development of specific strategies for the treatment of chronic pathologies affecting mucosal tissues.

AUTHOR CONTRIBUTIONS

L-MM, CM, and VM edited the topic and wrote the manuscript. All authors contributed to the article and approved the submitted version.

FUNDING

Funded by grants from Consejo de Investigaciones científicas y tecnológicas (CONICET) PIP 2017-0950.

ACKNOWLEDGMENTS

We thank Elke Schneider for reviewing the manuscript.

Conflict of Interest: The authors declare that the research was conducted in the absence of any commercial or financial relationships that could be construed as a potential conflict of interest.

frontiers in Immunology

ORIGINAL RESEARCH
published: 15 October 2019
doi: 10.3389/fimmu.2019.02399

Chymase-Cre; Mcl-1$^{fl/fl}$ Mice Exhibit Reduced Numbers of Mucosal Mast Cells

Ying Luo[1], *Nicole Meyer*[2], *Qingqing Jiao*[1], *Jörg Scheffel*[1], *Carolin Zimmermann*[1], *Martin Metz*[1], *Ana Zenclussen*[2], *Marcus Maurer*[1]* *and Frank Siebenhaar*[1]

[1] Dermatological Allrgology, Department of Dermatology and Allergy, Charité - Universitätsmedizin Berlin, Corporate Member of Freie Universität Berlin, Humboldt - Universität zu Berlin, and Berlin Institute of Health, Berlin, Germany, [2] Experimental Obstetrics and Gynecology, Medical Faculty, Otto-Von-Guericke-University, Magdeburg, Germany

Mast cells (MCs) are considered as key effector cells in the elicitation of allergic symptoms, and they are essential players in innate and adaptive immune responses. In mice, two main types of MCs have been described: connective tissue MCs (CTMCs) and mucosal MCs (MMCs). However, little is known about the biological functions of MMCs, which is due to the lack of suitable models to investigate MMCs *in vivo*. Here, we aimed to generate a mouse model selectively deficient in MMCs. It has been previously described that Cre expressed under the control of the baboon α-chymase promotor is predominantly localized in MMCs. Therefore, we mated α-chymase-Cre transgenic mice with mice bearing a floxed allele of the myeloid cell leukemia sequence 1 (Mcl-1). Mcl-1 encodes for an intracellular antiapoptotic factor in MCs; hence, a selective reduction in MMCs was expected. Our results show that this new mouse model contains markedly reduced numbers of MMCs in mucosal tissues, whereas numbers of CTMCs are normal. Thus, Chm-Cre; Mcl-1$^{fl/fl}$ mice are a useful tool for the investigation of the pathophysiological functions of MMCs *in vivo*.

Keywords: mast cells, mouse model, mucosa, connective tissue, chymase, Cre, Mcl-1

OPEN ACCESS

Edited by:
Maria Leite-de-Moraes, INSERM U1151 Institut Necker Enfants Malades Centre de médecine moléculaire (INEM), France

Reviewed by:
Adrian Piliponsky, Seattle Children's Research Institute, United States
Ulrich Blank, Institut National de la Santé et de la Recherche Médicale (INSERM), France

***Correspondence:**
Marcus Maurer
marcus.maurer@charite.de

Specialty section:
This article was submitted to Molecular Innate Immunity, a section of the journal Frontiers in Immunology

Received: *19 July 2019*
Accepted: *25 September 2019*
Published: *15 October 2019*

Citation:
Luo Y, Meyer N, Jiao Q, Scheffel J, Zimmermann C, Metz M, Zenclussen A, Maurer M and Siebenhaar F (2019) Chymase-Cre; Mcl-1$^{fl/fl}$ Mice Exhibit Reduced Numbers of Mucosal Mast Cells. Front. Immunol. 10:2399. doi: 10.3389/fimmu.2019.02399

INTRODUCTION

Mast cells (MCs) are potent inflammatory cells that are constitutively present in most tissues. MCs are key effector cells in the elicitation of allergic symptoms (1–3) and essential players in protective innate and adaptive immune responses to pathogens and other environmental threats (4–6).

MCs exhibit a diverse hematopoietic origin. As the bone marrow was previously believed the only site from which MCs can arise (7–9), it has been recently shown that MCs also originate from the yolk sac and from definite progenitors (10). Unlike other myeloid-derived cells, which differentiate and mature in the BM before being released to the blood, MCs egress the BM and circulate as immature progenitor cells (11–14) (generically termed MCps), which give rise to mature MCs when they migrate to their target tissues (15).

In mice, MCps differentiate into two major types of mature MCs, connective tissue MCs (CTMCs) and mucosal MCs (MMCs), classified according to their anatomical distribution: CTMCs are found in skin, peritoneum, and submucosa of the gastrointestinal tract, where they are predominantly located in close proximity to vessels and sensory nerve endings. In contrast, MMCs are present in mucosal tissues such as the gastrointestinal and respiratory mucosa as well as in the uterus where they coexist with CTMCs and an intermediate phenotype (15, 16).

CTMCs and MMCs also differ in their morphology, protease expression profiles, and biochemical and functional properties (15). CTMCs represent a robust and long-lived tissue population (17, 18), whereas MMCs are low in numbers under physiological conditions but show rapid and marked expansion under pathological conditions, such as parasitic infections (19–21) or food allergy (22). In addition, it has been reported that MMCs can expand during T cell-dependent immune responses (19, 23, 24), whereas CTMCs exhibit little or no T cell-dependent behavior and appear in athymic nude mice or rats in normal numbers. CTMCs are relatively well-characterized and studied as compared to MMCs. This is, in part, because animal models for the investigation of CTMC functions became available some decades ago. In contrast, very little is known about MMCs, and we are lacking suitable models to study their biological functions.

The role of MMCs in health and disease is largely unknown. In contrast to CTMCs, very little is known about the pathways of MMC activation, their physiological functions, mechanisms of proliferation and survival, as well as modulators of MMCs biology. We, therefore, aimed to generate a new mouse model that exhibits a specific reduction in MMCs, thus allowing for the investigation of MMC biology *in vivo*. To this end, we made use of the Cre/loxP recombination system for generating tissue-specific gene inactivation in mice (25, 26). It has been previously reported that Cre expression driven by the baboon α-chymase promotor correlates to MC-specific lineages present in colon and lungs, thereby suggesting an MMC-specific expression (27). Hence, in the present study, we mated chymase-Cre transgenic mice with mice bearing a floxed allele of the myeloid cell leukemia sequence 1 (Mcl-1), which encodes for an intracellular antiapoptotic factor in MCs (28). We hypothesized that the genetic inactivation of Mcl-1 under the control of the α-chymase promotor in this Chm-Cre; Mcl-$1^{fl/fl}$ mouse induces apoptosis in the target cell population and results in a specific reduction of MMCs.

RESULT

Chm-Cre; Mcl-$1^{fl/fl}$ Mice Have Markedly Reduced Numbers of Gastric and Duodenal MMCs

Chm-Cre; Mcl-$1^{fl/fl}$ mice showed markedly reduced numbers of MMCs in the glandular stomach as compared to control Chm-Cre; Mcl-$1^{+/+}$ mice (**Figure 1**, 1.6 ± 0.5 MCs/HPF vs. 4.12 ± 0.3/HPF). MMC numbers were also markedly reduced in the lamina propria of the duodenum of Chm-Cre; Mcl$1^{fl/fl}$ mice (Chm-Cre;Mcl-$1^{fl/fl}$: 0.6 ± 0.1 MC/HPF vs. Chm-Cre;Mcl-$1^{+/+}$: 1.3 ± 0.1 MC/HPF, −54%, $P < 0.01$). MCs in ileum and colon generally appear in very low numbers; hence, the reduction of MMCs in the lamina propria of the ileum and colon of Chm-Cre; Mcl-$1^{fl/fl}$ mice was detectable but not significant.

Chm-Cre; Mcl-$1^{fl/fl}$ Mice Exhibit Markedly Reduced Numbers of Uterus MCs and Decreased Placental Thickness

In consideration of the variation of uterine MC numbers (uMCs) during the fertile period in the uterus, which contains MMCs

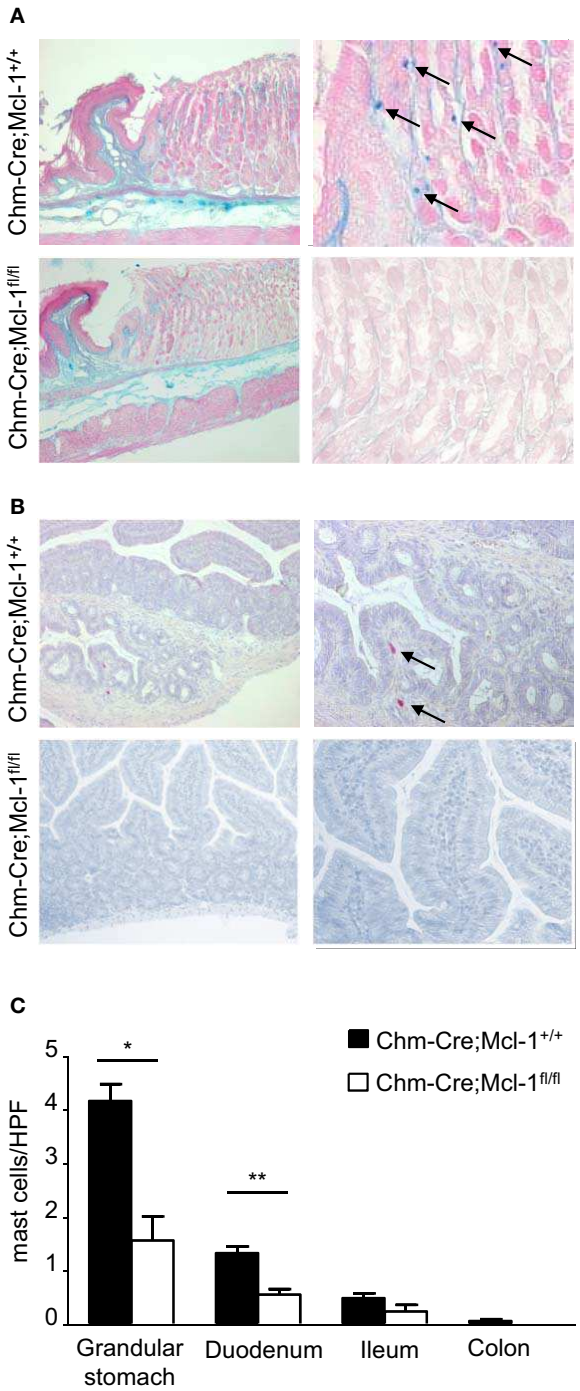

FIGURE 1 | Chm-Cre; Mcl-$1^{fl/fl}$ mice have markedly reduced numbers of representative mucosal mast cell (MMC) populations. **(A)** Alcian blue staining for stomach MCs of 5-μm-thick paraffin sections showed markedly reduced MCs numbers (blue) in Chm-Cre; Mcl-1fl/fl mice compared to control Chm-Cre; Mcl-$1^{+/+}$ mice. **(B)** Chloroacetate esterase staining for intestinal MCs showed decreased number of MCs (red) in duodenum of Chm-Cre; Mcl-$1^{fl/fl}$ mice compared to control Chm-Cre; Mcl-$1^{+/+}$ mice. **(C)** Numbers of MCs in different gastrointestinal tissues were assessed by quantitative histomorphometry analysis. **(A,B)** left: 100× magnification, **(A)** right: 400× magnification, **(B)** right: 200× magnification. Data were pooled from three independent experiments ($n = 5$ mice per group) and expressed as mean ± SEM (*$P < 0.05$, **$P < 0.01$, n.s., not significant).

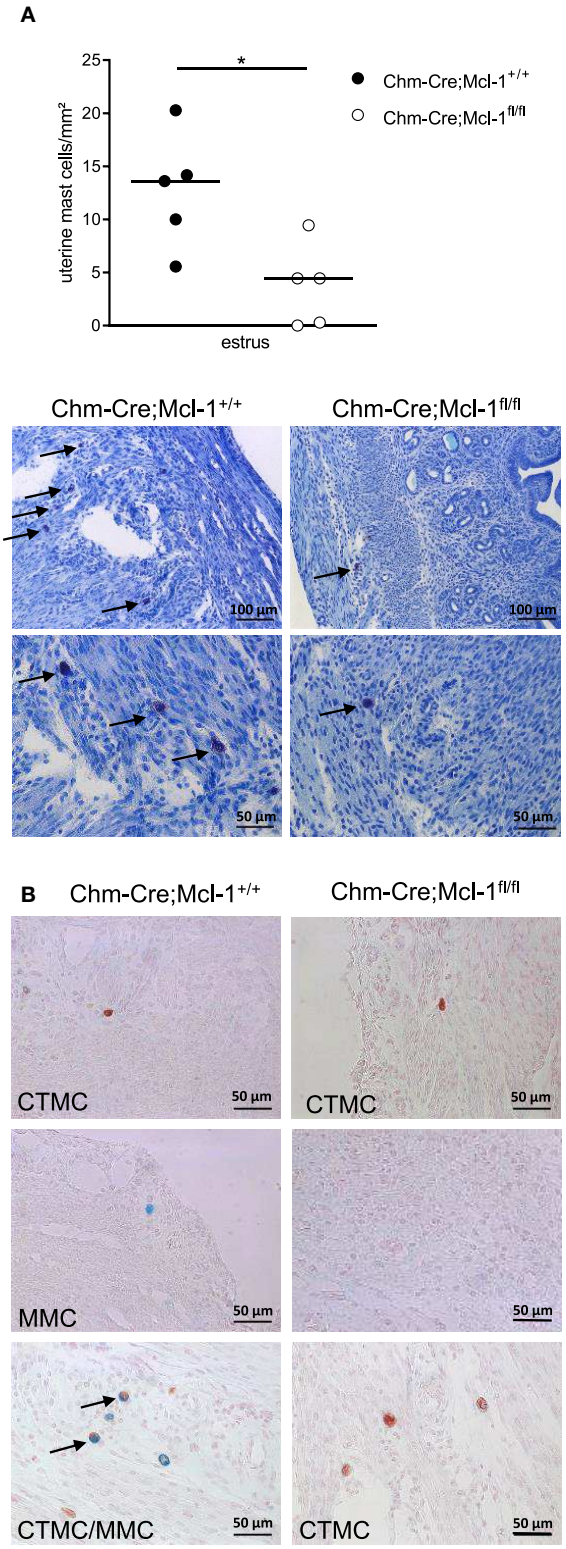

FIGURE 2 | Chm-Cre; Mcl-$1^{fl/fl}$ mice exhibit reduced numbers of uterus MCs. **(A)** Toluidine blue staining of 5-µm-thick paraffin uteri sections showed markedly reduced number of uterus MCs (uMCs) at the estrus cycle (arrows) in Chm-Cre; Mcl-$1^{fl/fl}$ mice compared to control Chm-Cre; Mcl-$1^{+/+}$ mice.

(Continued)

FIGURE 2 | (B) Representative images of alcian blue (MMCs) and safranin (CTMCs) staining of uterus from Chm-Cre; Mcl-$1^{+/+}$ and Chm-Cre; Mcl-$1^{fl/fl}$ at estrus. Results are presented as individual values and median. Statistical differences were obtained by using Mann–Whitney (*$P < 0.05$), 200× magnification.

and CTMCs, we quantified the number of uMCs/mm^2 in the uterus of virgin Chm-Cre; Mcl-$1^{fl/fl}$ and Chm-Cre; Mcl-$1^{+/+}$ female mice at the estrus. During the estrus cycle, Chm-Cre; Mcl-$1^{fl/fl}$ mice presented significantly reduced uMC numbers as compared to Chm-Cre; Mcl-$1^{+/+}$ mice (**Figure 2A**, 3.72 ± 1.72/mm^2, $n = 5$ vs. 12.72 ± 2.44/mm^2, $n = 5$, $P = 0.017$). Histomorphological analyses of uterine sections stained with alcian blue and safranin, to quantify MMCs and CTMCs, respectively, identified both CTMCs and MMCs during estrus in Chm-Cre; Mcl-$1^{+/+}$ control mice. Interestingly, we observed some alcian blue/safranin double-positive cells in the uterus of Chm-Cre; Mcl-$1^{+/+}$ mice, suggesting for an indistinct potentially intermediate phenotype. In contrast, Chm-Cre; Mcl-$1^{fl/fl}$ mice had CTMCs only, but no MMCs (**Figure 2B**).

To investigate whether the lack of MMCs in the uterus has an impact on fetal/placental growth, we performed ultrasound analyses of the gestation period at gd5 and gd10 assessing the implantation area, placental thickness, and diameter, as well as the placental diameter/thickness ratio of Balb/c-paired Chm-Cre; Mcl-$1^{fl/fl}$ mice ($n = 5$, placentas $n = 23$) and Chm-Cre; Mcl-$1^{+/+}$ mice ($n = 4$, placentas $n = 22$) at gd10 (**Figures 3A,B**). We observed significantly reduced placental thickness in Chm-Cre; Mcl-$1^{fl/fl}$ mice (**Figure 3B**), whereas the implantation area, placenta weight, as well as implantation and abortion rates were comparable to the one observed for Chm-Cre; Mcl-$1^{+/+}$ mice at gd5 and gd10 (**Figure 3C** and **Figures S1A–C**). Also, no differences in spiral artery (SA) parameters were found at gd10 (**Figure S1D**).

Chm-Cre; Mcl-$1^{fl/fl}$ Mice Exhibit No Difference in Cell Numbers or Morphology of Representative CTMC Populations

Chm-Cre; Mcl-$1^{fl/fl}$ mice and Chm-Cre; Mcl-$1^{+/+}$ mice were similar in their numbers of CTMCs obtained from the peritoneum (PMCs), and their PMCs were similar in their morphology and surface expression of c-kit and FcεRI as assessed by FACS analysis (**Figures 4A,B**). Numbers of CTMCs in the dorsal skin of Chm-Cre; Mcl-$1^{fl/fl}$ and Chm-Cre; Mcl-$1^{+/+}$ control mice were similar as assessed by quantitative histomorphometry (**Figures 4C,D**; Chm-Cre; Mcl-$1^{fl/fl}$: 10.1 ± 0.9 MCs/HPF; Chm-Cre; Mcl-$1^{+/+}$: 10,6 ± 0.8 MCs/HPF). Both strains also exhibited similar numbers of ear skin CTMCs (**Figure 4D**; Chm-Cre; Mcl-$1^{fl/fl}$: 11.2 ± 0.7 MCs/HPF; Chm-Cre; Mcl-$1^{+/+}$: 10.1 ± 0.9 MCs/HPF).

Bone Marrow-Derived Cultured MCs of Chm-Cre; Mcl-$1^{fl/fl}$ Mice-Exhibit Normal Proliferation and Differentiation

It has been previously reported that the α-chymase promotor is not expressed in bone marrow-derived cultured MCs

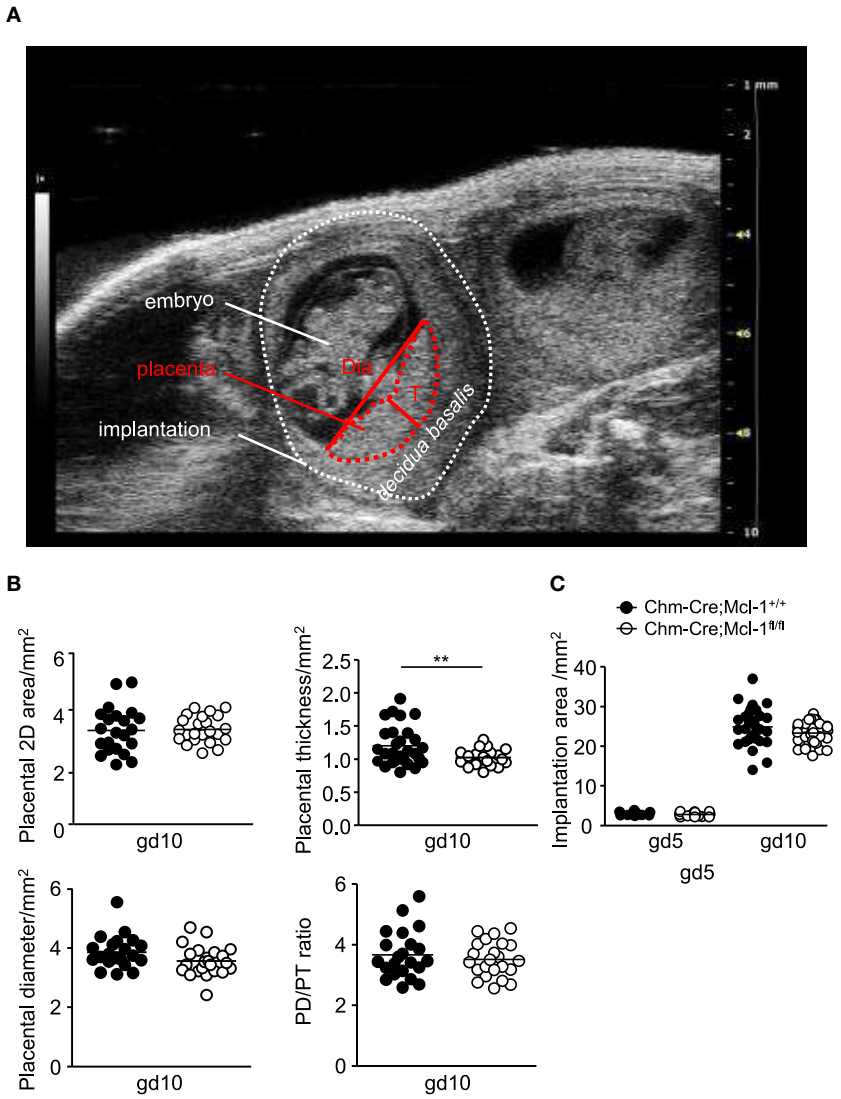

FIGURE 3 | Chm-Cre; Mcl-1$^{fl/fl}$ mice presented decreased placental thickness at gd10. **(A)** Representative ultrasound image of an implantation at gd10 showing the embryo, the *decidua basalis*, and the placenta with placenta thickness (T) and diameter (Dia). **(B)** Placental area, placental thickness, placental diameter, and placental diameter/thickness ratio from Balb/c-paired Chm-Cre; Mcl-1$^{+/+}$ (mice $n = 4$, placentas $n = 22$) and Chm-Cre; Mcl-1$^{fl/fl}$ mice (mice $n = 5$, placentas $n = 23$) at gd10. **(C)** Implantation areas in mm^2 from Balb/c-paired Chm-Cre; Mcl-1$^{+/+}$ (mice $n = 4$, implantations $n = 15$–32 per day) and Chm-Cre; Mcl-1$^{fl/fl}$ females (mice $n = 5$, implantations $n = 21$–36 per day) at gd5 and gd10. Results are presented as individual values for each single placenta with mean. Statistical differences were obtained using unpaired *t*-test (**$P < 0.01$). gd, gestation day; T, thickness; Dia, diameter.

(BMCMCs). As expected, cytological analyses showed cytoplasmic Giemsa-positive granules in both, BMCMCs generated from Chm-Cre; Mcl-1$^{fl/fl}$ and Chm-Cre; Mcl-1$^{+/+}$ mice, after 4 weeks of culture. Furthermore, BMCMCs derived from Chm-Cre; Mcl-1$^{fl/fl}$ and Chm-Cre; Mcl-1$^{+/+}$ mice were similar in size, granule distribution, and nucleus formation (**Figure 5A**). Chm-Cre; Mcl-1$^{fl/fl}$ and Chm-Cre; Mcl-1$^{+/+}$ BMCMCs also showed no differences in their rates of proliferation after 7, 14, 21, or 28 days of culture (**Figure 5B**). The differentiation of BMCMCs derived from Chm-Cre; Mcl-1$^{fl/fl}$ and Chm-Cre; Mcl-1$^{+/+}$ was also similar as assessed by flow cytometric analysis of the expression of the MC surface markers CD117 (c-kit) and FcεRIα at day 7, 14, 21, or 28 of culture. BMCMCs from both strains, after 28 days of culture, exhibited more than 95% double-positive cells (**Figure 5C**).

DISCUSSION

In this study, we developed a new mouse strain Chm-Cre; Mcl-1$^{fll/fl}$ that was used for the investigation and characterization of different populations of MCs (CTMCs and MMCs). Our data support the conclusion that Chm-Cre;

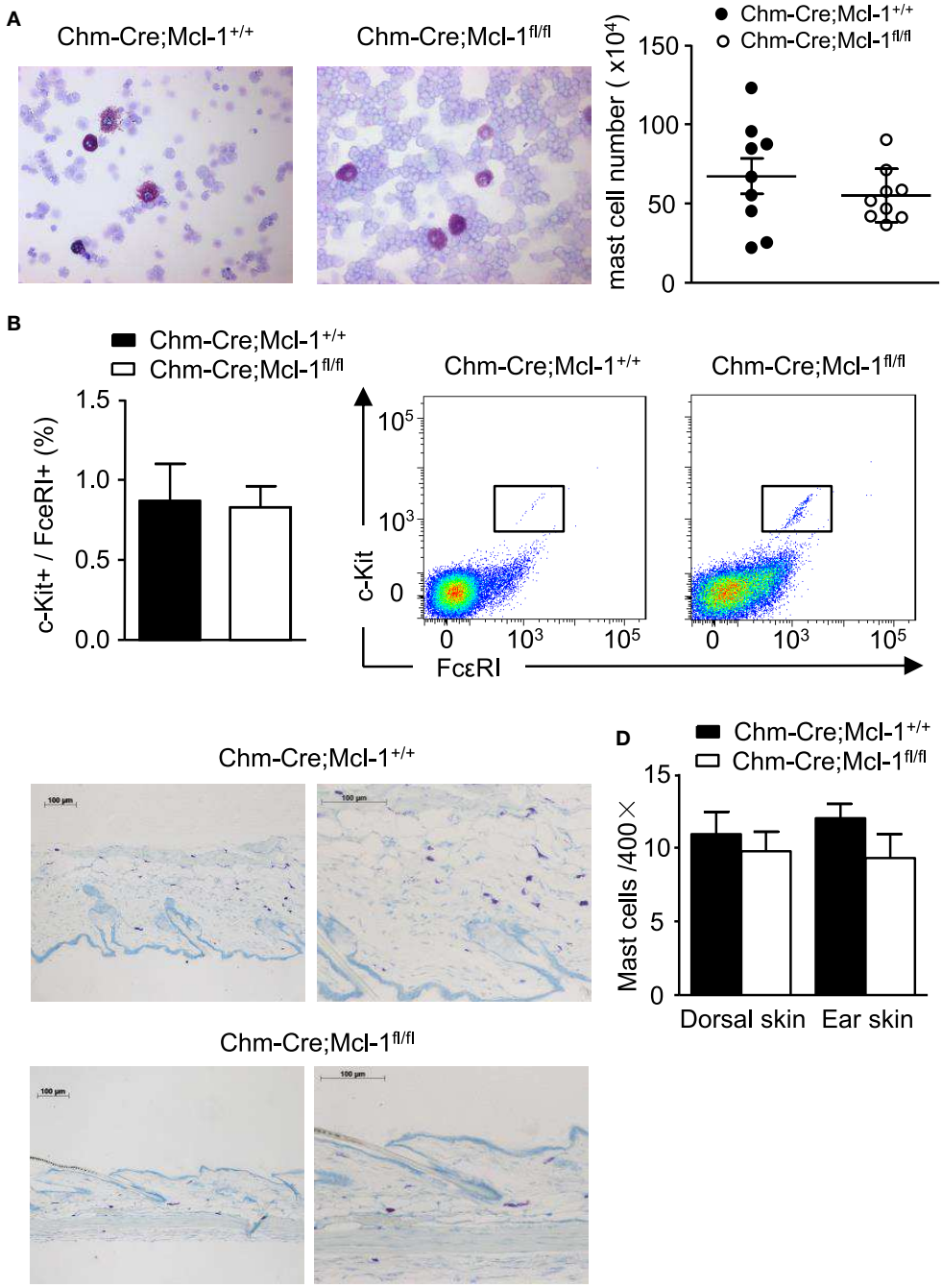

FIGURE 4 | Chm-Cre; Mcl-$1^{fl/fl}$ mice exhibit no variation of cell number in representative sites of connective tissue mast cell (CTMC) populations as compared to Chm-Cre; Mcl-$1^{+/+}$ mice. **(A)** Cytospins of peritoneal lavage fluid from Chm-Cre; Mcl-$1^{+/+}$ mice and Chm-Cre; Mcl-$1^{fl/fl}$ mice were stained with Giemsa solution and MC numbers were assessed by Neubauer Hemocytometry. Mice exhibit comparable numbers of PMCs (right) with similar morphological features. **(B)** Percentage of mast cell surface markers expression (left) and representative flow cytometry plots (right) showed comparable expression of c-kit and FcεRI on PMCs isolated from Chm-Cre; Mcl-$1^{+/+}$ mice and Chm-Cre; Mcl-$1^{fl/fl}$ mice. **(C)** Giemsa staining of 5-μm-thick paraffin sections of dorsal skin obtained from Chm-Cre; Mcl-$1^{+/+}$ and Chm-Cre; Mcl-$1^{fl/fl}$ mice show comparable numbers of MCs (purple). **(D)** MCs in dorsal and ear skin tissues show similar amounts of dermal MCs. **(A)** 400× magnification, **(C)** left: 100× magnification, **(C)** right: 200× magnification. Data were pooled from two (**A,B**; $n = 3$ mice per group ± SEM) or five independent experiment (**C,D**; $n = 5$ mice per group ± SEM).

Mcl-$1^{fl/fl}$ mice have markedly reduced numbers of MMCs in mucosal tissues of the glandular stomach and intestine, which contain only MMCs, as well as in the uterus, which contains both subtypes of MCs. In contrast, the numbers of CTMCs, in the dorsal skin, ear skin, and peritoneal cavity, are normal.

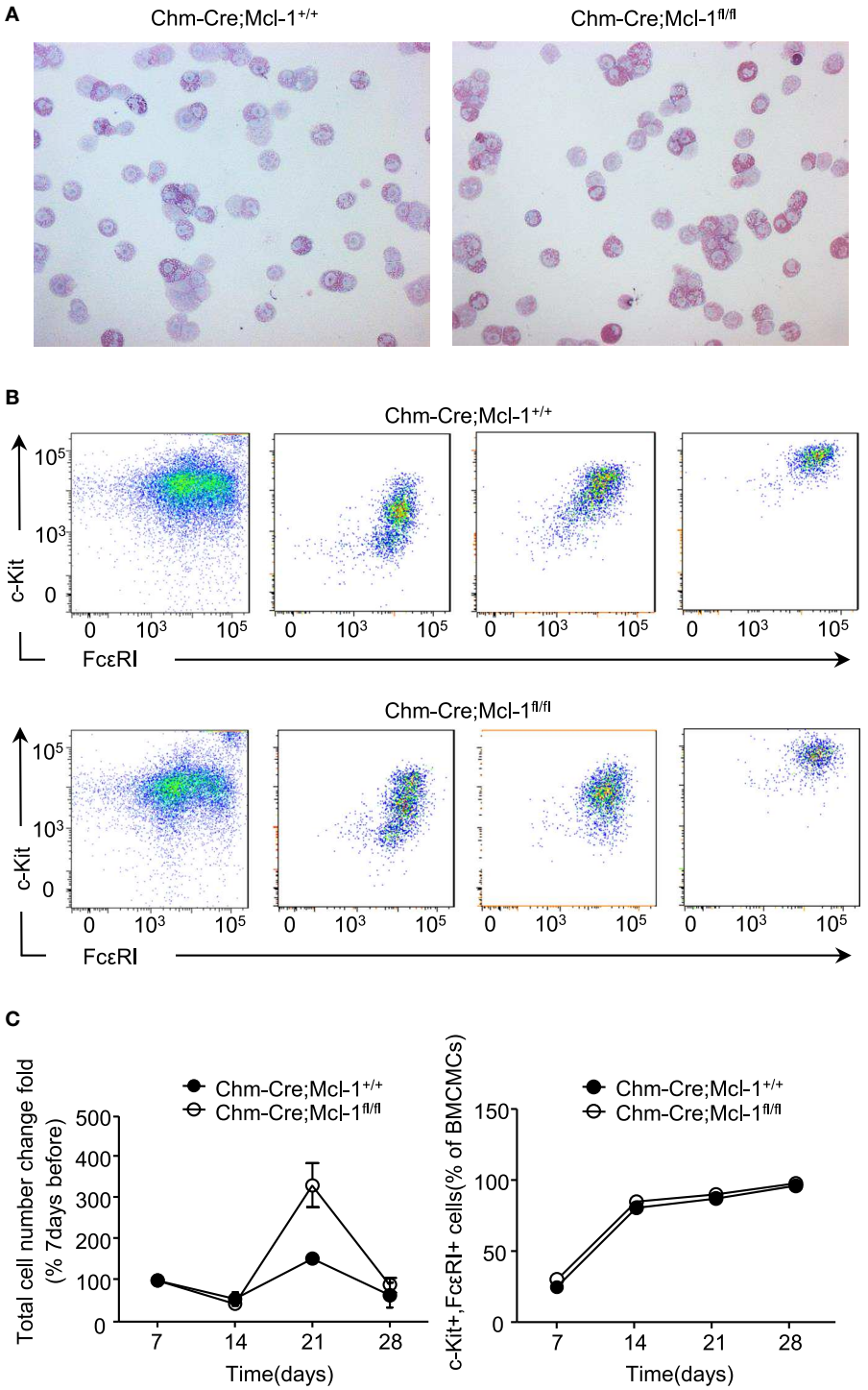

FIGURE 5 | Comparable proliferation and differentiation rates in bone marrow-derived cultured mast cells (BMCMCs). **(A)** Representative light micrograph shows comparable morphology of BMCMCs after 4 weeks of culture in IL-3-supplemented medium from Chm-Cre; Mcl-$1^{+/+}$ control mice and Chm-Cre; Mcl-$1^{fl/fl}$ mice. BMCMCs were identified morphologically on cytospin cell preparations stained with Giemsa solution. **(B)** Representative flow cytometry plots and percentage of c-kit and FcεRI expression show comparable differentiation rate on BMCMCs isolated from Chm-Cre; Mcl-$1^{+/+}$ mice and Chm-Cre;Mcl-$1^{fl/fl}$ mice after 7, 14, 21, and 28 days of culture. **(C)** The proliferation rate of BMCMCs was evaluated by calculating the fold change of cell number over time. Data show similar proliferation rates of BMCMCs after 7, 14, 21, and 28 days of culture from Chm-Cre; Mcl-$1^{+/+}$ mice and Chm-Cre; Mcl-$1^{fl/fl}$ mice. **(A)** 200× magnification. Data are pooled from three independent experiments ($n = 3$ mice per group ± SEM).

MMCs are found at relatively low numbers in most mucosal tissues, especially in the intestines (29). It was, therefore, not surprising to find that some of the intestinal tissues analyzed, such as the ileum and colon, contained barely any detectable MMCs (**Figure 1C**). Our data indicate that Chm-Cre; Mcl-$1^{fl/fl}$ mice exhibited a significantly reduced number of intestinal MMCs, even when the physiological number of MMCs in wild-type mice was very low (**Figure 1C**) as previously described (9). MMC populations of the gut are known to expand under inflammatory conditions, such as parasitic infections and allergic conditions (19–21). Further studies will be needed to characterize if and how intestinal MMC numbers change in Chm-Cre; Mcl-$1^{fl/fl}$ mice in these settings. This will help to characterize their role and relevance for intestinal immune responses against parasites and allergens.

Interestingly, we observed markedly reduced MMC numbers in uterine tissue of Chm-Cre; Mcl-$1^{fl/fl}$ mice (**Figure 2**). Previous studies have shown that uMCs have a positive influence on implantation, placentation, and remodeling of spiral arteries (SAs) as well as placenta size and fetal growth (16, 30, 31). In Chm-Cre; Mcl-$1^{fl/fl}$ mice, the placental and fetal development was largely normal (**Figure S1**), but we did find that placental thickness is decreased (**Figure 3**). It has been recently demonstrated that the complete absence of all MCs, i.e., of both CTMCs and MMCs, in Kit^{W-sh}/Kit^{W-sh} (sash) mice is linked to a severe impairment in reproduction. The selective depletion of Mcpt-5-positive CTMCs also negatively impacts fetal and placental development (30). Our study suggests that the selective absence of MMCs has no major impact on fetal and placental growth. Previous studies have shown that uterine natural killer cells (uNKs) are able to overcome the absence of uMCs by counterbalancing their effects at the feto-maternal interface to promote SA remodeling and placentation (30). In addition, regulatory T cells (Treg) are known as key regulators of placental implantation. Tregs transferred into abortion-prone mice, which present with insufficient numbers of uMCs, restore SA remodeling and placental development by promoting the expansion of uMCs (16). Further studies will help in understanding the functions of uNKs and Tregs in Chm-Cre; Mcl-$1^{fl/fl}$ mice. uNKs and Tregs may rescue the phenotype in Chm-Cre; Mcl-$1^{fl/fl}$ mice and thereby secure normal implantation and placental development.

Interestingly, we also observed alcian blue/safranin double-positive cells in Chm-Cre; Mcl-$1^{+/+}$ mice (**Figure S1**). Alcian blue staining is used to detect MMCs, and safranin stains CTMCs. The presence of double-positive MCs in the uterus has previously been reported (32–34). Whether these MCs are in a premature state or in a conversion process is yet unclear. It has been suggested by some authors that uMCs may be able to change their phenotype depending on the surrounding milieu (33, 34).

MCs can originate from bone marrow precursor cells, and they then differentiate into MMCs and CTMCs according to the local microenvironment. BMCMCs are used as an *in vitro* model for studying MC functions. They are a mucosal-like population of MCs since they share some characteristics with MMCs, like their protease composition. The generation of BMCMCs from Chm-Cre; Mcl-$1^{fl/fl}$ mice, however, revealed no differences when compared to Chm-Cre; Mcl-$1^{+/+}$ mice, suggesting that BMCMCs are immature MCs that are phenotypically distinct from both MMCs and CTMCs (35). BMCMCs from Chm-Cre; Mcl-$1^{fl/fl}$ mice were similar in proliferation and maturation as compared to cells derived from control mice (**Figures 5B,C**), indicating that the hematopoietic progenitor cell capacities for MC differentiation are retained in Chm-Cre; Mcl-$1^{fl/fl}$ mice. This is in line with previous findings showing that the BMCMC population derived from Chm:Cre mice exhibit no specific Cre activity (27), indicating that Cre-expression driven by the baboon α-chymase promotor is restricted to mature MMCs.

After their egress from the bone marrow or alternate stem cell reservoirs, MC progenitors undergo differentiation and maturation in their peripheral target tissues. MC progenitors that populate the skin or peritoneum become CTMCs, whereas those that differentiate and mature in mucosal epithelia and the lamina propria become MMCs. The most important finding of our study is that Chm-Cre; Mcl-$1^{fl/fl}$ mice exhibit a profound reduction of MMCs in mucosal tissues of the glandular stomach and intestine without affecting the number of CTMCs in connective tissues like the skin and the peritoneal cavity.

Although mammalian MCs were first described more than a century ago, their detailed functions remain to be elucidated. MCs are considered to be multifunctional immune cells implicated in several physiological and pathological processes. However, the knowledge about the biological functions of the different MC subtypes, especially MMCs, and the plasticity of MCs is limited due to the lack of suitable models for their investigation *in vivo*. Today, one of the most important challenges for the development of MC-targeting therapeutic applications is to understand their impact on different MC subpopulations. Genetic mouse models are an important tool for this, as well as for the identification and characterization of physiological and pathological functions of MCs *in vivo*. Several MC-deficient models have been described and used in the past: mice deficient for Kit (Kit^{W}/Kit^{W-v} mice and Kit^{W-sh}/Kit^{W-sh} mice), the receptor for stem cell factor (SCF), which is essential for MC growth and survival, have been used for more than 30 years to analyze MC populations and their functions *in vivo*. These mice exhibit a variety of non-MC-related phenotypic abnormalities, including abnormalities affecting hematopoietic cells other than MCs that can contribute to innate or adaptive immune responses, such as neutrophils, basophils, γδ T-cells, and myeloid suppressor cells (9, 11, 36). In recent years, Kit-independent models became available including Cpa3-Cre; Mcl-$1^{fl/fl}$ (28), $Cpa3^{Cre/+}$ ("Cre-Master") mice (37), and Mas-TRECK (38), as well as Mcpt5-Cre iDTR (39), Mcpt5-Cre R-DTA (40), and RMB mice (41) with an inducible or constitutive deficiency for either the entire MC compartment, CTMCs only, or both MCs and basophils. However, genetic mouse models with a specific focus on MMC populations had not be reported, and this has been a roadblock for improving our understanding of the biology of MMCs.

In this study, we report a novel model for studying MMCs, the Chm-Cre; Mcl-$1^{fl/fl}$ mouse, and we provide a phenotypic characterization of its MC populations. The selective reduction of numbers of MMCs in this novel mouse model is a useful tool

in MC research, especially for investigating the role and relevance of MMCs in health and disease.

METHODS

Mice

Genetically, Chm-Cre; Mcl-$1^{fl/fl}$ mice and congenic normal Chm-Cre; Mcl-$1^{+/+}$ mice (8–12 weeks old) were obtained from breeding colonies of the animal facilities of Charité-Universitätsmedizin Berlin. Mice were kept in community cages at the Animal Care Facilities at light periods of 12 h and were fed water and mouse chow *ad libitum*. All animal care and experimentation was conducted in accordance with current Institutional Animal Care and Use Committee guidelines at the Charité-Universitätsmedizin Berlin under official permissions of the State of Berlin, Germany.

Development of the Mouse Model

C57BL/6 alpha-chymase-Cre transgenic (Chm-Cre) mice previously described by Müsch et al. (27) were crossed to C57BL/6 Mcl-$1^{+/fl}$ mice for one generation to obtain heterozygote Chm-Cre; Mcl-$1^{+/fl}$ mice. The offspring was identified by PCR genotyping. The heterozygote Chm-Cre; Mcl-$1^{+/fl}$ mice were bred as breeder to obtain Chm-Cre; Mcl-$1^{+/+}$, Chm-Cre; Mcl-$1^{+/fl}$, and Chm-Cre; Mcl-$1^{fl/fl}$ mice.

Genotyping

Genotyping was performed by PCR. The genotype of transgenic offspring from Chm-Cre; Mcl-$1^{+/fl}$ mice was detected by ear biopsies DNA as described before (22). (Primers: Chm-CreFor: 5′ CGG CGC TAA GGA TGA CTC TGG TCA G 3′, Chm-CreRev: 5′ GTC CAA CGT TCC GTT CGC GCG G 3′, Mcl-1For: 5′ CGA TGC AAC GAG TGA TGA GG 3′, Mcl-1Rev: 5′ GCA TTG CTG TCA CTT GGT CGT 3′). Three reactions are performed during the genotyping, in brief: one to test for Chm-Cre, one to test for the wild-type Mcl-1 allele (PCR product: 360 bp), and one to test for the Mcl-1 flox allele (PCR product: 400 bp).

Cells

Mouse femoral and tibial BM cells from Chm-Cre; Mcl-1 mice were cultured for 4 weeks in complete IL-3-containing medium with 1% antibiotics to generate BM-derived cultured mast cells (BMCMCs). Peritoneal cells (PMCs) were obtained by injecting Chm-Cre; Mcl-1 mice i.p. with 5 ml of PBS for the peritoneal lavage. Morphological analysis of MCs was assessed by Alkaline-Giemsa staining of cytospins. MC differentiation was assessed by flow cytometric analysis for surface expression of CD117 (c-kit) and FcεRI.

Histology

Mice were euthanized, and samples of back skin, ear pinna, were fixed in 4% buffered formaldehyde (vendor); stomach, duodenum, ileum, and colon were fixed in 4% methanol-free formaldehyde, dehydrated, and embedded in paraffin ensuring a cross-sectional orientation of all tissues, and 5-μm sections were stained with alkaline-Giemsa solution for histologic examination and enumeration of MCs. To examine stomach MMCs, stomach samples were stained by alcian blue solution. To examine MMCs of the duodenum, jejunum, ileum, and colon, 5-μm sections of intestinal tissue were stained for chloroacetate esterase-positive MMCs, as previously described (35). To examine uMCs, 5-μm paraffin embedded uterus samples were stained by toluidine blue, alcian blue, or safranin. At least three random sections per mouse were analyzed. Ten high-power fields (HPF) per section have been analyzed.

Determination of MC Numbers

In all histological assessments, cell numbers were enumerated by a single observer not aware of the identity (mouse group) of the individual sections. Cell numbers were based on counting 10 medium-power fields (200×) or HPF (400×), and mean values were calculated. In this study, MCs were classified according to anatomic location as previously described (42). Skin MCs were quantified according to horizontal field length of dermis, uterine MCs were quantified according to area, and gastrointestinal MCs were quantified according to anatomical structure (per field of mucosa and submucosa). MCs superficial to the deep border of the muscular layer, including the epithelium and lamina propria, were classified as MMCs. Images were captured with a Zeiss Axioplan 2 Imaging microscope using a Zeiss AxioCam camera run by AxioVision Rel. 4.8 software.

Ultrasound Imaging

Serial high-frequency ultrasound measurements were performed with the Vevo® 2100 Imaging system (FujiFilm VisualSonics Inc.) by using the transducer MS550D-0421. Isoflurane (Baxter)-anesthetized mice were placed on the heating platform, abdominal hair was removed with depilatory cream (Reckitt Beckiser), and eye protection cream (Bayer) and prowarmed ultrasound gel (Gello GmbH Geltechnik) were applied. During measurements, ECG, body temperature, and respiratory physiology were controlled. B-Mode was used to visualize anatomical structures in 2D grayscale image. Ultrasound examinations were performed at gd5 (implantation size) and gd10 (implantation size, placenta area/thickness/diameter), and all implantations found within the mothers were imaged. Mice were never exposed longer than 1 h to gaseous anesthesia.

Statistics

Unless otherwise indicated, all data were tested for statistical significance using the unpaired Student's *t*-test and expressed as mean ± SEM. A $p \leq 0.05$ was considered to reflect statistical significance.

DATA AVAILABILITY STATEMENT

The datasets generated for this study are available on request to the corresponding author.

ETHICS STATEMENT

The animal study was reviewed and approved by Landesamt für Soziales und Gesundheit Berlin.

AUTHOR CONTRIBUTIONS

YL, QJ, CZ, and NM performed experiments. YL wrote the manuscript. JS and FS supervised experiments and revised the manuscript. AZ, MMe, and MM gave critical input to the experimental design and the manuscript. All authors contributed to the interpretation of the results.

FUNDING

This work was supported by grants from the German Research Foundation (DFG) SPP1394 to MM (MA1909/9-1 and MA1909/10-1) and by a scholarship from the China Scholarship Council to YL.

ACKNOWLEDGMENTS

We thank Sina Heydrich and Evelin Hagen for their excellent technical support. We further acknowledge support from the German Research Foundation and the Open Access Publication Fund of Charité-Universitätsmedizin Berlin.

SUPPLEMENTARY MATERIAL

The Supplementary Material for this article can be found online at: https://www.frontiersin.org/articles/10.3389/fimmu.2019.02399/full#supplementary-material

Figure S1 | Chm-Cre; Mcl1$^{fl/fl}$ mice exhibit no differences in the analyzed placental parameters comparing to Chm-Cre; Mcl1$^{+/+}$ mice. **(A)** Placental weight of Chm-Cre; Mcl-1$^{+/+}$ (mice $n = 4$, placentas $n = 21$) and Chm-Cre; Mcl-1$^{fl/fl}$ (mice $n = 5$, placentas $n = 34$) females paired with Balb/c males at gd10. **(B)** Number of implantations at gd5 or gd10, abortions, and abortion rate at gd10 from Chm-Cre; Mcl-1$^{+/+}$ ($n = 3$–4) and Chm-Cre; Mcl-1$^{fl/fl}$ ($n = 3$–5) females paired with Balb/c males at gd10. Results are presented as individual values ± median. **(C)** Representative bicorneal uteri of Chm-Cre; Mcl-1$^{+/+}$ and Chm-Cre; Mcl-1$^{fl/fl}$ mice at gd5 or gd10. **(D)** SA wall thickness and SA wall-to-lumen ratio from 3 to 9 SAs per mice of Balb/c-paired Chm-Cre; Mcl-1$^{+/+}$ ($n = 4$) and Chm-Cre; Mcl-1$^{fl/fl}$ ($n = 5$) females at gd10. Statistical differences were analyzed with the Mann–Whitney test. gd, gestation day; SA, spiral artery.

REFERENCES

1. Rivera J, Gilfillan AM. Molecular regulation of mast cell activation. *J Allergy Clin Immunol.* (2006) 117:1214–25; quiz 26. doi: 10.1016/j.jaci.2006.04.015
2. Grimbaldeston MA, Metz M, Yu M, Tsai M, Galli SJ. Effector and potential immunoregulatory roles of mast cells in IgE-associated acquired immune responses. *Curr Opin Immunol.* (2006) 18:751–60. doi: 10.1016/j.coi.2006.09.011
3. Gilfillan AM, Tkaczyk C. Integrated signalling pathways for mast-cell activation. *Nat Rev Immunol.* (2006) 6:218–30. doi: 10.1038/nri1782
4. Brown GD. Innate antifungal immunity: the key role of phagocytes. *Annu Rev Immunol.* (2011) 29:1–21. doi: 10.1146/annurev-immunol-030409-101229
5. Abraham SN, St John AL. Mast cell-orchestrated immunity to pathogens. *Nat Rev Immunol.* (2010) 10:440–52. doi: 10.1038/nri2782
6. St John AL, Abraham SN. Innate immunity and its regulation by mast cells. *J Immunol.* (2013) 190:4458–63. doi: 10.4049/jimmunol.1203420
7. Kitamura Y, Go S, Hatanaka K. Decrease of mast cells in W/Wv mice and their increase by bone marrow transplantation. *Blood.* (1978) 52:447–52.
8. Jamur MC, Grodzki AC, Berenstein EH, Hamawy MM, Siraganian RP, Oliver C. Identification and characterization of undifferentiated mast cells in mouse bone marrow. *Blood.* (2005) 105:4282–9. doi: 10.1182/blood-2004-02-0756
9. Chen CC, Grimbaldeston MA, Tsai M, Weissman IL, Galli SJ. Identification of mast cell progenitors in adult mice. *Proc Natl Acad Sci USA.* (2005) 102:11408–13. doi: 10.1073/pnas.0504197102
10. Gentek R, Ghigo C, Hoeffel G, Bulle MJ, Msallam R, Gautier G, et al. Hemogenic endothelial fate mapping reveals dual developmental origin of mast cells. *Immunity.* (2018) 48:1160–71.e5. doi: 10.1016/j.immuni.2018.04.025
11. Kitamura Y, Sonoda T, Nakano T, Hayashi C, Asai H. Differentiation processes of connective tissue mast cells in living mice. *Int Arch Allergy Appl Immunol.* (1985) 77:144–50. doi: 10.1159/000233769
12. Kitamura Y, Kasugai T, Arizono N, Matsuda H. Development of mast cells and basophils: processes and regulation mechanisms. *Am J Med Sci.* (1993) 306:185–91. doi: 10.1097/00000441-199309000-00011
13. Kroegel C. Biological and molecular aspects of mast cell and basophil differentiation and function. In: Kitamura Y, Yamamoto S, Galli SJ, Greaves MW, editors. *FEBS Letters*. New York, NY: Raven Press (1994). p. 270. doi: 10.1016/0014-5793(51)90001-4
14. Hallgren J, Gurish MF. Pathways of murine mast cell development and trafficking: tracking the roots and routes of the mast cell. *Immunol Rev.* (2007) 217:8–18. doi: 10.1111/j.1600-065X.2007.00502.x
15. Gurish MF, Austen KF. Developmental origin and functional specialization of mast cell subsets. *Immunity.* (2012) 37:25–33. doi: 10.1016/j.immuni.2012.07.003
16. Woidacki K, Meyer N, Schumacher A, Goldschmidt A, Maurer M, Zenclussen AC. Transfer of regulatory T cells into abortion-prone mice promotes the expansion of uterine mast cells and normalizes early pregnancy angiogenesis. *Sci Rep.* (2015) 5:13938. doi: 10.1038/srep13938
17. Fukuzumi T, Waki N, Kanakura Y, Nagoshi J, Hirota S, Yoshikawa K, et al. Differences in irradiation susceptibility and turnover between mucosal and connective tissue-type mast cells of mice. *Exp Hematol.* (1990) 18:843–7.
18. Kitamura Y, Shimada M, Hatanaka K, Miyano Y. Development of mast cells from grafted bone marrow cells in irradiated mice. *Nature.* (1977) 268:442–3. doi: 10.1038/268442a0
19. Ruitenberg EJ, Elgersma A. Absence of intestinal mast cell response in congenitally athymic mice during Trichinella spiralis infection. *Nature.* (1976) 264:258–60. doi: 10.1038/264258a0
20. Hepworth MR, Daniłowicz-Luebert E, Rausch S, Metz M, Klotz C, Maurer M, et al. Mast cells orchestrate type 2 immunity to helminths through regulation of tissue-derived cytokines. *Proc Natl Acad Sci USA.* (2012) 109:6644–9. doi: 10.1073/pnas.1112268109
21. McDermott JR, Bartram RE, Knight PA, Miller HR, Garrod DR, Grencis RK. Mast cells disrupt epithelial barrier function during enteric nematode infection. *Proc Natl Acad Sci USA.* (2003) 100:7761–6. doi: 10.1073/pnas.1231488100
22. Brandt EB, Strait RT, Hershko D, Wang Q, Muntel EE, Scribner TA, et al. Mast cells are required for experimental oral allergen-induced diarrhea. *J Clin Invest.* (2003) 112:1666–77. doi: 10.1172/JCI19785
23. Mayrhofer G, Fisher R. Mast cells in severely T-cell depleted rats and the response to infestation with Nippostrongylus brasiliensis. *Immunology.* (1979) 37:145–55.
24. Guy-Grand D, Dy M, Luffau G, Vassalli P. Gut mucosal mast cells. Origin, traffic, and differentiation. *J Exp Med.* (1984) 160:12–28. doi: 10.1084/jem.160.1.12
25. Kos CH. Methods in nutrition science: Cre/loxP system for generating tissue-specific knockout mouse models. *Nutr Rev.* (2004) 62:243–6. doi: 10.1301/nr2004.jun243-246
26. Rajewsky K, Gu H, Kuhn R, Betz UA, Muller W, Roes J, et al. Conditional gene targeting. *J Clin Invest.* (1996) 98:600–3. doi: 10.1172/JCI118828
27. Müsch W, Wege AK, Männel DN, Hehlgans T. Generation and characterization of alpha-chymase-Cre transgenic mice. *Genesis.* (2008) 46:163–6. doi: 10.1002/dvg.20378

28. Lilla JN, Chen CC, Mukai K, BenBarak MJ, Franco CB, Kalesnikoff J, et al. Reduced mast cell and basophil numbers and function in Cpa3-Cre; Mcl-1fl/fl mice. *Blood.* (2011) 118:6930–8. doi: 10.1182/blood-2011-03-343962
29. Reber LL, Sibilano R, Mukai K, Galli SJ. Potential effector and immunoregulatory functions of mast cells in mucosal immunity. *Mucosal Immunol.* (2015) 8:444–63. doi: 10.1038/mi.2014.131
30. Meyer N, Woidacki K, Knöfler M, Meinhardt G, Nowak D, Velicky P, et al. Chymase-producing cells of the innate immune system are required for decidual vascular remodeling and fetal growth. *Sci Rep.* (2017) 7:45106. doi: 10.1038/srep45106
31. Woidacki K, Popovic M, Metz M, Schumacher A, Linzke N, Teles A, et al. Mast cells rescue implantation defects caused by c-kit deficiency. *Cell Death Dis.* (2014) 4:e462. doi: 10.1038/cddis.2012.214
32. Combs J, Lagunoff D, Benditt E. Differentiation and proliferation of embryonic mast cells of the rat. *J Cell Biol.* (1965) 25:577–92. doi: 10.1083/jcb.25.3.577
33. Aydin Y, Tunçel N, Gürer F, Tunçel M, Koşar M, Oflaz G. Ovarian, uterine and brain mast cells in female rats: cyclic changes and contribution to tissue histamine. *Comp Biochem Physiol A Mol Integr Physiol.* (1998) 120:255–62. doi: 10.1016/S1095-6433(98)00027-0
34. Brandon JM, Evans JE. Changes in uterine mast cells during the estrous cycle in the Syrian hamster. *Am J Anat.* (1983) 167:241–7. doi: 10.1002/aja.1001670209
35. Yamada N, Matsushima H, Tagaya Y, Shimada S, Katz SI. Generation of a large number of connective tissue type mast cells by culture of murine fetal skin cells. *J Invest Dermatol.* (2003) 121:1425–32. doi: 10.1046/j.1523-1747.2003.12613.x
36. Galli SJ, Nakae S, Tsai M. Mast cells in the development of adaptive immune responses. *Nat Immunol.* (2005) 6:135–42. doi: 10.1038/ni1158
37. Feyerabend TB, Weiser A, Tietz A, Stassen M, Harris N, Kopf M, et al. Cre-mediated cell ablation contests mast cellcontribution in models of antibody- and T cell-mediated autoimmunity. *Immunity.* (2011) 35:832–44. doi: 10.1016/j.immuni.2011.09.015
38. Otsuka A, Kubo M, Honda T, Egawa G, Nakajima S, Tanizaki H, et al. Requirement of interaction between mast cells and skin dendritic cells to establish contact hypersensitivity. *PLoS ONE.* (2011) 6:e25538. doi: 10.1371/journal.pone.0025538
39. Reber LL, Marichal T, Mukai K, Kita Y, Tokuoka SM, Roers A, et al. Selective ablation of mast cells or basophils reduces peanut-induced anaphylaxis in mice. *J Allergy Clin Immunol.* (2013) 132:881–8.e11. doi: 10.1016/j.jaci.2013.06.008
40. Dudeck A, Dudeck J, Scholten J, Petzold A, Surianarayanan S, Kohler A, et al. Mast cells are key promoters of contact allergy that mediate the adjuvant effects of haptens. *Immunity.* (2011) 34:973–84. doi: 10.1016/j.immuni.2011.03.028
41. Dahdah A, Gautier G, Attout T, Fiore F, Lebourdais E, Msallam R, et al. Mast cells aggravate sepsis by inhibiting peritoneal macrophage phagocytosis. *J Clin Invest.* (2014) 124:4577–89. doi: 10.1172/JCI75212
42. Galli S, Wershil B, Bose R, Walker P, Szabo S. Ethanol-induced acute gastric injury in mast cell-deficient and congenic normal mice. Evidence that mast cells can augment the area of damage. *Am J Pathol.* (1987) 128:131–40.

Conflict of Interest: The authors declare that the research was conducted in the absence of any commercial or financial relationships that could be construed as a potential conflict of interest.

frontiers in Immunology

REVIEW
published: 03 December 2019
doi: 10.3389/fimmu.2019.02821

Bacterial Manipulation of Autophagic Responses in Infection and Inflammation

*Yang Jiao and Jun Sun**

Division of Gastroenterology and Hepatology, College of Medicine, University of Illinois at Chicago, Chicago, IL, United States

Eukaryotes have cell-autonomous defenses against environmental stress and pathogens. Autophagy is one of the main cellular defenses against intracellular bacteria. In turn, bacteria employ diverse mechanisms to interfere with autophagy initiation and progression to avoid elimination and even to subvert autophagy for their benefit. This review aims to discuss recent findings regarding the autophagic responses regulated by bacterial effectors. Effectors manipulate autophagy at different stages by using versatile strategies, such as interfering with autophagy-initiating signaling, preventing the recognition of autophagy-involved proteins, subverting autophagy component homeostasis, manipulating the autophagy process, and impacting other biological processes. We describe the barriers for intracellular bacteria in host cells and highlight the role of autophagy in the host-microbial interactions. Understanding the mechanisms through which bacterial effectors manipulate host responses will provide new insights into therapeutic approaches for prevention and treatment of chronic inflammation and infectious diseases.

Keywords: autophagy, effectors, bacteria, LC-3, innate immunity, microbiome

OPEN ACCESS

Edited by:
Elba Mónica Vermeulen, Instituto de Medicina Experimental (IMEX)-CONICET, Academia Nacional de Medicina, Argentina

Reviewed by:
Shashank Gupta, Brown University, United States
Sunil Joshi, Miller School of Medicine, University of Miami, United States

***Correspondence:**
Jun Sun
junsun7@uic.edu

Specialty section:
This article was submitted to Microbial Immunology, a section of the journal Frontiers in Immunology

Received: *07 September 2019*
Accepted: *15 November 2019*
Published: *03 December 2019*

Citation:
Jiao Y and Sun J (2019) Bacterial Manipulation of Autophagic Responses in Infection and Inflammation. Front. Immunol. 10:2821. doi: 10.3389/fimmu.2019.02821

INTRODUCTION

Autophagy, which literally means "self-eating," is an intrinsic process of eukaryotes that delivers cytoplasmic material to lysosomes for degradation. During this process, cytoplasmic material is enclosed by phagophores. Then, the phagophores elongate to form autophagosomes that fuse with lysosomes to form autolysosomes where the cargoes are degraded (1). Autophagy is an important biological process that is involved in immune responses, embryonic development, cell death, and cellular defense (2). It is important for host responding to nutrient stress as well as eliminating intracellular pathogens. Better understanding of autophagy mechanism will allow us to develop therapeutic drugs, vaccines, and host-directed strategies for successful control of intracellular microorganisms.

There are three forms of autophagy that are commonly described: chaperone-mediated autophagy (CMA), microautophagy, and macroautophagy. Macroautophagy is then divided into non-selective and selective autophagy. Various cargoes, such as defective mitochondria, defective endoplasmic reticulum (ER), lipids, and foreign organisms, are targeted by selective autophagy for degradation. When autophagy engulfs microorganisms for clearance, this pathway is called "xenophagy," which plays a central role in cellular defense (3).

To survive in host cells, bacteria employ multiple mechanisms to protect against cellular defenses. Effectors, one type of weapons used by bacteria, are proteins translocated from the bacterial cytoplasm to the host cell cytoplasm by a series of secretion systems (T1SS–T8SS) (4).

Bacterial effectors have the capacity to influence host cellular biological processes, including signaling pathways, tight junctions, phagocytosis, apoptosis, and autophagy (5, 6).

This review will discuss the recent research advancement (<6 years) in interactions between bacterial effectors and host autophagic responses. We synoptically describe the barriers for intracellular bacteria in host cells and highlight the role of autophagy in these processes. Furthermore, we emphasize the different strategies used by bacterial effectors from secretion systems (T3SS, T44SS, T6SS, and T7SS) to manipulate autophagic responses in host cells in infection and inflammation.

THE FATE OF INTRACELLULAR BACTERIA IN AUTOPHAGY

There is a constant battle between bacterial evasion mechanisms and host cellular defenses, and the fate of intracellular bacteria is determined by the outcome of this battle. Intracellular pathogens can be internalized by either phagocytic or non-phagocytic cells. After entry into host cells, bacteria are localized to internalization vacuoles, which are designated as phagosomes (**Figure 1**). To survive, bacterial effectors have different strategies to interfere with host, including affecting autophagy-initiating signaling, modifying LC3 protein, avoiding autophagosome-lysosome fusion, affecting lysosome function, deubiquitinating ubiquitinated substrate around intracellular bacteria, etc. Therefore, intracellular bacteria obtain nutrients to replicate or hide to wait for opportunities.

Pathogen-containing phagosomes fuse with lysosomes via phagocytosis to form phagolysosomes, where the bacteria are eliminated. Notably, recent reports have described a process called LC3-associated phagocytosis (LAP) that recruits the autophagy marker protein LC3 to pathogen-containing phagosomes, and the subsequent fusion of these phagosomes with lysosomes results in pathogen digestion (7). To prevent phagocytosis-mediated bacterial killing, bacteria can either modify the phagosomes to form pathogen-containing vacuoles, thus avoiding fusion with lysosomes (*Mycobacterium tuberculosis*), or disrupt the vacuoles to escape from the phagosomes (*Salmonella* Typhimurium) (8). Xenophagy plays a key role in cell resistance to these crafty bacteria by clearing pathogen-containing vacuoles, escaped pathogens, damaged vacuoles and pathogen-containing phagosomes. Pathogens have many unique ways to escape or subvert host xenophagy. These mechanisms are complex and fall outside the scope of this article; readers are referred to more comprehensive reviews of this subject (9, 10). Here, we focus on the effectors employed by Gram-negative bacteria to disrupt the autophagic responses of host cells.

Abbreviations: ATG protein, Autophagy-related protein; CCVs, *Coxiella*-containing vacuoles; DCs, Dendritic cells; ER, endoplasmic reticulum; JNK, c-Jun N-terminal kinase; LAP, LC3-associated phagocytosis; LUBAC, liner ubiquitin chain assembly complex; RAB proteins, the ras superfamily G-proteins; SCVs, *Salmonella*-containing vacuoles; SPI, *Salmonella* pathogenicity island; T3SS, type III secretion system; T4SS, type IV secretion system; T6SS, type VI secretion system; T7SS, type VII secretion system.

THE AUTOPHAGY MANIPULATION STRATEGIES OF T3SS EFFECTORS

Bacteria can be eliminated by autophagy, thus, Gram-negative bacteria use T3SS effectors to suppress or subvert this process. We summarized all related research work in **Table 1** and discussed the recent progress (<6 years) of different strategies bacteria used, e.g., interference with signaling or ATG proteins, prevention of recognition by autophagy mechanisms, subversion of autophagic components for bacterial survival, and escape from LC3-associated phagocytosis.

Interference With Signaling or ATG Proteins Involved in Autophagy

Shigella flexneri effector IcsB, was recently found to repress the early recruitment of LC3 during infection (11). During early infection (40 min), IcsB recruits the host protein Toca-1 to intracellular *S. flexneri* to suppress the recruitment of LC3 and NDP52 around these intracellular bacteria. LC3 is a marker of autophagosomes, it is also present in LC3-associated phagocytosis. Therefore, this research suggests that IcsB manipulates Toca-1 to inhibit LC3-associated phagocytosis and/or LC3 recruitment to vacuolar membrane remnants early during infection (11). However, this study lacks supporting morphological observations.

In macrophages, SPI-2 (*Salmonella* pathogenicity island-2) T3SS is responsible for suppressing autophagy by actively manipulating the recruitment of focal adhesion kinase (FAK) to *Salmonella*-containing vacuoles (SCVs) and then stimulating the Akt-mTORC1 signaling pathway. However, the effector(s) that are responsible for this process remain unclear (12). Furthermore, the effector AWR5 from the plant pathogen *Ralstonia solanacearum* can also affect the mTOR signaling pathway to activate autophagy (13). Research indicates that AWR5, which is expressed heterologously in yeast, induces growth inhibition and autophagic flux. AWR5 may exert its function by inhibiting TORC1 upstream of PP2A directly or indirectly and thus promoting autophagy.

The effector SseF and SseG secreted by *Salmonella* Typhimurium can inhibit autophagy in host cells by the same autophagy blockade (14). Mechanistically, SseF and SseG impair autophagy initiation by directly interacting with the small GTPase Rab1A in the host cell. And the disruption of Rab1A signaling blocked the recruitment and activation of Unc-51–like autophagy-activating kinase 1 (ULK1) and decreased phosphatidylinositol 3-phosphate biogenesis, which ultimately suppress autophagosome formation.

Salmonella T3SS effector SopF was found to be a general xenophagy inhibitor without affecting canonical autophagy. Using *Salmonella* Typhimurium Δ*sopF*, the researchers identified the V-ATPase-ATG16L1 axis that mediates xenophagy initiation in HeLa cells. And SopF can target ATP6V0C for ADP-ribosylation on Gln124, thereby blocking bacterial autophagy and infection-induced recruitment of ATG16L1 by the V-ATPase (15).

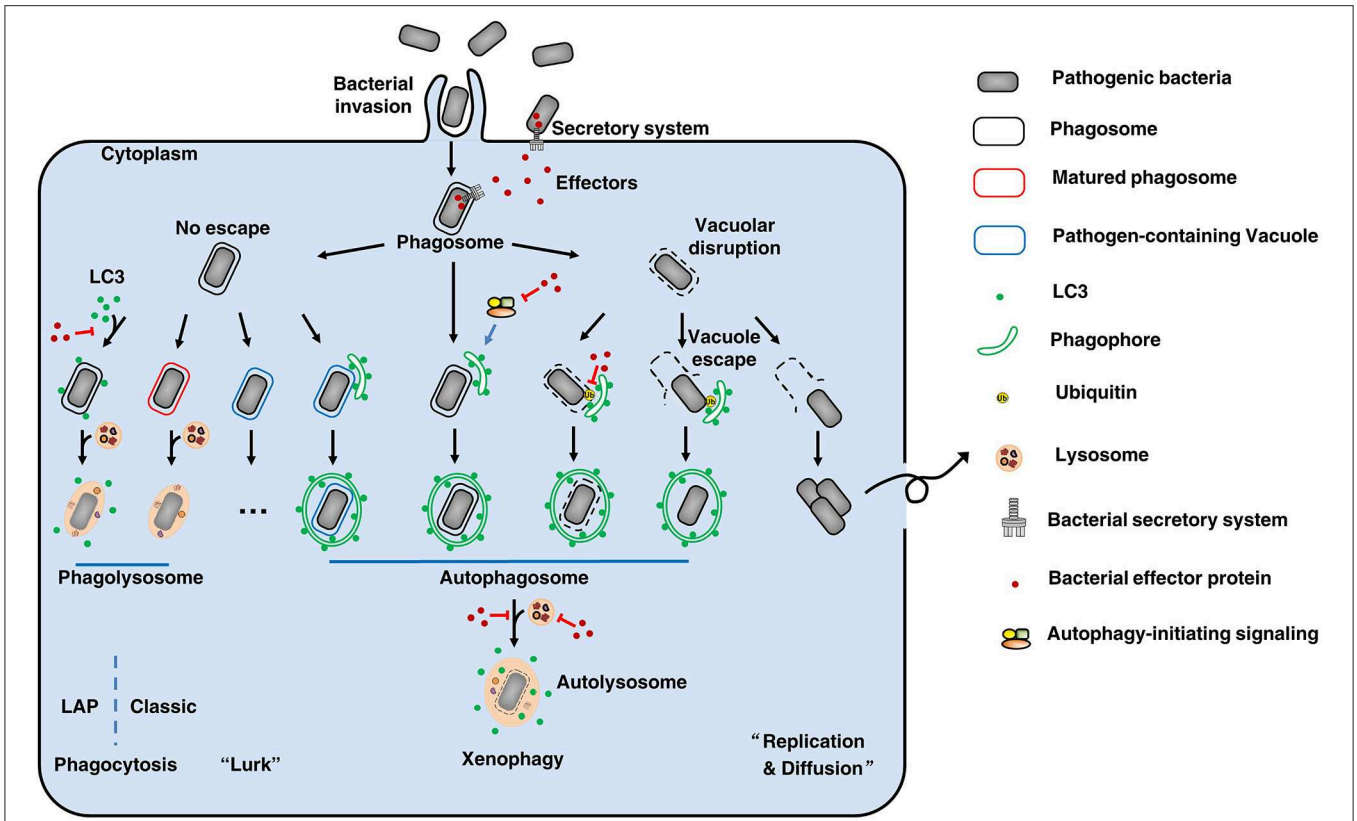

FIGURE 1 | The fate of intracellular bacteria. After entry into host cells, bacteria are localized to internalization vacuoles, which are designated as phagosomes To survive, bacteria employ diverse means to escape or subvert host cellular defenses, especially using its secretion systems and effectors. By various ways, some bacteria (like *Salmonella* Typhimurium) can damage the phagosomes and then escape to the cytoplasm, where can obtain nutrients to replicate and to diffuse. On the other hand, to clean up the bacteria remaining in phagosomes, the phagosomes will be mature and fuse with lysosomes to form phagolysosomes where the bacteria are degraded. This's the classic phagocytosis. To prevent phagocytosis-mediated bacterial killing, bacteria (such as *Mycobacterium tuberculosis*) can modify the phagosomes to form pathogen-containing vacuoles, thus avoiding fusion with lysosomes. These bacteria will lurk to wait for opportunities for their survival. Therefore, xenophagy plays a key role in cell resistance to these crafty bacteria by clearing pathogen-containing vacuoles, escaped pathogens, damaged vacuoles, and pathogen-containing phagosomes. During this process, above targets are enclosed by phagophores. Then, the phagophores elongate to form autophagosomes that fuse with lysosomes to form autolysosomes where the bacteria are eliminated. Notably, LC3-associated phagocytosis (LAP) can recruit the autophagy marker protein LC3 to pathogen-containing phagosomes, and the subsequent fusion of these phagosomes with lysosomes results in pathogen digestion. Additionally, there are other unmentioned cross-talk between xenophagy and phagocytosis. Back to our theme, effectors-autophagy interactions. Using effectors delivered by secretion systems, bacteria are able to interfere with autophagy-initiating signaling, modify LC3 protein, avoid autophagosome-lysosome fusion, affect lysosome function, and deubiquitinate ubiquitinated substrate around intracellular bacteria, etc. Thus, bacteria can suppress or subvert autophagic responses for their survival. Overall, there is a constant battle between bacterial evasion mechanisms and host cellular defenses, and the fate of intracellular bacteria is determined by the outcome of this battle.

We recently show that *Salmonella* Enteritidis effector AvrA can suppress autophagy (16). The AvrA protein is an effector that possesses acetyltransferase and deubiquitinase activity and inhibits the host c-Jun N-terminal kinase (JNK)/AP-1 and NF-κB signaling pathways; thus, AvrA inhibits host inflammatory responses and stabilizes intestinal tight junctions to the benefit of *Salmonella* survival (31, 32). We found that AvrA can inhibit autophagic responses by decreasing Beclin-1 protein levels, and this process occurs via JNK/c-Jun/AP-1 signaling pathway inhibition.

Prevention of Recognition by Autophagy Mechanisms

Bacterial T3SS effectors can interfere with autophagy recognition mechanisms, thus avoiding bacterial killing in the host. IcsB from *S. flexneri* is one of the best-known effectors with this capability. IcsB competes with ATG5 binding to VirG (a bacterial surface protein), thereby masking the bacteria from recognition by autophagy mechanisms. Therefore, IcsB mutants are targeted for autophagy during multiplication in host cells infected with *S. flexneri* (18). Taken together, it suggests that the *S. flexneri* effector IcsB modulates LC3 recruitment around intracellular bacteria at the early stage of infection and inhibits autophagy late during infection (11, 18).

The *S. flexneri* T3SS effector IpaH1.4 is another example of preventing recognition by autophagy mechanisms (19). The E3 ligase LUBAC (liner ubiquitin chain assembly complex) can generate linear (M1-linked) polyubiquitin patches in the ubiquitin coat of intracellular bacteria, which recruit Optineurin and Nemo for xenophagy. In contrast, the effector protein IpaH1.4, a bacterial secreted E3 ubiquitin ligase 30, antagonizes the LUBAC-mediated accumulation of M1-linked ubiquitin

TABLE 1 | Strategies used by T3SS effectors to manipulate autophagy.

Bacteria	Effectors	Host model	Description	Bacterial survival	References
Interfering with signaling or proteins involved in autophagy					
Shigella flexneri	IcsB	HeLa cells, 293T cells and MEFs	Recruits the host protein Toca-1 to repress the recruitment of LC3 around these intracellular bacteria	The absence of IcsB has no effect on bacterial survival up to 3 h of infection	(11)
Salmonella Typhimurium	Unknown	Mouse peritoneal macrophages	Recruits FAK to SCVs and then stimulates the Akt-mTORC1 signaling pathway	In FAK-deficient macrophages, Akt/mTOR signaling is attenuated and autophagic capture of intracellular bacteria is enhanced, resulting in reduced bacterial survival	(12)
Ralstonia solanacearum	AWR5	Yeast, *N. benthamiana*	Suppresses TOR signaling by inhibiting TORC1 upstream of PP2A	Not applicable	(13)
Salmonella Typhimurium	SseF and SseG	HeLa cells, Rab1A$^{-/-}$ RAW264.7 cell, Rab1A$^{-/-}$ mouse	Inhibits Rab1A-mediated autophagy	SseF or SseG-deficient bacterial strains exhibit reduced survival and growth in both mammalian cell lines and mouse infection models	(14)
Salmonella Typhimurium	SopF	HeLa cells	Targets ATP6V0C for ADP-ribosylation on Gln124, thereby blocking recruitment of ATG16L1 by the V-ATPase	ΔsopF grow less efficiently in HeLa cells than the WT strain. And this SopF-dependent replication was diminished in ATG16L1$^{-/-}$ cells, which were rescued by ATG16L1	(15)
Salmonella Enteritidis	AvrA	HCT116 cells, organoids and mice	Reduces the protein expression of Beclin-1 by inhibiting the JNK/c-Jun/AP-1 signaling pathway	AvrA-deficient bacterial strains colonized human epithelial cells show a decreased intracellular bacterial load compared to those colonized with wild type	(16)
Burkholderia pseudomallei	TTSS1 ATPase	RAW 264.7 cells	Decreases colocalization with LC3 but does not affect autophagy	TTSS1 ATPase-deficient bacterial strains has diminished survival and replicative capacity in RAW264.7 cells	(17)
Preventing recognition by autophagy mechanisms					
Shigella flexneri	IcsB	BHK cells, MDCK cells and *atg5*$^{-/-}$ MEFs	Competes with ATG5 binding to the bacterial surface protein VirG	The absence of IcsB has no effect on bacterial survival up to 3 h of infection	(18)
Shigella flexneri	IpaH1.4	MEFs	Antagonizing the LUBAC-mediated accumulation of M1-linked ubiquitin chains on bacterial surfaces, as well as the recruitment of Optineurin and Nemo	Not applicable	(19)
Salmonella Typhimurium	SseL	HeLa cells, RAW264.7 cells and BMM	Splits cytosolic aggregates around SCVs by its deubiquitinating activity	SseL contributes to bacterial replication in restrictive cellular environment	(20)
Subverting autophagic components for bacterial survival					
Vibrio parahaemolyticus	VopQ	HeLa cells	Forms a gated ion channel on lysosomes	VopQ attenuates phagocytosis of *Vibrio parahaemolyticus* during infection	(21–23)
Salmonella Typhimurium	SopB	HeLa cells	Increases the interaction of *Salmonella* with autophagosomes	Autophagy facilitates *Salmonella* replication in the cytosol of HeLa cells	(24)
Affecting autophagy by subverting host cell homeostasis					
Salmonella Typhimurium	SipB	BMDPM	Disrupts mitochondria to induce autophagy	Not applicable	(25)
Shigella flexneri	IcsB	MDAMC cells	Interacts with host cholesterol to evade autophagy	The absence of IcsB has no effect on bacterial survival up to 3 h of infection	(26)
Burkholderia pseudomallei	BopA	RAW 264.7 cells, MEFs, MDAMC cells	Interacts with host cholesterol to evade autophagy	Not applicable	(26, 27)
Manipulating autophagy via unknown mechanisms					
Vibrio alginolyticus	Unknown	Several mammalian cell lines	Activates autophagy via unknown mechanisms	Not applicable	(28)

(Continued)

TABLE 1 | Continued

Bacteria	Effectors	Host model	Description	Bacterial survival	References
Pseudomonas aeruginosa	Unknown	AEC line (A549 cells)	Unknown	Not applicable	(29)
Yersinia enterocolitica	Unknown	Murine J774A.1 macrophages	Suppresses autophagy via unknown mechanisms	Not applicable	(30)
Escaping LC3-associated phagocytosis					
Shigella flexneri	IcsB	HeLa cells, 293T cells and MEFs	Recruits the host protein Toca-1 to repress LC3 recruitment around these intracellular bacteria	The absence of IcsB has no effect on bacterial survival up to 3 h of infection	(11)
Burkholderia pseudomallei	BopA	RAW264.7 cells	Represses LC3 and LAMP1 recruitment via an unknown mechanism	*bopA* mutant bacteria show reduced intracellular survival	(7)

chains on bacterial surfaces, as well as the recruitment of Optineurin and Nemo. Therefore, *S. flexneri* profoundly cripples LUBAC-dependent cellular defense mechanisms–xenophagy.

Subversion of Autophagic Components for Bacterial Survival

T3SS effectors interact with autophagic components to interrupt autophagy. *Vibrio parahaemolyticus* VopQ is an effector that affects lysosomes. VopQ forms a gated ion channel in lysosomes to cause deacidification, thus disturbing autophagic flux. Moreover, VopQ binds directly to the V-ATPase V_o domain of lysosomes to block autophagosome-lysosome fusion (21–23).

It has been reported that *Salmonella* requires the RAB1 (the ras superfamily G-proteins-1)-mediated autophagy pathway for its survival (33). *Salmonella* Typhimurium SopB regulate this process to increases the interaction of *Salmonella* with autophagosomes for replication in HeLa cells. One possible reason for this finding is that SopB ubiquitination promotes the association of *Salmonella* and autophagosomes (24). Nevertheless, the detailed mechanism is still unclear.

Escape From LC3-Associated Phagocytosis

LAP is not a member of the autophagy pathway. However, the autophagy marker LC3 protein participates in this process, which makes it hard to be ignored. We should distinguish autophagy from LAP in research work. For instance, effector IcsB, which may manipulate Toca-1 to inhibit LAP (11). The T3SS effector BopA also plays a role in preventing bacterial killing via LAP. Because the BopA mutants showed higher levels of colocalization with LC3 and the lysosomal marker LAMP1, suggesting enhanced elimination through LAP (7).

MANIPULATING AUTOPHAGY VIA BACTERIAL EFFECTORS FROM OTHER SECRETION SYSTEMS

The effectors from other secretion systems of Gram-negative bacteria possess approaches for manipulating autophagy, as summarized in **Table 2** and discussed in the following text (papers within 6 years).

Interference With Signaling or ATG Proteins Involved in Autophagy

RavZ, is delivered by T4SS from *Legionella pneumophila*. RavZ can inhibit autophagy in HEK293 cells infected with *L. pneumophila* (34, 35). This protein uses its LIR motifs to bind to the LC3 protein and then extract LC3-PE (LC3- phosphatidylethanolamine) from the membrane of autophagosomes (35). RavZ hydrolyzes the amide bonds between glycine residues and aromatic residues at the carboxyl-terminal of the LC3 protein, using a catalytic mechanism similar to that of the Atg4. Thus, modified LC3 cannot be reconjugated by Atg7 and Atg3 in the process of autophagosome formation.

The protein VgrG2 from VpT6SS2 (T6SS-2 of *Vibrio parahaemolyticus*) induces autophagy by targeting the initial events of autophagic signaling (37). VgrG2 is a translocon of VpT6SS2. Heterogenous expression of VgrG2 increases LC3-II lipidation in macrophage cells and increases the accumulation of LC3-II in RAW264.7 cells treated with chloroquine (an inhibitor of autophagosome-lysosome fusion). Furthermore, VgrG2 mutants decrease the level of intracellular cAMP, which is necessary for the activation of the PRKA-AMPK-SIRT1 signaling pathway to induce autophagy in HUVECs treated with resveratrol (47). This finding suggests the possible role of targeting cAMP signaling in the VgrG2-mediated induction of autophagic responses (37).

A recent report has shown that *Ehrlichia chaffeensis* acquires nutrients from host cells by inducing RAB5-regulated autophagy via its T4SS-delivered effector Etf-1(6). Etf-1 interacts with RAB5, Beclin-1, VPS34, and autophagy-initiating PtdIns3K and is targeted to ehrlichial inclusions; through these mechanisms, Etf-1 induces autophagy to deliver host cytosolic nutrients for its replication while avoiding autophagic clearance (6).

Prevention of Recognition by Autophagy Mechanisms

Bartonella quintana T4SS effector BepE was identified to induce selective autophagy. The researchers found that ectopic expression of BepE specifically induced punctate structures that colocalized with LC3-II in host cells. Further study showed that host cells utilize selective autophagy to confine and degrade BepE via poly-ubiquitin chain of K63 linkage conjugation (38).

TABLE 2 | Strategies used by the effectors from T4SS, T6SS, and T7SS to manipulate autophagy.

Bacteria	Effectors	Host model	Description	Bacterial survival	References
Interfering with signaling or proteins involved in autophagy					
Legionella pneumophila	RavZ (T4SS)	HEK293 cells and MCF-7 cells	Cleaving LC3 off the membrane and modifying LC3 by its de-conjugating enzyme activity	Not applicable	(34, 35)
Anaplasma phagocytophilum	Ats-1 (T4SS)	THP-1 cells, RF/6A cells and *Beclin-1*$^{+/-}$ mice	Binds host Beclin-1 protein and hijacks Beclin-1-Atg14L autophagy initiation	Not applicable	(36)
Vibrio parahaemolyticus	VgrG2 (T6SS)	RAW264.7 cells	Possibly reduces the level of intracellular cAMP	Not applicable	(37)
Ehrlichia chaffeensis	Etf-1 (T4SS)	THP-1 cells, HEK293 cells and DH82 cells	Targets host RAB5, Beclin-1, VPS34, and autophagy - initiating PtdIns3K to ehrlichial inclusions to induce autophagy	*Ehrlichia chaffeensis* proliferation requires class III PtdIns3K activation and BECN1, and is enhanced by induction of autophagy with rapamycin	(6)
Preventing recognition by autophagy mechanisms					
Bartonella quintana	BepE (T4SS)	HeLa cells, HEK293 cells and HUVECs	Induces selective autophagy by conjugation with K63 poly-ubiquitin chain	Not applicable (But cells with BepE-induced autophagy are about 3-fold more effective at engulfing *Bartonella quintana* than cells with BepE-induced filopodia and membrane ruffles)	(38)
Subverting autophagic components for bacterial survival					
Legionella pneumophila	DrrA, LidA, RalF and LepB (T4SS)	Primary mouse macrophages	Interacts with RAB proteins to manipulate autophagosomal maturation	Not applicable	(39)
Coxiella burnetii	Cig2 (T4SS)	HeLa cells	Promotes the fusion of *Coxiella*-containing vacuoles with autophagosomes to maintain this vacuole in an autolysosomal stage of maturation	*Coxiella burnetii* is highly resistant to environmental stresses and is able to replicate in acidified lysosome-derived vacuoles	(40)
Mycobacterium tuberculosis (Note: this strain is not suitable for using Gram stain)	ESAT-6 (T7SS)	Human primary DCs	Impairs autophagosome-lysosome fusion	Not applicable	(41)
Mediating autophagy by subverting host cell homeostasis					
Legionella pneumophila	*Lp*Spl (T4SS)	HEK-293T cells and THP-1 macrophages	Inhibits autophagy by disrupting host sphingolipid biosynthesis	Not applicable	(42)
Pseudomonas aeruginosa	TplE (T6SS)	HeLa cells and HEK293T cells	Activates autophagy responses by subverting ER homeostasis	In intra- and inter-species competition studies show that the loss of *tplE* gave rise to a growth advantage of the recipient strain	(43)
Manipulating autophagy via unknown mechanisms					
Brucella	VceA (T4SS)	HPT-8 cells	Suppresses autophagy via unknown mechanisms	Not applicable	(44)
Escaping LC3-associated phagocytosis					
Legionella species	RavZ (T4SS)	HEK293 cells and MCF-7 cells	Cleaving LC3 off the membrane and modifying LC3 by its de-conjugating enzyme activity	Not applicable	(34, 45)
Legionella pneumophila	*Lp*Spl (T4SS)		May be responsible for inhibiting LAP	Not applicable	(42, 46)

Subversion of Autophagic Components for Bacterial Survival

The *Coxiella burnetii* protein Cig2 is a T4SS effector that hijacks host autophagosomes. *Coxiella burnetii* is highly resistant to environmental stresses and is able to replicate in acidified lysosome-derived vacuoles. *Coxiella*-containing vacuoles (CCVs) are highly fusogenic with each other and with other organelles of the endocytic pathway; therefore, good-sized vacuole formation is promoted (48). The effector Cig2 can promote the fusion of CCVs with autophagosomes to maintain these vacuoles in

an autolysosomal stage of maturation, thus promoting CCV homotypic fusion and influencing host infection tolerance in a moth model (40).

Mediating Autophagy by Subverting Host Cell Homeostasis

A T4SS effector and a T6SS effector have been confirmed to affect autophagy by regulating other biological processes. The protein *Lp*Spl is translocated by the T4SS of *L. pneumophila*. *Lp*Spl has a high degree of similarity to eukaryotic sphingosine-1 phosphate lyase. Interestingly, cells infected with *Lp*Spl mutants have significantly greater LC3 recruitment than WT-infected cells, suggesting that *Lp*Spl is responsible for suppressing autophagy during infection. Together, these data indicate that *Lp*Spl inhibits autophagy by disrupting host sphingolipid biosynthesis. However, the complete mechanism has not been elucidated (42).

T6SS effector TplE from *Pseudomonas aeruginosa* is a Tle4 phospholipase family protein that possesses inter-bacterial killing capacity (49). Noteworthy, TplE targets and disrupts the host ER (endoplasmic reticulum) via its eukaryotic PGAP1-like domain. ER homeostasis perturbation can lead to the activation of the unfolded protein response, which acts as a potent trigger of autophagy (50). Therefore, TplE activates autophagy responses by subverting ER homeostasis (43).

Manipulating Autophagy via Unknown Mechanisms

Effector VceA from *Brucella* T4SS is involved in host autophagic responses (44). As The Atg5, LC3-II, and Bcl-2 mRNA expression were significantly increased in the VceA mutant than the WT group. However, this study lacks the sufficient determining of autophagy process and the mechanism is still unclear.

Escape From LC3-Associated Phagocytosis

T4SS of *Legionella* species has been reported to play a role in suppressing LAP (46). The T4SS effector RavZ from *L. pneumophila* strains can inhibit LAP via its capability to irreversibly deconjugate LC3, which has been previously described (34, 45). However, this LAP escape is not due solely to the effector RavZ in *L. pneumophila*; an additional strategy is likely utilized (46). One possible reason for this proposal is that the T4SS effector *Lp*Spl may be used to inhibit LAP. Sphingosine-1 phosphate lyase (*Lp*Spl)can decrease LC3 recruitment around *L. pneumophila* strains in macrophage cells (42).

CONCLUSION, LIMITS, AND FUTURE DIRECTION

From host side, the innate immunity and mucosal barriers play critical roles to maintain the autophagic responses (51, 52). From the bacterial side, effectors manipulate autophagy at different stages by using various strategies, including interfering with autophagy-initiating signaling, preventing the recognition of autophagy-involved proteins, subverting autophagy component homeostasis, manipulating the autophagy process (e.g., autophagosome maturation and autophagosome-lysosome fusion) and impacting other biological processes to affect autophagy. The research on effectors and autophagy has started to reveal basic features of autophagy manipulated by bacterial proteins for the benefit of bacterial survival and replication.

The progress in some field have shown better understanding of consequent host responses when autophagy is disturbed, such as killing host cells [SipB (25) and T3SS of *Vibrio alginolyticus* (28)], influencing host infection tolerance [Cig2 (40)], and escaping DC-mediated immune responses [ESAT-6 (41)]. Remarkably, bacteria could use multiple effectors (*Salmonella* and *Legionella*), and even two secretion systems (*Vibrio parahaemolyticus*), to mediate autophagy. Meanwhile, some effectors are versatile in manipulating autophagy (IcsB). Moreover, in the study of the effector *Lp*Spl, the author found that the effector RavZ is not present in all strains of *L. pneumophila*, suggesting that this strain employs other effector, namely *Lp*Spl (42), to inhibit autophagy. Therefore, determining whether one effector (even the partial function of one effector) is required for altering autophagic responses will help us to find novel effectors and better understanding of host-bacterial interactions.

The commonly used methods for exploring the effectors that are responsible for manipulating autophagy are: (a) deleting entire secretion systems or single genes and then analyzing the changes in autophagic responses in host cells infected with WT/mutant strains; (b) similarity searches to seek effectors that exhibit similar structures to host proteins, such as RavZ (35) and *Lp*Spl (42); and (c) investigating effectors that can interact with autophagy-involved proteins and then exploring the underlying mechanisms, such as Ats-1 (36) and Etf-1 (6). Most of these studies were done *in vitro* and still lack *in vivo* models to verify the physiological relevance of the studies. We would like to advocate the organoid system to study the host-microbial interactions (53). *In vivo*, acute and chronic infectious models will help us to understand into the short-term and long-term effects of bacterial survival and suppressed autophagy. When studying the interaction between a target and autophagy, one single autophagy marker is not sufficient for determining changes in autophagic responses. Determining multiple related proteins in autophagy, having morphological observations, and monitoring autophagic flux will support more information for judgment and help us to differentiate autophagy from other biological process, like LAP (54).

Noteworthy, the studies on effectors-autophagy interactions in host cells is not only to determine the effectors, that can affect the host autophagic responses, and the underlying molecular mechanism. Some excellent researches are progressing in the direction for understanding autophagy and its regulators. Like the study of effector VopQ, VopQ can bind directly to the V-ATPase V_o domain, which appears to play a key role in the regulation of autophagy through amino acid sensing, and even more directly, autophagosome-lysosome membrane fusion. Though the details is unclear, this study enlighten us to further elucidate the role of V-ATPase in autophagosome fusion with the lysosome (21, 23). Additionally, Xu et al. recently found *Salmonella* effector SopF is a xenophagy-specific inhibitor. By determining the target of *sopF*, they were able to identify the

V-ATPase-ATG16L1 axis that mediates xenophagy initiation. Namely, upon infection, internalized bacteria cause damage to the residing vacuole, which is sensed by the vacuolar ATPase that then recruits ATG16L1 to initiate xenophagy. This study provides mechanistic insight into xenophagy recognition and initiation (15). It expands our knowledge to autophagic process, especially the crucial role of V-ATPase.

The causes of autophagy are numerous and complex. The mechanisms of effectors and autophagy have not been fully elucidated. Many important pathogenic Gram-negative bacteria still need to be tested. All the current studies focus on Gram-negative bacterial effectors, but Gram-positive and non-Gram stain bacterial effectors have been less attention (55). Moreover, the bacteria have abundant means/tools, not limited to effectors, to manipulate host autophagy. Most of these studies were focusing on uncovering the methods used by bacteria to inhibit autophagy, while ignoring the compensation of host cellular defense system. More studies are needed to understand the host cellular defense system in fighting back bacterial infection.

The physiological role of autophagy and its signaling mechanisms remain poorly understood. The study of interactions of bacterial effectors via pattern recognition receptors modulate the autophagy maybe uncover the underlying mechanisms. Overall, future directions could be focused on the following aspects in effectors-autophagy interactions to: (a) use various methods to determine multiple related proteins in autophagy, including morphological observations and monitoring autophagic flux to support accurate information about autophagic responses. Please refer to a comprehensive review of this subject (54); (b) understand the relationship between autophagy and immunological responses, which will uncover the link between autophagy and life activity. Most researchers pay attention to the effect of effectors to autophagic responses and the underlying cellular and molecular mechanism, but less attention to the immunological consequences of these affects; (c) study diverse immune and inflammatory signals modulate autophagy in host cell through pattern recognition receptors, such as toll-like receptors and nucleotide-binding oligomerization domain (NOD)-like receptors (56–59).

Studies on effectors-autophagy interactions in host cells will provide new insights into the pathogenic mechanisms of infections and inflammation. A better understanding of the mechanisms used by bacterial effectors to manipulate autophagy will help the study of mechanisms in immunity, drug design, and novel therapeutic approaches for infectious diseases and chronic inflammation.

AUTHOR CONTRIBUTIONS

JS designed the theme and topic and obtained research funds. YJ drafted the manuscript and organized the figure and tables. YJ and JS finalized the manuscript.

FUNDING

We would like to acknowledge the UIC Cancer Center, the NIDDK/National Institutes of Health grant R01 DK105118, and R01DK114126 to JS. The study sponsors play no role in the study design, data collection, analysis, and interpretation of data.

REFERENCES

1. Nakatogawa H, Suzuki K, Kamada Y, Ohsumi Y. Dynamics and diversity in autophagy mechanisms: lessons from yeast. *Nat Rev Mol Cell Biol.* (2009) 10:458–67. doi: 10.1038/nrm2708
2. Mizushima N. Autophagy: process and function. *Gene Dev.* (2007) 21:2861–73. doi: 10.1101/gad.1599207
3. Klionsky DJ, Cuervo AM, Dunn WA Jr, Levine B, van der Klei I, Seglen PO. How shall I eat thee? *Autophagy.* (2007) 3:413–6. doi: 10.4161/auto.4377
4. Desvaux M, Hebraud M, Talon R, Henderson IR. Secretion and subcellular localizations of bacterial proteins: a semantic awareness issue. *Trends Microbiol.* (2009) 17:139–45. doi: 10.1016/j.tim.2009.01.004
5. Hood RD, Singh P, Hsu F, Guvener T, Carl MA, Trinidad RR, et al. A type VI secretion system of *Pseudomonas aeruginosa* targets a toxin to bacteria. *Cell Host Microbe.* (2010) 7:25–37. doi: 10.1016/j.chom.2009.12.007
6. Lin M, Liu H, Xiong Q, Niu H, Cheng Z, Yamamoto A, et al. *Ehrlichia* secretes Etf-1 to induce autophagy and capture nutrients for its growth through RAB5 and class III phosphatidylinositol 3-kinase. *Autophagy.* (2016) 12:2145–66. doi: 10.1080/15548627.2016.1217369
7. Gong L, Cullinane M, Treerat P, Ramm G, Prescott M, Adler B, et al. The *Burkholderia pseudomallei* type III secretion system and BopA are required for evasion of LC3-associated phagocytosis. *PLoS ONE.* (2011) 6:e17852. doi: 10.1371/journal.pone.0017852
8. Flannagan RS, Cosio G, Grinstein S. Antimicrobial mechanisms of phagocytes and bacterial evasion strategies. *Nat Rev Microbiol.* (2009) 7:355–66. doi: 10.1038/nrmicro2128
9. Huang J, Brumell JH. Bacteria-autophagy interplay: a battle for survival. *Nat Rev Microbiol.* (2014) 12:101–14. doi: 10.1038/nrmicro3160
10. Siqueira MDS, Ribeiro RM, Travassos LH. Autophagy and its interaction with intracellular bacterial pathogens. *Front Immunol.* (2018) 9:935. doi: 10.3389/fimmu.2018.00935
11. Baxt LA, Goldberg MB. Host and bacterial proteins that repress recruitment of LC3 to *Shigella* early during infection. *PLoS ONE.* (2014) 9:e94653. doi: 10.1371/journal.pone.0094653
12. Owen KA, Meyer CB, Bouton AH, Casanova JE. Activation of focal adhesion kinase by *Salmonella* suppresses autophagy via an Akt/mTOR signaling pathway and promotes bacterial survival in macrophages. *PLoS Pathog.* (2014) 10:e1004159. doi: 10.1371/journal.ppat.1004159
13. Popa C, Li L, Gil S, Tatjer L, Hashii K, Tabuchi M, et al. The effector AWR5 from the plant pathogen *Ralstonia solanacearum* is an inhibitor of the TOR signalling pathway. *Sci Rep.* (2016) 6:27058. doi: 10.1038/srep 27058
14. Feng ZZ, Jiang AJ, Mao AW, Feng Y, Wang W, Li J, et al. The *Salmonella* effectors SseF and SseG inhibit Rab1A-mediated autophagy to facilitate intracellular bacterial survival and replication. *J Biol Chem.* (2018) 293:9662–73. doi: 10.1074/jbc.M117.811737
15. Xu Y, Zhou P, Cheng S, Lu Q, Nowak K, Hopp AK, et al. A Bacterial effector reveals the V-ATPase-ATG16L1 axis that initiates xenophagy. *Cell.* (2019) 178:552–66.e20. doi: 10.1016/j.cell.2019.06.007
16. Jiao Y, Lin Z, Zhang Y-G, Lu R, Mei S, Pan Z, et al. *Salmonella* Enteritidis effector protein AvrA inhibits Beclin-1-dependent autophagy. *Gastroenterology.* (2017) 152:S200. doi: 10.1016/S0016-5085(17)30974-5
17. D'Cruze T, Gong L, Treerat P, Ramm G, Boyce JD, Prescott M, et al. Role for the *Burkholderia pseudomallei* type three secretion system cluster 1 *bpscN* gene in virulence. *Infect Immun.* (2011) 79:3659–64. doi: 10.1128/IAI.01351-10

18. Ogawa M, Yoshimori T, Suzuki T, Sagara H, Mizushima N, Sasakawa C. Escape of intracellular *Shigella* from autophagy. *Science.* (2005) 307:727–31. doi: 10.1126/science.1106036
19. Noad J, von der Malsburg A, Pathe C, Michel MA, Komander D, Randow F. LUBAC-synthesized linear ubiquitin chains restrict cytosol-invading bacteria by activating autophagy and NF-κB. *Nat Microbiol.* (2017) 2:17063. doi: 10.1038/nmicrobiol.2017.63
20. Mesquita FS, Thomas M, Sachse M, Santos AJ, Figueira R, Holden DW. The *Salmonella* deubiquitinase SseL inhibits selective autophagy of cytosolic aggregates. *PLoS Pathog.* (2012) 8:e1002743. doi: 10.1371/journal.ppat.1002743
21. Sreelatha A, Bennett TL, Zheng H, Jiang QX, Orth K, Starai VJ. *Vibrio* effector protein, VopQ, forms a lysosomal gated channel that disrupts host ion homeostasis and autophagic flux. *Proc Natl Acad Sci USA.* (2013) 110:11559–64. doi: 10.1073/pnas.1307032110
22. Burdette DL, Seemann J, Orth K. *Vibrio* VopQ induces PI3-kinase-independent autophagy and antagonizes phagocytosis. *Mol Microbiol.* (2009) 73:639–49. doi: 10.1111/j.1365-2958.2009.06798.x
23. Sreelatha A, Orth K, Starai VJ. The pore-forming bacterial effector, VopQ, halts autophagic turnover. *Autophagy.* (2013) 9:2169–70. doi: 10.4161/auto.26449
24. Yu HB, Croxen MA, Marchiando AM, Ferreira RB, Cadwell K, Foster LJ, et al. Autophagy facilitates *Salmonella* replication in HeLa cells. *MBio.* (2014) 5:e00865–14. doi: 10.1128/mBio.00865-14
25. Hernandez LD, Pypaert M, Flavell RA, Galan JE. A *Salmonella* protein causes macrophage cell death by inducing autophagy. *J Cell Biol.* (2003) 163:1123–31. doi: 10.1083/jcb.200309161
26. Kayath CA, Hussey S, El hajjami N, Nagra K, Philpott D, Allaoui A. Escape of intracellular *Shigella* from autophagy requires binding to cholesterol through the type III effector, IcsB. *Microbes Infect.* (2010) 12:956–66. doi: 10.1016/j.micinf.2010.06.006
27. Cullinane M, Gong L, Li X, Lazar-Adler N, Tra T, Wolvetang E, et al. Stimulation of autophagy suppresses the intracellular survival of *Burkholderia pseudomallei* in mammalian cell lines. *Autophagy.* (2008) 4:744–53. doi: 10.4161/auto.6246
28. Zhao Z, Zhang L, Ren C, Zhao J, Chen C, Jiang X, et al. Autophagy is induced by the type III secretion system of *Vibrio alginolyticus* in several mammalian cell lines. *Arch Microbiol.* (2011) 193:53–61. doi: 10.1007/s00203-010-0646-9
29. De La Rosa I, Eissa NT, Xu Y. Negative regulation of autophagy by *Pseudomonas aeruginosa* type 3 secretion system in airway epithelial cells. *Am J Respir Crit Care Med.* (2013) 187:A4554. Available online at: https://www.atsjournals.org/doi/abs/10.1164/ajrccm-conference.2013.187.1_MeetingAbstracts.A4554
30. Deuretzbacher A, Czymmeck N, Reimer R, Trulzsch K, Gaus K, Hohenberg H, et al. β1 integrin-dependent engulfment of *Yersinia enterocolitica* by macrophages is coupled to the activation of autophagy and suppressed by type III protein secretion. *J Immun.* (2009) 183:5847–60. doi: 10.4049/jimmunol.0804242
31. Ye Z, Petrof EO, Boone D, Claud EC, Sun J. *Salmonella* effector AvrA regulation of colonic epithelial cell inflammation by deubiquitination. *Am J Pathol.* (2007) 171:882–92. doi: 10.2353/ajpath.2007.070220
32. Lin Z, Zhang YG, Xia Y, Xu X, Jiao X, Sun J. *Salmonella* enteritidis effector AvrA stabilizes intestinal tight junctions via the JNK pathway. *J Biol Chem.* (2016) 291:26837–49. doi: 10.1074/jbc.M116.757393
33. Huang J, Birmingham CL, Shahnazari S, Shiu J, Zheng YT, Smith AC, et al. Antibacterial autophagy occurs at PI(3)P-enriched domains of the endoplasmic reticulum and requires Rab1 GTPase. *Autophagy.* (2011) 7:17–26. doi: 10.4161/auto.7.1.13840
34. Choy A, Dancourt J, Mugo B, O'Connor TJ, Isberg RR, Melia TJ, et al. The *Legionell*a effector RavZ inhibits host autophagy through irreversible Atg8 deconjugation. *Science.* (2012) 338:1072–6. doi: 10.1126/science.1227026
35. Yang A, Pantoom S, Wu YW. Elucidation of the anti-autophagy mechanism of the *Legionella* effector RavZ using semisynthetic LC3 proteins. *Elife.* (2017) 6:e23905. doi: 10.7554/eLife.23905
36. Niu H, Xiong Q, Yamamoto A, Hayashi-Nishino M, Rikihisa Y. Autophagosomes induced by a bacterial Beclin-1 binding protein facilitate obligatory intracellular infection. *Proc Natl Acad Sci USA.* (2012) 109:20800–7. doi: 10.1073/pnas.1218674109
37. Yu Y, Fang L, Zhang Y, Sheng H, Fang W. VgrG2 of type VI secretion system 2 of *Vibrio parahaemolyticus* induces autophagy in macrophages. *Front Microbiol.* (2015) 6:168. doi: 10.3389/fmicb.2015.00168
38. Wang C, Fu J, Wang M, Cai Y, Hua X, Du Y, et al. *Bartonella quintana* type IV secretion effector BepE-induced selective autophagy by conjugation with K63 polyubiquitin chain. *Cell Microbiol.* (2019) 21:e12984. doi: 10.1111/cmi.12984
39. Joshi AD, Swanson MS. Secrets of a successful pathogen: *Legionella* resistance to progression along the autophagic pathway. *Front Microbiol.* (2011) 2:138. doi: 10.3389/fmicb.2011.00138
40. Kohler LJ, Reed Sh C, Sarraf SA, Arteaga DD, Newton HJ, Roy CR. Effector protein Cig2 decreases host tolerance of infection by directing constitutive fusion of autophagosomes with the *Coxiella*-containing vacuole. *MBio.* (2016) 7:e01127–16. doi: 10.1128/mBio.01127-16
41. Romagnoli A, Etna MP, Giacomini E, Pardini M, Remoli ME, Corazzari M, et al. ESX-1 dependent impairment of autophagic flux by *Mycobacterium tuberculosis* in human dendritic cells. *Autophagy.* (2012) 8:1357–70. doi: 10.4161/auto.20881
42. Rolando M, Escoll P, Nora T, Botti J, Boitez V, Bedia C, et al. *Legionella pneumophila* S1P-lyase targets host sphingolipid metabolism and restrains autophagy. *Proc Natl Acad Sci USA.* (2016) 113:1901–6. doi: 10.1073/pnas.1522067113
43. Jiang F, Wang X, Wang B, Chen L, Zhao Z, Waterfield NR, et al. The *Pseudomonas aeruginosa* type VI secretion PGAP1-like effector induces host autophagy by activating endoplasmic reticulum stress. *Cell Rep.* (2016) 16:1502–9. doi: 10.1016/j.celrep.2016.07.012
44. Zhang J, Li M, Li Z, Shi J, Zhang Y, Deng X, et al. Deletion of the type IV secretion system effector VceA promotes autophagy and inhibits apoptosis in *Brucella*-infected human trophoblast cells. *Curr Microbiol.* (2019) 76:510–9. doi: 10.1007/s00284-019-01651-6
45. Martinez J, Malireddi RK, Lu Q, Cunha LD, Pelletier S, Gingras S, et al. Molecular characterization of LC3-associated phagocytosis reveals distinct roles for Rubicon, NOX2 and autophagy proteins. *Nat Cell Biol.* (2015) 17:893–906. doi: 10.1038/ncb3192
46. Hubber A, Kubori T, Coban C, Matsuzawa T, Ogawa M, Kawabata T, et al. Bacterial secretion system skews the fate of *Legionella*-containing vacuoles towards LC3-associated phagocytosis. *Sci Rep.* (2017) 7:44795. doi: 10.1038/srep44795
47. Chen ML, Yi L, Jin X, Liang XY, Zhou Y, Zhang T, et al. Resveratrol attenuates vascular endothelial inflammation by inducing autophagy through the cAMP signaling pathway. *Autophagy.* (2013) 9:2033–45. doi: 10.4161/auto.26336
48. Howe D, Melnicakova J, Barak I, Heinzen RA. Fusogenicity of the *Coxiella burnetii* parasitophorous vacuole. *Ann NY Acad Sci.* (2003) 990:556–62. doi: 10.1111/j.1749-6632.2003.tb07426.x
49. Russell AB, LeRoux M, Hathazi K, Agnello DM, Ishikawa T, Wiggins PA, et al. Diverse type VI secretion phospholipases are functionally plastic antibacterial effectors. *Nature.* (2013) 496:508–12. doi: 10.1038/nature12074
50. Yorimitsu T, Nair U, Yang Z, Klionsky DJ. Endoplasmic reticulum stress triggers autophagy. *J Biol Chem.* (2006) 281:30299–304. doi: 10.1074/jbc.M607007200
51. Wu S, Zhang YG, Lu R, Xia Y, Zhou D, Petrof EO, et al. Intestinal epithelial vitamin D receptor deletion leads to defective autophagy in colitis. *Gut.* (2015) 64:1082–94. doi: 10.1136/gutjnl-2014-307436
52. Sun J. VDR/vitamin D receptor regulates autophagic activity through ATG16L1. *Autophagy.* (2016) 12:1057–8. doi: 10.1080/15548627.2015.1072670
53. Zhang YG, Zhu X, Lu R, Messer JS, Xia Y, Chang EB, et al. Intestinal epithelial HMGB1 inhibits bacterial infection via STAT3 regulation of autophagy. *Autophagy.* (2019) 15:1935–53. doi: 10.1080/15548627.2019.1596485
54. Klionsky DJ, Abdelmohsen K, Abe A, Abedin MJ, Abeliovich H, Acevedo Arozena A, et al. Guidelines for the use and interpretation of assays for monitoring autophagy (3rd edition). *Autophagy.* (2016) 12:1–222. doi: 10.1080/15548627.2015.1100356
55. Simeone R, Bottai D, Brosch R. ESX/type VII secretion systems and their role in host-pathogen interaction. *Curr Opin Microbiol.* (2009) 12:4–10. doi: 10.1016/j.mib.2008.11.003
56. Takahama M, Akira S, Saitoh T. Autophagy limits activation of the inflammasomes. *Immunol Rev.* (2018) 281:62–73. doi: 10.1111/imr.12613

57. Lee JW, Nam H, Kim LE, Jeon Y, Min H, Ha S, et al. TLR4 (toll-like receptor 4) activation suppresses autophagy through inhibition of FOXO3 and impairs phagocytic capacity of microglia. *Autophagy.* (2019) 15:753–70. doi: 10.1080/15548627.2018.1556946
58. Li J, Li B, Cheng Y, Meng Q, Wei L, Li W, et al. The synergistic effect of NOD2 and TLR4 on the activation of autophagy in human submandibular gland inflammation. *J Oral Pathol Med.* (2019) 48:87–95. doi: 10.1111/jop.12793
59. Li C, Ma L, Liu Y, Li Z, Wang Q, Chen Z, et al. TLR2 promotes development and progression of human glioma via enhancing autophagy. *Gene.* (2019) 700:52–9. doi: 10.1016/j.gene.2019.02.084

Conflict of Interest: The authors declare that the research was conducted in the absence of any commercial or financial relationships that could be construed as a potential conflict of interest.

frontiers in Immunology

ORIGINAL RESEARCH
published: 14 February 2020
doi: 10.3389/fimmu.2020.00209

Group 2 Innate Lymphoid Cells (ILC2) Suppress Beneficial Type 1 Immune Responses During Pulmonary Cryptococcosis

*Markus Kindermann[1], Lisa Knipfer[1], Stephanie Obermeyer[2], Uwe Müller[3], Gottfried Alber[3], Christian Bogdan[2,4], Ulrike Schleicher[2,4], Markus F. Neurath[1,4] and Stefan Wirtz[1,4]**

[1] Medizinische Klinik 1, Universitätsklinikum Erlangen, Friedrich-Alexander-Universität Erlangen-Nürnberg, Erlangen, Germany, [2] Mikrobiologisches Institut - Klinische Mikrobiologie, Immunologie und Hygiene, Friedrich-Alexander-Universität Erlangen-Nürnberg, Erlangen, Germany, [3] Centre for Biotechnology and Biomedicine, Institute of Immunology, College of Veterinary Medicine, University of Leipzig, Leipzig, Germany, [4] Medical Immunology Campus Erlangen, FAU Erlangen-Nürnberg, Erlangen, Germany

OPEN ACCESS

Edited by:
Maria Leite-de-Moraes, INSERM U1151 Institut Necker Enfants Malades Centre de Médecine Moléculaire (INEM), France

Reviewed by:
Karen L. Wozniak, Oklahoma State University, United States
Hans Yssel, Institut National de la Santé et de la Recherche Médicale (INSERM), France

***Correspondence:**
Stefan Wirtz
stefan.wirtz@uk-erlangen.de

Specialty section:
This article was submitted to Mucosal Immunity, a section of the journal Frontiers in Immunology

Received: 27 September 2019
Accepted: 27 January 2020
Published: 14 February 2020

Citation:
Kindermann M, Knipfer L, Obermeyer S, Müller U, Alber G, Bogdan C, Schleicher U, Neurath MF and Wirtz S (2020) Group 2 Innate Lymphoid Cells (ILC2) Suppress Beneficial Type 1 Immune Responses During Pulmonary Cryptococcosis. Front. Immunol. 11:209. doi: 10.3389/fimmu.2020.00209

Cryptococcus neoformans is an opportunistic fungal pathogen preferentially causing disease in immunocompromised individuals such as organ-transplant-recipients, patients receiving immunosuppressive medications or, in particular, individuals suffering from HIV infection. Numerous studies clearly indicated that the control of *C. neoformans* infections is strongly dependent on a prototypic type 1 immune response and classical macrophage activation, whereas type 2-biased immunity and alternative activation of macrophages has been rather implicated in disease progression and detrimental outcomes. However, little is known about regulatory pathways modulating and balancing immune responses during early phases of pulmonary cryptococcosis. Here, we analyzed the role of group 2 innate lymphoid cells (ILC2s) for the control of *C. neoformans* infection. Using an intranasal infection model with a highly virulent *C. neoformans* strain, we found that ILC2 numbers were strongly increased in *C. neoformans*-infected lungs along with induction of a type 2 response. Mice lacking ILC2s due to conditional deficiency of the transcription factor RAR-related orphan receptor alpha (Rora) displayed a massive downregulation of features of type 2 immunity as reflected by reduced levels of the type 2 signature cytokines IL-4, IL-5, and IL-13 at 14 days post-infection. Moreover, ILC2 deficiency was accompanied with increased type 1 immunity and classical macrophage activation, while the pulmonary numbers of eosinophils and alternatively activated macrophages were reduced in these mice. Importantly, this shift in pulmonary macrophage polarization in ILC2-deficient mice correlated with improved fungal control and prolonged survival of infected mice. Conversely, adoptive transfer of ILC2s was associated with a type 2 bias associated with less efficient anti-fungal immunity in lungs of recipient mice. Collectively, our date indicate a non-redundant role of ILC2 in orchestrating myeloid anti-cryptococcal immune responses toward a disease exacerbating phenotype.

Keywords: ILC2, fungi (Candida, *Cryptococcus*), innate immunity, lung infection, type 2 immune response

INTRODUCTION

Cryptococcus (*C.*) *neoformans* is an opportunistic fungal pathogen that causes disease predominantly in immunocompromised individuals, such as organ-transplant-recipients, patients receiving immunosuppressive medications or, in particular, individuals suffering from HIV infection [reviewed in (1, 2)]. In these patients inhalation of the fungus, either in form of desiccated yeast cells or as spores, typically leads to a pneumonia-like illness. As a consequence of an exacerbating disease progression, the fungi have the propensity to pass the blood-brain-barrier causing life threatening cryptococcal meningitis [reviewed in (3)]. While *C. neoformans* exposure most likely occurs ubiquitously already during childhood, the vast majority of immunocompetent individuals completely clear the infection or control the pathogen asymptomatically in encapsulated cryptococcomas (4). Despite increasing incidence in immunocompetent patients (5, 6), the highest infection rates and disease manifestations are found in immunocompromised patients suffering from AIDS. Noteworthy, for the year 2014 more than 200,000 cases of cryptococcal meningitis, leading to more than 180,000 deaths (7).

Although a well-balanced regulation of the immune cell network protects from fatal outcomes in pulmonary cryptococcosis, the precise immunological mechanisms that direct the development of protective or detrimental anti-cryptococcal immunity are not clearly understood. However, numerous studies in mice clearly indicated that the control and clearance of *C. neoformans* is strongly reliant on prototypic type 1 immune responses, characterized by the production of inflammatory cytokines such as Interleukin (IL)-2, Tumor necrosis factor (TNF), and particularly Interferon (IFN)-γ as well as the activation of classical macrophages [reviewed in (8)]. Conversely, type 2 biased immune responses have been implicated in disease progression and detrimental outcomes (8). At mucosal surfaces, the release of alarmins such as IL-25, IL-33, and thymic stromal lymphopoietin (TSLP) was identified as important early trigger of type 2 immunity, which is defined by production of the cytokines IL-4, IL-5, and IL-13 [reviewed in (9–11)]. As a result, eosinophils and alternatively activated macrophages (AAMs) are activated and recruited, while goblet cell hyperplasia and T helper (T_H)2 cell differentiation is induced (12). Indeed, detrimental *Cryptococcus*-induced type 2 immunity is characterized by elevated levels of the cytokines IL-4, IL-5, and IL-13, which seem to be important modulators of mucus hyperproduction, eosinophilia and AAM activation in the lungs of infected mice.

Recently, the immunomodulatory capacity of group 2 innate lymphoid cells (ILC2s) in the context of various infectious diseases became evident and ILC2s effector functions were considered as potentially important for shifting early immune responses toward a type 2 phenotype. ILC2s were shown to produce high amounts of type 2 cytokines upon activation by alarmin stimulation [reviewed in (10, 13, 14)]. It was recently demonstrated that the alarmin IL-33 is strongly induced during the development of pulmonary cryptococcosis. Because proliferation and activation of ILC2s are impaired in mice lacking the IL-33 receptor T1/ST2 (15, 16) and ILC2 effector cytokines such as IL-4, IL-5, and IL-13 exert critical effects in anti-cryptococcal immune responses (15–22), it is tempting to speculate that ILC2s may also play important roles during disease progression. However, direct effects of ILC2s during pulmonary *C. neoformans* infections still remain to be determined more precisely. Previous studies utilized IL-4R, T1/ST2, and IL17Rb/ST2 receptor knockout animals (16, 17) to address indirectly the involvement of ILC2s in the modulation of anti-cryptococcal immunity. However, in this broad approach, deficiencies of the immunological functions of AAMs, $ST2^+$/$Gata3^+$ T_H2 cells, and $ST2^+$ regulatory T cells most likely influenced the disease outcome, which essentially precluded firm conclusions on the role of ILC2s for the course of pulmonary *C. neoformans* infection.

In order to verify and substantiate the function of ILC2s during different phases of pulmonary cryptococcosis, we comprehensively studied the immune response in ILC2-deficient animals within the first 14 days of infection. Thereby, ILC2-deficient animals showed a massive downregulation of type 2 immunity, reflected by reduced levels of the type 2 signature cytokines IL-4 and IL-13. Importantly, ILC2-deficiency in mice was associated with an increase in type 1 immunity, increased pulmonary frequencies of classically activated macrophages, improved fungal control and prolonged survival. Collectively, these date corroborate a non-redundant role of ILC2 in orchestrating anti-cryptococcal immune responses toward a disease exacerbating phenotype.

RESULTS

ILC2 Deficiency Is Associated With Decreased Fungal Burden and Reduced Pulmonary Damage

Recently, the infection-dependent release of the alarmin IL-33 has been identified as one of the main initial events for establishment of a type 2 polarized immune response in murine cryptococcosis (15, 16, 23). Given the importance of extracellular IL-33 for activation of these cells, we aimed to address the role of pulmonary ILC2s in a well-established murine model of acute pulmonary cryptococcosis using the virulent *C. neoformans* serotype A strain ATCC 90112 (24). Therefore, we intranasally infected $Rora^{Cre}tdTomato^{flox}$ mice, in which ILC2s are marked by strong expression of the fluorescent reporter protein tdTomato due to their strong expression of the transcription factor *rora* (25). While only few $tdtomato^+$ cells were detectable at steady state, strongly increased numbers of labeled cells were present in lungs 2 weeks after infection as evidenced by confocal microscopy (**Figure 1A**). In line, flow cytometric analysis also demonstrated ILC2 accumulation in lungs of mice upon cryptococcal challenge (**Figure 1B**). Next, we analyzed $Tie2^{Cre}Rora^{flox}$ mice, which due to deficiency of the transcription factor *rora* in hematopoietic cells display an almost complete deletion of steady state pulmonary IL-5- and IL-13-producing ILC2s on day 14 pi (**Figures 1C,D**), but show normal development of T cell subsets including regulatory and T_H17

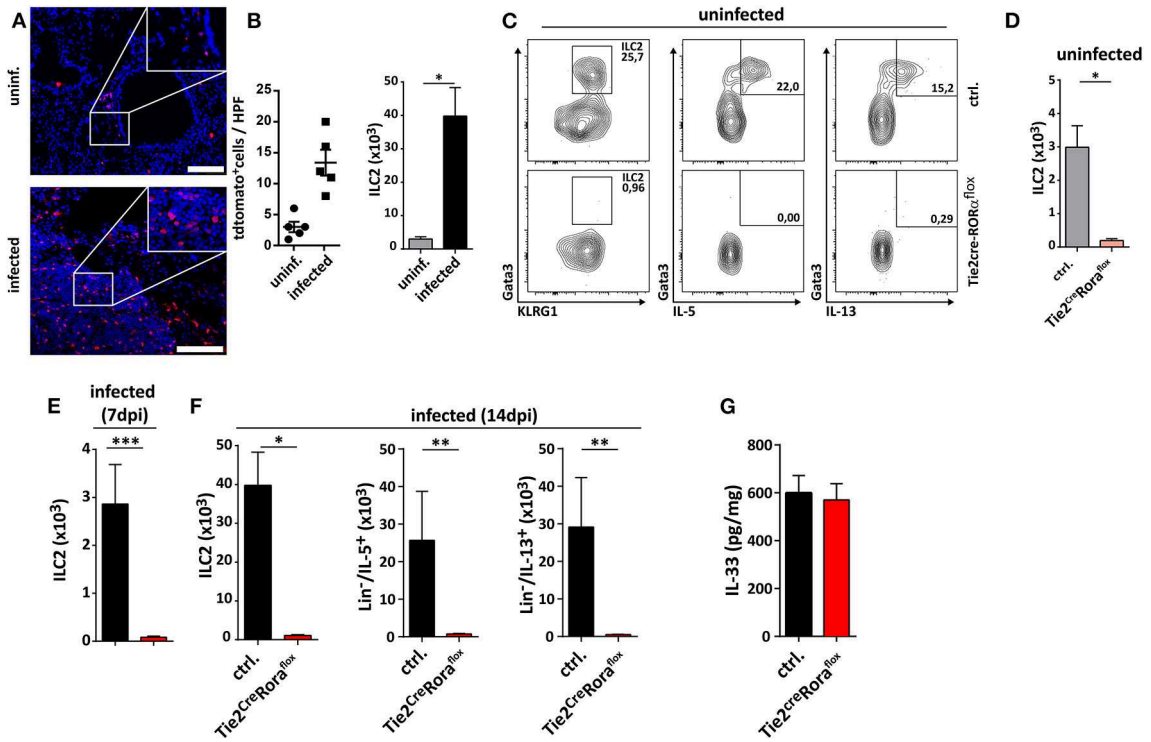

FIGURE 1 | Analysis of ILC2s in lungs of *C. neoformans* infected mice. **(A,B,E–G)** Mice were infected intranasally with 500 cfu *C. neoformans.* and analyzed 7 dpi **(E)** or **(A,B,F,G)** 14 dpi. **(A)** Representative IHC-pictures of lungs of Rora^{Cre}tdTomato^{flox} bone marrow chimeric mice and quantification of tdTomato expressing cells in naïve and *Cryptococcus*-challenged animals. **(B)** Pulmonary ILC2 counts of naïve and *C. neoformans* infected C57BL/6 mice (n = 4–5/group). **(C)** Representative flow cytometric plots of lung Lin$^-$/Thy1$^+$/Gata3$^+$/KLRG1$^+$ ILC2, Lin$^-$/Thy1$^+$/Gata3$^+$/IL-5$^+$ ILC2 and Lin$^-$/Thy1$^+$/Gata3$^+$/IL-13$^+$ ILC2 of healthy controls and Tie2^{cre}Rora^{flox} mice. **(D)** Quantification of naïve lung Lin$^-$/Thy1$^+$/ICOS$^+$/KLRG1$^+$ ILC2 in control (n = 4) and Tie2^{cre}Rora^{flox} mice (n = 4). **(E,F)** Quantification of Lin$^-$/Thy1$^+$/ICOS$^+$/KLRG1$^+$ ILC2 (n = 4), Lin$^-$/IL-5$^+$ (ctrl. n = 4, Tie2^{cre}Rora^{flox} mice n = 6), and Lin$^-$/IL-13$^+$ (ctrl. n = 4, Tie2^{cre}Rora^{flox} mice n = 6) populations in *C. neoformans*-challenged animals. **(G)** IL-33 concentration in lung tissue quantified per mg of total protein in control (n = 18) and Tie2^{cre}Rora^{flox} mice (n = 26). Data is shown as mean ± SEM for at least two independent experiments. *$P \leq 0.05$; **$P \leq 0.01$ and ***$P \leq 0.001$ using a Mann-Whitney U-test.

cells *in vitro* (**Supplemental Figures 1A,B**) (26). In contrast to control mice, cryptococcal challenge of Tie2^{cre}Rora^{flox} mice did not result in increased accumulation of pulmonary ILC2s producing IL-5 and IL-13 on day 7 and 14 pi (**Figures 1E,F**). Similar results were obtained in lethally irradiated C57BL/6 mice reconstituted with bone marrow from Tie2^{cre}Rora^{flox} mice (**Supplemental Figures 1C,D**). Notably, this outcome was not related to a differential presence of IL-33 protein (**Figure 1G**), a key cytokine responsible for directing early immunomodulatory pathways during the onset of pulmonary cryptococcosis (15).

In the next set of experiments, we analyzed whether ILC2-deficiency in Tie2^{cre}Rora^{flox} mice affected their capacity to control *C. neoformans* infection. At 7 dpi, there were no major differences in pulmonary fungal burdens between Tie2^{cre}Rora^{flox} mice and littermate controls (**Supplemental Figures 2A,B**). Strikingly, ILC2-deficient mice displayed significantly reduced cryptococcal burdens in lung tissues at 14 dpi compared to controls (**Figure 2A**). Moreover, the vast majority of the ILC2-deficient mice survived the infection for more than 40 days, while the infection-dependent lethality of control mice was substantially lower [mean survival of 33.5 days (**Figure 2B**)]. Furthermore, histologic assessment of hematoxylin/eosin (H&E) or Periodic acid-Schiff (PAS) stained lung tissue sections demonstrated that cryptococcal loads and the degree of tissue damage and mucosal inflammation was markedly reduced in the absence of ILC2s (**Figure 2C**). In line with this, magnetic resonance imaging (MRI) of whole lungs revealed a significantly higher presence of hypointense areas in infected control mice, which most likely represent local regions with concentrated fungal burden and strong immune cell infiltration (**Figures 2D,E**). Additionally, the volumes of hypointense areas relative to total lung volumes were significantly reduced in ILC2-deficient mice (**Figure 2F**). Further analyses also revealed that systemic spread and brain dissemination were tentatively lower in ILC2-deficient mice at 14 dpi as evidenced by analysis of liver and CNS fungal cultures (**Supplemental Figures 2C,D**).

To further ascertain the functional impact of ILC2 on the immune response to cryptococcal infection, we next adoptively transferred sort-purified and *in vitro* expanded ILC2s of C57BL/6 mice into *C. neoformans* infected Tie2^{cre}Rora^{flox} mice on a C57BL/6 background (27). These ILC2s are able to target the murine lung upon intravenous injection as we have recently shown in a model of type 2 mediated lung inflammation (27, 28), albeit rather high numbers of cells are required for effective long

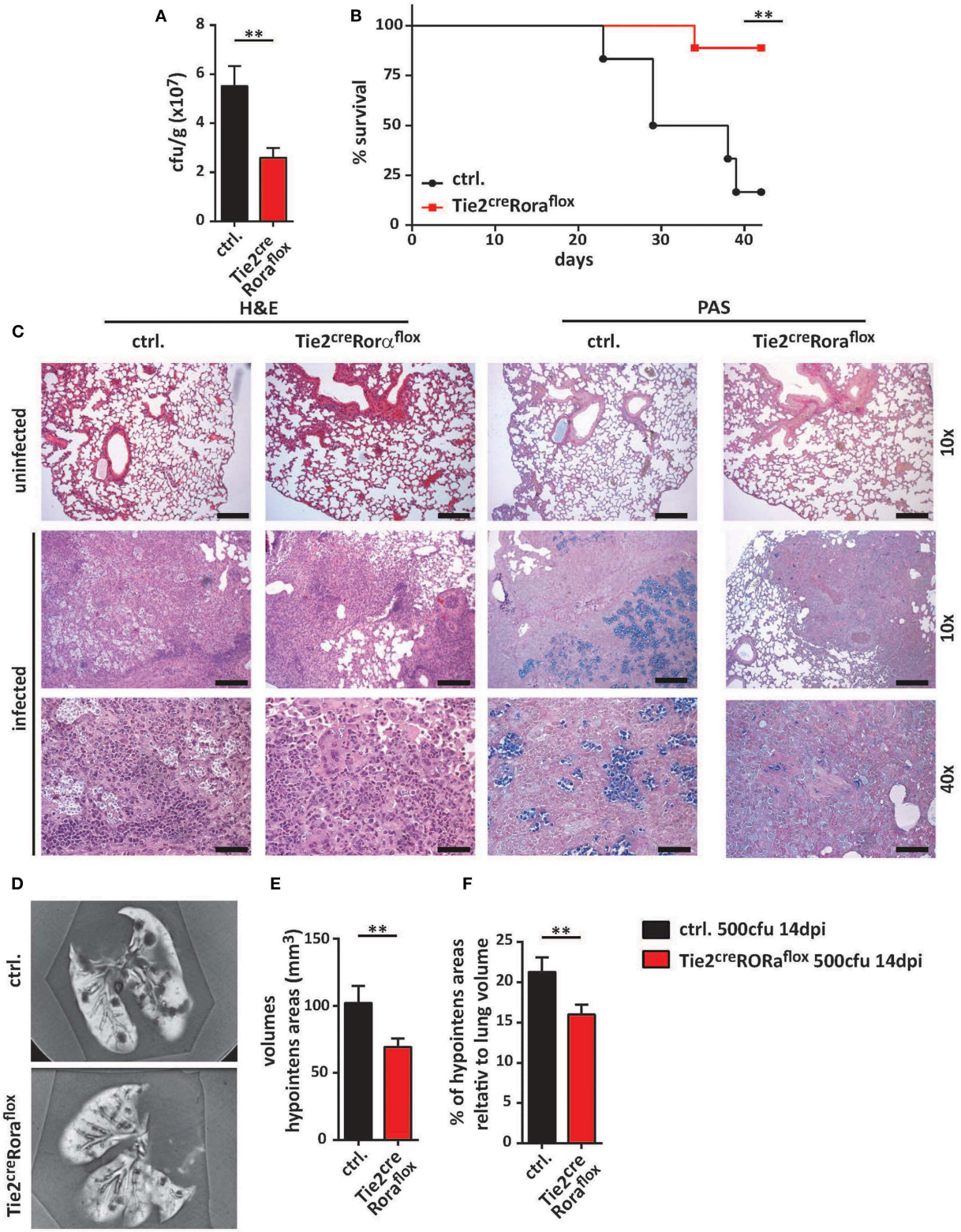

FIGURE 2 | Improved fungal control in ILC2-deficient mice. **(A–F)** Control and Tie2^{cre}Rora^{flox} mice were intranasally infected with 500 cfu of *C. neoformans* and sacrificed after 2 weeks. **(A)** Pulmonary fungal burden of control ($n = 13$) and Tie2^{cre}Rora^{flox} mice ($n = 17$) was determined by plating serial dilutions of organ homogenates on SAB-Agar. **(B)** Animal fitness was judged over the indicated time course and illustrated as % survival. **(C)** Representative H&E and PAS stainings of

(Continued)

FIGURE 2 | paraffin-embedded lung sections. Scale bar 10× magnification = 200 μm, scale bar 40× magnification = 50 μm. **(D)** *Ex-vivo* MRI images of lungs were used to determine **(E)** total and **(F)** relative volumes of T2 weighted hypointense cryptococcal and inflammatory cell accumulations in infected control and Tie2^{cre}Rora^{flox} mice ($n = 10$/group). Data is expressed as mean ± SEM, and pooled from **(B,D–F)** two or **(A)** three independent experiments $^{**}P \leq 0.01$ using a Mann-Whitney *U*-test.

term studies. Strikingly, reconstitution of the ILC2 compartment was found to be associated with significantly increased lung fungal burden at 14 dpi as revealed by cfu determination (**Figure 3A**) and histological staining compared to controls indicating that the immunomodulatory functions of ILC2s are sufficient to abrogate the protective phenotype in Tie2^{cre}Rora^{flox} mice (**Figure 3B**).

Collectively, these data suggest a critical and detrimental role of ILC2s during the pathogenesis of murine pulmonary cryptococcosis.

C. neoformans-Infected ILC2-Deficient Mice Display Reduced Pulmonary Type 2 Cytokine Production

The quality of the cytokine response plays a significant role in protective anti-cryptococcal immunity, and early detection and control by the immune response is necessary to prevent systemic dissemination of this fungal pathogen. Indeed, increasing concentrations of the type 2 cytokines IL-4, IL-5, and IL-13 in lung homogenates positively correlated with cryptococcal burdens in our experimental settings (**Figure 4A**). We therefore next analyzed, to which extent ILC2-deficency in Tie2^{cre}Rora^{flox} mice alters the pulmonary immune response upon cryptococcal infection. By profiling the expression of 84 T_H cell related genes by PCR array analysis, we found that total lung tissue homogenates of infected ILC2-deficient mice contained less transcripts of the type 2 cytokines IL-4, IL-5, and IL-13, while transcripts for the important T_H1-related cytokine IFN-γ and the cytotoxic factor granzyme B were increased in these mice (**Figure 4B**). Accordingly, specific ELISA analysis of lung homogenates also demonstrated decreased concentrations of T_H2 cytokines and increased presence of IFN-γ on protein level in lungs of infected Tie2^{cre}Rora^{flox} mice. By contrast, the concentrations of the cytokine IL-17, which at least in some reports has strongly been implicated in pathways related to protective anti-fungal immunity (29, 30), were not significantly altered between the two experimental groups (**Figure 4C**). On a cellular level, both IL-13-producing ILC2 and to a lesser extent T_H2 cells were reduced in Tie2^{cre}Rora^{flox} mice at 14 dpi as determined by flow cytometry compared to controls. Conversely, infected lungs of Tie2^{cre}Rora^{flox} mice contained more CD4$^+$ T cells producing IFN-γ, while the numbers of IFN-γ$^+$ ILCs were comparable between both groups (**Figure 4D**). Notably, the analysis of 4get reporter mice, which express enhanced green fluorescent protein (eGFP) from the 3′ UTR of the endogenous *Il4* gene, indicated that in addition to T cells, ILC2s could be readily identified as potential source of IL-4 in infected lungs (**Figure 4E**). Collectively, our data supports the importance of type 2 cytokine expression during the onset of pulmonary cryptococcosis and indicates that ILC2s critically contribute to a pathophysiologically relevant local cytokine milieu in the infected lung.

ILC2-Deficient Mice Display Alterations in Myeloid Cell Composition and Macrophage Polarization During *C. neoformans* Infection

Among the multiple immune cell subtypes infiltrating *C. neoformans*-infected lungs, the myeloid cell lineage and in particular macrophages are of primary importance for pathogen control and eventual clearance. Because our data so far were indicative of strong shifts in the expression patterns of important cytokines previously reported to regulate the plasticity of these cells, we next aimed to comprehensively compare the myeloid compartment in infected ILC2-deficient mice and control mice by flow cytometry. Multivariate analysis using non-linear dimensionality reduction with stochastic neighbor-embedding approach (t-SNE) revealed striking differences in the pulmonary myeloid cell compartment in Tie2^{cre}Rora^{flox} mice at 14 dpi (**Figures 5A,B**). Rather expectedly, numbers of eosinophils (CD11b$^+$/CD64$^-$/Ly6g$^-$/SiglecF$^+$), a cell type strongly dependent on IL-5 and eotaxin production by ILC2s (31), were massively reduced in ILC2-deficient mice at 14 dpi (**Figure 5C**). However, we did not observe a compensatory accumulation of CD11b$^+$/Ly6g$^+$/Ly6c$^+$ neutrophils granulocytes (**Figure 5D**), which was described previously (32). Interestingly, mice lacking ILC2s displayed an increased abundance of SiglecF$^-$/MHCII$^+$ cells compared to controls (**Figure 5E**), suggesting changes in the monocyte/macrophage compartment. Detailed analysis of the monocyte/macrophage lineage revealed significantly increased frequencies of SiglecF$^-$/CD64$^+$ interstitial macrophages (**Figure 5F**) and SiglecF$^-$/Ly6c$^+$ monocyte-derived cells (**Figure 5G**) in the context of ILC2-deficency, while CD11c$^{int/+}$/CD64$^+$/SiglecF$^+$ alveolar macrophages were seemingly unaffected (**Figure 5H**). Conversely, less myeloid cells expressing the mannose receptor (CD206) were present in lungs of mice lacking ILC2s indicating that the presence of ILC2s correlates to *Cryptococcus*-dependent accumulation of AAMs (**Figure 5I**). Notably, we observed no significant changes in myeloid cell populations at 7 dpi (**Supplemental Figures 3A–F**). We also compared the lung frequencies of dendritic cells (DCs). However, no significant changes were observed in the different DC subsets, including CD11c$^+$CD103$^+$ DCs, CD11c$^+$CD11b$^+$ DCs, and CD11c$^+$Ly6C$^+$ plasmacytoid DCs (**Supplemental Figures 3G–I**).

Collectively, these data support the notion that the presence of functional ILC2s is associated with compositional shifts in the myeloid cell compartment during pulmonary cryptococcosis.

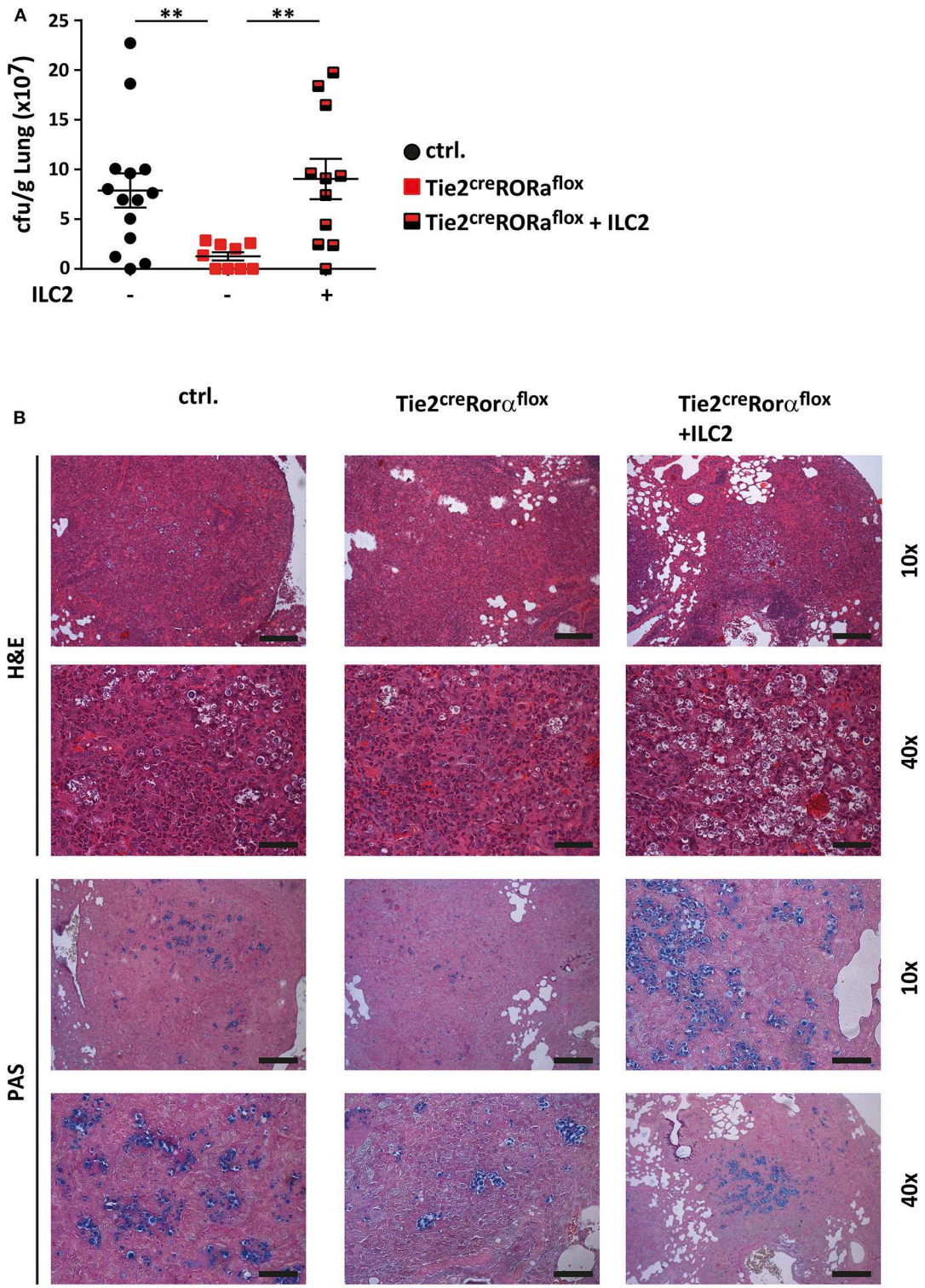

FIGURE 3 | ILC2 drive detrimental anti-cryptococcal immune responses. **(A,B)** Control and Tie2^{cre}Rora^{flox} mice were challenged with 500 cfu of *C.neoformans.* and analyzed 14 dpi. In addition, Tie2^{cre}Rora^{flox} mice were reconstituted with sort-purified and *in vitro* expanded ILC2 on day 1 and 7 of infection as described in the method section (Tie2^{cre}Rora^{flox} + ILC2). **(A)** Infection loads in affected lungs of ILC2 reconstituted Tie2^{cre}Rora^{flox} mice ($n = 11$) were quantified and compared to control. ($n = 14$) and Tie2^{cre}Rora^{flox} mice ($n = 9$). **(B)** Representative H&E and PAS stainings of control, Tie2^{cre}Rora^{flox} and ILC2 reconstituted Tie2^{cre}Rora^{flox} mice. Scale bar 10× magnification = 200 μm, scale bar 40× magnification = 50 μm. Data is expressed as mean ± SEM, and pooled from **(A)** three independent experiments $^{**}P \leq 0.01$ using a Mann-Whitney *U*-test.

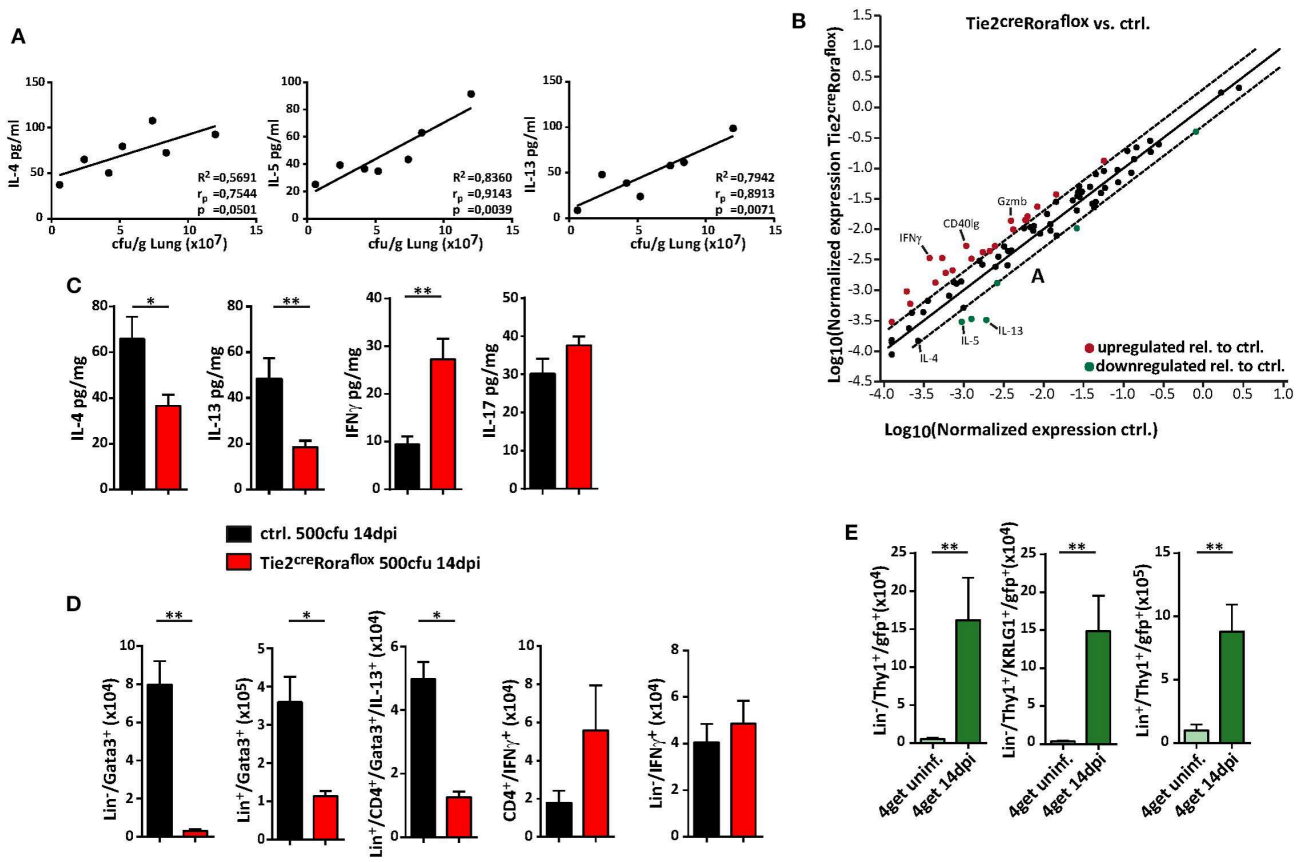

FIGURE 4 | ILC2 orchestrate the local pulmonary cytokine milieu during cryptococcosis. **(A–D)** Control and **(B–D)** conditional Rora deficient mice (Tie2^{cre}Rora^{flox}) were subjected to intranasal *C. neoformans* infection (500 cfu infection dose) for 14 days. **(A)** Correlation analysis of cytokine concentrations (IL-4, IL-5, and IL-13) with fungal burden ($n = 7$). **(B)** Scatter plot of differentially regulated genes in Tie2^{cre}Rora^{flox} compared to control mice. Data was generated by using RT^2 Profiler PCR Array PAMM-074 (Qiagen) and relative gene expression was analyzed in the web-based Qiagen Data Analysis Center. Boundaries mark threshold of 2-fold change ($n = 4$, pooled/group). **(C)** Total lung protein concentrations of IL-4 (ctrl. $n = 11$; Tie2^{cre}Rora^{flox} mice $n = 18$), IL-5 (ctrl. $n = 9$; Tie2^{cre}Rora^{flox} mice $n = 14$), IFNγ (ctrl. $n = 9$; Tie2^{cre}Rora^{flox} mice $n = 14$) and IL-17 (ctrl. $n = 11$; Tie2^{cre}Rora^{flox} mice $n = 18$) was quantified in response to *C. neoformans* infection. **(D)** Lung single cell preparations were stimulated with PMA/ionomycin in the presence of protein transport inhibitors for 4 h. Cell numbers of Lin$^-$/Gata3$^+$ ILC2, Lin$^+$/Gata3$^+$ cells, Lin$^+$/CD4$^+$/Gata3$^+$/IL-13$^+$ T cells, CD4$^+$/IFN-γ$^+$ T cells, and Lin$^-$/CD4$^-$/IFN-γ$^+$ ILC1 determined in lung tissue of infected mice (ctrl. $n = 8$; Tie2^{cre}Rora^{flox} mice $n = 11$). **(E)** Analysis of naïve or *C. neoformans* infected (14 dpi) 4get mice. Data is presented as mean ± SEM **(A)** representative of two experiments, **(B)** one experiment or **(C–E)** pooled from 2 to 3 experiments. $^*P \leq 0.05$; $^{**}P \leq 0.01$ defined by Mann-Whitney *U*-test.

DISCUSSION

Complex host-pathogen relationships characterize cryptococcal infections and an intricate balance between tolerance and resistance is required for effective pathogen control. There is a substantial body of literature that highlighted the critical role of T lymphocytes in the pulmonary immune response to *C. neoformans* challenge. Indeed, a number of studies have clearly emphasized the importance of T helper cell-mediated immunity in controlling cryptococcal infection. Thereby, resistance has been mainly associated to generation of polarized Th1/Th17 immune responses followed by STAT1-dependent activation of classical macrophages that ultimately facilitates fungal clearance (29, 33–35). Conversely, a dominance of type 2 immune responses and the activation of alternatively activated macrophages has been strongly linked to pathogen survival and systemic spread (36). However, with the recent description of ILCs as innate counterparts of T helper cells endowed with the potential to produce high amounts of important immunoregulatory cytokines, further research is warranted to address their relative contribution to anti-cryptococcal immunity. Here, we analyzed the role of ILC2s during pulmonary cryptococcosis using mice with specific deficiency in the ILC2 compartment. We observed that the numbers of ILC2 increased upon infection and that these cells were significant producers of type 2 signature cytokines. Notably, ILC2-deficiency was linked to increased pulmonary type 1 immunity and classical macrophage activation resulting in improved fungal control and prolonged survival, suggesting a detrimental role of ILC2 effector functions during *C. neoformans* infection.

Previous studies in Balb/c mice showed that the alarmin IL-33 derived from alveolar type 2 epithelial cells is an important trigger of lung type 2 cytokine production both at early and late phases of infection with a highly virulent *C. neoformans* strain

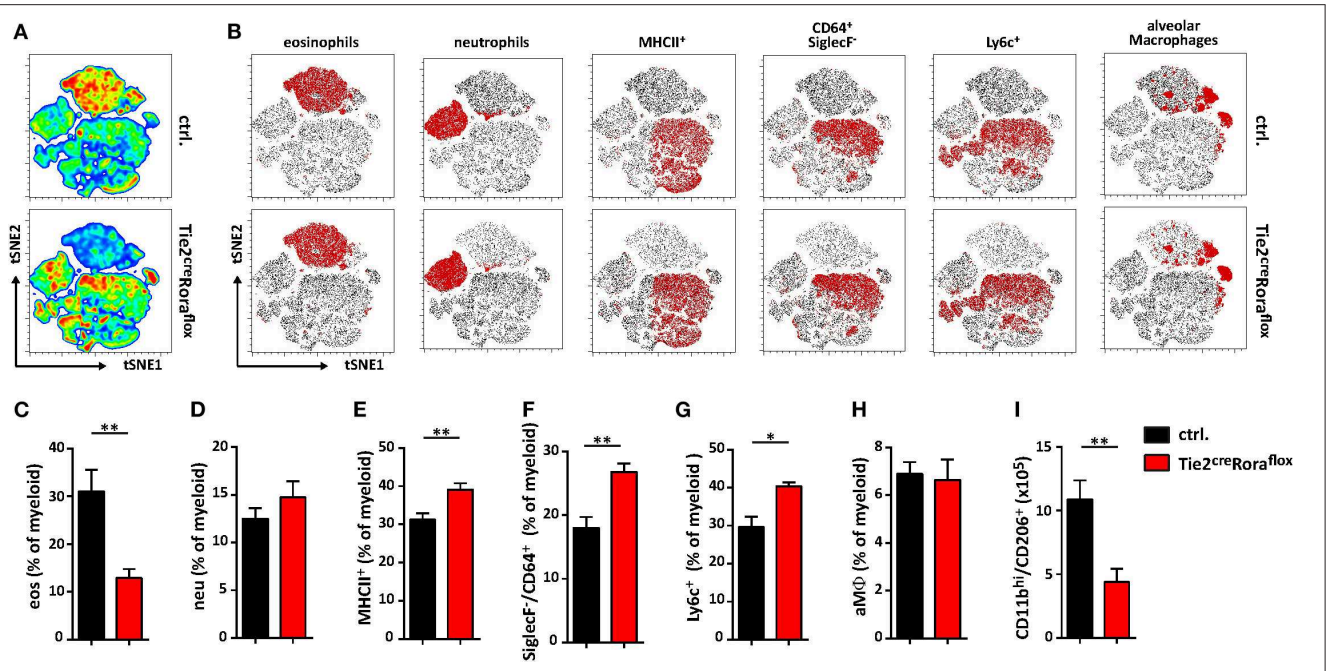

FIGURE 5 | Altered polarization patterns in the myeloid compartment in the absence of ILC2 mice. **(A–I)** Control and Tie2^{cre}Rora^{flox} mice were challenged intranasally with 500 cfu of *C. neoformans* and sacrificed 14 dpi. **(A)** t-SNE plots of flow cytometric analyzed pulmonary myeloid cell composition (t-SNE 1/t-SNE 2 represents individual marker expression of CD11b, CD11c, CD64, Ly6c, Ly6g, MHCII, and SiglecF of individual data points) in control and Tie2^{cre}Rora^{flox} mice. Color code depicted is reflecting relative cell density (blue = low, red = high; $n = 8$/genotype). **(B)** Representative t-SNE-maps of control and Tie2^{cre}Rora^{flox} mice show localization of respective surface marker positive cell clusters (red area) within t-SNE plots ($n = 8$). **(C–I)** Relative abundance of **(C)** CD11b^{+}/CD64^{-}/Ly6g^{-}/SiglecF^{+} eosinophil Granulocytes (eos), **(D)** CD11b^{+}/Ly6g^{+}/Ly6c^{+} neutrophil Granulocytes (neu), **(E)** SiglecF^{-}/MHCII^{+} cells, **(F)** SiglecF^{-}/CD64^{+}, **(G)** SiglecF^{-}/Ly6c^{+} and **(H)** CD11b$^{int/+}$/CD11c$^{int/+}$/CD64^{+}/SiglecF^{+} alveolar macrophages (aMϕ) referred to total myeloid cells in control (ctrl. $n = 8$) and Tie2^{cre}Rora^{flox} ($n = 7$) mice. **(I)** Quantification of CD11b^{hi}/CD206^{+} cells in total lung tissue of infected animals (ctrl. $n = 4$; Tie2^{cre}Rora^{flox} mice $n = 6$). **(A,B)** t-SNE analysis and **(C–I)** flow cytometry shown is representative for two individual experiments. **(C,I)** Data is expressed as mean ± SEM. *$P \leq 0.05$; **$P \leq 0.01$ defined by Mann-Whitney *U*-test.

(15, 16, 23, 37). While deficiency in IL-33 signaling attenuated infection-induced ILC2 numbers and their production of IL-13 and IL-5 in these studies, it remained unclear, whether ILC2s and their cytokine production significantly contributed to AAM differentiation and the severity of pulmonary disease. Using mice lacking ILC2s due to conditional deletion of the transcription factor Rorα in immune cells, we provide direct evidence that ILC2s functionally contribute to mechanisms of immune polarization during cryptococcosis. Although Rorα is not exclusively expressed in ILC2s, our data indicated that T helper cell subset differentiation was not affected in Tie2^{Cre}Rora$^{flox/sg}$ mice. Similarly, a broadly used strategy to delete Rorα using IL-7R^{Cre} deleter mice in CD127-expressing cells (e.g., T cells, ILCs, B cells) resulted in effective ILC2 depletion without obvious effects on Th2 cells during infection-dependent type 2-mediated lung inflammation (38).

Rorα deficiency in mice was reported to result in diminished Th17 responses *in vitro* and *in vivo* (39). However, we did not observe effects on the *in vitro* differentiation potential of naïve T cells toward Rorγt^{+} and IL-17 producing cells *in vitro*. Moreover, improved pathogen clearance in Tie2^{Cre}Rora$^{flox/sg}$ mice was not associated with changes in the frequencies of Th17 cells or IL-17 itself, which has been shown to protect from *C. neoformans*-induced lung pathology in some studies (29, 40). However, the role of IL-17 in cryptococcosis is controversial as in other studies IL-17 played no or only minor protective roles compared to IFN-γ-dependent classical macrophage activation (41, 42). In line with this, we observed no changes in the frequencies of lung infiltrating neutrophils in the absence of ILC2s in infected mice. Conversely, ILC2s were, most likely via the production of IL-5, essential for the pulmonary accumulation of eosinophils in our model. Notably, this ILC2-dependent increase in eosinophil numbers occurred in the presence of adaptive immune cells, while it was previously reported in Rag2$^{-/-}$ mice that ILCs and NKs can drive eosinophilia even in the absence of T cells (32). Although eosinophilia has been associated with cryptococcal disease in mice and potentially humans (43–45), it remains unclear whether reduced eosinophil numbers in Tie2^{Cre}Rora$^{flox/sg}$ mice are directly linked to improved pathogen control and survival. Enhanced Th1 and Th17 responses were reported in *C. neoformans*-infected eosinophil-deficient ΔdblGATA mice, although lung fungal burdens and brain dissemination were similar to wildtype control mice (46). In the same study, Piehler et al. identified eosinophils as important producers of the cytokine IL-4, which is a key immunoregulatory factor in cryptococcosis (47). However, IL-4 production by eosinophils and antigen-specific Th2 cells occurred rather late during infection, suggesting that other

IL-4 sources may contribute to Th2 polarization at early time points of the infection process. Using IL-4 reporter mice, we identified in the present study ILC2s as producers of IL-4 in infected lung tissue. Moreover, IL-4 transcripts were reduced in the context of ILC2-deficiency. Thus, IL-4 production by ILC2s may be positioned at the apex of a cascade leading to the development of Th2 polarization, while protective Th1 responses and the activation of classical macrophages are inhibited. Indeed, ILC2s have been shown to be substantial producers of IL-4 *in vivo* (26, 48). In addition, activated ILC2 are also well-known for their capacity to produce high amounts of IL-13, a cytokine with profound effects on macrophage cell biology in pathological microenvironments (49, 50). However, whether ILC2s directly via the production of prototypical cytokines or indirectly via other mechanisms such as direct cellular interaction contribute to macrophage polarization during *C. neoformans* still remains an open question. Further studies will have to dissect the individual contribution of ILC2 effector cytokines to T helper and macrophage polarization patterns in early *C. neoformans* infection.

In summary, we identified ILC2s as a critical regulatory cell lineage during pulmonary *C. neoformans* infections. Targeting ILC2s may therefore represent, in combination with other therapeutic strategies, a method to treat this severe inflammatory disease.

METHODS

Animals and Husbandry

$Tie2^{cre}Rora^{flox/sg}$ (C57BL/6 background) were described previously (26, 27). $Rora^{Cre}tdTomato^{flox}$ mice were generated by crossbreeding $Rora^{Cre}$ mice [kindly provided by Dennis O'Leary (51)] to ROSA26-LSL-tdTomato mice that contain a transgene encoding an enhanced tandem dimer tomato red fluorescent protein (tdTomato) in the ROSA26 locus with a lox-transcriptional stop-lox cassette inserted between exon 1 and exon 2 (52). 4get mice were kindly provided by David Vöhringer, Erlangen (53). C57BL/6 mice were purchased from The Jackson Laboratory. Animal husbandry and experiments were realized in accordance to the guidelines for "Tierhaltung Regierung Unterfranken" (accreditation no. 55.2-2532-2-827). Sterile drinking water and food were provided *ad libitum*. All animals were kept in individually ventilated cages (IVC), and the health status of the colony was assessed periodically for pathogens in adherence with the guidelines of the Federation of European Laboratory Animal Science Associations.

Culture of *C. neoformans* and Infection Model

C. neoformans var. *grubii* (ATCC 90112) was thawed from glycerol stocks and cultured in Sabouraud Dextrose Broth (SAB-Medium; 2% Dextrose, 1% Peptone; Sigma-Aldrich) at 30°C overnight. Fungi were harvested and washed twice in sterile phosphate-buffered saline (PBS) and cell numbers were determined with the help of a Neubauer-improved counting chamber. Afterwards, suspensions containing 2.5×10^4 cryptococci per ml in sterile PBS were prepared. Recipient mice were anesthetized intraperitoneally with 80 µl/10 g body weight of a ketamine/xylazine mixture [2.4 ml ketamine (50 mg/ml), 0.8 ml xylazine (20 mg/ml) in 6.8 ml sterile PBS] prior to intranasal application of a 20 µl inoculum to induce a low dose infection with 500 colony-forming-units (cfu). *C. neoformans* concentrations were verified by plating serial dilutions of the inoculum on Sabouraud Dextrose Agar (SAB-Agar; 4% dextrose, 1.5% agar, 0.5% casein, 0.5% animal tissue digest; Thermo Fisher Scientific) followed by incubation for 48 h at 30°C to determine the number of cfu. Infected mice were monitored daily with regard to their health status.

Determination of Lung Fungal Burden

Lung, liver or brain tissue was removed, weighted and covered with 1 ml SAB-Medium per mg of tissue. Lung tissue integrity was disrupted by processing with a homogenizer (MM400 mixer mill, Retsch, Germany) with metal beads at a frequency of 25 Hz for 2 min. Serial dilutions were plated on SAB-Agar plates and incubated for 48 h at 30°C. The numbers of cfu/g tissue were determined under consideration of the dilution factor.

Preparation of Pulmonary Leukocytes

For the preparation of lung leukocyte single cell suspensions, lung tissue was removed, rinsed in Hank's Balanced Salt Solution (HBSS; Sigma-Aldrich) and cut into small pieces. Subsequently, the lung tissue was digested in HBSS containing 0.2 mg/ml Liberase™ (Roche) and 1 µg/ml DNase1 (2,000 U/mg; Roche) in a final volume of 2.5 ml. Digestion was performed with the help of a gentleMACS™ Octo Dissociator with heaters running the program 37C_m_LDK_1 (Miltenyi Biotec). Subsequently, the suspension was passed through a 70 µm nylon-mesh (Corning) and washed in phosphate buffered saline supplemented with 0.5% bovine serum albumin and 2 mM EDTA (PEB-Buffer). In order to remove erythrocytes, the suspension was spun down, resuspended in 1 ml ACK-Lysis-Buffer (155 mM ammonium chloride, 10 mM potassium bicarbonate, 0.1 mM EDTA) and incubated for 30 s. Subsequently, cells were washed in PEB-Buffer and passed to Percoll-centrifugation. In brief, 80% Percoll (GE Healthcare) was overlayed with 40% Percoll containing lung leukocytes. After centrifugation at 1,400 rpm for 20 min at room temperature without breaks, interphases were collected and washed in PEB-Buffer. Finally, cell numbers were determined in a Neubauer-improved counting chamber and single cell suspensions were used for further *ex vivo* phenotyping.

Flow Cytometry

Lung leukocytes were incubated with anti-CD16/CD32 antibodies (anti-Fc-receptor; eBioscience) prior to specific surface marker and intracellular staining. For ILC2 identification, specific lineage preclusion was applied. In brief, Fc-receptor blocked cells were incubated with a custom made biotinylated lineage antibody cocktail (anti-B220, anti-CD3, anti-CD5, anti-CD11b, anti-GR1, anti-NK1.1, anti-SiglecF, anti-Ter119; Miltenyi Biotec). After washing, cells were passed to regular surface staining including streptavidin-Brilliant-Violet 421 (BV421; Biolegend) for labeling of biotinylated antibodies. Antibodies were purchased from Miltenyi Biotec if not otherwise

indicated. APC (Alexa647), BV510, BV650, FITC, PacificBlue (BV421, eFluor410, VioBlue), PE, PE-Cy7 or PerCP-Cy5.5 (PerCP-efluor710, PerCP-Vio700) conjugated antibodies were used. For surface staining, cells were incubated with different combinations of anti-CD4, anti-CD64 (BD Bioscience), anti-CD11b, anti-CD11c, anti-CD103 (Biolegend), anti-CD206 (Biolegend), anti-ICOS anti-KLRG1, anti-Ly6c (BD Bioscience), anti-Ly6g (eBioscience), anti-MHCII (eBioscience), anti-SiglecF, and anti-Thy1.2 antibodies.

In order to enable intracellular cytokine staining cells were stimulated with the 1× Cell Stimulation Cocktail (plus protein transport inhibitors) (eBioscience) for 4 h. For subsequent intracellular staining of transcription factors and/or Interleukins, cells were fixed and permeabilized with the FoxP3 Transcription Factor Staining Buffer according to manufacturer's instructions (eBioscience). For intracellular staining, antibody combinations of anti-IL-13-PE (eBioscience), anti-IFNγ-APC (eBioscience), anti-Gata3-APC, anti-T-bet-PE (eBioscience), anti-RORγt-PE (eBioscience), and/or anti-FoxP3-PE (eBioscience) were utilized. Samples were analyzed on a LRSFortessa cell analyzer (BD Bioscience) and evaluated with Flowjo 10 (Treestar). For gating strategies of specific immune cell populations see **Supplemental Figure 4**.

t-SNE analysis was performed with Flowjo 10 (Treestar). In brief, FCS files of individual specimens of control and Tie2^{cre}RORα^{flox} mice were down sampled randomly to 50,000 events per specimen and concatenated according to their originating genotype. t-SNE maps were generated by running the t-SNE analysis with following markers: CD11b, CD11c, CD64, Ly6c, Ly6g, MHCII, and SiglecF. Two dimensional reduction (t-SNE 1/t-SNE 2) was calculated by using the following parameters: 1,000 iterations, perplexity 30 and a learning rate (eta) of 56,000. Specific cell populations were defined according to their surface marker abundance.

ILC2 Isolation and Expansion

For ILC2 induction *in vivo*, an IL-25 expression vector was hydrodynamically administered and murine spleen and mesenteric lymph nodes were isolated 3 days later (54). To generate single cell suspensions, tissues were digested in RPMI (Sigma-Aldrich), supplemented with 10% FBS (Gibco), 1% penicillin-streptomycin (Sigma-Aldrich), 0.25 mg/ml collagenase B (Roche) and 0.05 mg/ml DNase1 (2,000 U/mg; Roche) using the gentleMACS™ Octo Dissociator with heaters running the program 37C_m_SDK_1 (Miltenyi Biotec) according to manufacturer's instructions. After washing and cell number determination, cell suspensions were passed to fluorescence-activated cell sorting and ILC2 were identified using the following panel: CD3 FITC$^-$ (17A2, BioLegend), CD5 FITC$^-$ (REA421, Miltenyi Biotec), CD11b APC-Vio770$^-$ (REA592, Miltenyi Biotec), CD11c APC-Vio770$^-$ (N418, Miltenyi Biotec), CD45R FITC$^-$ (REA755, Miltenyi Biotec), CD49b PE-Vio770$^-$ (REA981, Miltenyi Biotec), FcεR1a PE-Cy7$^-$ (MAR-1, Invitrogen), NK1.1 PE-Vio770$^-$ (PK136, Miltenyi Biotec), ICOS VioBlue$^+$ (7E.17G9, Miltenyi Biotec) and KLRG1 PE$^+$ (REA1016, Miltenyi Biotec). FACS was performed using a MoFlo Astrios EQ (Beckman Coulter) in the Core Unit Cell Sorting Erlangen.

For *ex vivo* expansion of sort-purified ILC2, cells were cultivated in DMEM GlutaMax medium (Sigma-Aldrich) supplemented with 10% FBS (Gibco), 1% penicillin-streptomycin (Sigma-Aldrich), 20 mM Hepes (Carl Roth), 1 mM sodium pyruvate (Gibco), 50 μM mercaptoethanol (Sigma-Aldrich) together with 20 ng/ml TSLP (Invitrogen) and 50 ng/ml of IL-2 (BioLegend), IL-7 (Immunotools), IL-25 (Immunotools), IL-33 (Immunotools) each.

Adoptive Transfer of ILC2 in *Cryptococcus neoformans*-Challenged Mice

ILC2-deficient Tie2^{cre}Rora^{flox} mice were adoptively transferred with 1 × 10^7 viable *in vitro* expanded ILC2 on day 1 and 7 of *C. neoformans* infection by intravenous administration. Thereafter, mice were sacrificed 14 dpi.

Bone Marrow Chimeras

In order to generate bone marrow chimeric mice, lethally irradiated (10 Gray) C57BL/6 mice were reconstituted with 1 × 10^7 femoral bone marrow cells of either control, Tie2^{cre}Rora^{flox} or Rora^{Cre}tdtomato^{flox} mice. Irradiated mice were kept in isolator cages and treated for 2 weeks with antibiotics (150 μl 24% Borgal® solution [200 mg sulfadoxine and 40 mg trimethoprim ad 1 ml aqua ad injectabilia; Virbac] in 300 ml drinking water). After 8 weeks of hematopoietic reconstitution, mice were challenged with *Cryptococcus neoformans*.

T Cell Differentiation

Before *in vitro* T cell differentiation, splenic single cell suspensions were generated by passing spleens through a 40 μm nylon mesh (Corning), followed by a washing step in R10+ medium (see **Table 1**). Erythrocytes were removed in 5 ml ACK-Lysis-Buffer (155 mM ammonium chloride, 10 mM potassium bicarbonate, 0.1 mM EDTA) for 5 min. Thereafter, the cell suspension was washed in R10+ medium and cell number was determined. Isolation of naïve T cells was performed with mouse CD4$^+$ T Cell Isolation and CD25 Isolation Kits (Miltenyi Biotec) according to manufacturer's instructions. For T cell differentiation, 1 × 10^6 CD4$^+$CD25$^-$ T cells were seeded in 48-well plates coated with anti-CD3/anti-CD28 antibodies (BioXcell, 10 μg/ml each). The differentiation of the respective T cell population was induced by stimulating the cells according to **Table 1** for 5 days.

Real-Time PCR

Lung tissue was snap-frozen in liquid nitrogen and stored at −80°C until RNA isolation. RNA was isolated using the RNeasy mini kit (Qiagen, Germany) according to manufacturer's instructions. cDNA was synthesized with the Script RT-PCR kit (Jena Bioscience, Jena Germany). For SYBR-green based quantitative real-time PCR (qRT-PCR) QuantiTect Primer assays (Qiagen) were analyzed in a CFX96 real-time detection system (Biorad). Probe-based assays (TaqMan Gene Expression Assays, ThermoFisher Scientific) were performed on a 7900HT Fast Real-Time PCR System (Applied Biosystems,

TABLE 1 | Stimulation media for T cell differentiation.

Subpopulation	Reagent	Concentration	Medium
T_H0	/	/	R10+ (RPMI 1640 [with L-Glutamine and sodium bicarbonate, Sigma-Aldrich], 1% penicillin/streptomycin [Sigma-Aldrich], 10% FCS [Gibco])
T_H1	anti-IL-4 rIL-12	5 μg/ml 20 ng/ml	R10+
T_H2	anti-IFNγ anti-IL-12 rIL-2 rIL-4	5 μg/ml 10 μg/ml 20 ng/ml 100 ng/ml	R10+
T_H17 (IL-23)	anti-IL-4 anti-IFNγ rIL-6 rIL-23 rIL-1β	5 μg/ml 5 μg/ml 100 ng/ml 50 ng/ml 20 ng/ml	X-Vivo+ (X-Vivo [Lonza] 1% penicillin/ streptomycin [Sigma-Aldrich])
T_H17 (TGF-β)	anti-IL-4 anti-IFNγ rIL-6 rTGF-β	5 μg/ml 5 ng/ml 100 ng/ml 5 ng/ml	I10+ (IMDM [PAA]), 1% penicillin/ streptomycin [Sigma-Aldrich], 10% FCS [Gibco]
T_{reg}	rTGF-β rIL-2	5 ng/ml 20 ng/ml	R10+

ThermoFisher Scientific). ΔCT values were calculated relative to *hprt* expression. For the generation of transcriptomic profiles, 0.5 μg RNA of total lung lysates of 4 control or $Tie2^{cre}Rora^{flox}$ mice were pooled, respectively. RT2 Profiler PCR Array PAMM-074 (Qiagen) was performed according to manufacturer's instructions. To calculate relative expression of genes and to generate scatter-plots the web-based Data analysis center (Qiagen) was used.

Histological Methods

Lung samples were fixed in Roti®-Histofix 4.5% (Carl-Roth, Germany) and embedded in paraffin. Six serial 3 μm slices of each lung sample were transferred on a microscope slide and subsequently stained either with hematoxylin and eosin (H&E) to examine immune cell infiltrates, tissue alterations and cryptococcoma formation or periodic acid Schiff's reagent (PAS) to visualize cryptococcal distribution and mucus production. Microscopy samples were analyzed on a Leica DMI 6000B.

Magnetic Resonance Imaging (MRI) of Lungs *ex vivo*

MRI was performed on a 7 Tesla small animal MRI scanner (ClinScan 70/30; Bruker) using a whole body mouse volume coil (Bruker). For preparation of lung tissue for MRI analysis, total lungs were removed and fixed for 24 h in 4% paraformaldehyde (PFA; Merck,). Subsequently, fixed tissue was embedded in 50 ml Tubes (Sarstedt) containing 1.5% low-melting agarose (Sea Plaque agarose, FMC BioProducts) to avoid motion artifacts during MRI. The measurement protocol consisted of a T2 weighted Turbo-Spin-Echo (TSE) sequence with the following parameters: Time to repetition (TR): 4,000 ms, time to echo (TE): 74 ms, bandwidth (bw): 125 Hz/px, 20 averages, matrix: 512. For image post processing and data analysis, a dedicated software package (Chimera GmbH,) was used to segment hypointense lung nodules on the TSE sequence to determine the respective volumes in mm^3. MRI was performed with the help of the Preclinical Imaging Platform Erlangen (PIPE).

Enzyme-Linked Immunosorbent Assays (ELISA)

In order to determine lung tissue specific concentration of IL-4, IL-5, IL-13, IL-17, and IFN-γ, snap-frozen tissue pieces were homogenized in M-PER™ Mammalian Protein Extraction Reagent (ThermoFisherScientific), supplemented with PhosSTOP™ (Roche) and cOmplete™ protease Inhibitor cocktails (Roche). Protein concentration was determined with a Roti®-Quant protein quantification assay (Carl-Roth). For assessment of cytokine concentrations, 100 mg/ml total protein was used either IL-4 (eBioscience), IL-5 (Biolegend), IL-13 (eBioscience), IL-17 (Biolegend), or IFN-γ (eBioscience) specific ELISA assays. ELISA assays were carried out according to manufacturer's instructions.

Statistics

Statistical tests were performed using Prism V7 (Graph Pad) software. If not otherwise indicated, a two-tailed Mann-Whitney *U* test with 95% confidence interval was performed for comparison of two groups ($^*P > 0.05$; $^{**}P > 0.01$; $^{***}P > 0.001$; NS = not significant).

DATA AVAILABILITY STATEMENT

All datasets generated for this study are included in the article/**Supplementary Material**.

ETHICS STATEMENT

The animal study was reviewed and approved by Regierung von Unterfranken.

AUTHOR CONTRIBUTIONS

MK, LK, and SO performed experiments and analyzed data. UM, GA, CB, US, and MN discussed the data and critically reviewed the manuscript. MK and SW conceptualized the project and wrote the paper.

FUNDING

This work was supported by funds from the German Research Foundation (DFG) to SW and MN (TRR241, A03; CRC1181, A08; FOR2886, TP01) and to US and CB (SPP1937; CRC1181, C04).

ACKNOWLEDGMENTS

The present work was performed in (partial) fulfillment of the requirements for obtaining the degree Dr. rer. nat. for MK. Cell sorting was supported by the FACS Core Unit at the Nikolaus-Fiebiger-Center, Erlangen. We thank the Optical Imaging Center Erlangen (OICE) of the Friedrich-Alexander-University Erlangen and the Preclinical Imaging Platform Erlangen (PIPE) of the University Hospital Erlangen for supporting imaging.

SUPPLEMENTARY MATERIAL

The Supplementary Material for this article can be found online at: https://www.frontiersin.org/articles/10.3389/fimmu.2020.00209/full#supplementary-material

Supplemental Figure 1 | (A,B) *In vitro* differentiated T cells obtained from control or Tie2^{cre}Rora^{flox} mice. **(A)** Expression of T cell subpopulation defining transcription factors in differentiated T cells. **(B)** Relative abundance of *in vitro* differentiated T cell subpopulations. **(C,D)** Bone marrow chimeric C57BL/6 or Tie2^{cre}Rora^{flox} mice were infected with 2,000 cfu of *C. neoformans* and analyzed 14 dpi. **(C)** Representative FACS plots and quantification of Lin$^-$/Thy1$^+$/ICOS$^+$/KLRG1$^+$ ILC2 in bone marrow chimeric mice ($n = 4$/group). **(D)** Fungal burden in lungs of infected bone marrow chimeric control and Tie2^{cre}Rora^{flox} mice ($n = 4$/group). Data is expressed as mean ± SEM of **(A,B)** 3 or **(C,D)** one single experiment.

Supplemental Figure 2 | (A–D) Control and Tie2^{cre}Rora^{flox} mice were challenged with 500 cfu of *C. neoformans* and analyzed **(A,B)** 7 dpi or **(F,D)** 14 dpi. **(A)** Cryptococcal burden in infected lungs 7 dpi of control ($n = 18$) and Tie2^{cre}RORa^{flox} ($n = 20$) mice assessed by plating serial dilutions of tissue homogenate on SAB-agar plates. **(B)** Representative H&E and PAS stainings of control and Tie2^{cre}RORa^{flox} mice 7 dpi. **(C,D)** Fungal burden of control ($n = 8$) and Tie2^{cre}RORa^{flox} ($n = 9$) mice in **(C)** brain and **(D)** liver 14 dpi determined by plating serial dilutions of tissue homogenates. Data is expressed as mean ± SEM pooled from **(A,C,D)** or representative **(B)** of two experiment.

Supplemental Figure 3 | (A–I) Control and Tie2^{cre}Rora^{flox} mice were challenged intranasally with 500 cfu *C. neoformans* and sacrificed **(A–F)** 7 dpi or **(G–H)** 14 dpi. **(A–F)** Quantification of pulmonary **(A)** CD11b$^+$/CD64$^-$/Ly6g$^-$/SiglecF$^+$ eosinophil granulocytes (eos), **(B)** CD11b$^+$/Ly6g$^+$/Ly6c$^+$ neutrophil granulocytes (neu), **(C)** SiglecF$^-$/MHCII$^+$ cells, **(D)** SiglecF$^-$/CD64$^+$ cells, **(E)** SiglecF$^-$/Ly6c$^+$ cells and **(F)** CD11b$^{int/+}$/CD11c$^{int/+}$/CD64$^+$/SiglecF$^+$ alveolar macrophages in control ($n = 10$) and Tie2^{cre}RORa^{flox} ($n = 12$) mice 7 dpi. **(G–I)** Quantification of **(G)** CD11b$^+$/CD11c$^+$/CD103$^+$, **(H)** CD11b$^+$/CD11c$^+$/CD24$^+$/Ly6c$^-$ cDCs and **(I)** CD11c$^+$/CD24$^+$/Ly6c$^+$ pDCs in lungs of infected control ($n = 8$) and Tie2^{cre}RORa^{flox} ($n = 9$) mice 14 dpi. Data is expressed as mean ± SEM pooled from two experiments.

Supplemental Figure 4 | Gating strategies used in flow cytometry. **(A)** Gating strategy for Lin$^-$/Thy1$^+$/ICOS$^+$/KLRG1$^+$ ILC2 in *C. neoformans* infected control and Tie2^{cre}Rora^{flox} mice 14 dpi. **(B)** Gating strategy for CD11b$^+$/CD64$^-$/Ly6g$^-$/SiglecF$^+$ eosinophilic granulocytes (eos), CD11b$^+$/Ly6g$^+$/Ly6c$^+$ neutrophil granulocytes (neu), SiglecF$^-$/MHCII$^+$ cells, SiglecF$^-$/CD64$^+$, SiglecF$^-$/Ly6c$^+$, and CD11b$^{int/+}$/CD11c$^{int/+}$/CD64$^+$/SiglecF$^+$ alveolar macrophages (aMϕ) representative shown for control mice 14 dpi after *C. neoformans* infection.

REFERENCES

1. Kronstad JW, Attarian R, Cadieux B, Choi J, D'Souza CA, Griffiths EJ, et al. Expanding fungal pathogenesis: Cryptococcus breaks out of the opportunistic box. *Nat Rev Microbiol.* (2011) 9:193–203. doi: 10.1038/nrmicro2522
2. Limper AH, Adenis A, Le T, Harrison TS. Fungal infections in HIV/AIDS. *Lancet Infect Dis.* (2017) 17:e334–43. doi: 10.1016/S1473-3099(17)30303-1
3. Williamson PR, Jarvis JN, Panackal AA, Fisher MC, Molloy SF, Loyse A, et al. Cryptococcal meningitis: epidemiology, immunology, diagnosis and therapy. *Nat Rev Neurol.* (2017) 13:13–24. doi: 10.1038/nrneurol.2016.167
4. Goldman DL, Khine H, Abadi J, Lindenberg DJ, Pirofski L, Niang R, et al. Serologic evidence for Cryptococcus neoformans infection in early childhood. *Pediatrics.* (2001) 107:E66. doi: 10.1542/peds.107.5.e66
5. Fischer M, Muller JP, Spies-Weisshart B, Grafe C, Kurzai O, Hunniger K, et al. Isoform localization of Dectin-1 regulates the signaling quality of anti-fungal immunity. *Eur J Immunol.* (2017) 47:848–59. doi: 10.1002/eji.201646849
6. Lui G, Lee N, Ip M, Choi KW, Tso YK, Lam E, et al. Cryptococcosis in apparently immunocompetent patients. *QJM.* (2006) 99:143–51. doi: 10.1093/qjmed/hcl014
7. Rajasingham R, Smith RM, Park BJ, Jarvis JN, Govender NP, Chiller TM, et al. Global burden of disease of HIV-associated cryptococcal meningitis: an updated analysis. *Lancet Infect Dis.* (2017) 17:873–81. doi: 10.1016/S1473-3099(17)30243-8
8. Denham ST, Brown JCS. Mechanisms of pulmonary escape and dissemination by cryptococcus neoformans. *J Fungi.* (2018) 4:E25. doi: 10.3390/jof4010025
9. Hammad H, Lambrecht BN. Barrier epithelial cells and the control of type 2 immunity. *Immunity.* (2015) 43:29–40. doi: 10.1016/j.immuni.2015.07.007
10. Kindermann M, Knipfer L, Atreya I, Wirtz S. ILC2s in infectious diseases and organ-specific fibrosis. *Semin Immunopathol.* (2018) 40:379–92. doi: 10.1007/s00281-018-0677-x
11. Roan F, Obata-Ninomiya K, Ziegler SF. Epithelial cell-derived cytokines: more than just signaling the alarm. *J Clin Invest.* (2019) 129:1441–51. doi: 10.1172/JCI124606
12. Kurowska-Stolarska M, Stolarski B, Kewin P, Murphy G, Corrigan CJ, Ying S, et al. IL-33 amplifies the polarization of alternatively activated macrophages that contribute to airway inflammation. *J Immunol.* (2009) 183:6469–77. doi: 10.4049/jimmunol.0901575
13. Kabata H, Moro K, Koyasu S. The group 2 innate lymphoid cell (ILC2) regulatory network and its underlying mechanisms. *Immunol Rev.* (2018) 286:37–52. doi: 10.1111/imr.12706
14. Mattner J, Wirtz S. Friend or foe? The ambiguous role of innate lymphoid cells in cancer development. *Trends Immunol.* (2017) 38:29–38. doi: 10.1016/j.it.2016.10.004
15. Flaczyk A, Duerr CU, Shourian M, Lafferty EI, Fritz JH, Qureshi ST. IL-33 signaling regulates innate and adaptive immunity to Cryptococcus neoformans. *J Immunol.* (2013) 191:2503–13. doi: 10.4049/jimmunol.1300426
16. Piehler D, Eschke M, Schulze B, Protschka M, Muller U, Grahnert A, et al. The IL-33 receptor (ST2) regulates early IL-13 production in fungus-induced allergic airway inflammation. *Mucosal Immunol.* (2016) 9:937–49. doi: 10.1038/mi.2015.106
17. Grahnert A, Richter T, Piehler D, Eschke M, Schulze B, Muller U, et al. IL-4 receptor-alpha-dependent control of Cryptococcus neoformans in the early phase of pulmonary infection. *PLoS ONE.* (2014) 9:e87341. doi: 10.1371/journal.pone.0087341
18. Muller U, Stenzel W, Kohler G, Werner C, Polte T, Hansen G, et al. IL-13 induces disease-promoting type 2 cytokines, alternatively activated macrophages and allergic inflammation during pulmonary infection of mice with Cryptococcus neoformans. *J Immunol.* (2007) 179:5367–77. doi: 10.4049/jimmunol.179.8.5367
19. Muller U, Stenzel W, Piehler D, Grahnert A, Protschka M, Kohler G, et al. Abrogation of IL-4 receptor-α-dependent alternatively activated macrophages is sufficient to confer resistance against pulmonary cryptococcosis despite an ongoing T(h)2 response. *Int Immunol.* (2013) 25:459–70. doi: 10.1093/intimm/dxt003
20. Stenzel W, Muller U, Kohler G, Heppner FL, Blessing M, McKenzie AN, et al. IL-4/IL-13-dependent alternative activation of macrophages but not microglial cells is associated with uncontrolled cerebral cryptococcosis. *Am J Pathol.* (2009) 174:486–96. doi: 10.2353/ajpath.2009.080598
21. Voelz K, Lammas DA, May RC. Cytokine signaling regulates the outcome of intracellular macrophage parasitism by Cryptococcus

neoformans. *Infect Immun.* (2009) 77:3450–7. doi: 10.1128/IAI.00297-09
22. Zhang Y, Wang F, Tompkins KC, McNamara A, Jain AV, Moore BB, et al. Robust Th1 and Th17 immunity supports pulmonary clearance but cannot prevent systemic dissemination of highly virulent Cryptococcus neoformans H99. *Am J Pathol.* (2009) 175:2489–500. doi: 10.2353/ajpath.2009.090530
23. Heyen L, Muller U, Siegemund S, Schulze B, Protschka M, Alber G, et al. Lung epithelium is the major source of IL-33 and is regulated by IL-33-dependent and IL-33-independent mechanisms in pulmonary cryptococcosis. *Pathog. Dis.* (2016) 74:ftw086. doi: 10.1093/femspd/ftw086
24. Alanio A, Desnos-Ollivier M, Dromer F. Dynamics of Cryptococcus neoformans-macrophage interactions reveal that fungal background influences outcome during cryptococcal meningoencephalitis in humans. *mBio.* (2011) 2:e00158-11. doi: 10.1128/mBio.00158-11
25. McHedlidze T, Kindermann M, Neves AT, Voehringer D, Neurath MF, Wirtz S. IL-27 suppresses type 2 immune responses *in vivo* via direct effects on group 2 innate lymphoid cells. *Mucosal Immunol.* (2016) 9:1384–94. doi: 10.1038/mi.2016.20
26. Omata Y, Frech M, Primbs T, Lucas S, Andreev D, Scholtysek C, et al. Group 2 innate lymphoid cells attenuate inflammatory arthritis and protect from bone destruction in mice. *Cell Rep.* (2018) 24:169–80. doi: 10.1016/j.celrep.2018.06.005
27. Knipfer L, Schulz-Kuhnt A, Kindermann M, Greif V, Symowski C, Voehringer D, et al. A CCL1/CCR8-dependent feed-forward mechanism drives ILC2 functions in type 2-mediated inflammation. *J Exp Med.* (2019) 216:2763–77. doi: 10.1084/jem.20182111
28. Schulz-Kuhnt A, Zundler S, Gruneboom A, Neufert C, Wirtz S, Neurath MF, et al. Advanced imaging of lung homing human lymphocytes in an experimental *in vivo* model of allergic inflammation based on light-sheet microscopy. *J. Vis. Exp.* (2019) 146:e59043. doi: 10.3791/59043
29. Murdock BJ, Huffnagle GB, Olszewski MA, Osterholzer JJ. Interleukin-17A enhances host defense against cryptococcal lung infection through effects mediated by leukocyte recruitment, activation, and gamma interferon production. *Infect Immun.* (2014) 82:937–48. doi: 10.1128/IAI.01477-13
30. Valdez PA, Vithayathil PJ, Janelsins BM, Shaffer AL, Williamson PR, Datta SK. Prostaglandin E2 suppresses antifungal immunity by inhibiting interferon regulatory factor 4 function and interleukin-17 expression in T cells. *Immunity.* (2012) 36:668–79. doi: 10.1016/j.immuni.2012.02.013
31. Nussbaum JC, Van Dyken SJ, von Moltke J, Cheng LE, Mohapatra A, Molofsky AB, et al. Type 2 innate lymphoid cells control eosinophil homeostasis. *Nature.* (2013) 502:245–8. doi: 10.1038/nature12526
32. Wiesner DL, Smith KD, Kashem SW, Bohjanen PR, Nielsen K. Different lymphocyte populations direct dichotomous eosinophil or neutrophil responses to pulmonary cryptococcus infection. *J Immunol.* (2017) 198:1627–37. doi: 10.4049/jimmunol.1600821
33. Hardison SE, Herrera G, Young ML, Hole CR, Wozniak KL, Wormley FL Jr. Protective immunity against pulmonary cryptococcosis is associated with STAT1-mediated classical macrophage activation. *J Immunol.* (2012) 189:4060–8. doi: 10.4049/jimmunol.1103455
34. Leopold Wager CM, Hole CR, Wozniak KL, Olszewski MA, Mueller M, Wormley FL Jr. STAT1 signaling within macrophages is required for antifungal activity against Cryptococcus neoformans. *Infect Immun.* (2015) 83:4513–27. doi: 10.1128/IAI.00935-15
35. Leopold Wager CM, Hole CR, Wozniak KL, Olszewski MA, Wormley FL Jr. STAT1 signaling is essential for protection against Cryptococcus neoformans infection in mice. *J Immunol.* (2014) 193:4060–71. doi: 10.4049/jimmunol.1400318
36. Leopold Wager CM, Wormley FL Jr. Classical versus alternative macrophage activation: the Ying and the Yang in host defense against pulmonary fungal infections. *Mucosal Immunol.* (2014) 7:1023–35. doi: 10.1038/mi.2014.65
37. Piehler D, Grahnert A, Eschke M, Richter T, Kohler G, Stenzel W, et al. T1/ST2 promotes T helper 2 cell activation and polyfunctionality in bronchopulmonary mycosis. *Mucosal Immunol.* (2013) 6:405–14. doi: 10.1038/mi.2012.84
38. Halim TYF, Rana BMJ, Walker JA, Kerscher B, Knolle MD, Jolin HE, et al. Tissue-restricted adaptive type 2 immunity is orchestrated by expression of the costimulatory molecule OX40L on group 2 innate lymphoid cells. *Immunity.* (2018) 48:1195–1207.e96. doi: 10.1016/j.immuni.2018.05.003
39. Yang XO, Pappu BP, Nurieva R, Akimzhanov A, Kang HS, Chung Y, et al. T helper 17 lineage differentiation is programmed by orphan nuclear receptors ROR alpha and ROR gamma. *Immunity.* (2008) 28:29–39. doi: 10.1016/j.immuni.2007.11.016
40. Szymczak WA, Sellers RS, Pirofski LA. IL-23 dampens the allergic response to Cryptococcus neoformans through IL-17-independent and -dependent mechanisms. *Am J Pathol.* (2012) 180:1547–59. doi: 10.1016/j.ajpath.2011.12.038
41. Hardison SE, Wozniak KL, Kolls JK, Wormley FL Jr. Interleukin-17 is not required for classical macrophage activation in a pulmonary mouse model of Cryptococcus neoformans infection. *Infect Immun.* (2010) 78:5341–51. doi: 10.1128/IAI.00845-10
42. Wozniak KL, Hardison SE, Kolls JK, Wormley FL. Role of IL-17A on resolution of pulmonary *C. neoformans infection PLoS ONE.* (2011) 6:e17204. doi: 10.1371/journal.pone.0017204
43. Feldmesser M, Casadevall A, Kress Y, Spira G, Orlofsky A. Eosinophil-Cryptococcus neoformans interactions *in vivo* and *in vitro*. *Infect Immun.* (1997) 65:1899–907. doi: 10.1128/IAI.65.5.1899-1907.1997
44. Huffnagle GB, Boyd MB, Street NE, Lipscomb MF. IL-5 is required for eosinophil recruitment, crystal deposition, and mononuclear cell recruitment during a pulmonary Cryptococcus neoformans infection in genetically susceptible mice (C57BL/6). *J Immunol.* (1998) 160:2393–400.
45. Marwaha RK, Trehan A, Jayashree K, Vasishta RK. Hypereosinophilia in disseminated cryptococcal disease. *Pediatr Infect Dis J.* (1995) 14:1102–3. doi: 10.1097/00006454-199512000-00015
46. Piehler D, Stenzel W, Grahnert A, Held J, Richter L, Kohler G, et al. Eosinophils contribute to IL-4 production and shape the T-helper cytokine profile and inflammatory response in pulmonary cryptococcosis. *Am J Pathol.* (2011) 179:733–44. doi: 10.1016/j.ajpath.2011.04.025
47. Muller U, Stenzel W, Kohler G, Polte T, Blessing M, Mann A, et al. A gene-dosage effect for interleukin-4 receptor alpha-chain expression has an impact on Th2-mediated allergic inflammation during bronchopulmonary mycosis. *J Infect Dis.* (2008) 198:1714–21. doi: 10.1086/593068
48. Pelly VS, Kannan Y, Coomes SM, Entwistle LJ, Ruckerl D, Seddon B, et al. IL-4-producing ILC2s are required for the differentiation of TH2 cells following Heligmosomoides polygyrus infection. *Mucosal Immunol.* (2016) 9:1407–17. doi: 10.1038/mi.2016.4
49. Gordon S, Martinez FO. Alternative activation of macrophages: mechanism and functions. *Immunity.* (2010) 32:593–604. doi: 10.1016/j.immuni.2010.05.007
50. Neill DR, Wong SH, Bellosi A, Flynn RJ, Daly M, Langford TK, et al. Nuocytes represent a new innate effector leukocyte that mediates type-2 immunity. *Nature.* (2010) 464:1367–70. doi: 10.1038/nature08900
51. Chou SJ, Babot Z, Leingartner A, Studer M, Nakagawa Y, O'Leary DD. Geniculocortical input drives genetic distinctions between primary and higher-order visual areas. *Science.* (2013) 340:1239–42. doi: 10.1126/science.1232806
52. Madisen L, Zwingman TA, Sunkin SM, Oh SW, Zariwala HA, Gu H, et al. A robust and high-throughput Cre reporting and characterization system for the whole mouse brain. *Nat Neurosci.* (2010) 13:133–40. doi: 10.1038/nn.2467
53. Mohrs M, Shinkai K, Mohrs K, Locksley RM. Analysis of type 2 immunity in vivo with a bicistronic IL-4 reporter. *Immunity.* (2001) 15:303–11. doi: 10.1016/S1074-7613(01)00186-8
54. McHedlidze T, Waldner M, Zopf S, Walker J, Rankin AL, Schuchmann M, et al. Interleukin-33-dependent innate lymphoid cells mediate hepatic fibrosis. *Immunity.* (2013) 39:357–71. doi: 10.1016/j.immuni.2013.07.018

Conflict of Interest: The authors declare that the research was conducted in the absence of any commercial or financial relationships that could be construed as a potential conflict of interest.

frontiers in Immunology

REVIEW
published: 28 February 2020
doi: 10.3389/fimmu.2020.00315

Myeloid Cell-Mediated Trained Innate Immunity in Mucosal AIDS Vaccine Development

Yongjun Sui and Jay A. Berzofsky**

Vaccine Branch, National Cancer Institute, National Institutes of Health (NIH), Bethesda, MD, United States

Trained innate immunity has recently emerged as a novel concept of innate immune cells, such as myeloid cells, exhibiting immune memory, and nonspecific heterologous immunity to protect against infections. The memory and specificity are mediated by epigenetic, metabolic, and functional reprogramming of the myeloid cells and myeloid progenitors (and/or NK cells) in the bone marrow and peripheral tissues such as gut and lung mucosa. A variety of agents, such as BCG, viruses, and their components, as well as TLR agonists, and cytokines have been shown to be involved in the induction of trained immunity. Since these agents have been widely used in AIDS vaccine development as antigen delivery vectors or adjuvants, myeloid cell mediated trained immunity might also play an important role in protecting against mucosal AIDS virus transmission or in control of virus replication in the major gut mucosal reservoir. Here we review the trained innate immunity induced by these vectors/adjuvants that have been used in AIDS vaccine studies and discuss their role in mucosal vaccine efficacy and possible utilization in AIDS vaccine development. Delineating the protective effect of the trained innate immunity mediated by myeloid cells will guide the design of novel AIDS vaccines.

Keywords: trained innate immunity, vaccinia virus, TLR ligands, IL-1, interferon, hematopoietic stem cell and progenitor cells

OPEN ACCESS

Edited by:
Maria Leite-de-Moraes, INSERM U1151 Institut Necker Enfants Malades Centre de Médecine Moléculaire (INEM), France

Reviewed by:
Mihai Netea, Radboud University Nijmegen, Netherlands
Suraj Sable, Centers for Disease Control and Prevention, United States

****Correspondence:***
Yongjun Sui
suiy@mail.nih.gov
Jay A. Berzofsky
berzofsj@mail.nih.gov

Specialty section:
This article was submitted to Molecular Innate Immunity, a section of the journal Frontiers in Immunology

Received: *17 December 2019*
Accepted: *07 February 2020*
Published: *28 February 2020*

Citation:
Sui Y and Berzofsky JA (2020) Myeloid Cell-Mediated Trained Innate Immunity in Mucosal AIDS Vaccine Development. Front. Immunol. 11:315. doi: 10.3389/fimmu.2020.00315

Trained immunity is a novel concept that innate immune cells, such as monocytes/macrophages, have certain level of immune "memory" properties to respond to second stimulations. Bacterial, fungal, and viral components, as well as cytokines and TLR agonists have the potential to induce trained immunity. Innate immune cells, after stimulation with these stimulants, can display long-term changes in their functional programs. This can be achieved through epigenetic or metabolic programming of the innate cells (1, 2). When they encounter a second stimulation, the trained innate cells produced either an increased level of cytokines/chemokines, or decreased level of immune mediators, which constitutes the two opposite programs of the trained immunity: namely, training and tolerance programs. Though there are still conflicting opinions on whether these changes can be accounted as true immune "memory," nevertheless, these changes can be maintained for a long period of time and can mediate protection or lead to auto-inflammatory diseases upon secondary stimulation. In this context, it should be noted that analogous epigenetic changes are also mediators of memory states in T lymphocytes at an individual cell level (3, 4). Thus, while innate cells do not have antigen-specific clones as do T and B cells that can undergo expansion to mediate memory at a population level, they are just as capable of epigenetic and metabolic changes at the individual cell level as lymphocytes to maintain a memory-cell state (**Figure 1**). Therefore, it should not be so surprising to see this type of memory state in innate cells like monocytes.

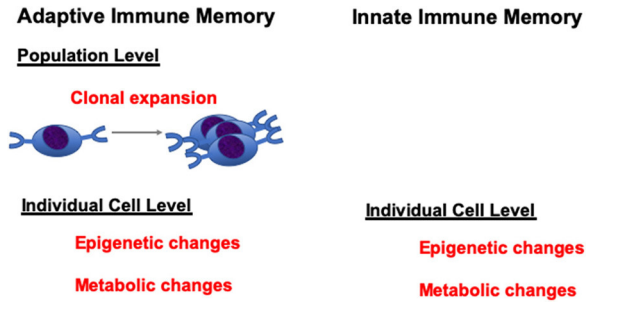

FIGURE 1 | Adaptive vs. innate immune memory.

Epigenetic and metabolic pathways are the substrates of trained immunity. The fungal product β-glucan, which provided the first evidence of trained immunity in vertebrates, induced stable and genome-wide changes in histone methylation by increasing the trimethylation of H3K4me3 of many genes including TNFα and IL-6 (5). The induced epigenetic program could be maintained for a long period of time and led to enhanced gene transcription upon the second challenges. Trained immunity was also found linked to metabolic pathways. Glycolysis, glutaminolysis, and the cholesterol synthesis pathway are essential for β-glucan-induced trained immunity (6, 7). Upregulation of glycolysis is required during immune cell activation (activated T cells and proinflammatory macrophages). Though less efficient, glycolysis generates faster production of ATP, which provides energy for cell activation in a timely fashion. Furthermore, epigenetic and metabolic pathways are interconnected. After priming with β-glucan, genes that are involved in glycolysis were epigenetically upregulated (8).

Developing an HIV vaccine is the ultimate solution to curtail the HIV pandemic. However, this remains a big challenge as only one out of six phase III HIV vaccine clinical trials showed efficacy to date (9, 10). Most HIV vaccine platforms include a complex regimen of viral vectors and adjuvants, which have the potential to induce trained immunity (**Figure 2**). Viral vectors, such as poxviral vectors, induce trained immunity. Trained immunity memory can also be generated directly by TLR ligands, or indirectly by IL-1 (promoted by alum adjuvant) and interferons (induced by TLR ligands or produced by vaccine-activated cells). Other diet factors or microbiota can affect the trained innate immunity as well. Trained immunity is especially important and may be helpful when effective HIV vaccines are currently not available. Here, we review data on trained immunity induced by these components in myeloid cells and discuss their possible involvement in mediating the vaccine efficacy of the previous published HIV vaccine studies. We also consider the possible utilization of trained immunity in future HIV vaccine development.

POXVIRUS-MEDIATED INDUCTION OF TRAINED IMMUNITY

As attenuated recombinant poxvirus vectors are safe and highly immunogenic against expressed foreign genes, they constitute excellent HIV/AIDS vaccine candidates (11). Aventis Pasteur live recombinant canarypox vector (ALVAC), modified Vaccinia Ankara (MVA), NYVAC and fowlpox are widely studied HIV poxvirus vectors (12). In the only HIV vaccine trial (RV144 trial) that showed efficacy (only 31%), four injections of recombinant HIV-ALVAC, and two injections of AIDSVAX B/E gp120 in alum were administrated (9). A later study found that the non-neutralizing IgG antibody responses against the V1V2 region of the envelope were correlated inversely with risk (13). However, several passive adoptive transfer studies with non-neutralizing anti-envelope antibodies in the macaque models failed to mediate protection (14–17). This raised the question whether there were other mechanisms involved. Trained immunity is one of the potential mechanisms.

Epidemiologic and experimental data showed that poxvirus itself could induce trained immunity. Smallpox vaccine, vaccinia, used to be a routine immunization until smallpox was eradicated in 1977. Several observational studies reported that immunization with vaccinia vaccine reduced the overall mortality in adults of Guinea-Bissau and Denmark (18–20). A sex bias was found in one of the studies with a stronger effect in females (18). Moreover, an inverse association of risk of non-Hodgkin lymphoma and melanoma was found with previous vaccinations with smallpox (21, 22). This non-specific protective effect suggested that vaccinia might induce trained immunity to mediate protection against other infectious diseases and cancers. Scherer et al. compared the gene expression pattern of human peripheral blood mononuclear cells following Aventis Pasteur smallpox vaccine (23). They found that smallpox vaccine upregulated genes associated monocytes or macrophages. A surprising number of genes, including IL-8 and IL-18, exhibited significant changes even 50–60 days post vaccination, supporting the induction of trained immunity (23). Similarly, monocyte and macrophages from vaccinia infected mice produced more TNF and IL-6 after being re-stimulated *in vitro* with HSV-infected cells, further suggesting training programs of trained immunity might be induced by vaccinia (24).

Recently, we and others found evidence that myeloid cell-mediated trained immunity might be involved in mediating protection using similar immunization protocols like RV144 in macaque models (25–27). Vaccari et al. found that hypoxia and inflammasome activation in CD14+CD16– monocytes are correlates of decreased risk of SIV acquisition after vaccination with DNA/ALVAC/gp120 platform in macaques (25, 27). We demonstrated in the macaques vaccinated with MVA/FLSC (full-length single chain recombinant gp120 fused with two domains of CD4 to maintain the CD4-induced conformation) with complex adjuvants that reduced infection risk was achieved in the absence of protective antibody responses against HIV envelope (26). The protection correlated with CD14+DR- monocytes induced by the vaccine; but not the viral-specific T cell responses induced by the vaccine. We proved that trained immunity was induced by re-exposing the monocytes *ex vivo* with challenge SHIV virus to mimic the *in vivo* scenario. The monocytes from vaccinated animals produced higher amounts of TNFα, IL-6, and MIP1α than those from the naïve animals upon re-stimulation with virus. Interestingly, the increased production

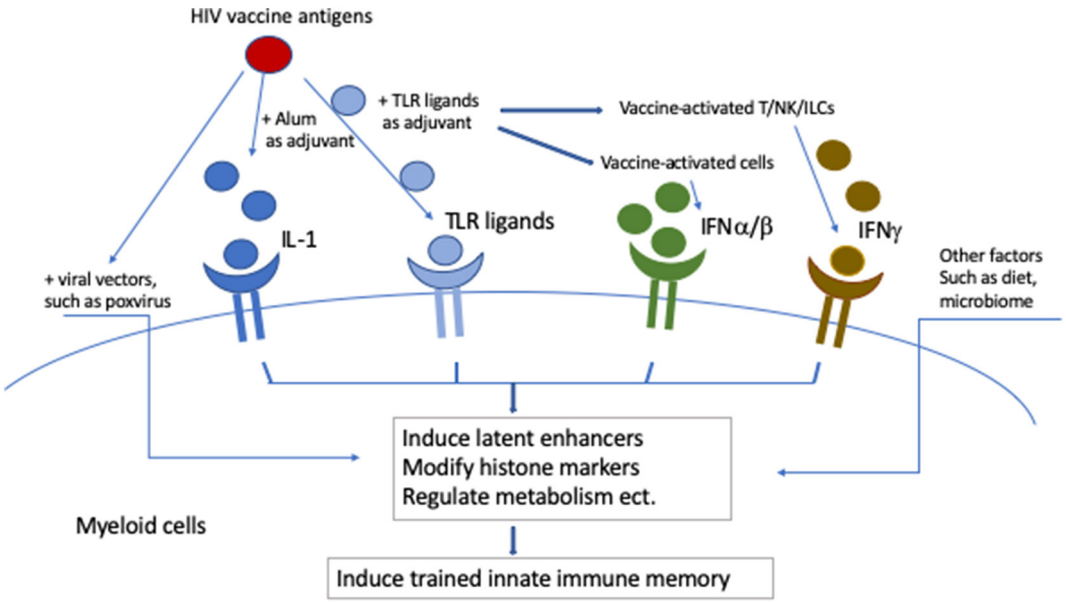

FIGURE 2 | Potential induction of trained innate immunity by complex HIV vaccines. Viral vectors, such as poxviral vectors, induce trained immunity. Trained immunity memory can also be generated directly by TLR ligands, or indirectly by IL-1 (promoted by alum adjuvant) and interferons (induced by TLR ligands or produced by vaccine activated cells). Other diet factors or microbiota can affect the trained innate immunity as well.

of cytokines/chemokine also correlated with *in vivo* challenge outcome, suggesting that trained immunity mediated protective efficacy. Since the interval between the last boost and first challenge was 8 weeks, we believe that trained immunity was induced and mediated protection in this RV144-like trial. However, since we have included multiple components in the vaccine, in this study we cannot dissect the mechanism of induced trained immunity to attribute it to MVA or TLR 2, 3, 9 agonists, IL-15 and mLT, or the combination. Further study is required to delineate the mechanisms.

Notably, different poxvirus vectors induced different innate immune profiles, which makes the interpretation of HIV vaccine studies difficult. One study found that after administrating ALVAC, MVA, and NYVAC poxvirus vaccine vectors to macaques, ALVAC induced a very different proinflammatory cytokine/chemokine profile from MVA and NYVAC, characterized by a higher induction of proinflammatory and IFN-related antiviral cytokines and chemokines at day 1 post vaccination (28). Furthermore, the stimulatory phenotypes were all reduced when the animals were re-exposed to these poxvirus vectors (28). Previous reports found that MVA induced stronger IFN-stimulated genes, while NYVAC promoted proinflammatory genes after infection in HeLa cells (29, 30). These differences might lead to potentially different biological effects, though it remains unknown to what extent these induced innate immune profiles contributed to vaccine efficacy. Nevertheless, the different innate immune responses induced by these vectors can potentially influence adaptive immunity, as well as trained immunity. Since not all trained immunity contributes to protection, studies to identify the distinct trained innate immunity profile which contributes to HIV/SIV vaccine efficacy are needed. This will facilitate the interpretation of vaccine results, and the manipulation of the reagents to induce protective trained immunity in future HIV/AIDS vaccine development.

ADJUVANT-, TOLL-LIKE RECEPTOR (TLR) AGONIST- AND CYTOKINE-MEDIATED INDUCTION OF TRAINED IMMUNITY

Both Toll-like receptor (TLR) agonists and cytokines have been widely used adjuvants in HIV/SIV vaccine development. Accumulating data from *in vivo* and *in vitro* studies support the notion that these adjuvants not only enhanced the antigen-specific T cell and B cell responses, but also induced trained immunity by imprinting the innate immune cells with epigenetic and metabolic modifications, which resulted in enhanced or decreased responses upon re-stimulation.

TLRs, type I transmembrane proteins, belonging to the pattern recognition receptor family, are expressed on the innate immune cells. Once engaged by their distinct ligands, TLRs activate innate immune cells, and participate in the initiation of adaptive immune responses (31). As adjuvants, TLR agonists enhanced the potency of vaccine-induced adaptive immunity. Ten TLRs have been identified in humans, and most of them, such as TLR, 2, 3, 4, 7, 8, and 9 agonists, have been tested as adjuvants in HIV/SIV vaccine studies (26, 32–36). In these studies, TLR agonists promoted efficient vaccine antigen delivery, induced more pronounced cell activation, and increased T follicular helper cell differentiation and germinal center formation, which led to stronger antigen-specific T cell and antibody immune responses.

Recent literature suggested that TLR agonists and cytokines also modulate the functional programming of monocytes/macrophages and render them "memory" properties for protection. One molecular mechanism of retaining the memory in myeloid cells was shown to be through the emergence of latent enhancers, which are the genomic regulatory elements unbound by transcriptional factors and unmarked in unstimulated cells (37). Upon activation with TLR agonists or cytokines, latent enhancers were induced, in addition to the activation or repression of the pre-existing poised enhancers. Interestingly, after washout of the stimuli, most of the enhancers returned to normal states, whereas a large fraction of latent enhancers remained stably epigenetically marked to keep the "memory" of the first stimulation. Specifically, selective retention of H3K4mel upon signal termination resulted in a faster and stronger responses upon re-stimulation (37). The complex repertoire of latent enhancers induced by various TLR agonists, including TLR, 2, 4, and 9, and cytokines such as IL-4, IFNγ, IL-1β, TNFα, and TGFβ have been uncovered (37). Each TLR agonist and cytokine stimulated a distinct repertoire of latent enhancers, which was considered as the epigenomic footprint of the stimulus (37).

Interestingly, the dose of the stimulation also determines the types of response. In the well-studied lipopolysaccharide (LPS) stimulation experiments, the concentration of LPS governed whether tolerance or priming of the monocytes was induced (38). LPS exposure induced several types of epigenetic modifications, including two gene-specific chromatin modifications that associated with silencing of pro-inflammatory mediators, or priming of antimicrobial effectors, which were the molecular mechanisms of tolerance and training (39). Similarly, *in vitro* exposure to other TLR agonists such as Pam3CSK4, Flagellin, polyIC, R848, and CpG, as well as NLR agonists TriDAp or MDP also altered the functional fates of monocytes and induced two opposing functional programs based on the nature and concentration of the agonists (40). High concentrations of the TLR agonists induced tolerance with the exception of CpG (for which tolerance is inherent at any dose), while low concentrations of TLR agonists generally abolished the tolerance and induced training of the monocytes. This led to a diminished or enhanced production of the cytokine/chemokine upon second stimulation (40). Mechanistically, the trained immunity in the monocytes induced by TLR agonists was dependent on histone methylation and acetylation (40).

Some viral vectors, such as vaccinia virus, have been demonstrated to be directly sensed by TLRs as well. Some reported that vaccinia virion was recognized by TLR2 (41–44), while the others found that TLR2 was not involved at all (45). Differences in effects may reflect differential pairing of TLR2 with TLR1 or TLR6. Specifically, TLR2/6 has been shown to mediate the innate immune sensing of MVA in macrophages to produce chemokines, IFNβ and IL-1β (42). In this respect, viral vectors can induce trained immunity by indirectly working through TLRs.

It worth mentioning that TLRs in collaboration with other innate receptors such as Nod-like receptors (NLRs), and C-type lectin receptors (CLRs) can shape innate/adaptive and maybe trained immunity, and some of the effects of adjuvants are not through TLRs, but through CLRs and NLRs (46–48).

Cytokines participate in the induction of trained immunity to potentially impact vaccine efficacy in several ways. First, cytokines can directly induce trained immunity. Cytokines such as TNFα, IL-4, IFNγ, or TGFβ induced latent enhancers, which were epigenetically modified after encounter with cytokines (37). Upon second stimulation, these cytokine-modified latent enhancers responded either more slowly or more quickly than the non-modified enhancers, which resulted in enhanced or decreased production of the gene products (37). Secondly, cytokines can be induced indirectly by other adjuvants. For example, alum, an adjuvant widely used in HIV and other vaccine development, induces the production of IL-1. IL-1 is one of the key components mediating the induction of trained immunity (49). As mentioned before, IL-1β induced trained immunity itself. Human monocytes treated with IL-1β *in vitro* had the potential to express high levels of TNFα and IL-6 upon re-stimulation (49, 50). The training was accomplished by the epigenetic modification of the promoter regions of TNFα, IL-6, and IL-1β (50). Furthermore, IL-1 was involved in the induction of trained immunity through modulation of metabolic pathways. Cheng et al. demonstrated that a complicated metabolic pathway shift led to the induction of trained immunity, where IL-1 and hypoxia-inducible factor 1α (HIF1α) were involved (8). Human monocytes treated with beta-glucan displayed a core metabolic shift from oxidative phosphorylation to aerobic glycolysis. This shift was mediated by the AKT/mTOR/ HIF1α pathway, and gene knock-out experiments showed that HIF1α is essential for the process. HIF1 is a heterodimeric transcription factor composed of HIF1α and HIF1β subunits, which regulate over 70 genes responding to hypoxia (51). HIF1β is constitutively expressed, while the expression of HIF1α is tightly regulated by O_2 concentration. Since the promoter region of IL-1β contains several binding sites of HIF1α, HIF1α can directly target the IL-1β gene (52, 53). Similarly, in the LPS-induced IL-1β production, LPS-treated macrophages increased the expression levels of succinate, which acted as a metabolite in innate immune signaling, and which then stabilized HIF1α. IL-1β, as a target of HIF1α, was induced after exposure to LPS (53). On the other hand, IL-1β can induce HIF1α under normoxic conditions via NF-κB/COX2 pathway (54). Altogether, accumulating evidence showed that high IL-1β level, possibly as a inducer or as a mediator of trained immunity, plays an important role in protecting against bacteria, candida and viral infections (55–58).

Another group of cytokines, which are widely induced by most vaccines, including HIV vaccines, are interferons (IFNs). During vaccination, IFNα/β are usually induced at the early stages, while IFNγ, mainly produced by vaccine-activated T cells, NK cells, and NKT cells, is produced at the later stages. IFNs are classified into three groups, Type I (IFNα/β), II(IFNγ), and III IFNs (IFN-λ), based on the structure of their receptors. IFNs, especially IFNγ, turned out to have much broader effects on both arms of the immune system than most of the cytokines (59). They have strong antiviral activity and have been widely used to treat viral infections (60). Different IFNs, used as adjuvants, have been

reported to induce distinct pathways to enhance the efficacy of vaccines (61).

Recent data suggested that exposure of monocytes/macrophages to IFNs leads to the induction of innate trained memory. IFNs induce chromatin remodeling, and lead to the demonstration of an "interferon epigenomic signature" in the treated monocyte/macrophages, which includes activation of latent enhancers, modulation of histone markers, regulation of chromatin accessibility, and alteration of enhancers and promotors (37, 62–68). For example, IFNβ induced epigenetic memory in fibroblasts and bone marrow-derived macrophages. Kamada et al. showed that IFNβ treatment led to faster and greater transcription of IFN-stimulated genes upon re-stimulation. This was achieved through accelerated recruitment of RNA polymerase II and phospho-STAT1 and coincided with histone H3.3 and H3K36 modifications. On the other hands, IFNγ was originally identified as "macrophage activating factor" and can polarize macrophages by modifying chromatin to reprogram transcriptional landscapes, which confer innate immunity to macrophages (69).

IFNs also interacted with TLR ligands to modulate immune responses. After stimulation with IFNγ and TLR ligands, human macrophages showed strong synergistic activation of inflammatory cytokine production, which was due to sustained occupancy of STAT1, IRF-1, and associated histone acetylation at promoter and enhancer regions of TNF and IL6 loci (63). IFNs have been observed to abrogate tolerance, which was induced by previously exposure to TLR ligands in macrophages (62). Furthermore, type I interferons cooperatively altered chromatin states of the macrophages with other cytokine such as TNF to induce transcriptional cascades to prevent the silencing of genes induced by TLR4 (67).

OTHER ADJUVANTS AND VECTORS: ADENOVIRUS-VECTORED VACCINE AND AIDS VIRUSES THEMSELVES

Recombinant attenuated adenovirus vectors, described as ideal platforms for vaccine delivery vectors, have been widely used in HIV/SIV clinical and experimental vaccine development. These vectors are safe, highly immunogenic, and able to express large amounts of antigens (70). However, two phase IIb clinical trials to evaluate the Merck human adenovirus serotype-5 vector expressing HIV gag/pol/nef did not demonstrate a decrease in HIV acquisition (71–74). To make matters worse, the STEP trial showed that the vaccination was associated with enhanced susceptibility to HIV infection in uncircumcised adenovirus serotype-5 seropositive men (71). The possibility that vaccination with adenovirus vector increased mucosal T cell activation was confirmed in some of the macaque studies (75), but not in others (76). Based on the recent finding that adenovirus can also induce trained immunity, it is tempting to hypothesize that trained immunity might affect the efficacy of these clinical trials. The fact that the enhanced HIV susceptibility occurred in adenovirus serotype-5 seropositive men indicated that these persons had been exposed to adenovirus 5 before. Whether the exposures to adenovirus led to the induction of trained immunity and/or epigenetic or metabolic modifications of innate cells such as myeloid cells are open questions, and worth investigation.

In addition, we recently found that a live attenuated AIDS virus, SHIV, could protect against intrarectal challenge with SIV in the absence of anti-envelope antibodies, through a mechanism involving trained innate immunity (77). The protection was also independent of CD8 T cells induced by the vaccine, as shown by CD8 T-cell depletion studies. Rather, epigenetic changes were detected in monocytes that may mediate such trained innate immunity. Thus, even AIDS viruses themselves can induce trained innate immunity.

TRAINED IMMUNITY MEMORY

Trained immunity memory has been defined as increased or decreased responsiveness to a secondary stimulation by innate immune cells. The short life span of these cells challenged the notion of long-term maintenance of trained immunity memory by matured innate cells. For example, in the cases of Bacillus Calmette-Guérin (BCG) vaccination, the epigenetic signature of innate cells lasts for up to 1 year (78). Thus, immune progenitor cells must be involved. Indeed, two recent studies found that hematopoietic stem cell (HSC) and progenitor cells (HPC) in the bone marrow were modulated with altered epigenetic landscapes and transcriptional profiles, which confer the memory properties for the trained immunity (79, 80). Kaufman et al. showed that BCG promoted myelopoiesis at the expense of lymphopoiesis, and altered the transcriptional profiles of HSC and HPC (79). Mitroulis et al. demonstrated that administration of fungal cell wall component β-glucan to mice led to expansion of myeloid progenitor cells, metabolic adaptions in glycolysis and cholesterol biosynthesis (80). In both studies, the trained immunity-induced myelopoiesis contributed to protection against M. tuberculosis infection or chemotherapy-induced DNA damage and cell death (79, 80). Similarly, Christ et al. revealed that a cholesterol-rich diet had persistent effects on the myeloid progenitor cells, which were epigenetically and transcriptional reprogrammed. The trained myeloid progenitor cells maintained these phenotypes for a long period of time. The shift back to normal chow diet did not change the augmented pro-inflammatory immune responses in macrophages, which were supposedly the offspring of trained myeloid progenitor cells (81).

Though it is still not fully understood, the training of the HSC and HPC could be through the TLRs expressed on these cells. Long-term HSC and HPC subsets express TLR2 and TLR4, and thus can directly respond to the agonists to drive their differentiation toward myeloid cells (82). *In vitro* and *in vivo* stimulation of HSC/HPC with Pam3CSK4 or LPS led to myeloid differentiation (82–84). Moreover, direct exposure of human and mouse HSC/HPC to TLR1/2 agonist Pam3CSK4 led to the generation of macrophages that produced lower levels of inflammatory cytokines, and reactive oxygen species (85). Further studies demonstrated

that the duration and the doses of the stimulation also played an important role to determine the nature of the responses. Short-term *in vivo* treatment with Pam3CSK4 led to a tolerance phenotype of *ex vivo* HSC/HPC-derived macrophages, whereas extended stimulation resulted in a trained phenotype. On the other hand, during the early stage of candidiasis infection, HSC/HPC differentiated to trained macrophages, while during the high candidiasis burden stage, HSC/HPC-derived macrophages was tolerized. Pam3CSK4-induced protection against candidiasis infection was abolished after HSC/HPC depletion, suggesting that the trained immunity memory was induced and maintained in the HSC/HPC population (86).

To develop a mucosal HIV/SIV vaccine, TLR2/6 agonist FSL-1 and MVA have been used as an adjuvant/delivery vector (26, 32). It is interesting to investigate the functionality of the monocyte/macrophages differentiated from FSL-1-primed HSC/HPC, especially when the signaling pathways through TLR1/2 and TLR2/6 had opposite roles to either silence or boost the immune responses (85).

Some long-lived tissue macrophages can maintain trained immunity memory. Respiratory viral infection induced trained immunity in alveolar macrophages, which mediated protection against bacterial infection with *Streptococcus pneumoniae*. The induction and maintenance of the memory was independent of monocyte or bone marrow progenitors (87).

Innate-like lymphocytes, which are present mainly in the mucosal surfaces and skin, also demonstrated immune memory (88). For example, Aspergillus protease-exposed Innate-lymphoid cell types 2 (ILC2) had a more vigorous cytokine production upon the re-challenge with papain (89). Moreover, NK and NK-like cells, as well as γδT cells from BCG-vaccinated individuals, produced more IFNγ (90). NKG2C^{+} NK cells have been reported to recognize HCMV-encoded UL40 peptides and to control the expansion and differentiation of adaptive NKG2C+ NK cells (91). NK cell mediated trained immunity memory has been recently reviewed (92), and will not be further discussed here.

Non-hematopoietic cells, like epithelial cells, can have memory to a previous contact with pathogen compounds (93). Pre-exposure of respiratory epithelia cells to Pseudomonas aeruginosa flagellin reduced or exacerbated inflammatory responses to a second non-related pathogen or LPS stimulation. By using histone acetyltransferase and methyltransferase inhibitors, the authors demonstrated that this was through epigenetic modifications.

OTHER FACTOR-INDUCED TRAINED IMMUNITY

To add an additional level of the complexity, other factors such as western diet (81, 94, 95), insulin (96), and microbiome, which have the potential to induce trained immunity, might also influence vaccine efficacy. To correctly interpret the immune correlates of protection for HIV/SIV vaccines, the contribution of trained immunity induced by these host factors needs to be taken into consideration.

Western-type diets (WDs) often include high calorically rich food that is lacking fiber, vitamins, and minerals. Long-term consumption of WDs can promote the activation of the immune system. While immune activation is the most important parameter to predict the susceptibility to HIV infection, recent studies also showed that WDs can alter *in vivo* LPS responses, and thus induce or alter trained innate immunity in monocyte/macrophages via NLRP3 (81, 95).

It has been known that trained immunity can be induced by endogenous metabolic products such as oxidized low-density lipoprotein (oxLDL), glucose glycylation end products, or fatty acids. For example, brief exposure of human monocytes to oxidized low-density lipoprotein (oxLDL) resulted in increased production of proinflammatory cytokines upon re-stimulation (97). This has been accomplished through trimethylation of lysine 4 at histone 3 (H3K4me3) in promoter regions of TNFα, IL-6, IL-18, the Matrix Metalloproteinase genes MMP2, MMP9, and the scavenger receptor CD36. Further study identified that ROS production, which was dependent on the AKT/mTOR signaling pathway, controlled the oxLDL-induced trained innate immunity phenotype (98).

Similarly, sustained activation of the AKT/mTOR signaling pathway leads to glycolysis in insulin resistance. Hyperglycemia facilitated sustained NF-κB gene activity due to increased H3K4 and reduced H3K9 methylation (99). Basal mTORC1 activity in the insulin-resistant macrophages was high. The macrophages showed an M2-like phenotype, and reduced their responses to LPS (100). Dietary changes also impact the gut microbiome, which has been shown to be associated with immune activation as well as HIV/SIV vaccine efficacy and susceptibility to infection (26, 101). In this context, western diet, or insulin signaling/insulin resistance signals have been viewed as modulators of trained immunity (98, 100, 102). Overall, various populations around the world might have potentially different responses to vaccines as they have different genetic backgrounds, diets, and microbiomes, which can affect innate and trained immunity.

HARNESSING THE POWER OF TRAINED IMMUNITY FOR AIDS VACCINE DEVELOPMENT

The delivery modality for HIV vaccines is critical for vaccine efficacy. A large variety of delivery vectors and adjuvants have been used in AIDS vaccine development in either macaque models or human clinical trials. Among them, a large proportion demonstrated the ability to induce trained innate immunity, which means that they can impact the vaccine efficacy in a much longer time frame than we have thought before. **Tables 1**, **2** summarize the delivery vectors and adjuvants that have shown evidence (**Table 1**) or have the potential (**Table 2**) to induce trained immunity in experimental HIV/AIDS vaccines. Moreover, the hosts might have pre-induced trained immunity by factors such

TABLE 1 | The vector/adjuvant combinations found to induce trained immunity in experimental HIV/AIDS vaccines.

Delivery vectors and adjuvants	Induced innate/trained immunity	Target cells involved	Associations with challenge outcomes	Minimum duration	Viral-specific adaptive immunity correlated	References
MVA/TLR agonists/IL-15	APOBEC3G	mDC	Inverse correlation with set-point SIVmac251 viral loads	7 weeks	T cell-responses	(32)
ALVAC/DNA-SIV/alum	Hypoxia and the inflammasome	CD14+CD16- monocytes	Correlation with decreased risk of SIVmac251 acquisition	4 weeks	Anti-env antibody responses	(25, 27)
MVA/TLR agonists/IL-15/mLT	TNFα, IL-6, and MIP1α	Myeloid cells	Correlation with reduced viral Gag expression and *in vivo* viral acquisition	7 weeks	No T & antibody responses	(26)

TABLE 2 | Adjuvants or vectors that have the potential to induce trained immunity in experimental HIV/AIDS vaccines.

Delivery vectors and adjuvants	Induced innate immunity	Sample	Associations with	Measurement time	References
TLR7/8 and 9 agonists	CXCL10	Plasma		Peak at 24 h, return to base level 1 week later	(34)
TLR7/8 agonist:R848		DC	Increased T cell responses		(35)
TLR4 and TLR7/8 agonists	Transcriptional profiling similar to live attenuated yellow fever vaccine	PBMC/monocyte	Anti-env antibody responses	24–96 h post immunization	(36)
ALVAC/MVA/NYVAC	Proinflammatory and antiviral cytokine/chemokine	Serum/PBMC		0–14 days post immunization	(28)

as diet, exposure history to other pathogens, and metabolic disorders. From these data one can speculate that trained innate immunity opens a new window for future HIV vaccine development: to design a novel HIV vaccine that combines the classical adaptive immunity as well as the protective trained immunity to mediate better protection than either one alone.

The concept of incorporation of protective trained immunity in HIV vaccine development is intriguing; however, it is far from being fully understood. Trained immunity induced by different stimuli or vaccinations might have these limitations: intermediate duration, non-specificity, limited local tissue distribution, and potential adverse effects such as potential enhancement of HIV/SIV viral acquisition. To harness the power of trained immunity in HIV/SIV vaccine development, we need to solve the following problems: (1) Practical assays to measure trained immunity; (2) Reliable methods/reagents to induce the two types of trained immunity, namely training and tolerance; (3) Long-term maintenance of the memory; (4) Identification of the protective trained immunity associated with HIV/SIV vaccine efficacy. Further studies to dissect whether sex bias plays any roles in trained immunity induction are also needed. Overall, long-lasting protective trained immunity provides new opportunities for innovative HIV vaccine design.

AUTHOR CONTRIBUTIONS

YS and JB designed the theme and topic and finalized the manuscript. YS drafted the manuscript. YS and JB drew the figure.

ACKNOWLEDGMENTS

We would like to thank Dr. Howard Young from the National Cancer Institute, and Dr. Keiko Ozato from the National institute of Child Health and Human Development for their critical review and valuable comments. This work was supported by intramural NCI funding under project #ZIA-C-004020.

REFERENCES

1. Netea MG, Joosten LA, Latz E, Mills KH, Natoli G, Stunnenberg HG, et al. Trained immunity: a program of innate immune memory in health and disease. *Science*. (2016) 352:aaf1098. doi: 10.1126/science.aaf1098
2. Monticelli S, Natoli G. Short-term memory of danger signals and environmental stimuli in immune cells. *Nat Immunol.* (2013) 14:777–84. doi: 10.1038/ni.2636
3. Masopust D, Kaech SM, Wherry EJ, Ahmed R. The role of programming in memory T-cell development. *Curr Opin Immunol.* (2004) 16:217–25. doi: 10.1016/j.coi.2004.02.005

4. Zediak VP, Wherry EJ, Berger SL. The contribution of epigenetic memory to immunologic memory. *Curr Opin Genet Dev.* (2011) 21:154–9. doi: 10.1016/j.gde.2011.01.016
5. Quintin J, Saeed S, Martens JHA, Giamarellos-Bourboulis EJ, Ifrim DC, Logie C, et al. *Candida albicans* infection affords protection against reinfection via functional reprogramming of monocytes. *Cell Host Microbe*. (2012) 12:223–32. doi: 10.1016/j.chom.2012.06.006
6. Bekkering S, Arts RJW, Novakovic B, Kourtzelis I, van der Heijden C, Li Y, et al. Metabolic induction of trained immunity through the mevalonate pathway. *Cell*. (2018) 172:135–146 e9. doi: 10.1016/j.cell.2017.11.025
7. Arts RJ, Novakovic B, Ter Horst R, Carvalho A, Bekkering S, Lachmandas E, et al. Glutaminolysis and fumarate accumulation integrate immunometabolic and epigenetic programs in trained immunity. *Cell Metab*. (2016) 24:807–19. doi: 10.1016/j.cmet.2016.10.008
8. Cheng SC, Quintin J, Cramer RA, Shepardson KM, Saeed S, Kumar V, et al. mTOR- and HIF-1alpha-mediated aerobic glycolysis as metabolic basis for trained immunity. *Science*. (2014) 345:1250684. doi: 10.1126/science.1250684
9. S. Rerks-Ngarm, Pitisuttithum P, Nitayaphan S, Kaewkungwal J, Chiu J, Paris R, et al. Vaccination with ALVAC and AIDSVAX to prevent HIV-1 infection in Thailand. *N Engl J Med*. (2009) 361:2209–20. doi: 10.1056/NEJMoa0908492
10. Hsu DC, O'Connell RJ. Progress in HIV vaccine development. *Hum Vaccin Immunother*. (2017) 13:1018–30. doi: 10.1080/21645515.2016.1276138
11. Price PJ, Torres-Dominguez LE, Brandmuller C, Sutter G, Lehmann MH. Modified Vaccinia virus Ankara: innate immune activation and induction of cellular signalling. *Vaccine*. (2013) 31:4231–4. doi: 10.1016/j.vaccine.2013.03.017
12. Gomez CE, Perdiguero B, Garcia-Arriaza J, Esteban M. Poxvirus vectors as HIV/AIDS vaccines in humans. *Hum Vaccin Immunother*. (2012) 8:1192–207. doi: 10.4161/hv.20778
13. Haynes BF, Gilbert PB, McElrath MJ, Zolla-Pazner S, Tomaras GD, Alam SM, et al. Immune-correlates analysis of an HIV-1 vaccine efficacy trial. *N Engl J Med*. (2012) 366:1275–86. doi: 10.1056/NEJMoa1113425
14. Burton DR, Hessell AJ, Keele BF, Klasse PJ, Ketas TA, Moldt B, et al. Limited or no protection by weakly or nonneutralizing antibodies against vaginal SHIV challenge of macaques compared with a strongly neutralizing antibody. *Proc Natl Acad Sci USA*. (2011) 108:11181–6. doi: 10.1073/pnas.1103012108
15. Nakane T, Nomura T, Shi S, Nakamura M, Naruse TK, Kimura A, et al. Limited impact of passive non-neutralizing antibody immunization in acute SIV infection on viremia control in rhesus macaques. *PLoS ONE*. (2013) 8:e73453. doi: 10.1371/journal.pone.0073453
16. Dugast AS, Chan Y, Hoffner M, Licht A, Nkolola J, Li H, et al. Lack of protection following passive transfer of polyclonal highly functional low-dose non-neutralizing antibodies. *PLoS ONE*. (2014) 9:e97229. doi: 10.1371/journal.pone.0097229
17. Bruel T, Guivel-Benhassine F, Lorin V, Lortat-Jacob H, Baleux F, Bourdic K, et al. Lack of ADCC breadth of human nonneutralizing anti-HIV-1 antibodies. *J Virol*. (2017) 91:1–9. doi: 10.1128/JVI.02440-16
18. Aaby P, Gustafson P, Roth A, Rodrigues A, Fernandes M, Sodemann M, et al. Vaccinia scars associated with better survival for adults. An observational study from Guinea-Bissau. *Vaccine*. (2006) 24:5718–25. doi: 10.1016/j.vaccine.2006.04.045
19. Jensen ML, Dave S, Schim van der Loeff M, da Costa C, Vincent T, Leligdowicz A, et al. Vaccinia scars associated with improved survival among adults in rural Guinea-Bissau. *PLoS ONE*. (2006) 1:e101. doi: 10.1371/journal.pone.0000101
20. Rieckmann A, Villumsen M, Sorup S, Haugaard LK, Ravn H, Roth A, et al. Vaccinations against smallpox and tuberculosis are associated with better long-term survival: a Danish case-cohort study 1971-2010. *Int J Epidemiol*. (2017) 46:695–705. doi: 10.1093/ije/dyw120
21. Pfahlberg A, Kolmel KF, Grange JM, Mastrangelo G, Krone B, Botev IN, et al. Inverse association between melanoma and previous vaccinations against tuberculosis and smallpox: results of the FEBIM study. *J Invest Dermatol*. (2002) 119:570–5. doi: 10.1046/j.1523-1747.2002.00643.x
22. Lankes HA, Fought AJ, Evens AM, Weisenburger DD, Chiu BC. Vaccination history and risk of non-Hodgkin lymphoma: a population-based, case-control study. *Cancer Causes Control*. (2009) 20:517–23. doi: 10.1007/s10552-008-9259-x
23. Scherer CA, Magness CL, Steiger KV, Poitinger ND, Caputo CM, Miner DG, et al. Distinct gene expression profiles in peripheral blood mononuclear cells from patients infected with vaccinia virus, yellow fever 17D virus, or upper respiratory infections. *Vaccine*. (2007) 25:6458–73. doi: 10.1016/j.vaccine.2007.06.035
24. Carpenter EA, Ruby J, Ramshaw IA. IFN-gamma, TNF, and IL-6 production by vaccinia virus immune spleen cells. An *in vitro* study. *J Immunol*. (1994) 152:2652–9.
25. Vaccari M, Fourati S, Gordon SN, Brown DR, Bissa M, Schifanella L, et al. HIV vaccine candidate activation of hypoxia and the inflammasome in $CD14^+$ monocytes is associated with a decreased risk of SIVmac251 acquisition. *Nat Med*. (2018) 24:847–56. doi: 10.1038/s41591-018-0025-7
26. Sui Y, Lewis GK, Wang Y, Berckmueller K, Frey B, Dzutsev A, et al. Mucosal vaccine efficacy against intrarectal SHIV is independent of anti-Env antibody response. *J Clin Invest*. (2019) 129:1314–28. doi: 10.1172/JCI122110
27. Vaccari M, Fourati S, Brown DR, Silva de Castro I, Bissa M, Schifanella L, et al. Myeloid cell crosstalk regulates the efficacy of the DNA/ALVAC/gp120 HIV vaccine candidate. *Front Immunol*. (2019) 10:1072. doi: 10.3389/fimmu.2019.01072
28. Teigler JE, Phogat S, Franchini G, Hirsch VM, Michael NL, Barouch DH. The canarypox virus vector ALVAC induces distinct cytokine responses compared to the vaccinia virus-based vectors MVA and NYVAC in rhesus monkeys. *J Virol*. (2014) 88:1809–14. doi: 10.1128/JVI.02386-13
29. Guerra S, Lopez-Fernandez LA, Conde R, Pascual-Montano A, Harshman K, Esteban M. Microarray analysis reveals characteristic changes of host cell gene expression in response to attenuated modified vaccinia virus Ankara infection of human HeLa cells. *J Virol*. (2004) 78:5820–34. doi: 10.1128/JVI.78.11.5820-5834.2004
30. Guerra S, Lopez-Fernandez LA, Pascual-Montano A, Najera JL, Zaballos A, Esteban M. Host response to the attenuated poxvirus vector NYVAC: upregulation of apoptotic genes and NF-kappaB-responsive genes in infected HeLa cells. *J Virol*. (2006) 80:985–98. doi: 10.1128/JVI.80.2.985-998.2006
31. Gay NJ, Gangloff M. Structure and function of Toll receptors and their ligands. *Annu Rev Biochem*. (2007) 76:141–65. doi: 10.1146/annurev.biochem.76.060305.151318
32. Sui Y, Zhu Q, Gagnon S, Dzutsev A, Terabe M, Vaccari M, et al. Innate and adaptive immune correlates of vaccine and adjuvant-induced control of mucosal transmission of SIV in macaques. *Proc Natl Acad Sci USA*. (2010) 107:9843–8. doi: 10.1073/pnas.0911932107
33. Sui Y, Hogg A, Wang Y, Frey B, Yu H, Xia Z, et al. Vaccine-induced myeloid cell population dampens protective immunity to SIV. *J Clin Invest*. (2014) 124:2538–49. doi: 10.1172/JCI73518
34. Moody MA, Santra S, Vandergrift NA, Sutherland LL, Gurley TC, Drinker MS, et al. Toll-like receptor 7/8 (TLR7/8) and TLR9 agonists cooperate to enhance HIV-1 envelope antibody responses in rhesus macaques. *J Virol*. (2014) 88:3329–39. doi: 10.1128/JVI.03309-13
35. Ding Y, Liu J, Lu S, Igweze J, Xu W, Kuang D, et al. Self-assembling peptide for co-delivery of HIV-1 CD8+ T cells epitope and Toll-like receptor 7/8 agonists R848 to induce maturation of monocyte derived dendritic cell and augment polyfunctional cytotoxic T lymphocyte (CTL) response. *J Control Release*. (2016) 236:22–30. doi: 10.1016/j.jconrel.2016.06.019
36. Kasturi SP, Kozlowski PA, Nakaya HI, Burger MC, Russo P, Pham M, et al. Adjuvanting a simian immunodeficiency virus vaccine with toll-like receptor ligands encapsulated in nanoparticles induces persistent antibody responses and enhanced protection in TRIM5alpha restrictive macaques. *J Virol*. (2017) 91:1–25. doi: 10.1128/JVI.01844-16
37. Ostuni R, Piccolo V, Barozzi I, Polletti S, Termanini A, Bonifacio S, et al. Latent enhancers activated by stimulation in differentiated cells. *Cell*. (2013) 152:157–71. doi: 10.1016/j.cell.2012.12.018
38. Maitra U, Deng H, Glaros T, Baker B, Capelluto DG, Li Z, et al. Molecular mechanisms responsible for the selective and low-grade induction of proinflammatory mediators in murine macrophages by lipopolysaccharide. *J Immunol*. (2012) 189:1014–23. doi: 10.4049/jimmunol.1200857

39. Foster SL, Hargreaves DC, Medzhitov R. Gene-specific control of inflammation by TLR-induced chromatin modifications. *Nature*. (2007) 447:972–8. doi: 10.1038/nature05836
40. Ifrim DC, Quintin J, Joosten LA, Jacobs C, Jansen T, Jacobs L, et al. Trained immunity or tolerance: opposing functional programs induced in human monocytes after engagement of various pattern recognition receptors. *Clin Vaccine Immunol.* (2014) 21:534–45. doi: 10.1128/CVI.00688-13
41. Zhu J, Martinez J, Huang X, Yang Y. Innate immunity against vaccinia virus is mediated by TLR2 and requires TLR-independent production of IFN-beta. *Blood*. (2007) 109:619–25. doi: 10.1182/blood-2006-06-027136
42. Delaloye J, Roger T, Steiner-Tardivel QG, Le Roy D, Knaup Reymond M, Akira S, et al. Innate immune sensing of modified vaccinia virus Ankara (MVA) is mediated by TLR2-TLR6, MDA-5 and the NALP3 inflammasome. *PLoS Pathog.* (2009) 5:e1000480. doi: 10.1371/journal.ppat.1000480
43. Barbalat R, Lau L, Locksley RM, Barton GM. Toll-like receptor 2 on inflammatory monocytes induces type I interferon in response to viral but not bacterial ligands. *Nat Immunol*. (2009) 10:1200–7. doi: 10.1038/ni.1792
44. O'Gorman WE, Sampath P, Simonds EF, Sikorski R, O'Malley M, Krutzik PO, et al. Alternate mechanisms of initial pattern recognition drive differential immune responses to related poxviruses. *Cell Host Microbe*. (2010) 8:174–85. doi: 10.1016/j.chom.2010.07.008
45. Davies ML, Sei JJ, Siciliano NA, Xu RH, Roscoe F, Sigal LJ, et al. MyD88-dependent immunity to a natural model of vaccinia virus infection does not involve Toll-like receptor 2. *J Virol.* (2014) 88:3557–67. doi: 10.1128/JVI.02776-13
46. Creagh EM,. O'Neill LA. TLRs, NLRs and RLRs: a trinity of pathogen sensors that co-operate in innate immunity. *Trends Immunol.* (2006) 27:352–7. doi: 10.1016/j.it.2006.06.003
47. Kawai T, Akira S. The roles of TLRs, RLRs and NLRs in pathogen recognition. *Int Immunol.* (2009) 21:317–37. doi: 10.1093/intimm/dxp017
48. Timmermans K, Plantinga TS, Kox M, Vaneker M, Scheffer GJ, Adema GJ, et al. Blueprints of signaling interactions between pattern recognition receptors: implications for the design of vaccine adjuvants. *Clin Vaccine Immunol.* (2013) 20:427–32. doi: 10.1128/CVI.00703-12
49. Moorlag S, Roring RJ, L.Joosten AB, Netea MG. The role of the interleukin-1 family in trained immunity. *Immunol Rev*. (2018) 281:28–39. doi: 10.1111/imr.12617
50. R.Arts JW, Moorlag S, Novakovic B, Li Y, Wang SY, Oosting M, et al. BCG Vaccination protects against experimental viral infection in humans through the induction of cytokines associated with trained immunity. *Cell Host Microbe*. (2018) 23:89–100 e5. doi: 10.1016/j.chom.2017.12.010
51. Semenza GL, Hydroxylation of HIF-1: oxygen sensing at the molecular level. *Physiology (Bethesda).* (2004) 19:176–82. doi: 10.1152/physiol.00001.2004
52. Zhang W, Petrovic JM, Callaghan D, Jones A, Cui H, Howlett C, et al. Evidence that hypoxia-inducible factor-1 (HIF-1) mediates transcriptional activation of interleukin-1beta (IL-1beta) in astrocyte cultures. *J Neuroimmunol.* (2006) 174:63–73. doi: 10.1016/j.jneuroim.2006.01.014
53. Tannahill GM, Curtis AM, Adamik J, Palsson-McDermott EM, McGettrick AF, Goel G, et al. Succinate is an inflammatory signal that induces IL-1beta through HIF-1alpha. *Nature*. (2013) 496:238–42. doi: 10.1038/nature11986
54. Jung YJ, Isaacs JS, Lee S, Trepel J, Neckers L. IL-1beta-mediated up-regulation of HIF-1alpha via an NFkappaB/COX-2 pathway identifies HIF-1 as a critical link between inflammation and oncogenesis. *FASEB J.* (2003) 17:2115–7. doi: 10.1096/fj.03-0329fje
55. Juffermans NP, Florquin S, Camoglio L, Verbon A, Kolk AH, Speelman P, et al. Interleukin-1 signaling is essential for host defense during murine pulmonary tuberculosis. *J Infect Dis.* (2000) 182:902–8. doi: 10.1086/315771
56. Vonk AG, Netea MG, van Krieken JH, Iwakura Y, van der Meer JW, Kullberg BJ. Endogenous interleukin (IL)-1 alpha and IL-1 beta are crucial for host defense against disseminated candidiasis. *J Infect Dis.* (2006) 193:1419–26. doi: 10.1086/503363
57. Sergerie Y, Rivest S, Boivin G. Tumor necrosis factor-alpha and interleukin-1 beta play a critical role in the resistance against lethal herpes simplex virus encephalitis. *J Infect Dis.* (2007) 196:853–60. doi: 10.1086/520094
58. Warren SE, Mao DP, Rodriguez AE, Miao EA, Aderem A. Multiple Nod-like receptors activate caspase 1 during Listeria monocytogenes infection. *J Immunol.* (2008) 180:7558–64. doi: 10.4049/jimmunol.180.11.7558
59. Young HA, Hardy KJ. Role of interferon-gamma in immune cell regulation. *J Leukoc Biol.* (1995) 58:373–81. doi: 10.1002/jlb.58.4.373
60. Lin FC, Young HA. Interferons: success in anti-viral immunotherapy. *Cytokine Growth Factor Rev.* (2014) 25:369–76. doi: 10.1016/j.cytogfr.2014.07.015
61. Ye L, Ohnemus A, Ong LC, Gad HH, Hartmann R, Lycke N, et al. Type I and Type III interferons differ in their adjuvant activities for influenza vaccines. *J Virol.* (2019) 93:1–8. doi: 10.1128/JVI.01262-19
62. Chen J, Ivashkiv LB. IFN-gamma abrogates endotoxin tolerance by facilitating Toll-like receptor-induced chromatin remodeling. *Proc Natl Acad Sci USA*. (2010) 107:19438–43. doi: 10.1073/pnas.1007816107
63. Qiao Y, Giannopoulou EG, Chan CH, Park SH, Gong S, Chen J, et al. Synergistic activation of inflammatory cytokine genes by interferon-gamma-induced chromatin remodeling and toll-like receptor signaling. *Immunity*. (2013) 39:454–69. doi: 10.1016/j.immuni.2013.08.009
64. Qiao Y, Kang K, Giannopoulou E, Fang C, Ivashkiv LB. IFN-gamma induces histone 3 lysine 27 trimethylation in a small subset of promoters to stably silence gene expression in human macrophages. *Cell Rep.* (2016) 16:3121–9. doi: 10.1016/j.celrep.2016.08.051
65. Barrat FJ, Crow MK, Ivashkiv LB. Interferon target-gene expression and epigenomic signatures in health and disease. *Nat Immunol.* (2019) 20:1574–83. doi: 10.1038/s41590-019-0466-2
66. Kang K, Park SH, Chen J, Qiao Y, Giannopoulou E, Berg K, et al. Interferon-gamma Represses M2 gene expression in human macrophages by disassembling enhancers bound by the transcription factor MAF. *Immunity*. (2017) 47:235–50 e4. doi: 10.1016/j.immuni.2017.07.017
67. Park SH, Kang K, Giannopoulou E, Qiao Y, Kang K, Kim G, et al. Type I interferons and the cytokine TNF cooperatively reprogram the macrophage epigenome to promote inflammatory activation. *Nat Immunol.* (2017) 18:1104–16. doi: 10.1038/ni.3818
68. Kamada R, Yang W, Zhang Y, Patel MC, Yang Y, Ouda R, et al. Interferon stimulation creates chromatin marks and establishes transcriptional memory. *Proc Natl Acad Sci USA*. (2018) 115:E9162–71. doi: 10.1073/pnas.1720930115
69. Ivashkiv LB. IFNgamma: signalling, epigenetics and roles in immunity, metabolism, disease and cancer immunotherapy. *Nat Rev Immunol.* (2018) 18:545–58. doi: 10.1038/s41577-018-0029-z
70. Barouch DH. Novel adenovirus vector-based vaccines for HIV-1. *Curr Opin HIV AIDS*. (2010) 5:386–90. doi: 10.1097/COH.0b013e32833cfe4c
71. Buchbinder SP, Mehrotra DV, Duerr A, Fitzgerald DW, Mogg R, Li D, et al. Efficacy assessment of a cell-mediated immunity HIV-1 vaccine (the Step Study): a double-blind, randomised, placebo-controlled, test-of-concept trial. *Lancet*. (2008) 372:1881–93. doi: 10.1016/S0140-6736(08)61591-3
72. Gray G, Buchbinder S, Duerr A. Overview of STEP and Phambili trial results: two phase IIb test-of-concept studies investigating the efficacy of MRK adenovirus type 5 gag/pol/nef subtype B HIV vaccine. *Curr Opin HIV AIDS*. (2010) 5:357–61. doi: 10.1097/COH.0b013e32833d2d2b
73. Gray GE, Allen M, Moodie Z, Churchyard G, Bekker LG, Nchabeleng M, et al. Safety and efficacy of the HVTN 503/Phambili study of a clade-B-based HIV-1 vaccine in South Africa: a double-blind, randomised, placebo-controlled test-of-concept phase 2b study. *Lancet Infect Dis.* (2011) 11:507–15. doi: 10.1016/S1473-3099(11)70098-6
74. Gray GE, Moodie Z, Metch B, Gilbert PB, Bekker LG, Churchyard G, et al. Recombinant adenovirus type 5 HIV gag/pol/nef vaccine in South Africa: unblinded, long-term follow-up of the phase 2b HVTN 503/Phambili study. *Lancet Infect Dis.* (2014) 14:388–96. doi: 10.1016/S1473-3099(14)70020-9
75. Bukh I, Calcedo R, Roy S, Carnathan DG, Grant R, Qin Q, et al. Increased mucosal $CD4^+$ T cell activation in rhesus macaques following vaccination with an adenoviral vector. *J Virol.* (2014) 88:8468–78. doi: 10.1128/JVI.03850-13
76. Brody IB, Calcedo R, Connell MJ, Carnathan DG, Nason M, Lawson BO, et al. Susceptibility to SIV infection after adenoviral vaccination in a low dose rhesus macaque challenge model. *Pathog Immun.* (2019) 4:1–20. doi: 10.20411/pai.v4i1.241
77. Sui Y, Keele B, Miller C, Berzofsky J. Protection against intrarectal SIV acquisition by live SHIV vaccine in the absence of anti-Env antibody responses. *Eur J Immuol.* (2019) 49:1695.

78. Kleinnijenhuis J, Quintin J, Preijers F, Benn CS, Joosten LA, Jacobs C, et al. Long-lasting effects of BCG vaccination on both heterologous Th1/Th17 responses and innate trained immunity. *J Innate Immun.* (2014) 6:152–8. doi: 10.1159/000355628
79. Kaufmann E, Sanz J, Dunn JL, Khan N, Mendonca LE, Pacis A, et al. BCG educates hematopoietic stem cells to generate protective innate immunity against tuberculosis. *Cell*. (2018) 172:176–90 e19. doi: 10.1016/j.cell.2017.12.031
80. Mitroulis I, Ruppova K, Wang B, Chen LS, Grzybek M, Grinenko T, et al. Modulation of myelopoiesis progenitors is an integral component of trained immunity. *Cell*. (2018) 172:147–61 e12. doi: 10.1016/j.cell.2017.11.034
81. Christ A, Gunther P, Lauterbach MAR, Duewell P, Biswas D, Pelka K, et al. Western diet triggers NLRP3-dependent innate immune reprogramming. *Cell*. (2018) 172:162–75 e14. doi: 10.1016/j.cell.2017.12.013
82. Megias J, Yanez A, Moriano S, O'Connor JE, Gozalbo D, Gil ML. Direct Toll-like receptor-mediated stimulation of hematopoietic stem and progenitor cells occurs *in vivo* and promotes differentiation toward macrophages. *Stem Cells*. (2012) 30:1486–95. doi: 10.1002/stem.1110
83. Granick JL, Falahee PC, Dahmubed D, Borjesson DL, Miller LS, Simon SI. *Staphylococcus aureus* recognition by hematopoietic stem and progenitor cells via TLR2/MyD88/PGE2 stimulates granulopoiesis in wounds. *Blood*. (2013) 122:1770–8. doi: 10.1182/blood-2012-11-466268
84. Megias J, Maneu V, Salvador P, Gozalbo D, Gil ML. *Candida albicans* stimulates *in vivo* differentiation of haematopoietic stem and progenitor cells towards macrophages by a TLR2-dependent signalling. *Cell Microbiol.* (2013) 15:1143–53. doi: 10.1111/cmi.12104
85. Nguyen MT, Uebele J, Kumari N, Nakayama H, Peter L, Ticha O, et al. Lipid moieties on lipoproteins of commensal and non-commensal staphylococci induce differential immune responses. *Nat Commun.* (2017) 8:2246. doi: 10.1038/s41467-017-02234-4
86. Martinez A, Bono C, Megias J, Yanez A, Gozalbo D, Gil ML. Systemic candidiasis and TLR2 agonist exposure impact the antifungal response of hematopoietic stem and progenitor cells. *Front Cell Infect Microbiol.* (2018) 8:309. doi: 10.3389/fcimb.2018.00309
87. Yao Y, Jeyanathan M, Haddadi S, Barra NG, Vaseghi-Shanjani M, Damjanovic D, et al. Induction of autonomous memory alveolar macrophages requires T cell help and is critical to trained immunity. *Cell*. (2018) 175:1634–50 e17. doi: 10.1016/j.cell.2018.09.042
88. Placek K, Schultze JL, Netea MG. Immune memory characteristics of innate lymphoid cells. *Curr Opin Infect Dis.* (2019) 32:196–203. doi: 10.1097/QCO.0000000000000540
89. Martinez-Gonzalez I, Matha L, Steer CA, Ghaedi M, Poon GF, Takei F. Allergen-experienced group 2 innate lymphoid cells acquire memory-like properties and enhance allergic lung inflammation. *Immunity*. (2016) 45:198–208. doi: 10.1016/j.immuni.2016.06.017
90. Suliman S, Geldenhuys H, Johnson JL, Hughes JE, Smit E, Murphy M, et al. Bacillus Calmette-Guerin (BCG) revaccination of adults with latent *Mycobacterium tuberculosis* infection induces long-lived BCG-reactive NK cell responses. *J Immunol.* (2016) 197:1100–10. doi: 10.4049/jimmunol.1501996
91. Hammer Q, Ruckert T, Borst EM, Dunst J, Haubner A, Durek P, et al. Peptide-specific recognition of human cytomegalovirus strains controls adaptive natural killer cells. *Nat Immunol.* (2018) 19:453–63. doi: 10.1038/s41590-018-0082-6
92. Hammer Q, Romagnani C. About training and memory: NK-cell adaptation to viral infections. *Adv Immunol.* (2017) 133:171–207. doi: 10.1016/bs.ai.2016.10.001
93. Bigot J, Guillot L, Guitard J, Ruffin M, Corvol H, Chignard M, et al. Respiratory epithelial cells can remember infection: a proof of concept study. *J Infect Dis.* (2019). doi: 10.1093/infdis/jiz569. [Epub ahead of print].
94. Samir P, R.Malireddi KS, Kanneganti TD. Food for training-western diet and inflammatory memory. *Cell Metab.* (2018) 27:481–2. doi: 10.1016/j.cmet.2018.02.012
95. Christ A, Lauterbach M, Latz E. Western diet and the immune system: an inflammatory connection. *Immunity*. (2019) 51:794–811. doi: 10.1016/j.immuni.2019.09.020
96. Ieronymaki E, Daskalaki MG, Lyroni K, Tsatsanis C. Insulin signaling and insulin resistance facilitate trained immunity in macrophages through metabolic and epigenetic changes. *Front Immunol.* (2019) 10:1330. doi: 10.3389/fimmu.2019.01330
97. Bekkering S, Quintin J, Joosten LA, van der Meer JW, Netea MG, Riksen NP. Oxidized low-density lipoprotein induces long-term proinflammatory cytokine production and foam cell formation via epigenetic reprogramming of monocytes. *Arterioscler Thromb Vasc Biol.* (2014) 34:1731–8. doi: 10.1161/ATVBAHA.114.303887
98. Sohrabi Y, Lagache SMM, Schnack L, Godfrey R, Kahles F, Bruemmer D, et al. mTOR-dependent oxidative stress regulates oxLDL-induced trained innate immunity in human monocytes. *Front Immunol.* (2018) 9:3155. doi: 10.3389/fimmu.2018.03155
99. Brasacchio D, Okabe J, Tikellis C, Balcerczyk A, George P, Baker EK, et al. Hyperglycemia induces a dynamic cooperativity of histone methylase and demethylase enzymes associated with gene-activating epigenetic marks that coexist on the lysine tail. *Diabetes*. (2009) 58:1229–36. doi: 10.2337/db08-1666
100. Ieronymaki E, Theodorakis EM, Lyroni K, Vergadi E, Lagoudaki E, Al-Qahtani A, et al. Insulin resistance in macrophages alters their metabolism and promotes an M2-like phenotype. *J Immunol.* (2019) 202:1786–97. doi: 10.4049/jimmunol.1800065
101. Sui Y, Dzutsev A, Venzon D, Frey B, Thovarai V, Trinchieri G, et al. Influence of gut microbiome on mucosal immune activation and SHIV viral transmission in naive macaques. *Mucosal Immunol.* (2018) 11:1219–29. doi: 10.1038/s41385-018-0029-0
102. Lancaster GI, Langley KG, Berglund NA, Kammoun HL, Reibe S, Estevez E, et al. Evidence that TLR4 is not a receptor for saturated fatty acids but mediates lipid-induced inflammation by reprogramming macrophage metabolism. *Cell Metab.* (2018) 27:1096–110 e5. doi: 10.1016/j.cmet.2018.03.014

Conflict of Interest: The authors declare that the research was conducted in the absence of any commercial or financial relationships that could be construed as a potential conflict of interest.

frontiers in Microbiology

ORIGINAL RESEARCH
published: 31 March 2020
doi: 10.3389/fmicb.2020.00497

Obacunone Protects Against Ulcerative Colitis in Mice by Modulating Gut Microbiota, Attenuating TLR4/NF-κB Signaling Cascades, and Improving Disrupted Epithelial Barriers

Xiaoping Luo†, Bei Yue†, Zhilun Yu, Yijing Ren, Jing Zhang, Junyu Ren, Zhengtao Wang and Wei Dou**

Shanghai Key Laboratory of Formulated Chinese Medicines, Institute of Chinese Materia Medica, Shanghai University of Traditional Chinese Medicine, Shanghai, China

OPEN ACCESS

Edited by:
Marcello Chieppa, European Biomedical Research Institute of Salerno (EBRIS), Italy

Reviewed by:
Ashok Kumar Pandurangan, B.S. Abdur Rahman Crescent Institute of Science and Technology, India
Marina Liso, National Institute of Gastroenterology "S. de Bellis" Research Hospital (IRCCS), Italy

***Correspondence:**
Zhengtao Wang
ztwang@shutcm.edu.cn; wzhengtao@yahoo.com
Wei Dou
douwei123456@126.com

† These authors have contributed equally to this work

Specialty section:
This article was submitted to Microbial Immunology, a section of the journal Frontiers in Microbiology

Received: *14 January 2020*
Accepted: *06 March 2020*
Published: *31 March 2020*

Citation:
Luo X, Yue B, Yu Z, Ren Y, Zhang J, Ren J, Wang Z and Dou W (2020) Obacunone Protects Against Ulcerative Colitis in Mice by Modulating Gut Microbiota, Attenuating TLR4/NF-κB Signaling Cascades, and Improving Disrupted Epithelial Barriers. Front. Microbiol. 11:497. doi: 10.3389/fmicb.2020.00497

Obacunone, a natural limonoid compound abundantly distributed in citrus fruits, possesses various biological properties, such as antitumor, antioxidant, and antiviral activities. Recent studies suggested an anti-inflammatory activity of obacunone *in vitro*, but its efficacy on intestinal inflammation remains unknown. This study was designed to evaluate the effects and mechanisms of obacunone in ameliorating intestinal inflammation in a mouse model of ulcerative colitis (UC). We found that obacunone efficiently alleviated the severity of dextran sulfate sodium (DSS)-induced mouse UC by modulating the abnormal composition of the gut microbiota and attenuating the excessive activation of toll-like receptor 4 (TLR4)/nuclear factor-kappa B (NF-κB) signaling. The intestinal epithelial barrier was disrupted in DSS colitis mice, which was associated with activation of inflammatory signaling cascades. However, obacunone promoted the expression of tight junction proteins (TJP1 and occludin) and repressed the activation of inflammatory signaling cascades. In summary, our findings demonstrated that obacunone attenuated the symptoms of experimental UC in mice through modulation of the gut microbiota, attenuation of TLR4/NF-κB signaling cascades, and restoration of intestinal epithelial barrier integrity.

Keywords: UC, gut microbiota, TLR4/NF-κB, epithelial barrier, obacunone

INTRODUCTION

Inflammatory bowel diseases (IBDs), consisting mainly of Crohn's disease and ulcerative colitis (UC), are common, chronic, and relapsing inflammatory disorders of the digestive tract (Kaplan, 2015). The clinical features of UC include recurrent, chronic, and persistent inflammation in the gastrointestinal tract. Furthermore, the symptoms of UC frequently include diarrhea, abdominal pain, weight loss, and malnutrition, which seriously affect the quality of life of UC patients (Rosen et al., 2015). The possible etiology of UC is complex and multifactorial including genetic, immune, microbiological, and environmental factors, each of which may lead to the occurrence of UC (Bernstein, 2017). Although the exact cause of UC remains unclear, accumulating evidence has

indicated that interaction between mucosal immunity and gut microbiota plays a key role in the pathogenesis of UC (Yue et al., 2019). Additionally, clinical studies have indicated that the composition of three major phyla of bacteria present in the gut microbiota of UC patients is disturbed, with a decrease in the proportion of *Firmicutes* and *Bacteroidetes* and an increase in that of *Proteobacteria* (Matsuoka and Kanai, 2015; Mirsepasi-Lauridsen et al., 2019). Administration of antibacterial agents and probiotics in UC patients has suggested that the gut microbiota does play a role in the onset of UC (Sokol, 2014).

Tight junction proteins (TJPs), localized at the interface between epithelial cells, are responsible for maintaining the integrity and function of the intestinal mucosal barrier (Bhat et al., 2018). Disruption of mucosal barrier in UC patients can trigger bacterial and endotoxin translocation, resulting in the loss of innate immunity, as well as aberrant activation of acquired immunity (Wang et al., 2019). Bacterial or endotoxin invasion is primarily recognized by toll-like receptor 4 (TLR4), a typical member of the pattern recognition receptors family. TLR4 recognizes bacterial components, such as lipopolysaccharide (LPS), which initiates a signaling cascade that results in the activation of nuclear factor-kappa B (NF-κB); this induces a series of pro-inflammatory immune responses by the host in an attempt to destroy the invading pathogens (Stephens and von der Weid, 2019; Yue et al., 2019).

There are various classical therapeutic approaches for UC, including anti-inflammatory, immunosuppressive, and biological therapies. However, a considerable number of UC patients have not benefited from these approaches, owing to insensitivity to these treatments or the presence of significant therapy-associated adverse effects (Neurath, 2017). Consequently, novel therapeutic options are constantly being developed, while traditional treatment approaches have attracted increasing attention in recent years. Obacunone is a triterpenoid limonoid compound isolated primarily from citrus fruits and plants of the *Rutaceae* family, such as *Phellodendron chinense* and *Tetradium ruticarpum* (Gao et al., 2018). Obacunone is found to display various pharmacological activities, including antioxidative, anti-inflammatory, antitumor, and hypoglycemic effects (Murthy et al., 2015). However, the effects of obacunone on UC and the underlying mechanisms have not been reported to date. In this study, we presented evidence that obacunone could alleviate UC-associated symptoms in mice, and this effect was mediated through modulation of the gut microbiota, attenuation of TLR4/NF-κB signaling cascades, and restoration of intestinal epithelial barrier integrity.

MATERIALS AND METHODS

Chemicals and Reagents

Obacunone ($C_{26}H_{30}O_7$, MW: 454.516, CAS: 751-03-1, HPLC purity ≥ 98%) was obtained from Meilun Biological Technology Co., Ltd. (Dalian, China). RAW264.7 mouse macrophage cells and NCM460 human colonic epithelial cells were obtained from the American Type Culture Collection (ATCC, Manassas, VA, United States). Dulbecco's modified Eagle's medium (DMEM), Roswell Park Memorial Institute (RPMI)-1640, and fetal bovine serum (FBS) were purchased from Gibco BRL (Grand Island, NY, United States). DEPC water, LPS, formalin, paraformaldehyde, and ethanol were from Sigma-Aldrich. Dimethyl sulfoxide (DMSO) and Tween 20 were obtained from Sangon Biotech Company (Shanghai, China). Antibodies against p-p65 (#SC-33039), p-IκBα (#SC-8404), and actin (#SC-47778) were from Santa Cruz Biotechnology (CA, United States). The anti-TLR4 (ab13556) and inducible nitric oxide (iNOS, ab129372) antibody were purchased from Abcam (Cambridge, MA, United States), while the anti-ZO-1 (A11417) and anti-occludin (A2601) antibodies were purchased from ABclonal Technology (Wuhan, China). All the other antibodies were from Cell Signaling Technology (Danvers, MA, United States), as follows: COX-2 (#12282P), IFN-γ (#3159), TNF-α (#3707S), and MyD88 (#42835). All reagents for quantitative polymerase chain reaction (qPCR) and the Reverse Transcriptase Kit were from Takara Biotechnology (Shiga, Japan). The Cell Counting Kit 8 (CCK-8) was from Meilun Biological Technology Co., Ltd. All other reagents were obtained from Thermo Fisher Scientific (Waltham, MA, United States).

Animals and DSS-Induced Colitis

Healthy C57BL/6 mice (8 weeks of age, 20–22 g) were purchased from the Shanghai Laboratory Animal Center. All mice were maintained in specific pathogen-free facility and kept under controlled conditions at a humidity of 60–70% and stationary temperature of 23–25°C with a 12 h light/dark cycle and with access to autoclaved food and drinking water. This study was carried out in accordance with the principles of the declaration recommendations of the Animal Experimentation Ethics Committee at Shanghai University of Traditional Chinese Medicine (Animal license key: SYXK2014-0008).

All mice were randomly divided into the following six groups (n = 10 mice per group): vehicle control group, obacunone-only group (100 mg/kg), dextran sulfate sodium (DSS) group, and three obacunone-treated groups (low dosage, middle dose, and high dose, respectively). The dosages of obacunone were 25, 50, and 100 mg/kg/day per body weight, respectively. Acute experimental colitis was induced in mice by administration of

TABLE 1 | The list of primers used for qPCR.

Gene	Primer sequence (5′–3′)
m IL-1α	F: ATGACCTGCAACAGGAAGTAAAA
	R:TGTGATGAGTTTTGGTGTTTCTG
m IL-1β	F: ATTGTGGCTGTGGAGAAG
	R: AAGATGAAGGAAAAGAAGGTG
m IL-16	F: GATACCACAGCCGAAGACCCTTGG
	R: GTGCTCGCTGGCTAGGCATCTTG
m iNOS	F: ATTGTGGCTGTGGAGAAG
	R: AAGATGAAGGAAAAGAAGGTG
m COX-2	F: GCCTTCCCTACTTCACAA
	R: ACAACTCTTTTCTCATTTCCAC
m β-actin	F: GGGAAATCGTGCGTGAC
	R: AGGCTGGAAAAGAGCCT

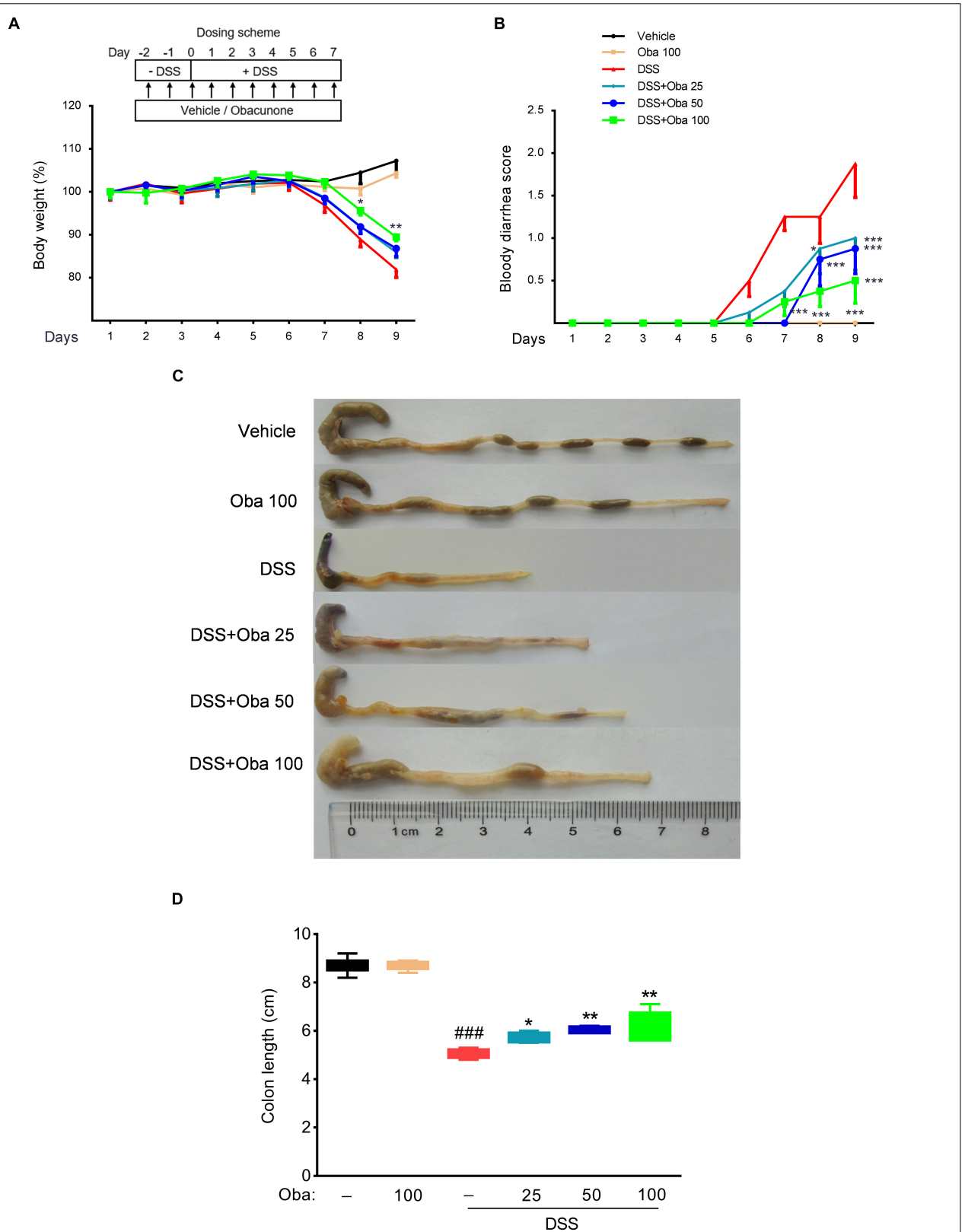

FIGURE 1 | Obacunone ameliorated body weight loss, bloody diarrhea, and colon shortening in IBD model mice. **(A)** Body weight was recorded after DSS induction of colitis. Data were plotted as a percentage of basal body weight. **(B)** The occurrence of bloody diarrhea. Data were plotted as the percentage of the total number of mice that had bloody diarrhea at different time points of DSS treatment. Macroscopic observation **(C)** and assessment of colon shortening **(D)** at the end of the study. Data were expressed as the mean ± SD (n = 6 mice per group). $^{*}p < 0.05$, $^{**}p < 0.01$, $^{***}p < 0.001$ vs. the DSS-treated group; $^{\#\#\#}p < 0.001$ vs. the control group.

3.5% DSS (MW: 36,000–50,000 Da, MP Biomedicals, Irvine, CA, United States) for 7 days as previously described (Yue et al., 2018). Obacunone was dissolved in 0.5% methylcellulose and administered by oral gavage once a day, starting from 2 days before DSS treatment and continuing to the end of the experiment. Body weight and bloody diarrhea were recorded daily. Mice were euthanized under anesthesia after the last oral gavage. The entire colon was removed and the total length was measured. After that, the distal colon tissues were collected for hematoxylin–eosin (H&E) staining. And the images were taken by the Olympus DP20 optical digital microscope camera (Tokyo, Japan). Histological injury was assessed by a combined score of inflammatory cell infiltration (score 0–3) and epithelial damage (score 0–3) using a double-blind method as described previously (Luo et al., 2017).

Cell Culture and Cell Viability Assay

Murine peritoneal macrophage RAW264.7 cells were cultured in DMEM supplemented with 10% FBS under 5% CO_2 at 37°C. Cells were treated with different concentrations of obacunone (0–100 μM) for 24 h. NCM460 human colonic epithelial cells were cultured in RPMI-1640 supplemented with 10% FBS under 5% CO_2 at 37°C. NCM460 cells were treated with different concentrations of obacunone (0–100 μM) for 2 h followed by coincubation with tumor necrosis factor (TNF-α) (20 ng/mL) for an additional 22 h. A CCK-8 assay was then performed to measure cell viability. The absorption values were measured at 540 nm using a microplate reader.

Nitric Oxide (NO) Assay

RAW264.7 cells were incubated with different concentrations of obacunone (0–100 μM) for 2 h before being stimulated by LPS (1 μg/mL) for an additional 22 h. The supernatant was then collected and a Griess assay was performed to measure the relative NO secretion levels in each group. Finally, the absorbance of each well was measured at 450 nm using a microplate reader as previously described (Luo et al., 2017).

Immunoblotting and RNA Analysis

Colon segments (∼1.5 cm near the anus) or cultured cells were homogenized or lysed in lysis buffer (Thermo Fisher Scientific, Mannheim, MA, United States) containing protease and phosphatase inhibitor cocktail tablets (Roche Diagnostics GmbH, Mannheim, GER). The lysate was centrifuged (4°C, 12,000 × *g*, 15 min) and the supernatant was collected. The procedure for immunoblotting was performed as previously described (Yue et al., 2018). In brief, proteins (30 μg) was separated by 10% SDS-PAGE and transferred onto a PVDF membrane. The membrane was blocked in 5% (w/v) skim milk for 2 h at room temperature and immunoblotted with primary antibody. Then blots were washed and incubated with HRP-coupled secondary antibody at room temperature. Finally, the blots were observed by enhanced chemiluminescence (ECL) detection reagents. Protein expressions were analyzed by a GS-700 imaging densitometer (Bio-Rad, CA, United States). β-actin (Santa Cruz, CA, United States) was used as an internal control.

RAW264.7 cells were treated with different concentrations of obacunone (0–100 μM) for 2 h before being stimulated by LPS (1 μg/mL) for an additional 22 h. Total RNA was extracted from cultured cells using TRIzol reagent. Reverse transcription and qPCR were carried out using SYBR Premix ExTaq Mix in an ABI Prism 7900HT Sequence Detection System (Life Technologies, Carlsbad, CA, United States) as previously described (Dou et al., 2012). The following thermal cycler parameters were used: 1 cycle of 95°C for 30 s and 40 cycles of denaturation (95°C, 5 s) and combined annealing/extension (60°C, 30 s). Relative mRNA expression levels were calculated by the comparative Ct method, and the values were normalized as the ratio of the optimal density relative to β-actin. The sequences of the primers were listed in **Table 1**.

Microbiota Sequencing Analysis

Mice feces were collected and stored at −80°C. Genomic DNA was extracted from the fecal samples using the E.Z.N.A. Soil DNA Kit (Omega Bio-tek, GA, United States), according to the manufacturer's protocol. A NanoDrop 2000 UV-vis spectrophotometer (Thermo Fisher Scientific, DE, United States) was used to assess the concentration and quality of the DNA. The V3–V4 hypervariable regions of

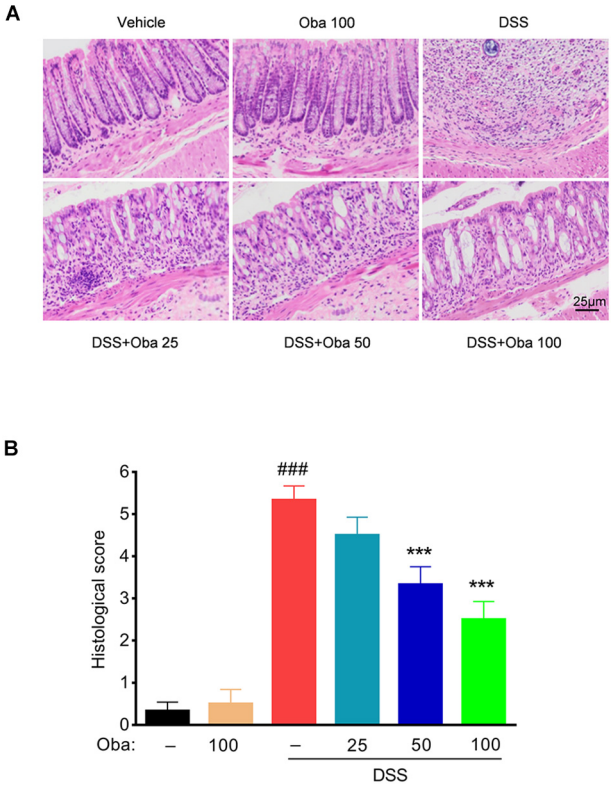

FIGURE 2 | Obacunone ameliorated inflammatory infiltration and histopathological injury in IBD model mice. Representative hematoxylin–eosin (H&E)-stained colon sections **(A)** and histological score **(B)**. Scale bar, 25 μm. Data were expressed as the mean ± SD (n = 6 mice per group). $^{***}p < 0.001$ vs. the DSS-treated group; $^{###}p < 0.001$ vs. the control group.

the bacterial 16S rRNA gene were amplified using primers 338F (5′-ACTCCTACGGGAGGCAGCAG-3′) and 806R (5′-GGACTACHVGGGTWTCTAAT-3′) in a GeneAmp 9700 ABI thermocycler PCR system (Carlsbad, CA, United States). PCR reaction was conducted using the following cycling conditions: an initial denaturation at 95°C for 3 min, followed by 27 cycles of denaturation at 95°C for 30 s, annealing at 55°C for 30 s, and elongation at 72°C for 45 s, and a final extension at 72°C for 10 min. Sequencing was performed using the high-throughput Illumina MiSeq platform (Illumina, CA, United States) according to standard protocols (Majorbio, Shanghai, China). Raw fastq files were quality-filtered by Trimmomatic and merged by FLASH. All the results were based on sequenced reads and operational taxonomic unit (OTU) clustering was performed with a 97% similarity cutoff and a 70% confidence threshold.

Statistics

Significance between groups was evaluated by one-way analysis of variance (ANOVA) using GraphPad Prism 7 software (GraphPad Software, La Jolla, CA, United States). All data were presented as the mean ± standard deviation (SD). p-values < 0.05 (two-sided) were considered significant ($^{*}p < 0.05$, $^{**}p < 0.01$, $^{***}p < 0.001$). All the 16S rDNA

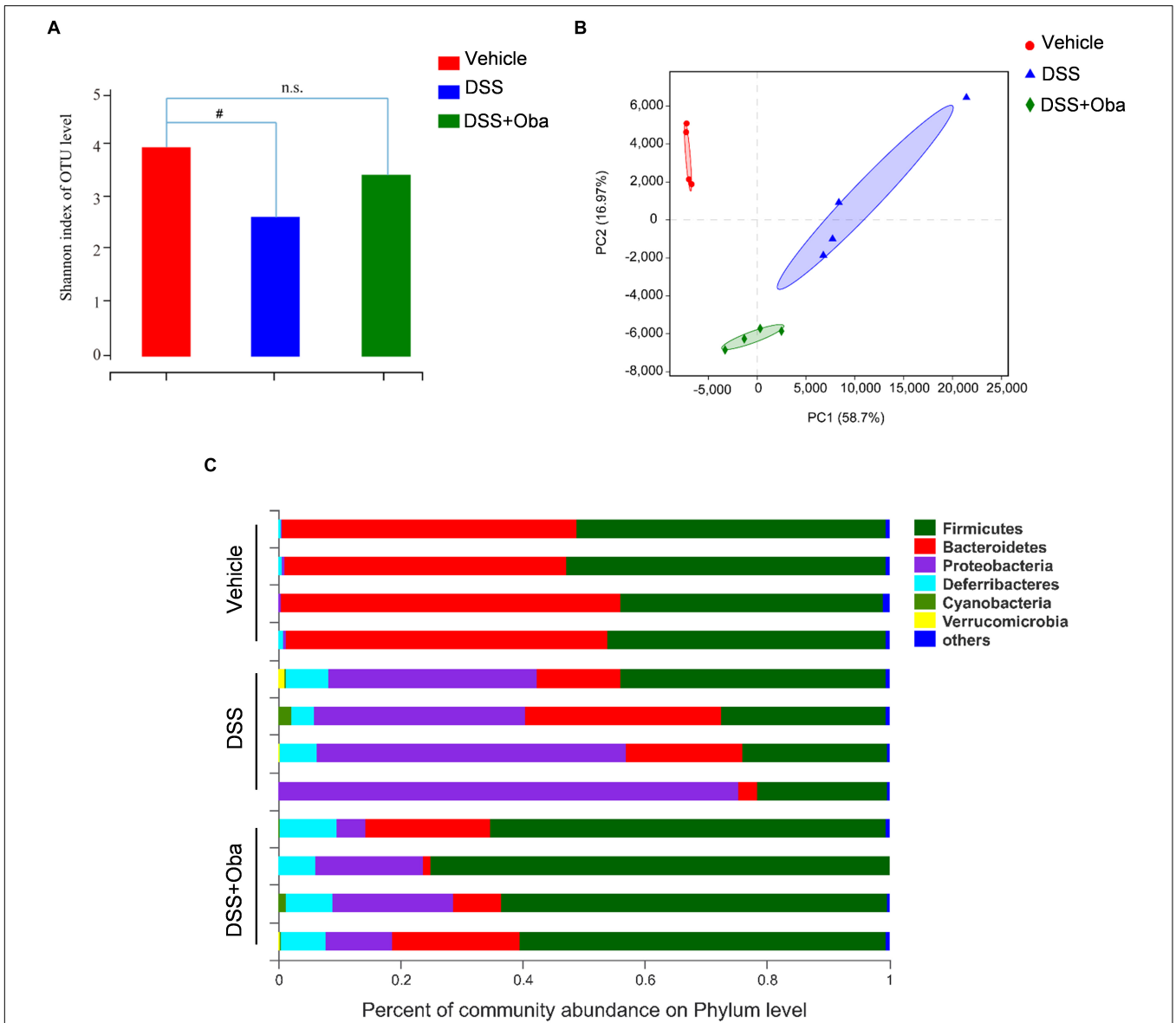

FIGURE 3 | Obacunone modulated the composition of gut microbiota in DSS-treated mice. **(A)** Index-group Difference Test of Shannon Value in Sample Hierarchical Cluster Tree alpha-Diversity. Student's *t*-test. Classification level: OTU. **(B)** Graph of principal component analysis (PCA) at the genus level. **(C)** The proportion of dominant communities at the phylum level in each group of samples. Phylum-level communities presenting in less than 5% of the samples were merged into others. Data = mean (n = 4 mice per group). $^{\#}p < 0.05$ vs. the control group; n.s., no significance.

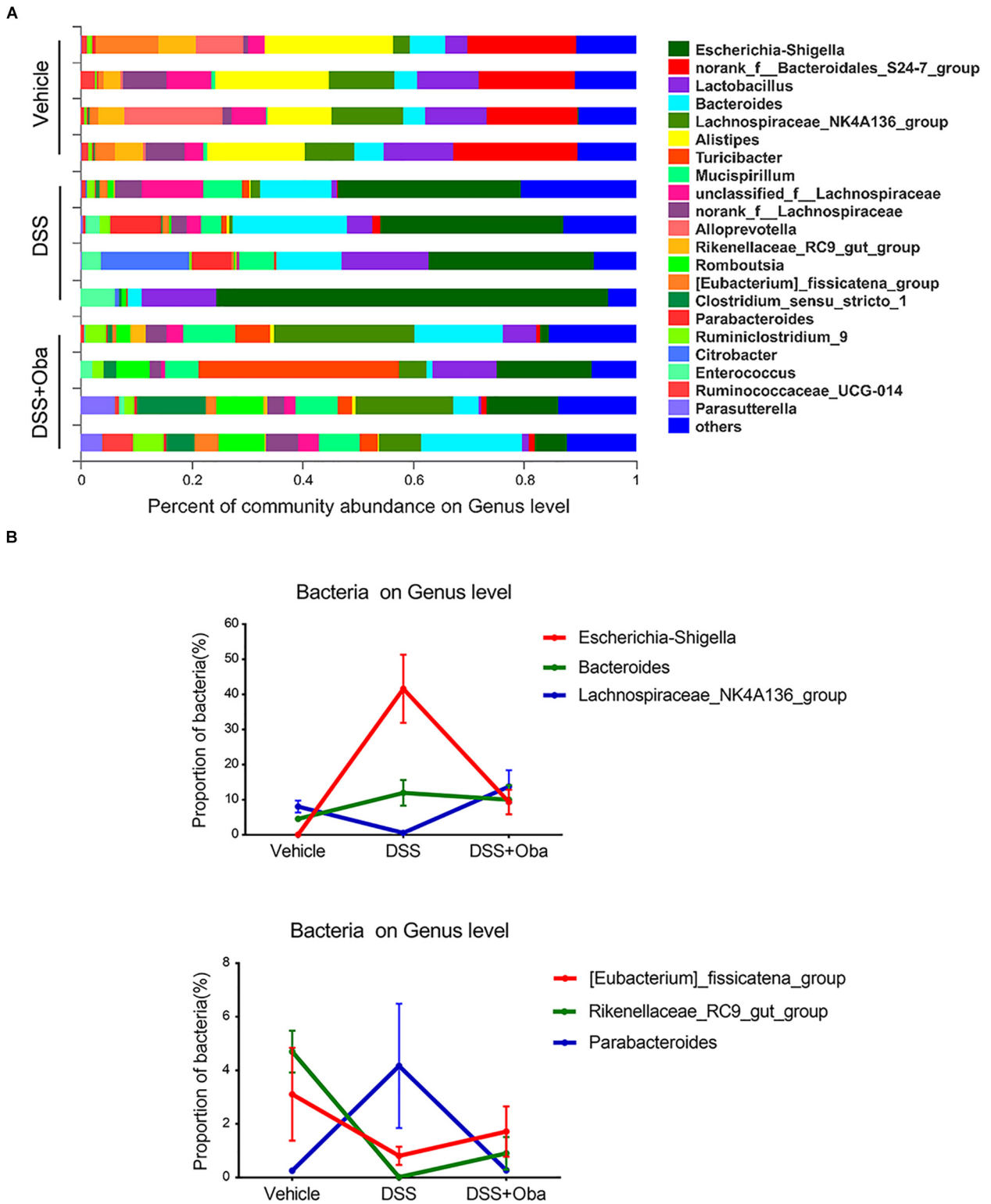

FIGURE 4 | Composition and abundance of gut microbiota at the genus level. **(A)** The proportion of dominant genera in each group of samples. Genus-level communities presenting in less than 5% of the samples were merged into others. **(B)** Distribution of *Escherichia–Shigella*, *Bacteroides*, Lachnospiraceae_NK4A136_group, *(Eubacterium)_fissicatena_group*, *Rikenellaceae_RC9_gut_group*, and *Parabacteroides* in each group. Data were expressed as the mean ± SD (n = 4 mice per group).

sequencing data were analyzed on the online Majorbio I-Sanger Cloud Platform[1].

RESULTS

Obacunone Exerted Protective Effects Against DSS-Induced Colitis in Mice

Dextran sulfate sodium-induced colitic mice exhibited body weight loss, accompanied by diarrhea, and bloody stools, compared with vehicle- or obacunone only-treated mice. However, treatment with obacunone (50 or 100 mg/kg) significantly attenuated disease symptoms in DSS-treated mice, including weight loss, diarrhea, bloody stool, and colonic shortening (**Figures 1A–D**). Moreover, the mice in the obacunone (100 mg/kg)-only treatment group showed an almost identical disease hallmark to that of vehicle-treated mice, indicating that obacunone had no obvious toxic side effects.

Additionally, examination of pathological colon tissue sections showed that DSS treatment resulted in severe intestinal epithelial injury, including crypt loss, mucosal ulceration, muscle thickening, and neutrophil infiltration. Obacunone (25, 50, or 100 mg/kg)-treated mice presented reduced loss of mucosal architecture, fewer ulcerations, and less cellular infiltration (**Figures 2A,B**). Because obacunone treatment at 100 mg/kg produced the best phenotypes, 100 mg/kg treatment group was used in the subsequent experimental analyses.

Obacunone Exerted a Modulating Effect on the Disordered Gut Microbiota of IBD Mice

Bacterial 16S rRNA gene sequencing was used to evaluate the effect of obacunone on DSS-induced changes in gut microbiota composition. Principal component analysis (PCA) revealed that each group was clustered separately (**Figures 3A,B**). The Shannon index was used to characterize the overall microbial diversity. The results showed that microbial diversity was significantly decreased in DSS-treated mice, whereas obacunone treatment mitigated these changes (**Figure 3A**), although the difference was not significant. The major intestinal bacteria at the phylum level included *Firmicutes*, *Bacteroidetes*, *Proteobacteria*, *Deferribacteres*, *Cyanobacteria*, and *Verrucomicrobia* (**Figure 3C**). Moreover, DSS treatment decreased the relative abundance of *Bacteroidetes* and enriched the abundance of *Proteobacteria* compared with that of the vehicle-treated group; however, obacunone treatment mitigated the DSS-induced phylum-level changes (**Supplementary Table 1**). At the genus level, the DSS-treated group exhibited proportional decreases in the abundances of *Lachnospiraceae-NK4A136-group*, *Rikenellaceae-RC9-gut-group*, and *(Eubacterium)-fissicatena-group*, but these changes were attenuated by obacunone administration (**Figures 4A,B**). Furthermore, the abundance of some pathogenic bacteria such as *Escherichia–Shigella* and *Enterococcus*, was significantly increased in DSS-treated group, whereas the abundance of *Escherichia–Shigella* and *Enterococcus* was decreased as a result of obacunone treatment (**Figures 4A,B** and **Supplementary Table 2**). Collectively, our results revealed that DSS treatment disturbed gut microbiota homeostasis, and this gut microbiota imbalance could be reversed by obacunone treatment.

Obacunone Exerted a Protective Effect on the Integrity of the Intestinal Barrier in Colitic Mice

To assess the integrity of the intestinal barrier in colitic mice, we determined the expression levels of the tight junction proteins, TJP1 and occludin, in colonic tissue of DSS-induced colitic mice. The results showed that the expression levels of TJP1 and occludin were markedly downregulated in DSS-treated mice (**Figures 5A,B**). However, obacunone treatment significantly rescued the reduced expression of these barrier proteins, indicating that obacunone might exert a protective effect against DSS-induced disruption of intestinal epithelial barrier integrity.

Obacunone Inhibited the TLR4/NF-κB Signaling Cascade in Colitic Mice

To investigate the mechanisms underlying obacunone-associated attenuation in DSS-induced intestinal inflammation, we evaluated the effect of obacunone on the protein expression

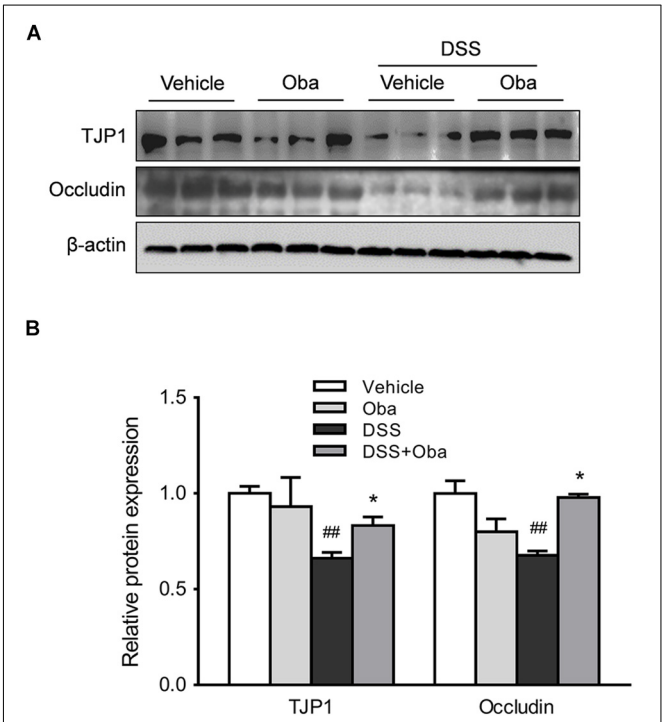

FIGURE 5 | Obacunone inhibited the DSS-induced loss of TJP1 and occludin protein expression. Effect of obacunone on tight junction protein (TJP1 and occludin) expression in colonic tissues. Representative western blots **(A)** and quantitative analysis **(B)** of the TJP1 and occludin proteins. Data were expressed as the mean ± SD (n = 3 mice per group). $^{*}p < 0.05$ vs. the DSS-treated group; $^{\#\#}p < 0.01$ vs. the control group.

[1]www.i-sanger.com

levels of inflammatory mediators. Significant increase in the expression levels of nitric oxide synthase, cyclooxygenase 2 (COX-2), interferon gamma (IFN-γ), and TNF-α was observed in the colon of DSS-induced colitic mice (**Figures 6A,B**). However, obacunone administration greatly reduced the expression levels of these inflammatory mediators in the colons of colitic mice. Moreover, the protein expression levels of TLR4, myeloid differentiation primary response gene 88 (MyD88), p-p65 (a subunit of NF-κB), and p-IκBα (an inhibitor of NF-κB) in colonic tissue was significantly increased after DSS treatment (**Figures 6C,D**). However, all these abnormally increased expression levels were markedly downregulated in colitic mice with obacunone treatment. Combined, these results indicated that obacunone exerted a protective effect against DSS-induced colitis through attenuation of TLR4/NF-κB signaling cascades.

Obacunone Decreased the LPS-Induced Production of Proinflammatory Mediators in RAW264.7 Macrophages

RAW264.7 mouse macrophages were used to further evaluate the anti-inflammatory effects of obacunone. The initial cytotoxicity evaluation suggested that obacunone was almost non-cytotoxic at dosages up to 100 μM (**Figure 7A**). Additionally, we found that obacunone markedly suppressed LPS-stimulated NO production in RAW264.7 cells in a concentration-dependent manner (0–100 μM) (**Figure 7B**). Meanwhile, the protein expression levels of the proinflammatory mediators iNOS and COX-2 were significantly increased in RAW264.7 cells after exposure to LPS. However, obacunone concentration-dependently decreased the LPS-induced increase in the levels of iNOS and COX-2 (**Figures 7C,D**). We then quantified the mRNA expression levels of pro-inflammatory mediators. The results showed that the mRNA levels of IL-1α, IL-1β, IL-16, COX-2, and iNOS were markedly upregulated in LPS-stimulated macrophages; however, obacunone treatment attenuated the LPS-induced increase in the mRNA levels of these proinflammatory mediators (**Figure 7E**).

Obacunone Exerted a Protective Effect on Intestinal Epithelial Barrier Integrity in Epithelial Cells

The human colonic epithelial cell line NCM460 is commonly used to investigate the mechanisms of inflammatory damage and repair in intestinal epithelial barrier (Tsoi et al., 2017). We found that obacunone markedly increased NCM460 cell viability in a concentration-dependent manner (**Figure 8A**). Further, our study showed that TNF-α treatment downregulated the expression levels of the tight junction proteins TJP1 and occludin; however, these decreased expression levels were significantly reversed by obacunone treatment (**Figure 8B**).

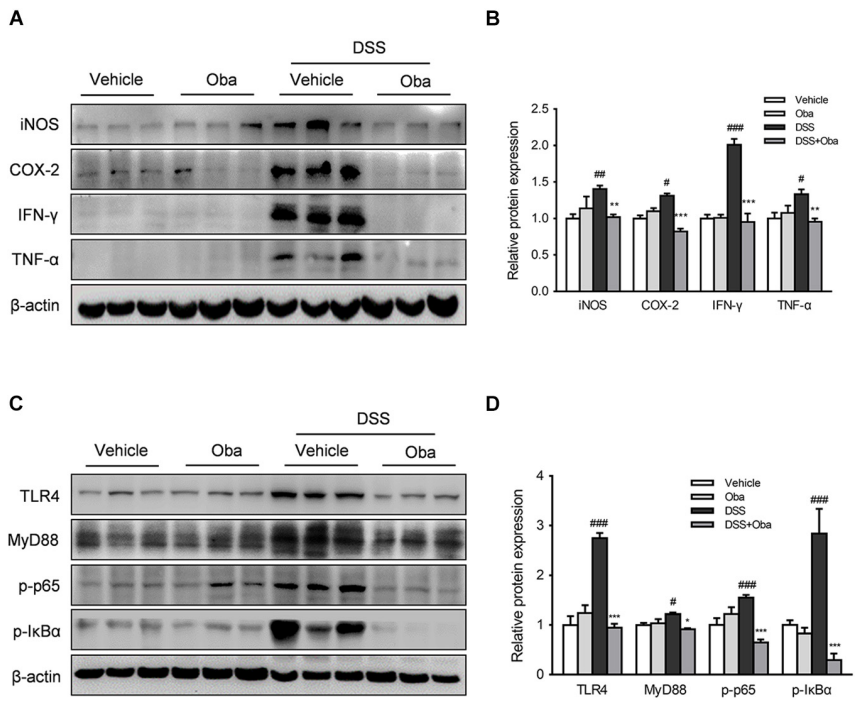

FIGURE 6 | Obacunone inhibited TLR4/NF-κB signaling *in vivo*. After the mice had been euthanized, colon samples were removed and evaluated. **(A,B)** Effect of obacunone on the protein expression levels of inflammatory mediators in colon tissue. Western blot analysis of the expression of iNOS, COX-2, IFN-γ, and TNF-α in each group. A representative blot is shown. The expression levels of all the proteins were normalized to actin. **(C,D)** Western blot analysis of the expression of TLR4, MyD88, p-IκBα, and p-p65 in each group. A representative blot is shown. Data were presented as the mean ± SD ($n = 3$). $^{*}p < 0.05$, $^{**}p < 0.01$, $^{***}p < 0.001$ vs. the DSS-treated group; $^{\#}p < 0.05$, $^{\#\#}p < 0.01$, $^{\#\#\#}p < 0.001$ vs. the control group.

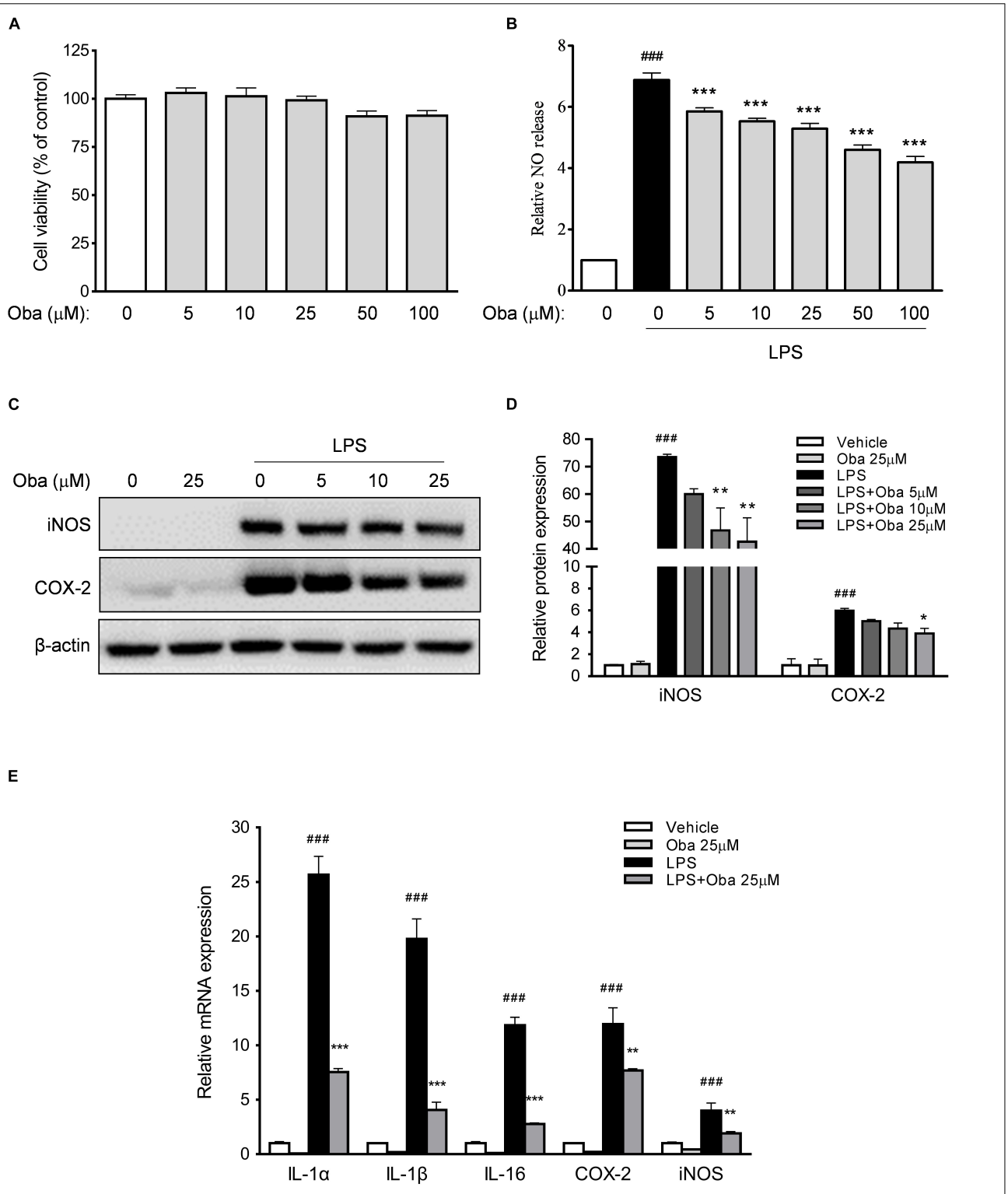

FIGURE 7 | Obacunone inhibited the expression of pro-inflammatory mediators *in vitro*. **(A,B)** Effect of obacunone on the viability and NO secretion levels of LPS-induced RAW264.7 macrophages. Cells were treated with obacunone (0–100 μM) for 24 h, after which cell viability and NO production were determined. **(C,D)** RAW264.7 macrophages were treated as described in section "Materials and Methods." The protein expression levels of iNOS and COX-2 in RAW264.7 cells were determined by western blot. Protein expression levels were normalized to that of actin. **(E)** Effect of obacunone on the mRNA expression of proinflammatory mediators in LPS-induced cells. RAW264.7 macrophages were treated as described in section "Materials and Methods," following which the mRNA expression levels of IL-1α, IL-1β, IL-16, COX-2, and iNOS were determined by qRT-PCR. All mRNA expression levels were normalized to that of actin. Data were presented as the mean ± SD ($n = 3$). $^{*}p < 0.05$, $^{**}p < 0.01$, $^{***}p < 0.001$ vs. the DSS-treated group; $^{\#\#\#}p < 0.001$ vs. the control group.

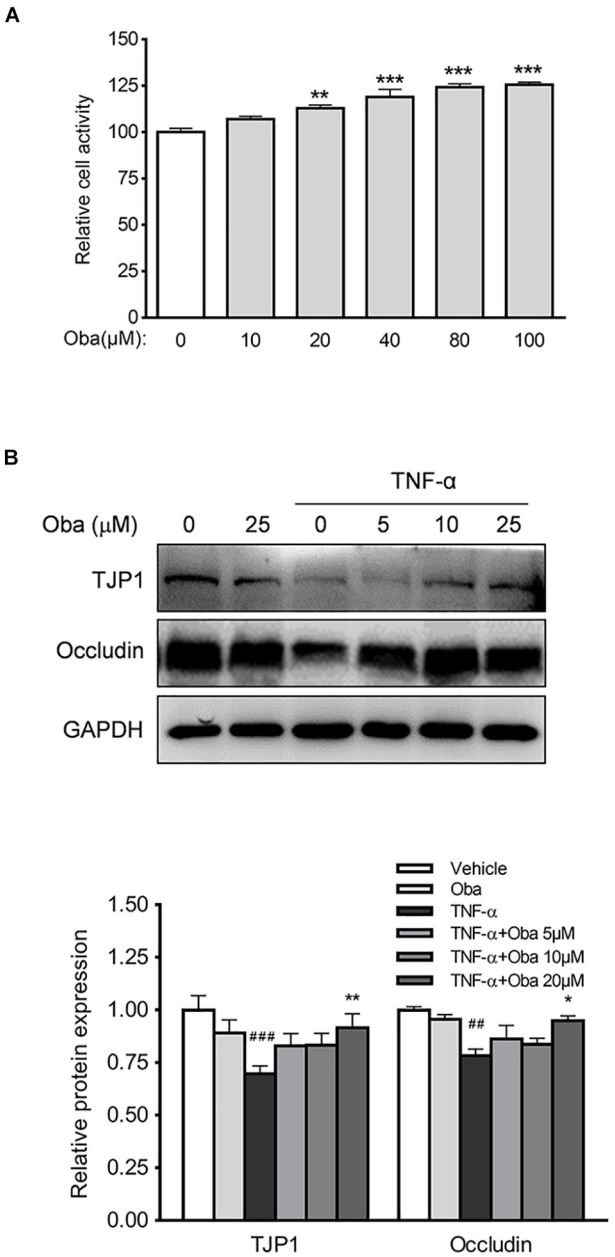

FIGURE 8 | Obacunone inhibited TNF-α-induced loss of TJP1 and occludin. **(A)** Effect of obacunone on the viability of NCM460 cells. The cells were treated with obacunone (0–100 μM) for 24 h and cell viability was then measured. **(B)** Effect of obacunone on the expression of the tight junction proteins TJP1 and occludin in TNF-α-stimulated NCM460 cells. Representative western blots and quantitative analysis of TJP1 and occludin protein. Data were expressed as the mean ± SD (n = 3 mice per group). $^{*}p < 0.05$, $^{**}p < 0.01$, $^{***}p < 0.001$ vs. the DSS-treated group; $^{\#\#}p < 0.01$, $^{\#\#\#}p < 0.001$ vs. control group.

DISCUSSION

Ulcerative colitis is a refractory inflammatory condition that affects the digestive tract, and the lesions are mainly located in the colon, rectum, or entire colorectal mucosa. Although the global incidence of UC has shown a gradual increase (Yue et al., 2018), therapeutic drugs with limited side effects are still not available for the treatment of UC patients. Consequently, the pathogenesis of UC and the optimal treatment approaches for this condition have attracted increasing attention in recent years (Zhang and Li, 2014).

Animal models with clinical characteristics and pathological changes similar to those observed in UC patients are important tools for investigating drug discovery, action mechanisms, and therapeutic exploration associated with the pathogenesis of UC (Bamias et al., 2017). As a well-known experimental UC model, the DSS-induced disease symptoms of disrupted epithelial barrier function and thereby increased exposure of innate immune elements in lamina propria to the invasive gut microbiota, are distinguished and are resemble with that of UC patients (Eichele and Kharbanda, 2017). In the current study, we found that mice with DSS treatment exhibited severe intestinal inflammation, which was accompanied with body weight loss, bloody diarrhea, the formation of large ulcers, diffuse necrosis, and neutrophil infiltration. However, obacunone treatment markedly alleviated these DSS-induced symptoms of colitis. Moreover, no toxic reaction was observed in the obacunone-treated mice, suggesting the relative safety for obacunone's potential clinical application.

Changes in the composition of gut microbiota were recently shown to be highly correlated with the incidence of UC. Severe dysbacteriosis has been reported in patients with UC, which is reflected in a reduced abundance of the commensal intestinal bacteria, *Firmicutes* and *Bacteroidetes*, and an increased abundance of pathogenic *Proteobacteria* (Ni et al., 2017; Sommer et al., 2017). Through 16S rRNA gene sequencing, we also found differences in gut bacterial community composition between DSS-treated group and normal control group, which included a decrease in the commensal intestinal bacteria (such as *Firmicutes* and *Bacteroidetes*) and an increase in pathogenic bacteria (such as *Proteobacteria*). However, after obacunone treatment, there was a shift in the composition of the bacterial community, which became more alike that of the vehicle group, indicative of an improving trend. Furthermore, a new study showed that there is a greater abundance of *Escherichia–Shigella* (a *Proteobacteria*) in the inflamed mucosae than in non-inflamed mucosae in UC patients (Baumgart et al., 2007; Xu et al., 2018). Moreover, *Escherichia–Shigella* is a Gram-negative bacterium that invades the human colonic epithelium and induces inflammatory responses owing to the presence of LPS in its outer membrane (Gronbach et al., 2014; Stephens and von der Weid, 2019). In our study, DSS treatment also led to an increase in the abundance of *Escherichia–Shigella*; however, this increase was attenuated with obacunone treatment.

Toll-like receptor 4, as the first identified human toll-like receptor, has been extensively investigated. TLR4 recognizes the exogenous bacterial ligand, LPS, and activates a signaling cascade that leads to pro-inflammatory response to destroy the invading pathogens (Liu et al., 2014; Holdbrook et al., 2019). Activation of TLR4 is known to trigger both MyD88-dependent and MyD88-independent pathways, which in turn lead to the activation

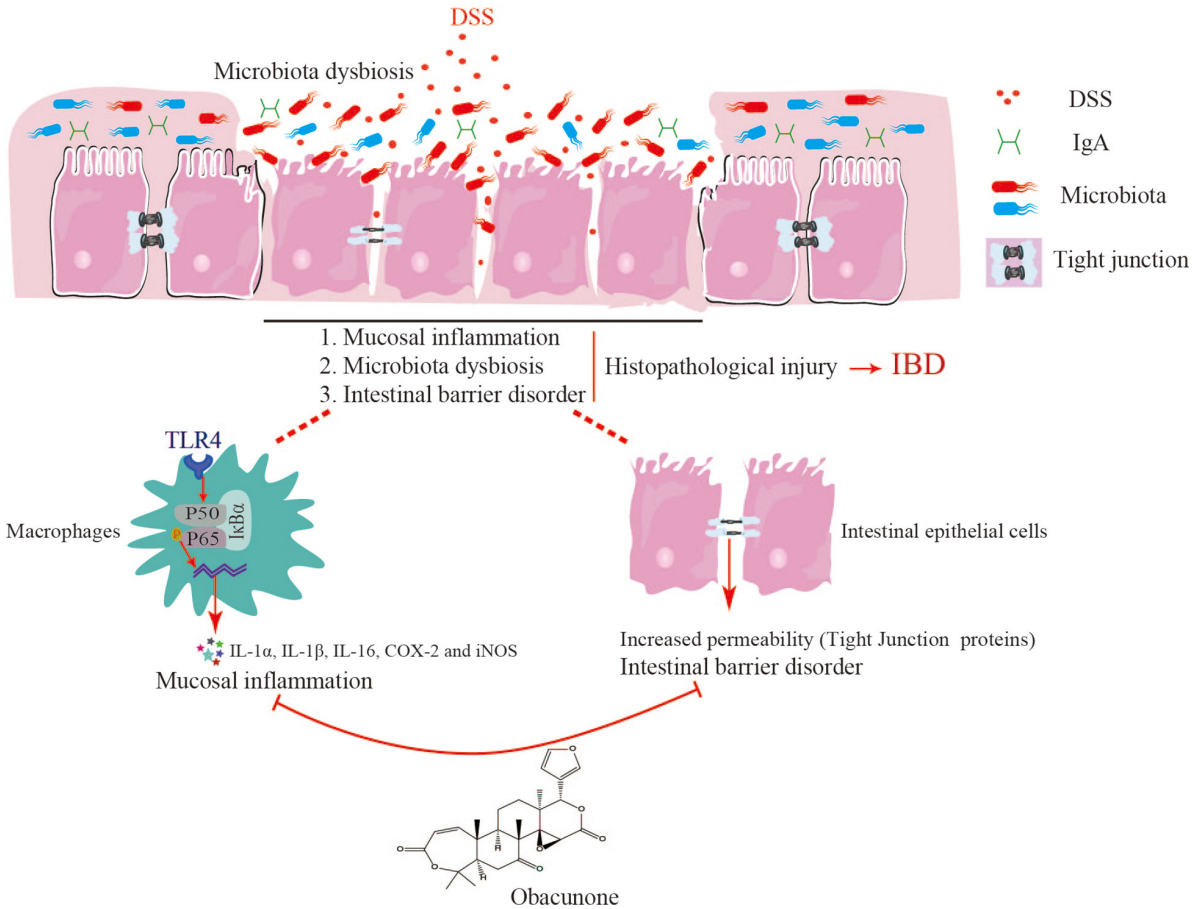

FIGURE 9 | Obacunone presented an anti-colitis efficacy, at least partially, via the modulation of the gut microbiota and attenuation of TLR4/NF-κB signaling cascades, as well as protection against disruption of the intestinal epithelial barrier.

of NF-κB and production of inflammatory mediators (O'Neill, 2002). It is widely accepted that TLR4 is a double-edged sword, as minor activation of TLR4 is essential in the maintenance of immune homeostasis, while excessive TLR4 activation can lead to the induction of host inflammatory responses (Steimle et al., 2019). TLR4 is highly expressed in the colon tissues of UC patients and DSS-induced colitic mice, and is considered to be a contributing factor to the initiation and development of intestinal inflammation in UC (Taniguchi et al., 2009; Murad, 2014; Yue et al., 2019). We found that the protein expression levels of TLR4, MyD88, p-p65, and p-IκBα were significantly increased in DSS-induced colitic mice; however, the expression levels of TLR4 and its downstream proteins were markedly decreased by obacunone treatment. Our results were consistent with the previous reports (Shi et al., 2019).

Furthermore, as the first line of immune defense, the intestinal epithelial barrier is crucial for the protection of the host against invasive pathogenic bacteria or viruses. With the loss of intestinal barrier integrity, bacteria (e.g., *Escherichia–Shigella*) and toxic substances (e.g., LPS) can penetrate through the intestinal wall and trigger the aforementioned feedback cycle (Chelakkot et al., 2018; Marin et al., 2019). TJPs are vital for the maintenance of epithelium integrity, and dysregulation of tight junctions is frequently correlated with the loss of intestinal barrier integrity (Turner et al., 2014). In our study, we used a human intestinal epithelial cell line NCM460 to explore the effects of obacunone on the expression of TJPs. Interestingly, we found that the protein expression levels of TJP1 and occludin were increased by obacunone treatment, whereas the levels of the barrier proteins were decreased in UC mice, as well as in TNF-α-stimulated NCM460 cells.

CONCLUSION

In summary, for the first time, our study indicated that obacunone alleviated intestinal damage, bloody stools, and diarrhea symptoms in DSS-induced colitic mice. Moreover, the anti-inflammatory effect of obacunone was exerted, at least partially, via the modulation of the gut microbiota and attenuation of TLR4/NF-κB signaling cascades, as well as protection against disruption of the intestinal epithelial barrier (**Figure 9**). Importantly, non of mice that received obacunone alone exhibited apparent clinical lesions or mucosal damage

throughout the study, indicating the relative safety of obacunone management. The current results strongly suggest that obacunone could be a potential therapeutic drug in colitis. This work allow us to hypothesized the potential application of obacunone on other bowel diseases such as Crohn's disease and colitis associated colorectal cancer. However, the further studies are required to confirm these hypotheses.

DATA AVAILABILITY STATEMENT

The raw data supporting the conclusions of this article will be made available by the authors, without undue reservation, to any qualified researcher.

ETHICS STATEMENT

The animal study was reviewed and approved by the Animal Experimentation Ethics Committee at Shanghai University of Traditional Chinese Medicine (Animal license key: SYXK2014-0008).

AUTHOR CONTRIBUTIONS

ZW and WD conceived and designed the experiments. XL, BY, ZY, YR, JZ, and JR performed the experiments and collected the data. XL, BY, ZY, and YR analyzed the data. BY and WD wrote the manuscript. XL, ZW, and WD supervised the study.

FUNDING

This work was funded through the National Natural Science Foundation of China (Grant Nos. 81920108033 and 81530096) and Natural Science Foundation of Shanghai (Grant No. 17ZR1427800).

SUPPLEMENTARY MATERIAL

The Supplementary Material for this article can be found online at: https://www.frontiersin.org/articles/10.3389/fmicb.2020.00497/full#supplementary-material

REFERENCES

Bamias, G., Arseneau, K. O., and Cominelli, F. (2017). Mouse models of inflammatory bowel disease for investigating mucosal immunity in the intestine. *Curr. Opin. Gastroenterol.* 33, 411–416. doi: 10.1097/MOG.0000000000000402

Baumgart, M., Dogan, B., Rishniw, M., Weitzman, G., Bosworth, B., Yantiss, R., et al. (2007). Culture independent analysis of ileal mucosa reveals a selective increase in invasive *Escherichia coli* of novel phylogeny relative to depletion of Clostridiales in Crohn's disease involving the ileum. *ISME J.* 1, 403–418. doi: 10.1038/ismej.2007.52

Bernstein, C. N. (2017). Review article: changes in the epidemiology of inflammatory bowel disease-clues for aetiology. *Aliment. Pharmacol. Ther.* 46, 911–919. doi: 10.1111/apt.14338

Bhat, A. A., Uppada, S., Achkar, I. W., Hashem, S., Yadav, S. K., Shanmugakonar, M., et al. (2018). Tight junction proteins and signaling pathways in cancer and inflammation: a functional crosstalk. *Front. Physiol.* 9:1942. doi: 10.3389/fphys.2018.01942

Chelakkot, C., Ghim, J., and Ryu, S. H. (2018). Mechanisms regulating intestinal barrier integrity and its pathological implications. *Exp. Mol. Med.* 50:103. doi: 10.1038/s12276-018-0126-x

Dou, W., Mukherjee, S., Li, H., Venkatesh, M., Wang, H., Kortagere, S., et al. (2012). Alleviation of gut inflammation by Cdx2/Pxr pathway in a mouse model of chemical colitis. *PLoS One* 7:e36075. doi: 10.1371/journal.pone.0036075

Eichele, D. D., and Kharbanda, K. K. (2017). Dextran sodium sulfate colitis murine model: an indispensable tool for advancing our understanding of inflammatory bowel diseases pathogenesis. *World J. Gastroenterol.* 23, 6016–6029. doi: 10.3748/wjg.v23.i33.6016

Gao, Y., Hou, R., Liu, F., Liu, H., Fei, Q., Han, Y., et al. (2018). Obacunone causes sustained expression of MKP-1 thus inactivating p38 MAPK to suppress pro-inflammatory mediators through intracellular MIF. *J. Cell Biochem.* 119, 837–849. doi: 10.1002/jcb.26248

Gronbach, K., Flade, I., Holst, O., Lindner, B., Ruscheweyh, H. J., Wittmann, A., et al. (2014). Endotoxicity of lipopolysaccharide as a determinant of T-cell-mediated colitis induction in mice. *Gastroenterology* 146, 765–775. doi: 10.1053/j.gastro.2013.11.033

Holdbrook, D. A., Huber, R. G., Marzinek, J. K., Stubbusch, A., Schmidtchen, A., and Bond, P. J. (2019). Multiscale modeling of innate immune receptors: endotoxin recognition and regulation by host defense peptides. *Pharmacol. Res.* 147:104372. doi: 10.1016/j.phrs.2019.104372

Kaplan, G. G. (2015). The global burden of IBD: from 2015 to 2025. *Nat. Rev. Gastroenterol. Hepatol.* 12, 720–727. doi: 10.1038/nrgastro.2015.150

Liu, Y., Yin, H., Zhao, M., and Lu, Q. (2014). TLR2 and TLR4 in autoimmune diseases: a comprehensive review. *Clin. Rev. Allergy Immunol.* 47, 136–147. doi: 10.1007/s12016-013-8402-y

Luo, X., Yu, Z., Deng, C., Zhang, J., Ren, G., Sun, A., et al. (2017). Baicalein ameliorates TNBS-induced colitis by suppressing TLR4/MyD88 signaling cascade and NLRP3 inflammasome activation in mice. *Sci. Rep.* 7:16374. doi: 10.1038/s41598-017-12562-6

Marin, M., Holani, R., Blyth, G., Drouin, D., Odeon, A., and Cobo, E. R. (2019). Human cathelicidin improves colonic epithelial defenses against *Salmonella* typhimurium by modulating bacterial invasion. TLR4 and pro-inflammatory cytokines. *Cell Tissue Res.* 376, 433–442. doi: 10.1007/s00441-018-02984-7

Matsuoka, K., and Kanai, T. (2015). The gut microbiota and inflammatory bowel disease. *Semin. Immunopathol.* 37, 47–55. doi: 10.1007/s00281-014-0454-4

Mirsepasi-Lauridsen, H. C., Vallance, B. A., Krogfelt, K. A., and Petersen, A. M. (2019). *Escherichia coli* pathobionts associated with inflammatory bowel disease. *Clin. Microbiol. Rev.* 32:e00060-18. doi: 10.1128/CMR.00060-18

Murad, S. (2014). Toll-like receptor 4 in inflammation and angiogenesis: a double-edged sword. *Front. Immunol.* 5:313. doi: 10.3389/fimmu.2014.00313

Murthy, K. N., Jayaprakasha, G. K., and Patil, B. S. (2015). Cytotoxicity of obacunone and obacunone glucoside in human prostate cancer cells involves Akt-mediated programmed cell death. *Toxicology* 329, 88–97. doi: 10.1016/j.tox.2015.01.008

Neurath, M. F. (2017). Current and emerging therapeutic targets for IBD. *Nat. Rev. Gastroenterol. Hepatol.* 14, 269–278. doi: 10.1038/nrgastro.2016.208

Ni, J., Wu, G. D., Albenberg, L., and Tomov, V. T. (2017). Gut microbiota and IBD: causation or correlation? *Nat. Rev. Gastroenterol. Hepatol.* 14, 573–584. doi: 10.1038/nrgastro.2017.88

O'Neill, L. A. (2002). Signal transduction pathways activated by the IL-1 receptor/toll-like receptor superfamily. *Curr. Top. Microbiol. Immunol.* 270, 47–61. doi: 10.1007/978-3-642-59430-4_3

Rosen, M. J., Dhawan, A., and Saeed, S. A. (2015). Inflammatory bowel disease in children and adolescents. *JAMA Pediatr.* 169, 1053–1060. doi: 10.1001/jamapediatrics.2015.1982

Shi, Y. J., Gong, H. F., Zhao, Q. Q., Liu, X. S., Liu, C., and Wang, H. (2019). Critical role of toll-like receptor 4 (TLR4) in dextran sulfate sodium (DSS)-induced intestinal injury and repair. *Toxicol. Lett.* 15, 23–30. doi: 10.1016/j.toxlet.2019.08.012

Sokol, H. (2014). Probiotics and antibiotics in IBD. *Dig. Dis.* 32(Suppl. 1), 10–17. doi: 10.1159/000367820

Sommer, F., Anderson, J. M., Bharti, R., Raes, J., and Rosenstiel, P. (2017). The resilience of the intestinal microbiota influences health and disease. *Nat. Rev. Microbiol.* 15, 630–638. doi: 10.1038/nrmicro.2017.58

Steimle, A., Michaelis, L., Di Lorenzo, F., Kliem, T., Munzner, T., Maerz, J. K., et al. (2019). Weak agonistic LPS restores intestinal immune homeostasis. *Mol. Ther.* 27, 1974–1991. doi: 10.1016/j.ymthe.2019.07.007

Stephens, M., and von der Weid, P. Y. (2019). Lipopolysaccharides modulate intestinal epithelial permeability and inflammation in a species-specific manner. *Gut Microbes* 16, 1–12. doi: 10.1080/19490976.2019.1629235

Taniguchi, Y., Yoshioka, N., Nakata, K., Nishizawa, T., Inagawa, H., Kohchi, C., et al. (2009). Mechanism for maintaining homeostasis in the immune system of the intestine. *Anticancer Res.* 29, 4855–4860.

Tsoi, H., Chu, E., Zhang, X., Sheng, J., Nakatsu, G., Ng, S. C., et al. (2017). Peptostreptococcus anaerobius induces intracellular cholesterol biosynthesis in colon cells to induce proliferation and causes dysplasia in mice. *Gastroenterology* 152, 1419–1433. doi: 10.1053/j.gastro.2017.01.009

Turner, J. R., Buschmann, M. M., Romero-Calvo, I., Sailer, A., and Shen, L. (2014). The role of molecular remodeling in differential regulation of tight junction permeability. *Semin. Cell Dev. Biol.* 36, 204–212. doi: 10.1016/j.semcdb.2014.09.022

Wang, C., Li, Q., and Ren, J. (2019). Microbiota-Immune interaction in the pathogenesis of gut-derived infection. *Front. Immunol.* 10:1873. doi: 10.3389/fimmu.2019.01873

Xu, J., Chen, N., Wu, Z., Song, Y., Zhang, Y., Wu, N., et al. (2018). 5-Aminosalicylic acid alters the gut bacterial microbiota in patients with ulcerative colitis. *Front. Microbiol.* 9:1274. doi: 10.3389/fmicb.2018.01274

Yue, B., Luo, X., Yu, Z., Mani, S., Wang, Z., and Dou, W. (2019). Inflammatory bowel disease: a potential result from the collusion between gut microbiota and mucosal immune system. *Microorganisms* 7:E440. doi: 10.3390/microorganisms7100440

Yue, B., Ren, Y. J., Zhang, J. J., Luo, X. P., Yu, Z. L., Ren, G. Y., et al. (2018). Anti-inflammatory effects of fargesin on chemically induced inflammatory bowel disease in mice. *Molecules* 23:1380. doi: 10.3390/molecules23061380

Zhang, Y. Z., and Li, Y. Y. (2014). Inflammatory bowel disease: pathogenesis. *World J. Gastroenterol.* 20, 91–99. doi: 10.3748/wjg.v20.i1.91

Conflict of Interest: The authors declare that the research was conducted in the absence of any commercial or financial relationships that could be construed as a potential conflict of interest.

frontiers in Immunology

ORIGINAL RESEARCH
published: 23 April 2020
doi: 10.3389/fimmu.2020.00692

Allergen-Specific Immunotherapy With Liposome Containing CpG-ODN in Murine Model of Asthma Relies on MyD88 Signaling in Dendritic Cells

*Ricardo Wesley Alberca-Custodio[1], Lucas D. Faustino[2], Eliane Gomes[1], Fernanda Peixoto Barbosa Nunes[1], Mirian Krystel de Siqueira[1], Alexis Labrada[3], Rafael Ribeiro Almeida[1], Niels Olsen Saraiva Câmara[1], Denise Morais da Fonseca[1] and Momtchilo Russo[1]**

[1] Institute of Biomedical Sciences, Department of Immunology, University of São Paulo, São Paulo, Brazil, [2] Center for Immunology and Inflammatory Diseases, Division of Rheumatology, Allergy and Immunology, Massachusetts General Hospital, Harvard Medical School, Boston, MA, United States, [3] Department of Allergens, National Center of Bioproducts (BIOCEN), Havana, Cuba

OPEN ACCESS

Edited by:
Marcello Chieppa,
European Biomedical Research Institute of Salerno, Italy

Reviewed by:
Attila Bacsi,
University of Debrecen, Hungary
Lakshna Mahajan,
University of Delhi, India

***Correspondence:**
Momtchilo Russo
momrusso@usp.br;
momrusso@icb.usp.br

Specialty section:
This article was submitted to Molecular Innate Immunity, a section of the journal Frontiers in Immunology

Received: 17 December 2019
Accepted: 26 March 2020
Published: 23 April 2020

Citation:
Alberca-Custodio RW, Faustino LD, Gomes E, Nunes FPB, de Siqueira MK, Labrada A, Almeida RR, Câmara NOS, da Fonseca DM and Russo M (2020) Allergen-Specific Immunotherapy With Liposome Containing CpG-ODN in Murine Model of Asthma Relies on MyD88 Signaling in Dendritic Cells. Front. Immunol. 11:692. doi: 10.3389/fimmu.2020.00692

Changing the immune responses to allergens is the cornerstone of allergen immunotherapy. Allergen-specific immunotherapy that consists of repeated administration of increasing doses of allergen extract is potentially curative. The major inconveniences of allergen-specific immunotherapy include failure to modify immune responses, long-term treatment leading to non-compliance and the potential for developing life-threating anaphylaxis. Here we investigated the effect of a novel liposomal formulation carrying low dose of allergen combined with CpG-ODN, a synthetic TLR9 agonist, on established allergic lung inflammation. We found that challenge with allergen (OVA) encapsulated in cationic liposome induced significantly less severe cutaneous anaphylactic reaction. Notably, short-term treatment (three doses) with a liposomal formulation containing co-encapsulated allergen plus CpG-ODN, but not allergen or CpG-ODN alone, reversed an established allergic lung inflammation and provided long-term protection. This liposomal formulation was also effective against allergens derived from *Blomia tropicalis* mite extract. The attenuation of allergic inflammation was not associated with increased numbers of Foxp3-positive or IL-10-producing regulatory T cells or with increased levels of IFN-gamma in the lungs. Instead, the anti-allergic effect of the liposomal formulation was dependent of the innate immune signal transduction generated in CD11c-positive putative dendritic cells expressing MyD88 molecule. Therefore, we highlight the pivotal role of dendritic cells in mediating the attenuation of established allergic lung inflammation following immunotherapy with a liposomal formulation containing allergen plus CpG-ODN.

Keywords: allergen, immunotherapy, dendritic cell, MyD88, asthma

INTRODUCTION

Asthma is a complex chronic respiratory disorder characterized by episodes of cough and wheezing with increased mucus secretion that results in variable airflow limitation and airway hyper-responsiveness (1). Nowadays, it is becoming clear that asthma is a syndrome that encompasses various clinical phenotypes generally divided in "Th2 high" and "Th2 low" forms that correspond respectively to atopic or non-atopic asthma (2), with a wide variation in prevalence and severity (3). Patients with a high Th2 endotype show elevated levels of IL-4, IL-5, IL-9, and IL-13 in the airways (4, 5). These cytokines mediate allergic eosinophilic inflammation and isotype switching to IgE (6).

It is postulated that asthma can be either prevented or suppressed by intrinsic and/or extrinsic factors that collectively modify the immune responses to airborne allergens (7). Among extrinsic factors, the "hygiene hypothesis" gained special interest by postulating that early life infections are required for reduced predisposition to develop allergic diseases (8). However, the cellular and molecular mechanisms of the immunological switch against airborne allergens are still elusive. Different mechanisms such as maturation of the immune system, immune-deviation toward a Th1 profile, active suppression by different regulatory cells including Foxp3-expressing regulatory T (Treg) cells, IL-10-producing T or B regulatory cells, or anergy have been proposed (9). Whatever the mechanism, the clinical course of asthma suffers significant influence by life-style, nutrition, infections and microbial products (10). Indeed, bacteria and helminths in the digestive tract offer protection against asthma and allergies (11–14). Moreover, numerous reports have shown the inhibitory effects of bacterial components on allergic responses (15). For example, children that live in rural areas are exposed to higher concentrations of dust muramic acid, a constituent of peptidoglycan present in gram-negative and gram-positive bacteria, showed a lower prevalence of asthma and wheezing compared with children that live in urban areas (16). Experimentally, the hygiene hypothesis could be approached using microbial infections or microbial products that signal through toll-like receptors (TLR). Many bacterial components have previously been used in experimental asthma models aiming to improve the treatment effectiveness (17–20). We have previously shown that among TLR agonists studied, the TLR9 agonist CpG-oligodeoxynucleotides, hereafter denominated CpG, was the most effective in preventing allergic sensitization (21).

Changing the immune responses to allergens is the golden-standard of allergen-specific immunotherapy since its introduction in 1911 (22). Allergen specific immunotherapy consists of repeated and long-term applications of increasing doses of a particular allergen or group of allergens by subcutaneous or sublingual routes. However, there are numerous inconveniences of allergen-specific immunotherapy including failure to modify the immune system, long-term treatment that results in non-compliance, allergy exacerbation and the potential for developing systemic allergic reactions and life-threating anaphylaxis. Here, we sought to investigate the effect of a novel immunotherapy formulation in a murine model of asthma that consisted of short-term treatment (three doses) with low concentrations of allergen and CpG co-encapsulated in a cationic liposome composed of N-[1-(2,3-Dioleoyloxy) propyl] -NN, N, N-trimethylammonium-(DOTAP). The use of liposomal formulation to encapsulate allergen and CpG was chosen due to its ability to transport DNA, RNA, and other negatively-charged molecules into eukaryotic cells (23) and, therefore, with the potential to limit the contact of the allergen with anaphylactic antibodies and consequent anaphylaxis while enhancing CpG signaling through endosomal TLR9 (24).

MATERIALS AND METHODS

Animals

Six-to-eight-week-old female 129S1, C57BL/6 mice (WT), MyD88-KO were originally purchased from Jackson Laboratories (Bar Harbor, ME). Mice expressing the recombinase Cre under the control of Itgax promoter (CD11c-Cre) (25) and *Myd88 fl/fl* mice (26) were bred together to generate CD11cMyD88$^{-/-}$ (DC-MyD88$^{-/-}$) and proper littermates CD11cMyD88$^{+/+}$ (DC-MyD88$^{+/+}$). Mice were kept in a specific pathogen-free breeding unit at the Institute of Biomedical Sciences of the University of São Paulo (ICB IV-USP). 10BiT that report Thy1.1 on the cell surface under the control of *Il10* promoter (27) were crossed with Foxp3^{gfp} reporter mice (28) to generate 10BiT.Foxp3^{gfp} dual reporter mice and were kept at specific-pathogen-free conditions at the animal facility of the Massachusetts General Hospital. All mice were kept in cages with a ventilated system, at a maximum of five animals per cage, with temperature-controlled rooms, food, and water *ad libitum*, in a 12 h light/dark cycle. Mice were treated according to animal welfare guidelines of ICB (Ethic Protocol 009/2015) under National Legislation-11.794 Law or under a study protocol approved by Massachusetts General Hospital Subcommittee on Research Animal Care.

Experimental Protocol

Mice were sensitized subcutaneously (s.c.) to OVA (4 μg) or *Blomia tropicalis* (Bt) (4 μg) with alum adjuvant gel (1.6 mg) on days 0 and 7. Mice were intranasally challenged with OVA (10 μg) or Bt (10 μg) in 40 μL of PBS on days 14, 38 and 45. Mice were treated on days 17, 24, and 31 according to specifications in each experiment. The final concentrations or volume of each reagent in one dose of the liposomal formulation was: 4 μg of allergen (OVA or Bt), 10 μg of CpG and 70 μL of DOTAP. More specifically, for the preparation of the immunotherapy OVA + CpG/DOTAP was: OVA (4 μg) in a volume of 4 μL and CpG (10 μg) in a volume of 3 μL were slowly mixed, and 70 μL of DOTAP was added to the mixture and slowly mixed with the aid of the pipette for 1 min. The liposomal formulation was kept at room temperature for 15 min followed by the addition of 123 μL of PBS. Control mice consisted of non-manipulated animals. All procedures (sensitization, challenges, and treatment) were done under anesthesia with ketamine (50 mg/kg) and xylazine (20 mg/kg). On day 46, animals were euthanized with inhaled halothane and samples were collected.

Reagents

CpG-ODN 2395 Class C, a TLR9 agonist, was purchased from Invivogen (San Diego, CA, United States). The allergens used were OVA (Sigma-Aldrich, United States) and *B. tropicalis* extract (BIOCEN, Cuba). The OVA was depleted of endotoxin (LPS) using four cycles of Triton X-114 extractions. The endotoxin level of purified OVA was below the limit of detection of Limulus assay lysate (less than 0.1 Endotoxin Units). DOTAP (DOTAP Liposomal Transfection Reagent) was purchased from Sigma–Aldrich (Sigma–Aldrich, St. Louis, MO, United States).

Blood and Bronchoalveolar Lavage (BAL) Collections

Blood samples were collected by cardiac puncture, centrifuged, and serum was stored at –20°C. The BAL fluid was obtained after lung washing with 1 ml of cold PBS via the trachea. Total and differential cell counts of BAL fluids were determined by hemacytometer (Sigma–Aldrich, Sant Louis, United States) and cytospin (Thermo Fisher Scientific, Waltham, United States) preparation, stained with H&E (Instant-Prov, Newprov, Brazil), a stain based on Romanowsky formulation.

ELISA for Cytokines

Cytokines (IL-5 and IFN-γ) levels in BAL were measured by sandwich kit enzyme-linked immunosorbent assay (ELISA) according to the manufacturer's recommendation (BD Biosciences, United States). Values were expressed as pg/ml deduced from a standards curve of recombinant cytokines ran in parallel.

Lung Harvest and Flow Cytometry

Lungs were digested with 0.52 U/ml Liberase TM (Roche) and 60 U/ml DNase I (Roche) in RPMI 1640 (Cellgro), at 37°C for 30 min. Lung leukocyte enrichment was performed by using a 30% Percoll gradient and the cell suspension obtained after erythrocyte lysis. Single cells were then incubated with anti-mouse CD16/32 (93, TruStain fcX, BioLegend) to block Fc receptors. Staining was performed with Fixable Viability Dye eF780 (eBioscience), to identify dead cells, and the following fluorochrome-conjugated anti-mouse monoclonal antibodies (mAbs): CD45-PerCP/Cy5.5 (30-F11), CD4-BV785 (GK1.5) (all from BioLegend), and CD3e-BUV395 (145-2C11) (from BD Biosciences). At least 1,000,000 events were recorded for each sample. Only viable and non-doublet cells were considered. Flow cytometric analysis was performed using a LSRFortessa X-20 flow cytometer (BD Biosciences) and FlowJo software (Tree Star).

Active Cutaneous Anaphylaxis (ACA) Assay

Mice were sensitized as described above and challenged intranasally on day 14. On day 16, the dorsal region was shaved with a trimmer ER389 (Panasonic, Japan) and on day 17, the animals were anesthetized with ketamine and xylazine and received an intradermal injection of OVA (10 ug) or PBS followed by an intravenous injection of 100 μl of Evans Blue dye (1 mg/mL). Thirty minutes later, the animals were euthanized and the skin of the dorsal region was removed for photographic registration. Skin spots were weighted and dye extraction performed with formamide (8 mL/mg of dry weight) for 72 h (29) and quantified by measuring dye absorbance at 620 nm. Results are expressed as μg/mL determined by a standard curve with known concentrations of Evans blue dye.

Lung Histopathology

After the BAL collection, 10 mL of cold PBS was perfused through the right ventricle of the heart, the lungs were fixed in 10% PBS-formalin for 24 h and then in 70% ethanol until embedding in paraffin. Sections of five-micrometer were stained with hematoxylin/eosin for determinations of lung inflammation or periodic acid-Schiff for mucus quantification. Lung inflammation score was performed by measurement of the peribronchial cellular infiltrates divided by the girth of the bronchial basal membrane. The mucus score was calculated as the percentage (%) of mucus positive area divided by the girth of the bronchial basal membrane.

ELISA for Antibody Determinations

Mice were euthanized with overdose of anesthesia and blood samples were collected by cardiac puncture, centrifuged and serum was stored at -20°C. Serum antibodies were determined by ELISA as described previously (30).

Statistical Analysis

Statistical analyses were performed using the software GraphPad Prism (V.5; GraphPad Software, United States). One-way ANOVA followed by Tukey post-test was performed, as appropriate. Differences were considered statistically significant when p-value ≤ 0.05. Data represent the mean ± SE.

RESULTS

Allergen (OVA) Encapsulation in a Cationic Liposome Attenuates Active Cutaneous Anaphylaxis

A major problem of allergen-specific immunotherapy is the development of life-threating anaphylaxis during treatment (31, 32). To circumvent this side effect, we postulated that encapsulation of the allergen (OVA) in a cationic liposome (DOTAP) would reduce the risks of anaphylaxis by preventing the allergen from the contact with allergen-specific IgE (33). To test this, we performed an ACA assay in C57BL/6 mice sensitized with OVA/Alum s.c. on days 0 and 7 and challenged with i.n OVA on day 14 (Allergic). ACA was induced with intradermal injection (i.d.) of OVA at day 17 in the dorsal region followed by i.v Evans Blue dye injection. Dye extravasation in the dorsal skin was measured 30 min later. As shown in **Figure 1**, challenge with encapsulated OVA (DOTAP + OVA group) in allergic mice, resulted in a significant decrease of dye extravasation when compared with non-encapsulated OVA

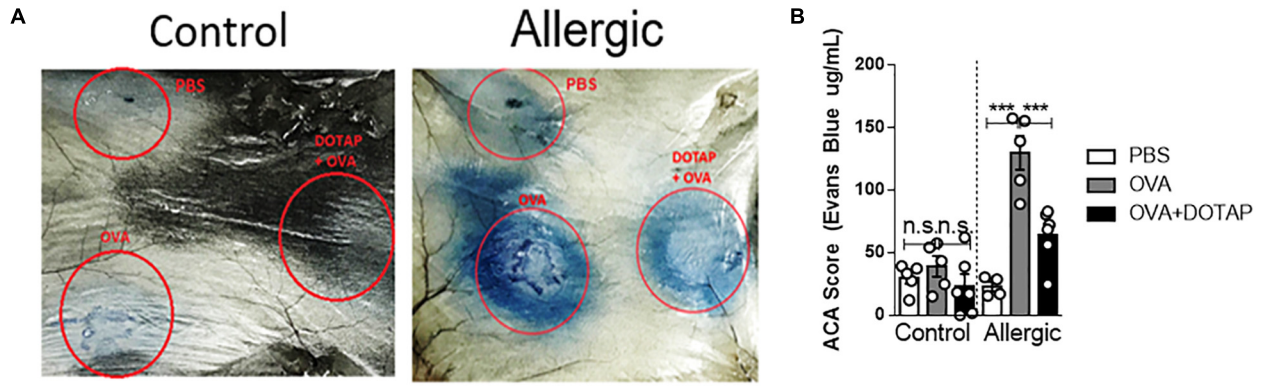

FIGURE 1 | Active cutaneous anaphylaxis with free or encapsulated allergen. C57BL/6 wild-type mice were sensitized with OVA/Alum on days 0 and 7 and challenged with OVA on day 14 to establish airway inflammation. Control group consisted of non-manipulated naive mice. On day 17 (Control and Allergic) groups received an intradermal injection of PBS or OVA alone or OVA encapsulated in DOTAP liposome in the dorsal region followed by i.v. injection of Evans Blue dye. **(A)** Representative pictures of active cutaneous anaphylaxis (ACA) in the dorsal skin 30 min after Evans Blue dye injection in Control or Allergic groups; **(B)** ACA scores were determined in Control or Allergic groups after Evans Blue dye extraction with formamide as described in M&M. Each symbol represents one mouse. Values represent the mean ± SEM and are representative of three independent experiments. One-way ANOVA: ***$p < 0.001$; n.s. non-significant.

group (**Figures 1A,B**). As expected, we did not observe any anaphylactic cutaneous reactions in non-sensitized (Control) group (**Figures 1A,B**). Thus, encapsulated OVA in cationic liposome trigger less severe allergen-induced ACA than non-encapsulated OVA.

Treatment With Liposomal Formulation Containing Allergen Plus CpG Reverses Established Asthma

Since CpG signals through endosomal TLR9 (34), its activity could be increased after endocytosis of the liposome containing CpG. Therefore, we investigated whether treatment with a liposomal formulation containing the allergen plus CpG could alter the immune response of mice with established asthma following OVA challenge. For this, we compared mice with established allergic airway inflammation treated subcutaneously on days 17, 24, and 31 with PBS (Allergic group) with mice treated with OVA in liposome alone (OVA/DOTAP), or with CpG in liposome alone (CpG/DOTAP), or with OVA plus CpG in liposome (OVA + CpG/DOTAP) and challenged with OVA on days 38 and 45 as despicted in **Figure 2A**. Control group consisted of non-manipulated naive animals. Experiments were performed 24 h after the last OVA challenge on day 46. Allergic group had increased number of total cells and eosinophils in the BAL after OVA challenges when compared with Control group (**Figures 2B,C**). All groups treated with liposome in combination with OVA (OVA/DOTAP), CpG (CpG/DOTAP), or OVA + CpG (OVA + CpG/DOTAP) showed a significant reduction in the number of eosinophils in the BAL when compared with the Allergic group (**Figure 2C**). However, only the OVA + CpG/DOTAP group had a dramatic inhibition in the number of total cells and eosinophils, and a robust reduction in the levels of IL-5, but not IFN-γ levels in the BAL compared with Allergic group (**Figures 2B–E**). No differences were observed in the numbers of neutrophils or in the levels of IL-12 in BAL (data not shown). Notably, histopathological analysis of lung sections stained for H&E or periodic acid-Schiff (PAS) revealed that only animals treated with the liposomal formulation containing OVA plus CpG had a significant reduction in peribronchovascular inflammatory cell infiltrates and mucus formation, respectively (**Figures 2F–H**). We also determined the effect of liposomal formulation containing OVA and CpG on antibody production. We found that the serum levels of total IgE and OVA-specific IgE and IgG1 or IgG2c were increased in Allergic group when compared to Control group (**Supplementary Figure S1**). Treatment with the liposomal formulation reduced the total levels of IgE when compared with non-treated Allergic group (**Supplementary Figure S1A**). OVA-specific IgE and IgG1 were similar in OVA + CpG/DOTAP and Allergic group (**Supplementary Figures S1B,C**) while OVA-specific IgG2c antibodies reached higher levels in OVA + CpG/DOTAP group when compared to the Allergic group (**Supplementary Figure S1D**). Altogether, our results indicate that treatment with allergen plus CpG encapsulated in cationic liposome attenuates all parameters of Th2-mediated allergic lung inflammation and total IgE production, increases IgG2c production and does not affect the levels of OVA-specific IgE and IgG1 isotypes.

Treatment With Liposomal Formulation Is Long-Lasting, Not Restricted to C57BL/6 Mouse Strain and Is Extended to Allergens Derived From House Dust Mite

Allergen-specific immunotherapy aims to provide sustained inhibition of the disease symptoms (35). Given that T cell memory is long-lasting in the OVA-induced allergic respiratory model (36) and that allergen-specific immunotherapy usually require many weeks or years of treatment (37, 38) we then next investigated whether our short-term (three-dose) treatment provides a long-lasting effect. For this, after the treatment, the

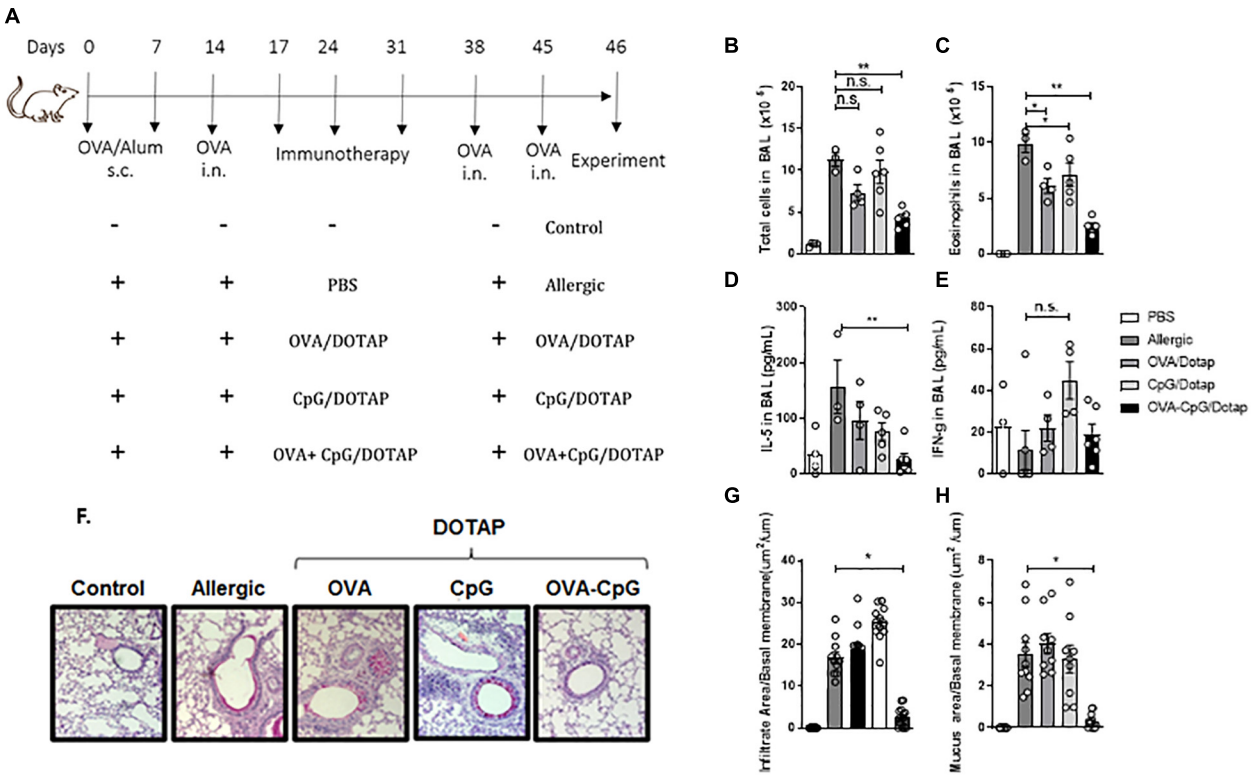

FIGURE 2 | Liposomal formulation containing allergen plus CpG attenuates airway inflammation. C57BL/6 WT mice were sensitized s.c. with OVA/Alum on days 0 and 7 and challenged with i.n. OVA on days 14 to establish airway inflammation. Mice were treated subcutaneously with PBS (Allergic); or with encapsulated OVA in DOTAP (OVA/DOTAP); or with encapsulated CpG in DOTAP (CpG/DOTAP); or with OVA and CpG co-encapsulated in DOTAP (OVA + CpG/DOTAP) on days 17, 24 and 31 and challenged with i.n. OVA on days 38 and 45. Experiments were performed on day 46. Control group consisted of non-manipulated naive animals. **(A)** Schematic protocol of immunotherapy. **(B)** Total number of cells and **(C)** eosinophil counts; **(D)** IL-5 and **(E)** IFN-gamma levels in BAL. **(F)** Representative microphotographs of lung sections stained with periodic acid-Schiff, **(G)** lung inflammation score and **(H)** lung mucus score. Each symbol represents one mouse. Values represent the mean ± SEM and are representative of two independent experiments. One-way ANOVA: $*p < 0.05$; $**p < 0.01$; n.s. non-significant.

mice were rested for 60 days and then challenged twice with i.n. OVA at days 91 and 98 as depicted in **Figure 3A**. We found that while the total number of cells and eosinophils were increased in BAL of allergic mice after OVA challenges compared to Control group, the treatment with liposomal formulation containing allergen and CpG significantly reduced the total cell and eosinophil counts in BAL when compared to Allergic group (**Figures 3B,C**). Histological analysis confirmed that the treatment was also effective in reducing lung allergic inflammation and mucus formation (**Figures 3D–F**). It is important to note that allergen-specific immunotherapy require several weeks or years of treatment (37, 38) while our treatment with liposomal formulation containing allergen and CpG was effective using a short-term treatment and low dose of allergen. In order to determine whether the efficacy of our short-term protocol treatment could be effective in other mouse strain, we tested our liposomal formulation in the 129S1 mice (**Figure 3G**), a mouse strain that is widely used in the production of targeted mutations (39). We found that the treatment with the liposomal formulation significantly inhibited all analyzed parameters of allergic inflammation such as airway total cell count and eosinophilia in BAL, peribronchial inflammatory infiltrates and mucus formation (**Figures 3H–L**), indicating that the treatment was also effective in 129S1 mouse strains. Finally, we aimed to determine whether liposomal formulation with specific allergen plus CpG could also be effective using allergens extracted from *B. tropicalis* (Bt) mite, a clinical relevant respiratory allergen. For this, we used a model recently described by our group that consists of subcutaneous sensitization with Bt mite extract adsorbed to alum adjuvant and a challenge with Bt i.n. to establish airway inflammation (40), followed by treatment with Bt + CpG liposomal formulation and challenges with Bt i.n. Allergic inflammation was determined 24 h after the last Bt i.n. challenge as depicted in **Figure 3M**. As in the OVA model, the treatment with the Bt + CpG liposomal formulation (Bt + CpG/DOTAP group) significantly inhibited the total number of cells and eosinophils in the BAL, as well as diminished the peribronchial inflammatory cell infiltrates and mucus formation in the lungs when compared with Allergic group (**Figures 3N–R**). We conclude that treatment with co-encapsulated allergen with CpG is effective in attenuating established asthma induced in a different mouse strains as well as induced by different allergens.

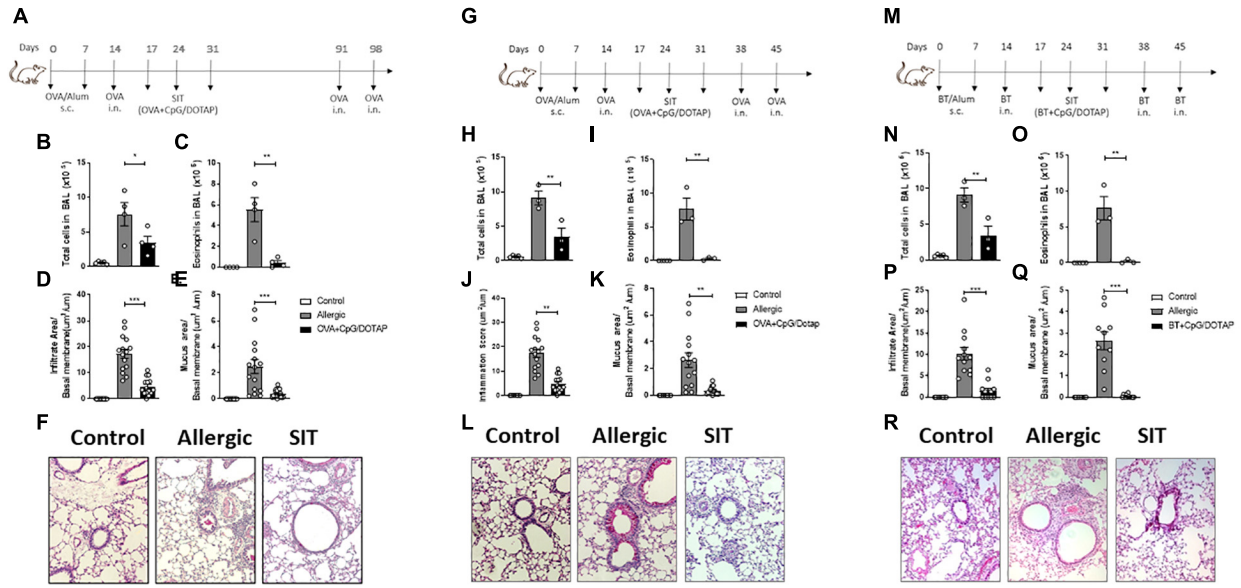

FIGURE 3 | Treatment with liposomal formulation is long-lasting, not restricted to C57BL/mice and is extended to allergens derived from *Blomia tropicalis*. C57BL/6 WT mice were sensitized s.c. with OVA/Alum on days 0 and 7 and challenged with i.n. OVA on days 14 to establish airway inflammation. Mice were treated subcutaneously with PBS (Allergic) or with co-encapsulated OVA and CpG in DOTAP (OVA + CpG/DOTAP) on days 17, 24 and 31. **(A)** Schematic representation of the long-lasting allergen-specific immunotherapy protocol. Mice were challenged with i.n. OVA on days 91 and 98 and experiments were performed on day 99. Control group consisted of non-manipulated naive animals. **(B)** Total number of cells and **(C)** eosinophil counts in the BAL; **(D)** Lung inflammation score and **(E)** lung mucus score. **(F)** Representative microphotographs of lung sections stained with periodic acid-Schiff. **(G)** Schematic representation of allergen-specific immunotherapy protocol. 129S1 mice were sensitized with OVA/Alum s.c. on days 0 and 7 and challenged with OVA i.n. on days 14 to establish airway inflammation. Mice were treated subcutaneously with PBS (Allergic) or with co-encapsulated OVA and CpG in DOTAP (OVA + CpG/DOTAP) on days 17, 24 and 31 challenged with i.n. OVA on days 38 and 45. Experiments performed on day 46. **(H)** Total number of cells and **(I)** eosinophil counts in the BAL. **(J)** Lung inflammation score and **(K)** lung mucus score. **(L)** Representative microphotographs of lung sections stained with periodic acid-Schiff. **(M)** Schematic representation of allergen-specific immunotherapy protocol. C57Bl/6 wild-type (WT) mice were sensitized s.c. with *Blomia tropicalis* (Bt)/Alum on days 0 and 7 and challenged with i.n. Bt on day 14 to establish airway inflammation. Mice were treated subcutaneously with PBS (Allergic) or treated with (Bt) and CpG encapsulated in DOTAP (Bt + CpG/DOTAP) on days 17, 24, and 31 and challenged with i.n. Bt on days 38 and 45. Experiments were performed on day 46. **(N)** Total number cells and **(O)** eosinophil counts in the BAL. **(P)** Lung inflammation score and **(Q)** lung mucus score; **(R)** Representative microphotographs of lung sections stained with periodic acid-Schiff. Each symbol represents one mouse. Values represent the mean ± SEM and are representative of two independent experiments. One-way ANOVA: $^{*}p < 0.05$; $^{**}p < 0.01$; $^{***}p < 0.001$; n.s. non-significant.

Attenuation of Established Asthma by Liposomal Formulation Is Not Associated With Increased Number of Lung Regulatory T Cells

Previous studies indicate that reduced activity of regulatory T cells, such as IL-10-producing Tr1 cells or Foxp3^{+} Treg cells is associated with allergic disease (41, 42) and that allergen-specific immunotherapy might increase their activity (43). To investigate the Foxp3^{+} and IL-10-producing regulatory T cell response *in vivo*, we crossed mice that express the Thy1.1 reporter under the control of *Il10* (10BiT) with mice that express the green fluorescent protein (GFP) under the control of *Foxp3* (Foxp3^{gfp}) to generate 10BiT.Foxp3^{gfp} mice (27). These "dual-reporter" mice enable simultaneous detection of *Il10* and *Foxp3* expression in individual cells. Interestingly, we did not observe any difference in the percentage and number of Foxp3^{+} Treg cells, or in putative IL-10-producing Foxp3^{+} Treg or Foxp3^{-} Tr1 cells in the lung of allergic mice treated with the liposomal formulation OVA/DOTAP or OVA + CpG/DOTAP when compared with allergic mice treated with PBS (Allergic group) (**Figures 4A–D**). Thus, the inhibition of allergic lung inflammation by liposomal formulation in our OVA-model was not associated with an expansion of Foxp3^{+} or IL-10-producing regulatory T cells in the lung or a cell-based increase in IL-10 production.

MyD88 Adaptor Molecule Is Essential for the Immunotherapeutic Effect of Liposomal Formulation

CpG signals through endosomal TLR9 via the MyD88 pathway (44), although it has been reported that high doses of CpG could signal through TRIF pathway (45). We have previously demonstrated that CpG has a prophylactic effect in allergic asthma that is dependent of MyD88 signaling (21). Here we sought to determine whether MyD88 signaling is also crucial for the therapeutic effect our liposomal formulation containing OVA + CpG. Using MyD88-deficient mice (MyD88KO) and C57BL/6 wild-type (WT) mice we found that treatment with liposomal formulation reduced the number of total cells, eosinophils, and the levels of IL-5 in the BAL in WT but not in MyD88KO mice when compared with the respective Allergic

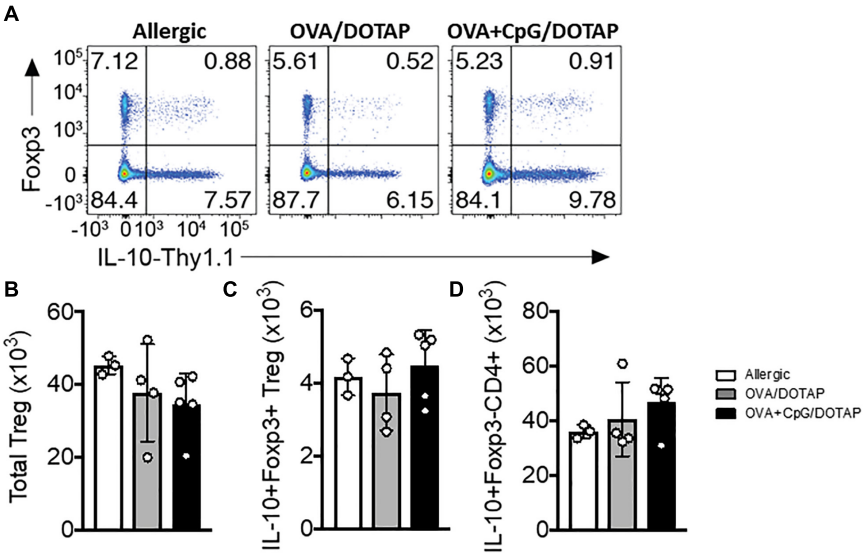

FIGURE 4 | Regulatory T cells in the lung after allergen-specific immunotherapy. 10BiT.Foxp3^{gfp} mice were sensitized with OVA/Alum s.c. on days 0 and 7 and challenged with OVA i.n. on day 14 to establish airway inflammation. Mice were treated subcutaneously with PBS (Allergic) or with encapsulated OVA in DOTAP (OVA/DOTAP), or with co-encapsulated OVA and CpG in DOTAP (OVA + CpG/DOTAP) on days 17, 24 and 31 and challenged with i.n. OVA on days 38 and 45. Experiments were performed on day 46. Control group consisted of non-manipulated naive animals. **(A)** Flow cytometric analysis showing expression of Foxp3 and Thy1.1 (IL-10) in lung CD4$^+$ T cells. **(B)** Total number of Foxp3$^+$ Treg cells, **(C)** IL-10$^+$Foxp3$^+$ Treg cells, and **(D)** IL-10$^+$Foxp3$^-$CD4$^+$ T (Tr1) cells. Each symbol represents one mouse. Values represent the mean ± SEM and are representative of one independent experiment.

groups (**Figures 5A–C**). Further, histopathological analysis of lung sections confirmed that WT but not MyD88KO treated with OVA + CpG/DOTAP showed attenuated lung infiltration compared with the Allergic group (**Figures 5D–E**). These results show that MyD88 signaling is required to the attenuation of the established allergic lung inflammation induced by treatment with the liposomal formulation containing allergen and CpG.

Dendritic Cells Expressing MyD88 Molecule Are Necessary and Sufficient for Reversal of Established Asthma by Liposomal Formulation

Recently we showed that dendritic cells (DCs) expressing MyD88 molecule are crucial for CpG-induced inhibition of IgE production (30). Therefore, we next focused on the role of *Myd88* expression on dendritic cells known to respond to CpG signaling and are involved in antigen presentation (30, 46, 47). For this, we used mice with specific deletion of *Myd88* gene on cells expressing CD11c integrin (DCs-MyD88$^{-/-}$) and their littermates' controls (DCs-MyD88$^{+/+}$). We found that DC-MyD88$^{+/+}$ and DC-MyD88$^{-/-}$ mice do develop allergic lung inflammation. Importantly, treatment with liposomal formulation containing co-encapsulated OVA and CpG reduced the number of total cells and, eosinophils in BAL as well as IL-5 production in DCs-MyD88$^{+/+}$, but not in DCs-MyD88$^{-/-}$ mice when compared with the respective Allergic groups (**Figures 6A–C**). DC-MyD88$^{+/+}$ mice also showed reduced lung inflammation as revealed by lung histopathology analysis compared with DC-MyD88$^{-/-}$ mice treated with liposomal formulation (**Figures 6D–E**). Thus, our data indicates that the therapeutic effect of liposomal formulation in established asthma requires CpG signaling through MyD88 molecule expressed on CD11c-positive putative DCs.

DISCUSSION

Currently, pharmacological and immunological interventions are used for asthma control. Pharmacological treatment aims to control airway inflammation by the use of oral or inhaled corticosteroids and long-acting bronchodilators and as such the treatment is essentially symptomatic. Immunological treatment with monoclonal antibodies against anaphylactic IgE or against type 2 cytokines such as IL-5 and IL-4/IL-13 is another way to control asthma symptoms. In contrast, allergen-specific immunotherapy, a type of therapy that has been used in humans for more than a century (22, 48), has the potential of changing definitively the immune responses to specific allergens and has been indicated for non-responsive patient to pharmacological treatment (22, 49). Conventional allergen-specific immunotherapy consists of administration of repeated and increasing doses of the sensitizing allergen for long periods of time (35). In the present study, we introduced some variables to conventional allergen-specific immunotherapy, such as: (1) Instead of free-allergen we used encapsulated allergen in cationic liposome in order to avoid interaction with anaphylactic antibodies; (2) We added CpG to cationic liposome containing allergen to target directly endosomal TLR9; and (3) We used short-term (three doses) immunotherapy treatment and a low

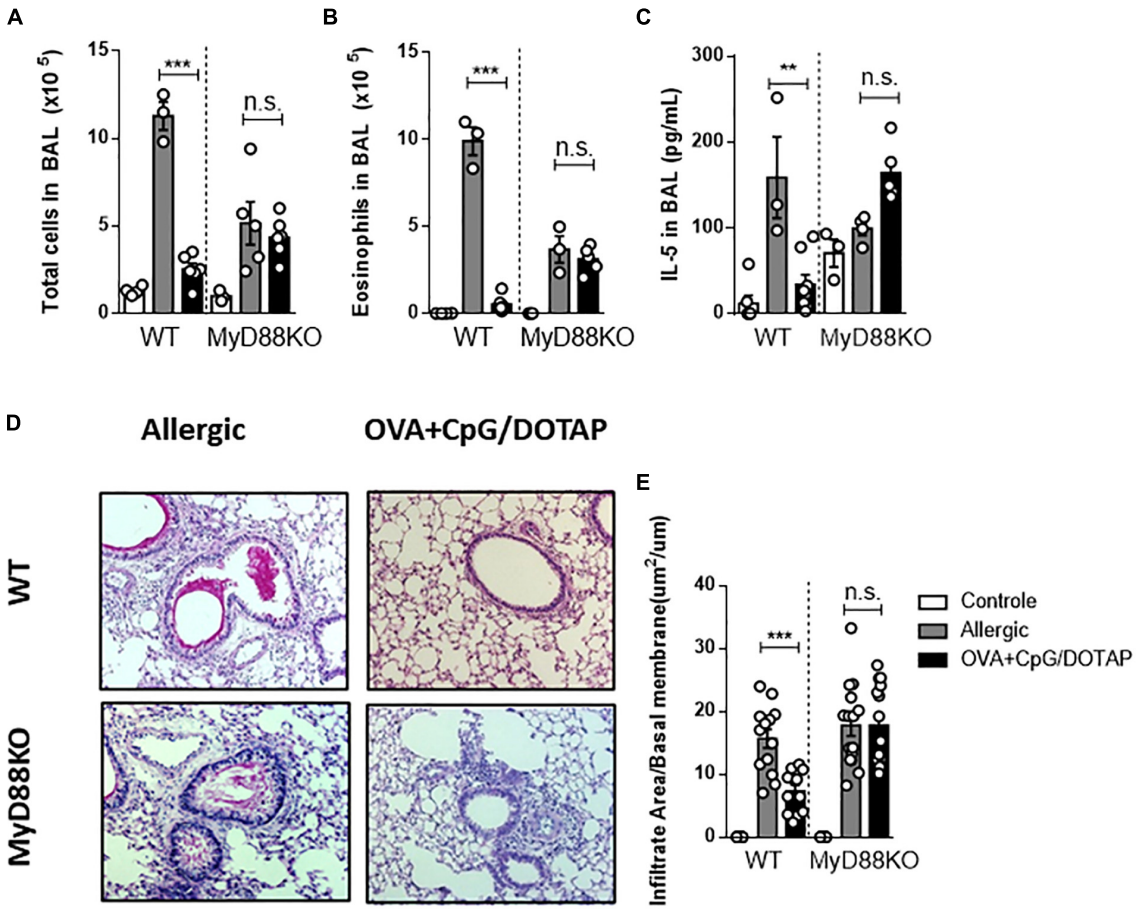

FIGURE 5 | Involvement of MyD88 adaptor molecule in allergen-specific immunotherapy. C57BL/6 wild-type (WT) or MyD88-deficient (MyD88KO) mice were sensitized s.c. with OVA/Alum on days 0 and 7 and challenged with i.n. OVA on days 14 to establish airway inflammation. Mice were treated subcutaneously with PBS (Allergic) or with co-encapsulated OVA and CpG in DOTAP (OVA + CpG/DOTAP) on days 17, 24 and 31 and challenged with i.n. OVA on days 38 and 45. Experiments were performed on day 46. Control group consisted of non-manipulated naive animals. **(A)** Total number of cells and **(B)** eosinophil counts in BAL. **(C)** IL-5 levels in BAL. **(D)** Representative microphotographs of lung sections stained with periodic acid-Schiff. **(E)** Inflammation score. Each symbol represents one mouse. Values represent the mean ± SEM and are representative of two independent experiments. One-way ANOVA: $^{*}p < 0.05$; $^{**}p < 0.01$; $^{***}p < 0.001$; n.s., non-significant.

dose of allergen. We first found that the encapsulation of OVA alone (without CpG) in liposome was indeed effective in attenuating ACA as well as systemic anaphylaxis (data not shown). However, it is notewhorty that immunotherapy with encapsulated OVA alone, without CpG, was ineffective in reversing established allergic lung inflammation. Currently many variations of immunotherapy are being evaluated such as peptide immunotherapy (50), sublingual immunotherapy (51), intranasal (52, 53), oral (54) and subcutaneous (55). The gold standard for immunotherapy route is the subcutaneous route due to its efficacy (56), but sublingual treatment is on the rise. Our finding with encapsulated OVA is of clinical relevance since one of the major drawbacks of allergen-specific treatment is the development of life-threating anaphylaxis (57). Although treatment of allergic mice with encapsulated allergen alone was effective in attenuating cutaneous anaphylaxis of allergic mice, this treatment was ineffective, in reversing established allergic lung inflammation. Also, treatment with encapsulated CpG was also ineffective in reversing airway eosinophilic inflammation, a finding that is in line with a previous report (20). However, in contrast to our findings, allergen-free immunotherapy has been evaluated previously in a model of house dust mite asthma, using CpG and unrelated proteins from *Mycobacteria tuberculosis* cultures. It was found that the experimental respiratory allergy was down modulated when mice were treated concomitantly with CpG and culture proteins from *M. tuberculosis*. The inhibition of respiratory allergy was IFNγ-dependent indicating that immune responses to proteins of *M. tuberculosis* inhibited Derp1-induced allergic responses by a bystander mechanism (58). In addition, it was shown that encapsulation of CpG could improve its stimulatory effect signaling through endosomal TLR9 (26, 59–61) without increasing the toxicity of the compound (62–64). Notably, in our model, treatment with a liposomal formulation containing both OVA and CpG, but not CpG alone, reversed

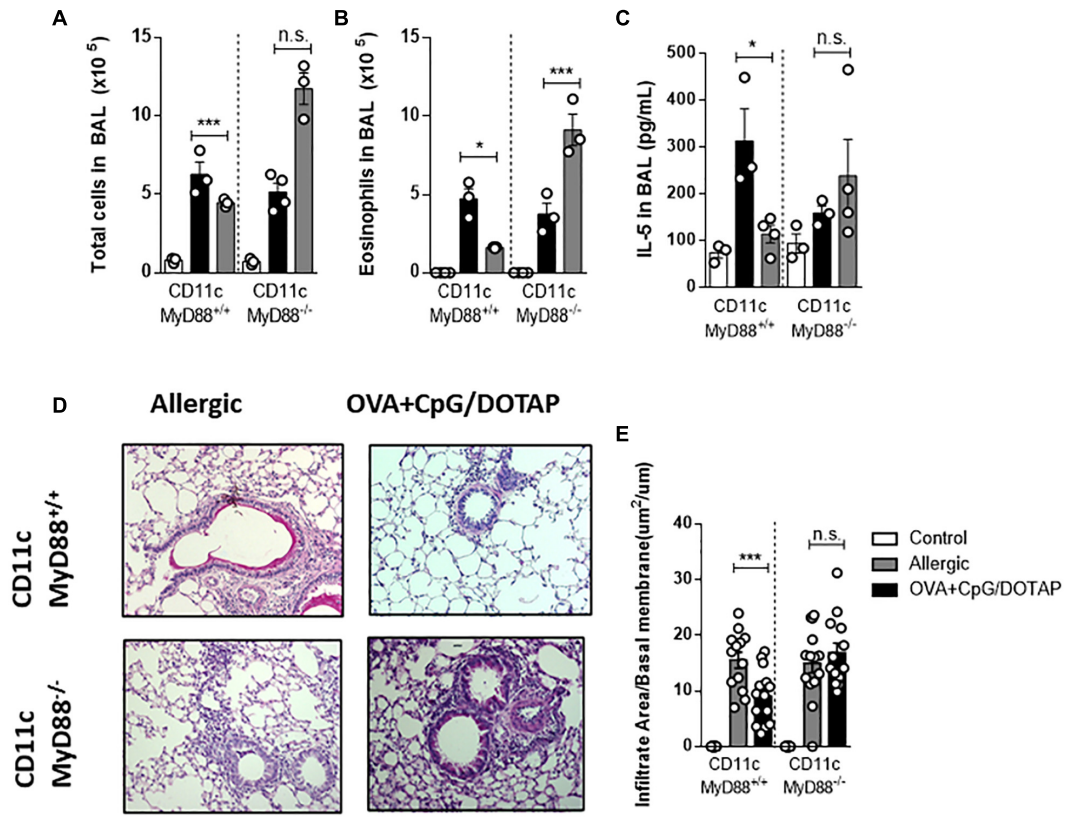

FIGURE 6 | Dendritic cells expressing MyD88 molecule are fundamental for allergen-specific immunotherapy. Mice lacking *Myd88* expression on CD11c-positive dendritic cells (DC-MyD88$^{-/-}$ and littermate controls (DC-MyD88$^{+/+}$) were sensitized with OVA/Alum s.c. on days 0 and 7 and challenged with i.n OVA on day 14 to establish airway inflammation. Mice were also treated subcutaneously with PBS (Allergic) or treated with OVA and CpG encapsulated in DOTAP (OVA + CpG/DOTAP) on days 17, 24, and 31 and challenged with i.n. OVA on days 38 and 45. Experiments were performed on day 46. Control group consisted of non-manipulated naive animals. **(A)** Total number of cells and **(B)** eosinophil counts in BAL. **(C)** IL-5 levels of in BAL. **(D)** Representative microphotographs of lung sections stained with periodic acid-Schiff. **(E)** Lung inflammation score. Each symbol represents one mouse. Values represent the mean ± SEM and are representative of two independent experiments. One-way ANOVA: $^{*}p < 0.05$; $^{***}p < 0.001$; n.s., non-significant.

established asthma, attenuating allergic lung inflammation and decreasing type 2 cytokine production in BAL without increasing airway IFN-γ production. We showed previously that IFN-γ was not involved in CpG-induced inhibition of allergic sensitization (21, 30, 40). In contrast, some reports demonstrate that CpG (65) or OVA plus CpG or co-encapsulation of OVA and CpG (66) resulted in increased IFN-γ production. These differences might be related to different protocols used, the compartment of the body where IFN-γ was detected and whether the measurements were performed *in vitro* or *ex vivo*. More specifically, our results are in line with the work of Jain et al. (67) that showed that mucosal (nasal) administration with CpG and OVA reversed established allergic inflammation, reducing type 2 cytokines production in BAL without changing IFN-γ levels in BAL. In line with Jain et al. (67), we also found that our liposomal formulation was effective in attenuating established asthma when administered by the intranasal route without increasing IFN-γ (data not shown). Besides lung inflammation, allergen-specific immunotherapy aims to module also anaphylactic antibody productions. We found that our treatment with liposomal formulation containing OVA and CpG reduced the serum levels of total IgE but not the production OVA-specific IgE or IgG1 while it increased the production of OVA-specific IgG2c antibodies when compared with allergic group (**Supplementary Figure S1**). How these findings are related to the attenuation of allergic inflammation remain elusive. It is anticipated that either adaptive memory T cells (immune deviation) or regulatory T cells might participate in this process. Because we did not find evidence for IFN-γ-mediated immune deviation, we focused on the participation of regulatory T cells and IL-10 in the inhibition of allergic inflammation. Therefore, we investigated whether inhibition of established allergic lung inflammation could be associated with increased number of IL-10-producing regulatory Tr1 cells or with Foxp3-positive Tregs cells in the airways. Our results with IL-10 and Foxp3 double reporter mice clearly indicated that reversal of allergic inflammation by treatment with co-encapsulated OVA and CpG in cationic liposome was not associated with an increase of IL-10-producing putative Tr1 cells or with Foxp3-expressing putative Tregs after last OVA challenge. However, we cannot exclude de participation

of regulatory T cell in other body compartments outside of the lung. Since the exact mechanism by which established adaptive Th2-mediated allergic responses were affected remained elusive, we focused on the role of MyD88 adaptor molecule in this process. CpG activates different innate cell types mainly signaling through MyD88 pathway via TLR9 (68), although it was reported that at high dose, CpG signaling through the TRIF pathway inhibited allergic bronchopulmonary aspergillosis (45). We first verified that MyD88 molecule was essential for CpG-mediated attenuation of the allergic reaction, ruling out the participation of TRIF pathway in this process. Since CpG activates different innate cell types (47, 69, 70) we next tested the participation of MyD88 molecule on CD11c-positive dendritic cells. For this, we used mouse engineered via Cre-lox technology with specific ablation of the mouse *Myd88* gene in CD11c-positive putative dendritic cells (25). As a control we used littermates mice with MyD88-expressing CD11c-positive cells. We found that DCs expressing MyD88 molecule were necessary and sufficient for CpG-induced attenuation of established asthma. Our results with DC-MyD88$^{-/-}$ mice reinforce the notion that DCs expressing MyD88 molecule are key target cells for CpG-mediated immunomodulation (21, 26, 30, 71). Allergen-specific immunotherapy require long-term treatment and adherence to the treatment (72) to achieve protection against allergic reactions and symptoms (73). Usually, successful treatment is long lasting (38), but there are some conflicting reports as to whether the protective effect of immunotherapy persist after discontinuation (74, 75). It appears that the optimum duration for long-term modulation of allergic symptoms in humans by allergen-specific immunotherapy is approximately three years (76), while in mice allergen-specific immunotherapy appears to require at least 8-weeks (77). Here we showed that short-term treatment with low dose of allergens and CpG efficiently reduced key features of allergic asthma. In addition, we also evaluated whether this type of immunotherapy could be applied to a relevant respiratory allergens obtained from *B. tropicalis* mite extract, one of the most prevalent mites in tropical countries (78) and found that the treatment with co-encapsulated Bt allergens and CpG reversed the established allergic lung responses. These results demonstrate the potential applications of our formulation to different allergens and highlight the importance of correct diagnosis for developing a specific allergen treatment (79). Since allergic T cell memory is long-lasting (80), we investigated whether our immunotherapy protocol had a long lasting effect by performing experiments 2 months after the end of the immunotherapy. We found that our allergen-specific immunotherapy has a long lasting modulation on OVA-induced allergic responses. Collectively, our work highlights an improved short-term immunotherapy protocol using co-encapsulated allergens and CpG that has the advantage to protect against anaphylaxis during allergen-specific immunotherapy treatment, which uses low doses of allergens, is effective against different allergens and is long lasting. Our results suggest that this type of immunotherapy might be of potential use to treat eosinophilic (type 2 high) asthma endotype (2, 81) and indicate the pivotal role of dendritic cell expressing *Myd88* in this process.

DATA AVAILABILITY STATEMENT

All datasets generated for this study are included in the article/**Supplementary Material**.

ETHICS STATEMENT

Mice were treated according to animal welfare guidelines of ICB (Ethic Protocol 009/2015) under National Legislation-11.794 Law or under a study protocol approved by the Massachusetts General Hospital Subcommittee on Research Animal Care.

AUTHOR CONTRIBUTIONS

RA-C designed the study, performed the experiments, analyzed the results, and wrote the manuscript. LF performed the experiments with IL-10 reporter mice and contributed to writing. MS, DF, FN, and EG performed the experiments. AL contributed with Bt-model of asthma. RA and NC provided the mouse strains, analyzed the results, and contributed to the writing. MR designed the study and wrote the manuscript. All authors read, edited, and approved the manuscript.

FUNDING

This study was supported by the São Paulo Research Foundation – FAPESP (grants 2013/24694-1, 2014/19906-2, 2015/16728-9, 2015/25364-0, 2016/16602-8, and 2017/05264-7) and the Conselho Nacional de Desenvolvimento Científico e Tecnológico – CNPq (grant 311055/2013-3). This study was supported in part by the Coordenação de Aperfeiçoamento de Pessoal de Nível Superior – Brasil (CAPES) – Finance Code 001.

SUPPLEMENTARY MATERIAL

The Supplementary Material for this article can be found online at: https://www.frontiersin.org/articles/10.3389/fimmu.2020.00692/full#supplementary-material

FIGURE S1 | Effect of liposomal formulation containing allergen plus CpG on antibody production. C57BL/6 WT mice were sensitized s.c. with OVA/Alum on days 0 and 7 and challenged with i.n. OVA on days 14 to establish airway inflammation. Mice were treated subcutaneously with PBS (Allergic); or with encapsulated OVA in DOTAP (OVA/DOTAP) on days 17, 24, and 31 and challenged with i.n. OVA on days 38 and 45. Serum levels of antibodies were determined on day 46. Control group consisted of non-manipulated naive animals. **(A)** Total IgE levels, **(B)** OVA-specific IgE antibodies, **(C)** OVA-specific IgG1 antibodies, and **(D)** OVA-specific IgG2c antibodies. Values represent the mean ± SEM and are representative of two independent experiments. One-way ANOVA: $^{*}p < 0.05$; $^{**}p < 0.01$.

REFERENCES

1. Global Strategy GINA. For asthma management and prevention: GINA executive summary. *Eur Respir J*. (2018) 31:143–78. doi: 10.1183/09031936.00138707
2. Zakeri A, Russo M. Dual role of toll-like receptors in human and experimental asthma models. *Front Immunol*. (2018) 9:1027. doi: 10.3389/fimmu.2018.01027
3. Lai CKW, Beasley R, Crane J, Foliaki S, Shah J, Weiland S, et al. Global variation in the prevalence and severity of asthma symptoms: phase three of the international study of asthma and allergies in childhood (ISAAC). *Thorax*. (2009) 64:476–83. doi: 10.1136/thx.2008.106609
4. Lin TY, Poon AH, Hamid Q. Asthma phenotypes and endotypes. *Curr Opin Pulm Med*. (2013) 19:18–23. doi: 10.1097/MCP.0b013e32835b10ec
5. Lötvall J, Akdis CA, Bacharier LB, Bjermer L, Casale TB, Custovic A, et al. Asthma endotypes: a new approach to classification of disease entities within the asthma syndrome. *J Allergy Clin Immunol*. (2011) 127:355–60. doi: 10.1016/j.jaci.2010.11.037
6. Stone KD, Prussin C, Metcalfe DD. IgE, mast cells, basophils, and eosinophils. *J Allergy Clin Immunol*. (2010) 125(2 Suppl 2):S73–80. doi: 10.1016/j.jaci.2009.11.017
7. Von Mutius E. The environmental predictors of allergic disease. *J Allergy Clin Immunol*. (2000) 105:9–19. doi: 10.1016/S0091-6749(00)90171-4
8. Strachan DP. Hay fever, hygiene, and household size. *BMJ*. (1989) 299:1259. doi: 10.1136/bmj.299.6710.1259
9. Romagnani S. The increased prevalence of allergy and the hygiene hypothesis: missing immune deviation, reduced immune suppression, or both? *Immunology*. (2004) 112:352–63. doi: 10.1111/j.1365-2567.2004.01925.x
10. Kozyrskyj AL, Bahreinian S, Azad MB. Early life exposures: impact on asthma and allergic disease. *Curr Opin Allergy Clin Immunol*. (2011) 11:400–6. doi: 10.1097/ACI.0b013e328349b166
11. Cooper PJ. Interactions between helminth parasites and allergy. *Curr Opin Allergy Clin Immunol*. (2009) 9:29–37. doi: 10.1097/ACI.0b013e32831f44a6
12. Sitcharungsi R, Sirivichayakul C. Allergic diseases and helminth infections. *Pathog Glob Health*. (2013) 107:110–5. doi: 10.1179/2047773213Y.0000000080
13. Shirakawa T, Enomoto T, Shimazu SI, Hopkin JM. The inverse association between tuberculin responses and atopic disorder. *Science*. (1997) 275:77–9. doi: 10.1126/science.275.5296.77
14. Choi IS. Immunomodulating approach to asthma using mycobacteria. *Allergy Asthma Immunol Res*. (2014) 6:187. doi: 10.4168/aair.2014.6.3.187
15. Prescott SL. Allergy takes its toll: the role of toll-like receptors in allergy pathogenesis. *World Allergy Organ J*. (2008) 1:4–8. doi: 10.1097/wox.0b013e3181625d9f
16. Van Strien RT, Engel R, Holst O, Bufe A, Eder W, Waser M, et al. Microbial exposure of rural school children, as assessed by levels of N-acetyl-muramic acid in mattress dust, and its association with respiratory health. *J Allergy Clin Immunol*. (2004) 113:860–7. doi: 10.1016/j.jaci.2004.01.783
17. Beeh KM, Kanniess F, Wagner F, Schilder C, Naudts I, Hammann-Haenni A, et al. The novel TLR-9 agonist QbG10 shows clinical efficacy in persistent allergic asthma. *J Allergy Clin Immunol*. (2013) 131:866–74. doi: 10.1016/j.jaci.2012.12.1561
18. Senti G, Johansen P, Haug S, Bull C, Gottschaller C, Müller P, et al. Use of A-type CpG oligodeoxynucleotides as an adjuvant in allergen-specific immunotherapy in humans: a phase I/IIa clinical trial. *Clin Exp Allergy*. (2009) 39:562–70. doi: 10.1111/j.1365-2222.2008.03191.x
19. Santeliz JV, Van NG, Traquina P, Larsen E, Wills-Karp M. Amb a 1-linked CpG oligodeoxynucleotides reverse established airway hyperresponsiveness in a murine model of asthma. *J Allergy Clin Immunol*. (2002) 109:455–62. doi: 10.1067/mai.2002.122156
20. Fonseca DM, Wowk PF, Paula MO, Gembre AF, Baruffi MD, Fermino ML, et al. Requirement of MyD88 and Fas pathways for the efficacy of allergen-free immunotherapy. *Allergy Eur J Allergy Clin Immunol*. (2015) 70:275–84. doi: 10.1111/all.12555
21. Mirotti L, Custódio RWA, Gomes E, Rammauro F, de Araujo EF, Calich VLG, et al. CpG-ODN shapes alum adjuvant activity signaling Via MyD88 and IL-10. *Front Immunol*. (2017) 8:47. doi: 10.3389/fimmu.2017.00047
22. Larenas Linnemann DES. One hundred years of immunotherapy: review of the first landmark studies. *Allergy Asthma Proc*. (2012) 33:122–8. doi: 10.2500/aap.2012.33.3515
23. Zohra FT, Chowdhury EH, Akaike T. High performance mRNA transfection through carbonate apatite-cationic liposome conjugates. *Biomaterials*. (2009) 30:4006–13. doi: 10.1016/j.biomaterials.2009.02.050
24. Latz E, Schoenemeyer A, Visintin A, Fitzgerald KA, Monks BG, Knetter CF, et al. TLR9 signals after translocating from the ER to CpG DNA in the lysosome. *Nat Immunol*. (2004) 5:190–8. doi: 10.1038/ni1028
25. Caton ML, Smith-Raska MR, Reizis B. Notch–RBP-J signaling controls the homeostasis of CD8 $^{-}$ dendritic cells in the spleen. *J Exp Med*. (2007) 204:1653–64. doi: 10.1084/jem.20062648
26. Hou B, Reizis B, DeFranco AL. Toll-like receptors activate innate and adaptive immunity by using dendritic cell-intrinsic and -extrinsic mechanisms. *Immunity*. (2008) 29:272–82. doi: 10.1016/j.immuni.2008.05.016
27. Maynard CL, Harrington LE, Janowski KM, Oliver JR, Zindl CL, Rudensky AY, et al. Regulatory T cells expressing interleukin 10 develop from Foxp3+ and Foxp3- precursor cells in the absence of interleukin 10. *Nat Immunol*. (2007) 8:931–41. doi: 10.1038/ni1504
28. Bettelli E, Carrier Y, Gao W, Korn T, Strom TB, Oukka M, et al. Reciprocal developmental pathways for the generation of pathogenic effector TH17 and regulatory T cells. *Nature*. (2006) 441:235–8. doi: 10.1038/nature04753
29. Radu M, Chernoff J. An in vivo assay to test blood vessel permeability. *J Vis Exp*. (2013) 73:e50062. doi: 10.3791/50062
30. Alberca Custodio RW, Mirotti L, Gomes E, Nunes FPB, Vieira RS, Graça L, et al. Dendritic cells expressing MyD88 molecule are necessary and sufficient for CpG-mediated inhibition of IgE production in vivo. *Cells*. (2019) 8:1165. doi: 10.3390/cells8101165
31. Cappella A, Durham S. Allergen immunotherapy for allergic respiratory diseases. *Hum Vaccin Immunother*. (2012) 8:1499–512. doi: 10.4161/hv.21629
32. Calderon MA, Rodriguez Del RP, Vidal C, Pfaar O, Just J, Worm M, et al. The European survey on adverse systemic reactions due to allergen immunotherapy: the "EASSI" pilot survey. *Allergy Eur J Allergy Clin Immunol*. (2013). 4:4. doi: 10.1186/2045-7022-4-22
33. Akdis CA. Therapies for allergic inflammation: refining strategies to induce tolerance. *Nat Med*. (2012) 18:736–49. doi: 10.1038/nm.2754
34. Lee BL, Barton GM. Trafficking of endosomal Toll-like receptors. *Trends Cell Biol*. (2014) 24:360–9. doi: 10.1016/j.tcb.2013.12.002
35. Eifan AO, Shamji MH, Durham SR. Long-term clinical and immunological effects of allergen immunotherapy. *Curr Opin Allergy Clin Immunol*. (2011) 11:586–93. doi: 10.1097/ACI.0b013e32834cb994
36. Bošnjak B, Kazemi S, Altenburger LM, Mokroviæ G, Epstein MM. Th2-TRMs maintain life-long allergic memory in experimental asthma in mice. *Front Immunol*. (2019) 10:840. doi: 10.3389/fimmu.2019.00840
37. Tabar AI, Arroabarren E, Echechipía S, García BE, Martin S, Alvarez-Puebla MJ. Three years of specific immunotherapy may be sufficient in house dust mite respiratory allergy. *J Allergy Clin Immunol*. (2011) 127:.57–63.e1–3. doi: 10.1016/j.jaci.2010.10.025
38. Marogna M, Spadolini I, Massolo A, Canonica GW, Passalacqua G. Long-lasting effects of sublingual immunotherapy according to its duration: a 15-year prospective study. *J Allergy Clin Immunol*. (2010) 126:969–75. doi: 10.1016/j.jaci.2010.08.030
39. Simpson EM, Linder CC, Sargent EE, Davisson MT, Mobraaten LE, Sharp JJ. Genetic variation among 129 substrains and its importance for targeted mutagenesis in mice. *Nat Genet*. (1997) 16:19–27. doi: 10.1038/ng0597-19
40. Nunes FPB, Alberca—Custódio RW, Gomes E, Fonseca DM, Yokoyama NH, Labrada A, et al. TLR9 agonist adsorbed to alum adjuvant prevents asthma—like responses induced by *Blomia tropicalis* mite extract. *J Leukoc Biol*. (2019) 106:653–64. doi: 10.1002/jlb.ma1218-475rr
41. Matsuoka T, Shamji MH, Durham SR. Allergen immunotherapy and tolerance. *Allergol Int*. (2013) 62:403–13. doi: 10.2332/allergolint.13-RAI-0650
42. Maazi H, Shirinbak S, Willart M, Hammad HM, Cabanski M, Boon L, et al. Contribution of regulatory T cells to alleviation of experimental allergic asthma after specific immunotherapy. *Clin Exp Allergy*. (2012) 42:1519–28. doi: 10.1111/j.1365-2222.2012.04064.x
43. Akdis CA, Akdis M. Mechanisms of allergen-specific immunotherapy. *J Allergy Clin Immunol*. (2011) 127:18–27. doi: 10.1016/j.jaci.2010.11.030
44. Hemmi H, Kaisho T, Takeda K, Akira S. The roles of toll-like receptor 9, MyD88, and DNA-dependent protein kinase catalytic subunit in the effects

of two distinct CpG DNAs on dendritic cell subsets. *J Immunol*. (2003) 170:3059–64. doi: 10.4049/jimmunol.170.6.3059
45. Volpi C, Fallarino F, Pallotta MT, Bianchi R, Vacca C, Belladonna ML, et al. High doses of CpG oligodeoxynucleotides stimulate a tolerogenic TLR9-TRIF pathway. *Nat Commun*. (2013) 4:1852. doi: 10.1038/ncomms2874
46. Krieg AM. CpG motifs in bacterial DNA and their immune effects. *Annu Rev Immunol*. (2002) 20:709–60. doi: 10.1146/annurev.immunol.20.100301.064842
47. Häcker H. Signal transduction pathways activated by CpG-DNA, in Raz E editor. *Microbial DNA and Host Immunity*. Totowa, NJ: Humana Press. (2002).
48. Ring J, Gutermuth J. 100 years of hyposensitization: history of allergen-specific immunotherapy (ASIT). *Allergy Eur J Allergy Clin Immunol*. (2011) 66:713–24. doi: 10.1111/j.1398-9995.2010.02541.x
49. Fujita H, Soyka MB, Akdis M, Akdis CA. Mechanisms of allergen-specific immunotherapy. *Clin Transl Allergy*. (2012) 2:2. doi: 10.1186/2045-7022-2-2
50. MacKenzie KJ, Fitch PM, Leech MD, Ilchmann A, Wilson C, McFarlane AJ, et al. Combination peptide immunotherapy based on T-cell epitope mapping reduces allergen-specific IgE and eosinophilia in allergic airway inflammation. *Immunology*. (2013) 138:258–68. doi: 10.1111/imm.12032
51. Canonica GW, Cox L, Pawankar R, Baena-Cagnani CE, Blaiss M, Bonini S, et al. Sublingual immunotherapy: world allergy organization position paper 2013 update. *World Allergy Organ J*. (2014) 7:6. doi: 10.1186/1939-4551-7-6
52. Takabayashi K, Libet L, Chisholm D, Zubeldia J, Horner AA. Intranasal immunotherapy is more effective than intradermal immunotherapy for the induction of airway allergen tolerance in Th2-sensitized mice. *J Immunol*. (2003) 170:3898–905. doi: 10.4049/jimmunol.170.7.3898
53. Georgitis JW, Reisman RE, Clayton WF, Mueller UR, Wypych JI, Arbesman CE. Local intranasal immunotherapy for grass-allergic rhinitis. *J Allergy Clin Immunol*. (1983) 71(1 Pt 1):71–6. doi: 10.1016/S0002-9610(34)90165-3
54. Kitagaki K, Businga TR, Kline JN. Oral administration of CpG-ODNs suppresses antigen-induced asthma in mice. *Clin Exp Immunol*. (2006) 143:249–59. doi: 10.1111/j.1365-2249.2005.03003.x
55. Cox L, Calderón M, Pfaar O. Subcutaneous allergen immunotherapy for allergic disease: examining efficacy, safety and cost-effectiveness of current and novel formulations. *Immunotherapy*. (2012) 4:606–16. doi: 10.2217/imt.12.36
56. Normansell R, Kew KM. Sublingual immunotherapy for asthma. *Cochrane Database Syst Rev*. (2014) 2015:CD011293. doi: 10.1002/14651858.CD011293
57. Lieberman P. The risk and management of anaphylaxis in the setting of immunotherapy. *Am J Rhinol Allergy*. (2012) 26:469–74. doi: 10.2500/ajra.2012.26.3811
58. Fonseca DM, Wowk PF, Paula MO, Campos LW, Gembre AF, Turato WM, et al. Recombinant DNA immunotherapy ameliorate established airway allergy in a IL-10 dependent pathway. *Clin Exp Allergy*. (2012) 42:131–43. doi: 10.1111/j.1365-2222.2011.03845.x
59. Yasuda K, Richez C, Uccellini MB, Richards RJ, Bonegio RG, Akira S, et al. Requirement for DNA CpG content in TLR9-dependent dendritic cell activation induced by DNA-containing immune complexes. *J Immunol*. (2009) 183:3109–17. doi: 10.4049/jimmunol.0900399
60. Yotsumoto S, Saegusa K, Aramaki Y. Endosomal translocation of CpG-oligodeoxynucleotides inhibits DNA-PKcs-dependent IL-10 production in macrophages. *J Immunol*. (2008) 180:809–16. doi: 10.4049/jimmunol.180.2.809
61. Mansourian M, Badiee A, Jalali SA, Shariat S, Yazdani M, Amin M, et al. Effective induction of anti-tumor immunity using p5 HER-2/neu derived peptide encapsulated in fusogenic DOTAP cationic liposomes co-administrated with CpG-ODN. *Immunol Lett*. (2014) 162(1 Pt A):87–93. doi: 10.1016/j.imlet.2014.07.008
62. Tada R, Muto S, Iwata T, Hidaka A, Kiyono H, Kunisawa J, et al. Attachment of class B CpG ODN onto DOTAP/DC-chol liposome in nasal vaccine formulations augments antigen-specific immune responses in mice. *BMC Res Notes*. (2017) 10:68. doi: 10.1186/s13104-017-2380-8
63. Tada R, Hidaka A, Iwase N, Takahashi S, Yamakita Y, Iwata T, et al. Intranasal immunization with dotap cationic liposomes combined with DC-cholesterol induces potent antigen-specific mucosal and systemic immune responses in mice. *PLoS One*. (2015) 10:e0139785. doi: 10.1371/journal.pone.0139785
64. Lv H, Zhang S, Wang B, Cui S, Yan J. Toxicity of cationic lipids and cationic polymers in gene delivery. *J Control Release*. (2006) 114:100–9. doi: 10.1016/j.jconrel.2006.04.014
65. Hemmi H, Takeuchi O, Kawai T, Kaisho T, Sato S, Sanjo H, et al. A Toll-like receptor recognizes bacterial DNA. *Nature*. (2000) 408:740–5. doi: 10.1038/35047123
66. Bal SM, Hortensius S, Ding Z, Jiskoot W, Bouwstra JA. Co-encapsulation of antigen and Toll-like receptor ligand in cationic liposomes affects the quality of the immune response in mice after intradermal vaccination. *Vaccine*. (2011) 29:1045–52. doi: 10.1016/j.vaccine.2010.11.061
67. Jain VV, Businga TR, Kitagaki K, George CL, O'Shaughnessy PT, Kline JN. Mucosal immunotherapy with CpG oligodeoxynucleotides reverses a murine model of chronic asthma induced by repeated antigen exposure. *Am J Physiol Lung Cell Mol Physiol*. (2003) 285:L1137–46. doi: 10.1152/ajplung.00073.2003
68. Chen L, Arora M, Yarlagadda M, Oriss TB, Krishnamoorthy N, Ray A, et al. Distinct responses of lung and spleen dendritic cells to the TLR9 agonist CpG oligodeoxynucleotide. *J Immunol*. (2006) 177:2373–83. doi: 10.4049/jimmunol.177.4.2373
69. Liu M, O'Connor RS, Trefely S, Graham K, Snyder NW, Beatty GL. Metabolic rewiring of macrophages by CpG potentiates clearance of cancer cells and overcomes tumor-expressed CD47-mediated 'don't-eat-me' signal. *Nat Immunol*. (2019) 20:265–75. doi: 10.1038/s41590-018-0292-y
70. Hou B, Reizis B, DeFranco A. Toll-like receptor-mediated dendritic cell-dependent and-independent stimulation of innate and adaptive immunity. *Immunity*. (2008) 29:272–82. doi: 10.1016/j.immuni.2008.05.016
71. Hou B, Saudan P, Ott G, Wheeler ML, Ji M, Kuzmich L, et al. Selective utilization of toll-like receptor and Myd88 signaling in B cells for enhancement of the antiviral germinal center response. *Immunity*. (2011) 34:375–84. doi: 10.1016/j.immuni.2011.01.011
72. Valovirta E, Petersen TH, Piotrowska T, Laursen MK, Andersen JS, Sørensen HF, et al. Results from the 5-year SQ grass sublingual immunotherapy tablet asthma prevention (GAP) trial in children with grass pollen allergy. *J Allergy Clin Immunol*. (2018) 141:529–38.e13. doi: 10.1016/j.jaci.2017.06.014
73. Jacobsen L, Wahn U, Bilo MB. Allergen-specific immunotherapy provides immediate, long-term and preventive clinical effects in children and adults: the effects of immunotherapy can be categorised by level of benefit -the centenary of allergen specific subcutaneous immunotherapy. *Clin Transl Allergy*. (2012) 2:8. doi: 10.1186/2045-7022-2-8
74. Kristiansen M, Dhami S, Netuveli G, Halken S, Muraro A, Roberts G, et al. Allergen immunotherapy for the prevention of allergy: a systematic review and meta-analysis. *Pediatr Allergy Immunol*. (2017) 28:18–29. doi: 10.1111/pai.12661
75. Halken S, Larenas-Linnemann D, Roberts G, Calderón MA, Angier E, Pfaar O, et al. EAACI guidelines on allergen immunotherapy: prevention of allergy. *Pediatr Allergy Immunol*. (2017) 28:728–74. doi: 10.1111/pai.12807
76. Penagos M, Eifan AO, Durham SR, Scadding GW. Duration of allergen immunotherapy for long-term efficacy in allergic rhinoconjunctivitis. *Curr Treat Options Allergy*. (2018) 5:275–90. doi: 10.1007/s40521-018-0176-2
77. Van Hove CL, Maes T, Joos GF, Tournoy KG. Prolonged inhaled allergen exposure can induce persistent tolerance. *Am J Respir Cell Mol Biol*. (2007) 36: 573–584. doi: 10.1165/rcmb.2006-0385OC
78. Santos Da Silva E, Asam C, Lackner P, Hofer H, Wallner M, Silva Pinheiro C, et al. Allergens of *Blomia tropicalis*: an overview of recombinant molecules. *Int Arch Allergy Immunol*. (2017) 172:203–14. doi: 10.1159/000464325
79. Rusznak C, Davies RJ. ABC of allergies: Diagnosing allergy BMJ. *BMJ*. (1998). 316:686. doi: 10.1136/bmj.316.7132.686
80. Crotty S, Ahmed R. Immunological memory in humans. *Semin Immunol*. (2004) 16:197–203. doi: 10.1016/j.smim.2004.02.008
81. Kuruvilla ME, Lee FEH, Lee GB. Understanding asthma phenotypes, endotypes, and mechanisms of disease. *Clin Rev Allergy Immunol*. (2019) 56:219–33. doi: 10.1007/s12016-018-8712-1

Conflict of Interest: The authors declare that the research was conducted in the absence of any commercial or financial relationships that could be construed as a potential conflict of interest.

frontiers in Immunology

ORIGINAL RESEARCH
published: 07 May 2020
doi: 10.3389/fimmu.2020.00691

ILC2 Lung-Homing in Cystic Fibrosis Patients: Functional Involvement of CCR6 and Impact on Respiratory Failure

Anja Schulz-Kuhnt[1], Vicky Greif[1], Kai Hildner[1], Lisa Knipfer[1], Michael Döbrönti[1], Sabine Zirlik[1], Florian Fuchs[1], Raja Atreya[1], Sebastian Zundler[1], Rocío López-Posadas[1], Clemens Neufert[1], Andreas Ramming[2], Alexander Kiefer[3], Anika Grüneboom[2], Erwin Strasser[4], Stefan Wirtz[1], Markus F. Neurath[1†] and Imke Atreya[1†]*

[1] Department of Medicine 1, University Hospital of Erlangen, Erlangen, Germany, [2] Department of Medicine 3, University Hospital of Erlangen, Erlangen, Germany, [3] Department of Pediatrics and Adolescent Medicine, University Hospital of Erlangen, Erlangen, Germany, [4] Department of Transfusion Medicine and Haemostaseology, University Hospital of Erlangen, Erlangen, Germany

Cystic fibrosis patients suffer from a progressive, often fatal lung disease, which is based on a complex interplay between chronic infections, locally accumulating immune cells and pulmonary tissue remodeling. Although group-2 innate lymphoid cells (ILC2s) act as crucial initiators of lung inflammation, our understanding of their involvement in the pathogenesis of cystic fibrosis remains incomplete. Here we report a marked decrease of circulating CCR6$^+$ ILC2s in the blood of cystic fibrosis patients, which significantly correlated with high disease severity and advanced pulmonary failure, strongly implicating increased ILC2 homing from the peripheral blood to the chronically inflamed lung tissue in cystic fibrosis patients. On a functional level, the CCR6 ligand CCL20 was identified as potent promoter of lung-directed ILC2 migration upon inflammatory conditions *in vitro* and *in vivo* using a new humanized mouse model with light-sheet fluorescence microscopic visualization of lung-accumulated human ILC2s. In the lung, blood-derived human ILC2s were able to augment local eosinophil and neutrophil accumulation and induced a marked upregulation of pulmonary type-VI collagen expression. Studies in primary human lung fibroblasts additionally revealed ILC2-derived IL-4 and IL-13 as important mediators of this type-VI collagen-inducing effect. Taken together, the here acquired results suggest that pathologically increased CCL20 levels in cystic fibrosis airways induce CCR6-mediated lung homing of circulating human ILC2s. Subsequent ILC2 activation then triggers local production of type-VI collagen and might thereby drive extracellular matrix remodeling potentially influencing pulmonary tissue destruction in cystic fibrosis patients. Thus, modulating the lung homing capacity of circulating ILC2s and their local effector functions opens new therapeutic avenues for cystic fibrosis treatment.

Keywords: group-2 innate lymphoid cells, cystic fibrosis, CCR6, type-VI collagen, tissue remodeling

OPEN ACCESS

Edited by:
Maria Leite-de-Moraes, Institut Necker Enfants Malades, France

Reviewed by:
Jorg Hermann Fritz, McGill University, Canada
Attila Bacsi, University of Debrecen, Hungary

***Correspondence:**
Imke Atreya
imke.atreya@uk-erlangen.de

† These authors have contributed equally to this work

Specialty section:
This article was submitted to Molecular Innate Immunity, a section of the journal Frontiers in Immunology

Received: *18 December 2019*
Accepted: *26 March 2020*
Published: *07 May 2020*

Citation:
Schulz-Kuhnt A, Greif V, Hildner K, Knipfer L, Döbrönti M, Zirlik S, Fuchs F, Atreya R, Zundler S, López-Posadas R, Neufert C, Ramming A, Kiefer A, Grüneboom A, Strasser E, Wirtz S, Neurath MF and Atreya I (2020) ILC2 Lung-Homing in Cystic Fibrosis Patients: Functional Involvement of CCR6 and Impact on Respiratory Failure. Front. Immunol. 11:691. doi: 10.3389/fimmu.2020.00691

INTRODUCTION

Cystic fibrosis (CF) represents the most common inherited disease in Caucasians and an epidemiological study performed in 2016 even predicts an increase of about 50% in the overall number of patients diagnosed for this life-threatening disease by the year 2025 in Western European countries (1, 2). The pathophysiology of CF is based on defined mutations in the cystic fibrosis transmembrane conductance regulator (*CFTR*) gene, which cause dysfunction of the CFTR chloride channel and, subsequently, an impaired epithelial chloride and bicarbonate transport resulting in viscid mucus production (3, 4). Although CF pathology involves various organ systems, respiratory failure as consequence of progressive lung disease appears as the leading cause of disease-associated morbidity and mortality (3–5).

Fibrosis and bronchiectasis represent key characteristics of pulmonary CF manifestation (4, 6, 7). It is well-accepted that the etiology of bronchiectasis depends on a complex interplay between chronic lung infections, progressive pulmonary tissue remodeling and an accumulation of pro-inflammatory immune cells (8). Mainly as consequence of viscid mucus production and impaired mucociliary clearance, airways of CF patients are highly susceptible to bacterial colonization and infection. This permanent crosstalk of microbial pathogens with the CFTR-dysfunctional airway epithelium triggers a pro-inflammatory but yet inefficient mucosal immune response (4, 9) dominated by a marked accumulation of neutrophils (10). Due to a complex dysregulation of adaptive and innate immune cell function and interplay (11, 12), the lung tissue, bronchoalveolar lavage (BAL) and sputum of CF patients are characterized by increased levels of inflammation-promoting chemokines and cytokines, including for instance IL-8, GM-CSF, IL-6, CCL2, CCL3, CCL4, CCL20, TNF-α, IL-1β, IL-17, IL-23, G-CSF, IL-9, and IL-33 (10, 13–16). Within this inflammatory milieu, neutrophil-derived elastase and matrix metalloproteinases represent crucial mediators of extracellular matrix degradation and CF-associated pulmonary tissue remodeling (17–19). In addition to chronic airway infections as inflammatory triggers, immune responses have been suggested to be partly driven by intrinsic alterations independent from non-self recognition in CF patients (20) and thus gained new research interest.

During the last decade, innate lymphoid cells (ILCs) emerged as rare but exceptionally potent representatives of the innate immune system. They are of particular importance for host defense at epithelial barrier surfaces (21), but also contribute to the systemic pool of circulating immune cells (22, 23). Characterized by a type-2 cytokine profile and the expression of signature surface molecules (e.g., CD127 and CRTH2) (24, 25) and transcription factors (e.g., GATA3) (26), group-2 ILCs (ILC2s) represent a predominant helper ILC population in the lung under steady state conditions (27, 28). There they are preferentially located in direct proximity to the airway epithelium or accumulate within infected foci (27, 29). This predisposes pulmonary ILC2s for sensing epithelial injury and participating in a first line of immunological defense against invading pathogens. In case of allergic or infectious lung diseases, inflammatory mediators like IL-33, IL-25, and thymic stromal lymphopoetin are locally released by damaged epithelial cells and potently stimulate ILC2 activity (30–35). Mainly via the secretion of characteristic cytokines (e.g., IL-5, IL-13, IL-9, and IL-4) and growth factors, but also based on cell contact-dependent mechanisms, activated ILC2s promote type-2 immune responses, support mucosal wound healing and, thereby, crucially impact on the maintenance and reconstitution of tissue homeostasis (27, 36–40). Overwhelming ILC2 activation, however, was found to be involved in chronic inflammation, allergy, and fibrotic tissue remodeling (24, 41, 42). Although published RNA-seq. data from bronchial brush samples implicated that the lung pathology in CF is predominated by Th17 and Th1 gene signatures (43), the increased pulmonary presence of the ILC2-activating cytokine IL-33 and augmented levels of the type-2 effector cytokines IL-5, IL-9, and IL-13 in CF BAL and sputum samples as well as the upregulation of local Th2 responses upon chronic infections with *Pseudomonas aeruginosa* in CF patients strongly argued for a potential, albeit less elucidated, involvement of ILC2s in CF pathogenesis (13, 14, 42, 44–46). Accordingly, the risk of asthma, a prototypical ILC2-initiated allergic disease (47), was found to be significantly higher in CF patients compared to non-carriers of a *CFTR* mutation (48), implicating exaggerated ILC2 activities in CF. In line with this, $Cftr^{-/-}$ mice showed elongated ILC2 responses compared to C57Bl/6 wild type mice upon infection with *Aspergillus fumigatus* (14). Furthermore, mainly based on analyses in preclinical murine models with CF-like pathology, Moretti et al. demonstrated that ILC2-derived IL-9 triggers an auto-amplifying pro-inflammatory cycle via activation of mast cells, which in turn supports ILC2 functions by producing the growth factor IL-2, indicating an orchestrating role of lung-resident ILC2s in CF-associated inflammation (14). However, the direct clinical relevance of ILC2 function for pulmonary manifestation of human CF disease as well as the origin of activated lung ILC2s remain undefined. Therefore, we here analyzed the functional significance of circulating human ILC2s in the peripheral blood (pb) for the development of CF–associated fibro-inflammatory changes in the lung. To address this, we examined pb ILC2 function in CF by taking advantage of human blood samples and *in vivo* studies in a new humanized mouse model for ILC2 lung homing. Our results identified the CCR6 - CCL20 axis as regulator of pulmonary ILC2 migration and suggest local ILC2 activation as a potential driver of pulmonary type-VI collagen production in CF patients.

MATERIALS AND METHODS

Human Blood Samples

After informed written consent, peripheral blood was collected in EDTA-coated tubes from patients with cystic fibrosis (n = 59), inflammatory bowel diseases (n = 19), and rheumatoid arthritis (n = 17), as well as healthy control subjects (n = 61). Characteristics of all study subjects are summarized in **Table S1**. Patient material was obtained from the Department of Medicine 1 and 3 as well as the Department of Pediatrics and Adolescent Medicine of the University Hospital of Erlangen, Germany. Leukocyte cones were derived from the Department

of Transfusion Medicine and Haemostaseology of the University Hospital of Erlangen, Germany. Blood donation was approved by the local ethical committee and the institutional review board of the University of Erlangen-Nuremberg, Germany.

Primary Human Blood Cell Isolation

Peripheral blood mononuclear cells (PBMCs) were isolated from whole blood, leukocyte cones and buffy coat blood via density gradient centrifugation using Pancoll human (PAN-Biotech) or Lymphocyte separation media (Anprotec). Where indicated, PBMCs were further enriched for $CD4^+$ or $CRTH2^+$ cells using magnetic bead-based isolation according to the manufacturer's instructions (Miltenyi Biotec).

Flow Cytometric Characterization of Human ILCs

To identify human ILC2s, ILC1s, and ILC3s, single cell suspensions were treated with FcR blocking reagent (Miltenyi Biotec) before incubation with the following fluorochrome-conjugated anti-human antibodies: hematopoietic lineage cocktail [eFlour450, including CD2 (RPA-2), CD3 (OKT3), CD14 (61D3), CD16 (CB16), CD19 (HIB19), CD56 (CB56), and CD235a (HIR2), eBioscience], CD11c (VioBlue, MJ4-27G12, Miltenyi Biotec), CD127 (APC-Vio770, REA614, Miltenyi Biotec), CD161 (FITC, 191B8, Miltenyi Biotec), CD7 (FITC, CD7-6B7, BioLegend), CD117 (APC, 104D2, BioLegend), and CRTH2 (PE, BM16, Miltenyi Biotec). To further analyze human ILC subgroups, specific antibodies targeting CCR4 (APC, L291H4, BioLegend), CCR5 (Alexa Flour 647, HEK/1/85a, BioLegend), CCR6 (PE/Cy7, G034E3, BioLegend), CCR9 (PerCP/Cy5.5, L053E8, BioLegend), CXCR3 (APC, G025H7, BioLegend), CD4 (PerCP/Cy5.5, OKT4, BioLegend), CD45 (APC, HI30, BioLegend), CD69 (APC, FN50, BioLegend), CD123 (PerCP/Cy5.5, 6H6, BioLegend), TCRα/β (APC, IP26, BioLegend), TCRγ/δ (APC, B1, BioLegend), and respective isotype control antibodies were used. Surface-stained cells were uniformly fixed in 1x BD CellFix (eBioscience) according to the manufacturer's specifications or measured directly after staining. For intracellular staining, the Foxp3/Transcription Factor Staining Buffer Set (eBioscience) in combination with a specific fluorochrome-conjugated antibody targeting human GATA3 (APC, REA174, Miltenyi Biotec) was used. LSR Fortessa (BD Bioscience) or MACSQuant 10 (Miltenyi Biotec) cell analyzers allowed data acquisition. For further data processing, the FlowJo single cell analysis software 7.6.5 and 10.06.1 (Tree Star Inc.) was used. Samples with <20 acquired ILC2s were excluded from further ILC2 phenotyping.

Ex vivo Expansion and Stimulation of Human pb ILC2s

To *ex vivo* expand human pb ILC2s, they were isolated from total PBMCs, derived from CF patients or healthy volunteers, via fluorescence-activated cell sorting (FACS) as $Lin^{neg}CD127^+CD161^+CRTH2^+$ lymphoid cells using a FACSAria II (BD Bioscience) or a MoFlo Astrios (Beckman Coulter) cell sorter. PBMCs from 3 different donors were γ-irradiated (45 Gray) and pooled to serve as feeder cells. Sort-purified human ILC2s (100/well) were then co-cultured with feeder cells (4×10^5/well) in 96 well-round bottom plates in 200 µl Yssel's Medium with 1% human serum AB (BioConnect) and 1% penicillin/streptomycin (P/S) per well. ILC2 expansion was stimulated with phytohaemagglutinin (PHA, 1 µg/ml, Sigma), rh IL-2 (100 IU/ml, Miltenyi Biotec), rh IL-25 (50 ng/ml, eBioscience) and rh IL-33 (50 ng/ml, BioLegend). Medium and cytokines were replenished every 3 to 4 days for 13–15 days. Afterwards, the ILC2 expansion factor was calculated based on flow cytometric enumeration of Lin^{neg} $CD127^+CD161^+CRTH2^+$ ILC2s per well. Expanded ILC2s were then rested in rh IL-2 (20 IU/ml, Miltenyi Biotec) alone for 2 days. For restimulation, expanded and rested cells were re-seeded at 1×10^5 or 3×10^5 cells/well and stimulated with rh IL-2 (100 IU/ml, Miltenyi Biotec), rh IL-25 (50 ng/ml, eBioscience) and rh IL-33 (50 ng/ml, BioLegend) for 3 additional days or overnight, respectively. Supernatants collected between day 11 and 15 of the expansion phase or after 3 days of restimulating adjusted cell numbers of expanded control subject-derived and CF-derived ILC2s were used as ILC2 conditioned media in fibroblast experiments as indicated. Conditioned medium of stimulated feeder cells alone served as control.

Enzyme Linked Immunosorbent Assay (ELISA)

Cytokine concentrations in cell culture supernatants derived from restimulated human ILC2s were quantified via ELISA analyses of human IL-4 (BioLegend), IL-5 (eBioscience, Invitrogen), IL-9 (BioLegend) and IL-13 (eBioscience, Invitrogen). ILC2 conditioned supernatants were used undiluted or diluted up to 1:1000. The optical density was measured using a NOVOstar plate reader (BMG Labtech).

In vitro Transmigration Assay

To analyze the migratory capacity of circulating human ILC2s under defined experimental conditions, freshly isolated $CRTH2^+$ human blood cells were labeled with the hematopoietic lineage cocktail (eFlour450, eBioscience) and fluorescent antibodies targeting CD11c (VioBlue, MJ4-27G12, Miltenyi Biotec), CD161 (FITC, 191B8, Miltenyi Biotec) and CRTH2 (PE, BM16, Miltenyi Biotec). 1.6×10^5 stained $CRTH2^+$ cells were suspended in 80 µl *X-Vivo* 15 medium (Lonza, 1% P/S) and applied to the upper insert of a 96 well-plate with 3 µm pore size (Corning). If indicated, a CCR6 blocking antibody (50 µg/ml in the insert, MAB195, R&D) or the respective isotype control antibody (BioLegend) were added. The bottom well was filled with 235 µl *X-Vivo* 15 medium and rh CCL20 (10 ng/ml and 100 ng/ml, Immunotools) as indicated. CCL25 (100 ng/ml, Immunotools) served as negative control, PGD2 (10 nM, Merck) as positive control (31). After 4 h at 37°C the number of migrated ILC2s in the bottom chamber was determined as $Lin^{neg}CD161^+CRTH2^+$ lymphoid cells via flow cytometry. The migration index was defined as relative migration of $Lin^{neg}CD161^+CRTH2^+$ cells attracted toward a chemotactic stimulus compared to those attracted by medium alone.

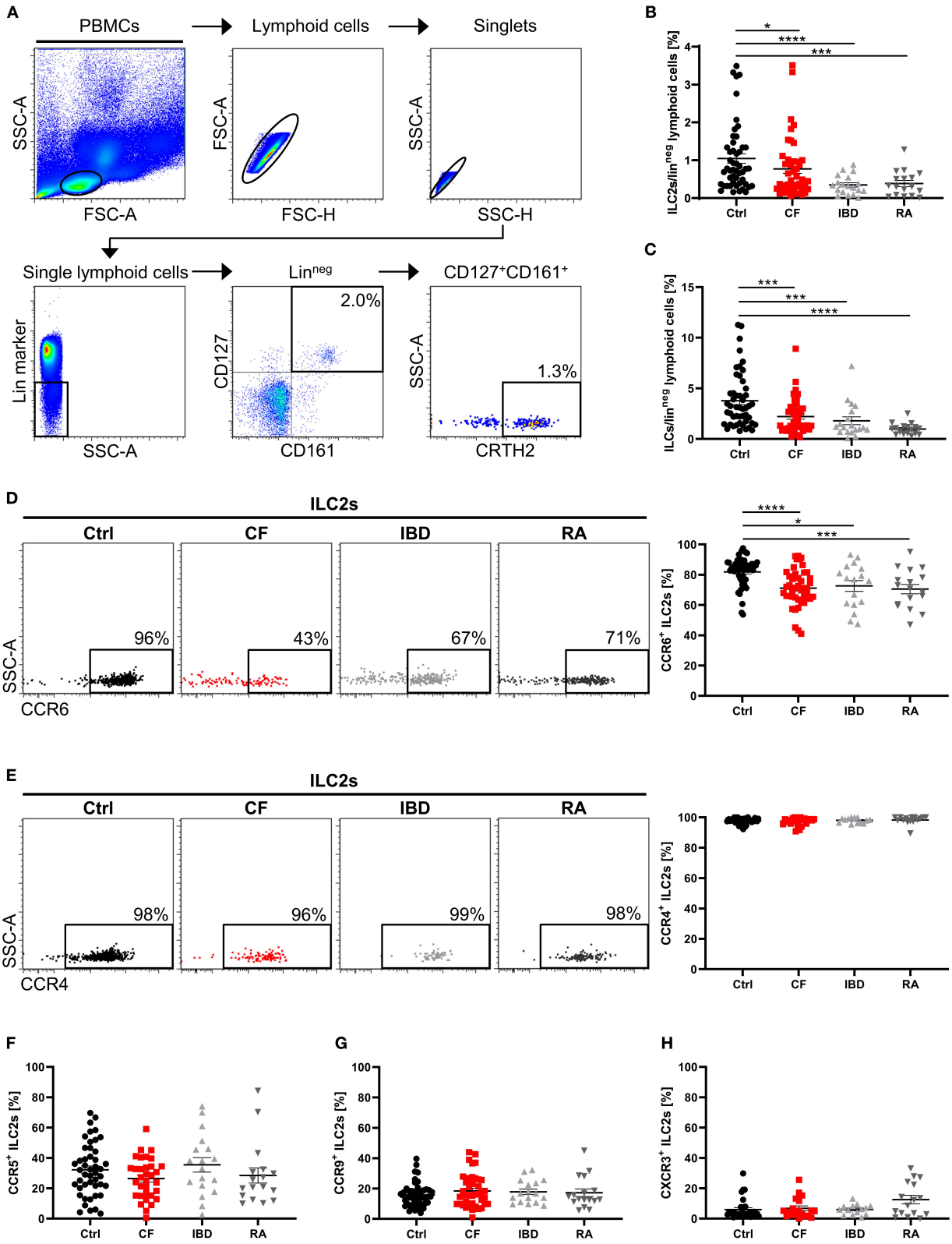

FIGURE 1 | Altered ILC2 profile in the peripheral blood of patients with chronic inflammatory diseases. **(A)** Representative gating scheme for the flow cytometric identification of human pb ILC2s as $Lin^{neg}CD127^{+}CD161^{+}CRTH2^{+}$ lymphoid cells in total PBMCs. Percent values indicate frequencies of gated cell populations on

(Continued)

FIGURE 1 | Lin^{neg} lymphoid cells. **(B)** Quantified proportion of pb ILC2s among Lin^{neg} lymphoid cells in the peripheral blood from healthy controls (ctrl) and patients suffering from cystic fibrosis (CF), inflammatory bowel diseases (IBD) and rheumatoid arthritis (RA) ($n = 17–50$). **(C)** Quantified percentage of total ILCs ($Lin^{neg}CD127^{+}$ lymphoid cells) on Lin^{neg} lymphoid cells ($n = 17–49$). **(D,E)** CCR6 ($n = 17–49$) and CCR4 ($n = 14–39$) expression on human pb ILC2s in ctrl, CF, IBD and RA subjects; representative gating and corresponding quantification. **(F–H)** Quantification of the CCR5 ($n = 17–46$), CCR9 ($n = 17–46$) and CXCR3 ($n = 14–31$) expression on pb ILC2s. Statistical significance was determined using the Mann–Whitney test. Single outliers across all cohorts were detected via the Grubbs' test.
$^{*}p < 0.05, ^{***}p < 0.001, ^{****}p < 0.0001$.

Animals and Papain-Induced Airway Inflammation

C57BL/6 mice were housed under specific pathogen-free conditions in individually ventilated cages with a regular day-night cycle. For the induction of lung inflammation, age-matched mice were anesthetized by *i.p.* injection of ketamine/xylazin and were intranasally treated with 50 μg papain (Merck) for 3 consecutive days. All experiments involving animals were approved by the Government of Lower Franconia, Germany.

In vivo Lung Homing Assay

To investigate the migratory capacity of human blood cells under *in vivo* inflammatory conditions, $CD4^{+}$ human cells or expanded, rested and overnight restimulated human ILC2s with a purity of at least 95% of Lin^{neg} cells were used. If necessary, magnetic bead-based enrichment of Lin^{neg} cells was performed (Miltenyi Biotec). Prior to injection, cells were labeled with the cell proliferation dye eFlour670 (eBioscience) and resuspended in 1x phosphate buffered saline (PBS). 1.5×10^{5} to 1×10^{6} labeled cells were injected intravenously into the tail vein of C57BL/6 mice with papain-induced lung inflammation. Mice without cell transfer served as negative control. If indicated, 2 μg of rh CCL20 (Immunotools) was administered intranasally to anesthetized mice 15 min prior to cell transfer. After 24 h of recirculation, mice were euthanized and the pulmonary circulation was perfused with 5 mM EDTA in 1x PBS via the right ventricle. For the collection of BAL, lungs were carefully flushed three times with PBS supplemented with 0.1 mM EDTA via the trachea. Obtained BAL cells were labeled with fluorochrome-conjugated antibodies targeting CD11c (VioBlue, N418, Miltenyi Biotec) and SiglecF (PE-Vio770, ES22-10D8, Miltenyi Biotec) in order to flow cytometrically determine BAL eosinophils. To inflate the lung tissue to its physiological size prior to removal, 0.75% agarose or 4% paraformaldehyde (PFA) was inserted via the trachea as demonstrated earlier (49). The lung tissue and ileum, if indicated, were then harvested and further subjected to the indicated analyses. During lung perfusion, peripheral blood was collected and erythrocytes were lysed using ammonium-chloride-potassium lysis buffer (155 mM ammonium chloride; 19 mM potassium hydrogen carbonate and 0.68 mM EDTA; pH 7.27) allowing the flow cytometric identification and characterization of injected labeled cells retained in the blood circulation. In order to differentiate between live and dead cells, blood cells were stained with the fixable viability dye eFlour405 (eBioscience) and fixed with the Foxp3/Transcription Factor Staining Buffer Set (eBioscience) prior to flow cytometry.

Light-Sheet Fluorescence Microscopy

For light-sheet microscopic visualization of lung-accumulated human blood ILC2s, the lung tissue was prepared as described elsewhere (50). In short, lung lobes were fixed in 4% PFA for 2 h at 4°C under constant rotation. Dehydration was performed in an ascending ethanol series of 50, 70, and 100% (2x) for at least 4 h each. Dehydrated samples were then cleared with ethyl cinnamate (Sigma) at room temperature and imaged with the UltraMicroscope II (LaVision, BioTec). 3D reconstruction and quantification of accumulated human blood ILC2s within the pulmonary tissue were performed with the Imaris Image Analysis software 9.0.2 (Bitplane) as described in detail earlier (49). Accumulated labeled cells were counted in 2 to 3 lung cubes with defined volume per lung with a mean cell count of 156 labeled ILC2s per lung cube.

Immunohistochemistry

Cryosections of murine lung tissue were fixed in 4% PFA followed by blocking with 5% BSA, Roti-ImmunoBlock (Carl Roth) and donkey serum. Primary antibodies targeting Col VI (1:250, EPR17072, Abcam), Col I (1:200, polyclonal, Abcam) or myeloperoxidase (MPO, 1:100, Abcam) were incubated overnight. Collagens were then stained with the secondary antibody donkey anti-rabbit Cy3 (1:200, Poly4064, BioLegend) that was incubated for 1 h at room temperature. Slides treated with the secondary antibody alone served as control. For MPO staining, slides were incubated with a donkey anti-rabbit biotin antibody (1:200, Dianova), followed by Streptavidin-Cy3 (1:200, BioLegend). Nuclei were counterstained using Hoechst 33342 (ThermoFisher Scientific). Image acquisition was performed with the fluorescence microscope DM600B (Leica) for quantitative images and the confocal microscope SP8 (Leica) for representative images. Data analysis and quantification were performed with Fiji (National Institutes of Health). Therefore, the signal intensity of peribronchial Col VI and Col I relative to the Hoechst signal was determined. MPO^{+} cells were counted manually.

Fibroblast Culture

Primary human lung fibroblasts, fetal (Sigma) were cultured in DMEM/F12 medium (Gibco) supplemented with 10% heat-inactivated fetal bovine serum (FBS), 1% P/S, 0.5% L-glutamine and 0.2% amphotericin B and were maintained at 37°C in a humidified incubator containing 5% CO_2. Prior to stimulation, 1×10^{5} fibroblasts were seeded per well of 6 well-plates and rested in 0.1% FBS overnight. Fibroblasts were then stimulated for 48 h with fresh medium supplemented with rh IL-4 (1 pg/ml and 5 pg/ml, Immunotools) and rh IL-13 (10 ng/ml, Immunotools) or 1:5 diluted conditioned ILC2 supernatants derived from *ex vivo* stimulated human ILC2s (collected between d11 to d15 or after 3 days of restimulating adjusted numbers of expanded ILC2s). When indicated, anti-human IL-4 (10 ng/ml, eBioscience), anti-human IL-13 (20 ng/ml, BioLegend) or combinations of these

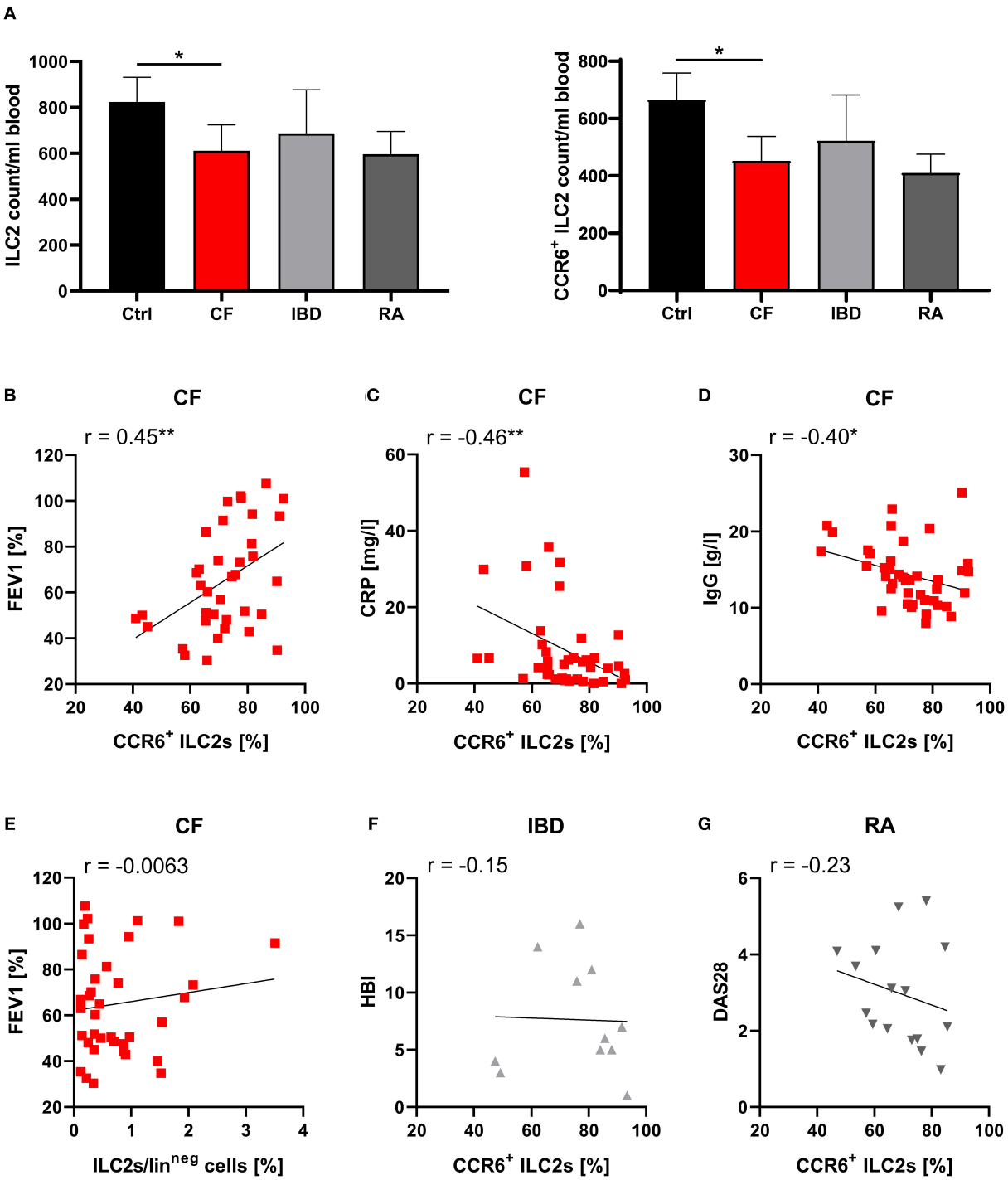

FIGURE 2 | Specific role of CCR6$^+$ pb ILC2s on disease severity in CF patients. **(A)** Total counts of human pb ILC2s and CCR6$^+$ ILC2s per ml blood donated by healthy controls (ctrl, $n = 40$–41) and patients with CF ($n = 35$), IBD ($n = 12$–13), or RA ($n = 17$). Total counts were calculated based on PBMC numbers/ml blood (determined by Neubauer counting chamber) and the proportion of ILC2s and CCR6$^+$ ILC2s among total PBMCs (determined by flow cytometry). The Mann–Whitney test was applied. **(B–D)** Correlation of the percentage of CCR6$^+$ pb ILC2s and disease severity in CF patients based on FEV1% (B; $n = 37$), CRP (C; $n = 41$) and IgG serum levels (D; $n = 41$). The included raw data on CCR6 expressing pb ILC2s were partly also used in **Figure 1D**. **(E)** Correlation of the pb ILC2 frequency and FEV1% in CF patients ($n = 37$). **(F,G)** Correlation of the frequency of CCR6$^+$ pb ILC2s and disease severity in Crohn's disease patients (F; Harvey-Bradshaw Index - HBI; $n = 11$) and RA patients (G; Disease Activity Score 28 - DAS28; $n = 16$). Spearman's r and regression lines are indicated. *$p < 0.05$, **$p < 0.01$.

were added. Conditioned supernatant derived from stimulated feeder cells alone or 1:5 diluted Yssel's medium (1% human serum AB, 1% P/S) supplemented with the cytokine cocktails used for ILC2 expansion (PHA, IL-2, IL-33 and IL-25) or restimulation (IL-2, IL-33, and IL-25) served as control. Fibroblasts up to passage eleven were used.

Immunoblotting

Proteins were isolated from tissue or cells by using mammalian protein extraction reagent (ThermoFisher Scientific) containing protease and phosphatase inhibitors (Roche Diagnostics). Protein concentrations were determined via Bradford assay (Carl Roth) or using the Nanodrop 2000 spectrophotometer (ThermoFisher Scientific). Proteins were then denatured at 99°C in NuPAGEsample Buffer (Life Technologies) and separated by SDS-PAGE gels. After blotting proteins onto nitrocellulose membranes, blocking was performed in 5% non-fat milk. Membranes were incubated overnight at 4°C with the following primary antibodies: Col VI (Abcam), Col I (Cell Signaling Technology), phospho-STAT3 (Cell Signaling Technology), STAT3 (Cell Signaling Technology), phospho-STAT6 (Cell Signaling Technology) and STAT6 (Cell Signaling Technology). β-Actin (Cell Signaling Technology) and tubulin (Cell Signaling Technology) served as loading controls. If necessary, a horseradish-peroxidase conjugated secondary antibody (goat anti-rabbit IgG, Cell Signaling Technology) was incubated for 1 h at room temperature. Chemiluminescence was detected using the ECL Western blotting substrate (ThermoFisher Scientific) by the Amersham Imager 600 (GE Healthcare Bio-Sciences). Quantification of protein levels relative to the loading control was performed using Fiji (National Institutes of Health).

Statistical Analysis

Statistical analyses were performed using the Prism 8 software (GraphPad). Either the two-tailed Student's *t*-test with Welch correction, if necessary, or the Mann-Whitney test was performed. Relative data were analyzed using the one-sample *t*-test. If indicated, single outliers were detected by the Grubbs' test ($\alpha = 0.05$). Results are displayed as bar graphs or scatter plots indicating mean ± SEM. Correlations were calculated by the Spearman or Pearson test as indicated. $P < 0.05$ were considered statistical significant in all tests with asterisks indicating the following levels of significance: $^{*}p < 0.05$, $^{**}p < 0.01$, $^{***}p < 0.001$, $^{****}p < 0.0001$.

RESULTS

Advanced Respiratory Failure Is Associated With a Decrease of Circulating CCR6^{+} ILC2s in CF Patients

Recent insights into the *in vivo* behavior of ILC2s implicate that these cells are present in the systemic circulation and migrate into tissues dependent on inflammatory triggers (51, 52), thus potentially adapting the pool of tissue-resident ILCs to local requirements. In accordance with this, we found a significantly decreased frequency of circulating pb ILC2s (defined as Lin^{neg}CD127^{+}CD161^{+}CRTH2^{+} lymphoid cells) in patients suffering from various chronic inflammatory and fibrotic diseases affecting different organ systems (cystic fibrosis - CF, inflammatory bowel diseases - IBD and rheumatoid arthritis - RA) compared to healthy controls (**Figures 1A,B**). The applied flow cytometric strategy for the identification of human pb ILC2s was successfully validated by confirming the absence of T cells (TCR^{+}, CD4^{+}) and DCs (CD123^{+}) in the indicated target cell population, which in addition showed positive staining for the common immune cell marker CD45 and the ILC2-associated transcription factor GATA3 (**Figure S1A**). Since the reduction of ILC2s in the blood of CF, IBD and RA patients was accompanied by a parallel decrease of total circulating ILCs (**Figure 1C**), it is unlikely that the observed effect can fully be explained by transdifferentiation of pb ILC2s into other ILC subsets, as described for ILC2s in nasal polyps of CF patients or COPD-affected lungs (30, 53). To explore the possibility that reduced systemic ILC2 frequencies in patients diagnosed for chronic inflammatory diseases (including CF, RA and IBD) are due to augmented tissue homing instead, we next focused on the chemokine receptor profile of circulating ILC2s. Examining a panel of defined chemokine receptors with a well-established function in inflammation-driven tissue homing of T cells (54, 55), we observed, in accordance with literature (56), that a high percentage of human pb ILC2s derived from healthy donors expressed CCR4 and CCR6. In contrast, the fractions of CCR5^{+} and especially CCR9^{+} and CXCR3^{+} pb ILC2s were markedly smaller (**Figures S1B,C**). Interestingly, we noted a significantly reduced frequency of CCR6^{+} cells within the circulating ILC2 fraction of CF, IBD and RA patients compared to healthy controls (**Figure 1D**), potentially implicating a general relevance of CCR6 for ILC2 homing into chronically inflamed tissue sites. In contrast to CCR6, neither the fraction of CCR4^{+}, CCR5^{+}, CCR9^{+}, nor CXCR3^{+} pb ILC2s showed an altered frequency in the considered disorders (**Figures 1E–H**). And even though sex-specific differences in the frequency of ILC2s were suggested in asthmatic patients (57), the here observed phenomenon turned out to be gender-independent (**Figure S1D**).

On the level of absolute cell counts per defined blood volume, the observed ILC2 reduction as well as the decrease in CCR6^{+} ILC2s was clearly detectable in CF patients (**Figure 2A**). Notably, we found that phases of impaired respiratory function (determined by low levels of the forced expiratory volume in 1 s - FEV1%) and high inflammatory activity (determined by high C-reactive protein - CRP, and IgG levels) were associated with a more pronounced decrease of CCR6^{+} ILC2 frequencies (**Figures 2B–D**), while this phenomenon was not influenced by the type of the disease-underlying *CFTR* mutation (**Figure S2**A). The inverse correlation with disease severity was only seen in the subgroup of CCR6^{+} but not in total ILC2s (**Figure 2E**). Moreover, in contrast to CF patients, neither clinical exacerbation of IBD nor RA was associated with decreasing rates of circulating CCR6^{+} ILC2s (**Figures 2F,G**), indicating a distinct functional role of CCR6^{+} pb ILC2s in CF. And despite CF being often described as a Th17-dominated disorder (58), the disease-dependent reduction of CCR6^{+} pb ILCs was restricted to the ILC2 subset rather than ILC3s or ILC1s (**Figures S2B,C**). Taken

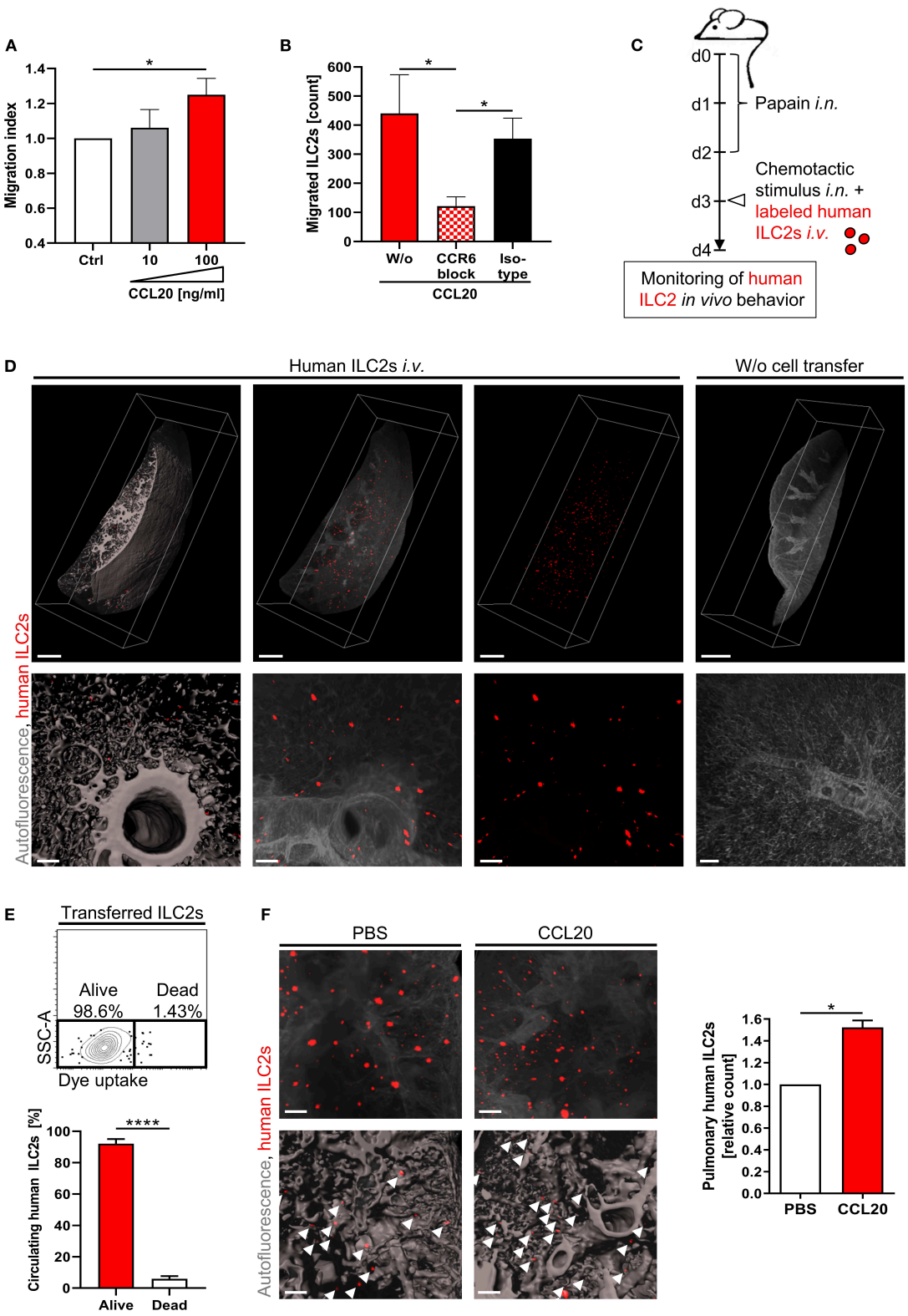

FIGURE 3 | CCR6-CCL20-dependent accumulation of human pb ILC2s in the inflamed lung. **(A)** *In vitro* migration of CRTH2$^+$ human PBMCs derived from healthy subjects towards CCL20. Migrated ILC2s (Lin^{neg}CD161$^+$CRTH2$^+$ lymphoid cells) were flow cytometrically quantified in the bottom chamber ($n = 9$). **(B)** Effect of a

(Continued)

FIGURE 3 | CCR6 blocking antibody (50 μg/ml) on the *in vitro* migration of human ILC2s from control subjects toward CCL20 (100 ng/ml) ($n = 9$, isotype $n = 3$). **(C)** Experimental workflow of the *in vivo* lung homing assay. **(D)** Representative 3D-reconstructed LSFM images (≥ 11 independent experiments) of lung-accumulated human ILC2s (displayed in red). Overview (scale bars: 1,000 μm) and detailed images (scale bars: 100 μm) are depicted (left panel: surface mode, middle/right panels: maximum intensity projection - MIP). Mice without cell transfer served as control. **(E)** Viability of labeled human ILC2s in the murine blood 24 h after transfer; representative FACS plot and corresponding quantification (pooled data from $n = 4$ ctrl ILC2s and $n = 3$ CF ILC2s). The paired *t*-test was applied. **(F)** Pulmonary enrichment of *i.v.* injected labeled ctrl ILC2s after intranasal administration of CCL20 or PBS. Representative LSFM images (scale bars: 200 μm; top panel: MIP; bottom panel: surface mode) and corresponding quantification of accumulated labeled cells (indicated by arrows) ($n = 3$). Single outliers were detected by the Grubbs' test. The Mann-Whitney test was applied, if not indicated otherwise. For relative data the one-sample *t*-test was used. $^{*}p < 0.05$, $^{****}p < 0.0001$.

together, the here depicted data collectively pointed to a potential role of CCR6 signaling during inflammation-triggered lung migration of circulating human ILC2s in CF.

The CCR6 Ligand CCL20 Promotes Pulmonary Accumulation of Human pb ILC2s

While CCR6 represents a well-known mediator of T cell recruitment (59), its potential involvement in the directed movement of circulating ILC2s remained to be investigated. This aspect might be of particular relevance in CF, as affected patients showed increased levels of the CCR6 ligand CCL20 in BAL fluid (15). To study the role of CCL20 for ILC2 migration, we performed chemotaxis assays with primary human $CRTH2^{+}$ pb cells. The CRTH2 ligand prostaglandin D2 (PGD2) and the CCR9 ligand CCL25 served as positive and negative control, respectively (**Figures S3A,B**), (31, 60). Performed analyses revealed a CCL20-induced enrichment of migrated $Lin^{neg}CD161^{+}CRTH2^{+}$ ILC2s in the bottom compartment of the transwell (**Figure 3A**). Of note, the CCL20 concentration (100 ng/ml), which was found to successfully chemoattract human ILC2s in our experimental system (**Figure 3A**), was comparable to increased CCL20 protein levels reported in the airway surface liquid of CF patients (15). As the ILC2 migration in the presence of CCL20 was efficiently inhibited by antibody-mediated blockade of CCR6 (**Figure 3B**), our data identified CCR6 as crucial mediator of human ILC2 chemotaxis.

To gain further insights into the lung homing capacity of human pb ILC2s under *in vivo* conditions, we took advantage of a new humanized mouse model in which fluorescence labeled human ILC2s were intravenously transferred into recipient wildtype mice (49). Using light-sheet fluorescence microscopy (LSFM) imaging, this model allows to visualize the pulmonary accumulation of human ILC2s in the context of papain-induced airway inflammation (**Figures 3C,D**; **Movies S1A,B**). 24 hours after cell transfer, LSFM images of the murine lung depicted a pulmonary enrichment of human ILC2s, while transferred cells did not accumulate in the intestinal mucosa of recipient animals (**Figure 3D**; **Figure S3**C). Flow cytometric detection of transferred ILC2s in the blood of recipient mice ensured good survival of human ILC2s within the murine organism for the entire period of the experimental procedure (**Figure 3E**). In accordance with our *in vitro* data, intranasal administration of rh CCL20 prior to the transfer of fully labeled human ILC2s resulted in a significantly increased pulmonary accumulation of human ILC2s (**Figure 3F**; **Figure S3D**), while comparable numbers of human ILC2s in the blood of both groups confirmed equal numbers of initially transferred cells (**Figure S3**E). Overall, these data strongly suggest CCR6 signaling as potent chemotactic trigger for the directed migration of circulating human ILC2s toward inflammatory tissue sites in the lung.

Pb-Derived Human ILC2s Drive Pulmonary Type-VI Collagen Production

The capacity of pb human ILC2s for pulmonary migration together with the observed association between decreased frequencies of circulating ILC2s and respiratory dysfunction in CF patients strongly implicated a direct impact of these cells on local fibro-inflammatory lung pathology. Indeed, ILC2-transferred recipient mice showed an increased frequency of eosinophils in the BAL and a significant pulmonary accumulation of neutrophils (**Figures 4A,B**). As the induction of airway eosinophilia represents a well-described consequence of lung ILC2 activation (61), these data indicated that transferred human ILC2s stably retained their type-2 immune function after pulmonary migration. Moreover, excessive neutrophilia as well as eosinophil activation represent hallmarks of human CF lung pathology (10, 62), suggesting an orchestrating function of blood-derived pulmonary ILC2s on local CF-associated lung inflammation. Besides the impact of ILC2s on inflammatory cell infiltrates, strikingly, we observed that the inflammation-driven accumulation of lung ILC2s relevantly influenced the composition of the extracellular matrix as well. *Ex vivo* analyses revealed a significantly upregulated protein expression of non-fibrillary type-VI collagen (Col VI) in lungs of ILC2-transferred recipient mice (**Figures 4C,D**), which could not be observed in extrapulmonary tissue (**Figure S4A**) or when human $CD4^{+}$ T cells instead of ILC2s were administered intravenously (**Figure 4E**). This finding was of particular interest, as Col VI critically affects the pulmonary elasticity and its increased expression has been suggested to represent an early event within the pathogenesis of lung fibrosis (63, 64). In contrast, expression levels of fibril-forming type-I collagen (Col I), which represents the most abundant collagen type in lung tissue (65), was not found to be significantly upregulated in the presence of transferred human ILC2s (**Figure 4C**). In accordance with this *in vivo* observation, analyses of cultured primary human lung fibroblasts indicated a significant induction of Col VI expression after exposure to ILC2-conditioned cell culture medium, suggesting ILC2-secreted soluble factors as key mediators of this phenomenon (**Figure 4F**; **Figure S4B**). Furthermore, as an indicator of an advanced pro-fibrotic activation status (66), a marked upregulation of STAT3 phosphorylation was observed (**Figure 4G**), while the expression of Col I remained unaffected

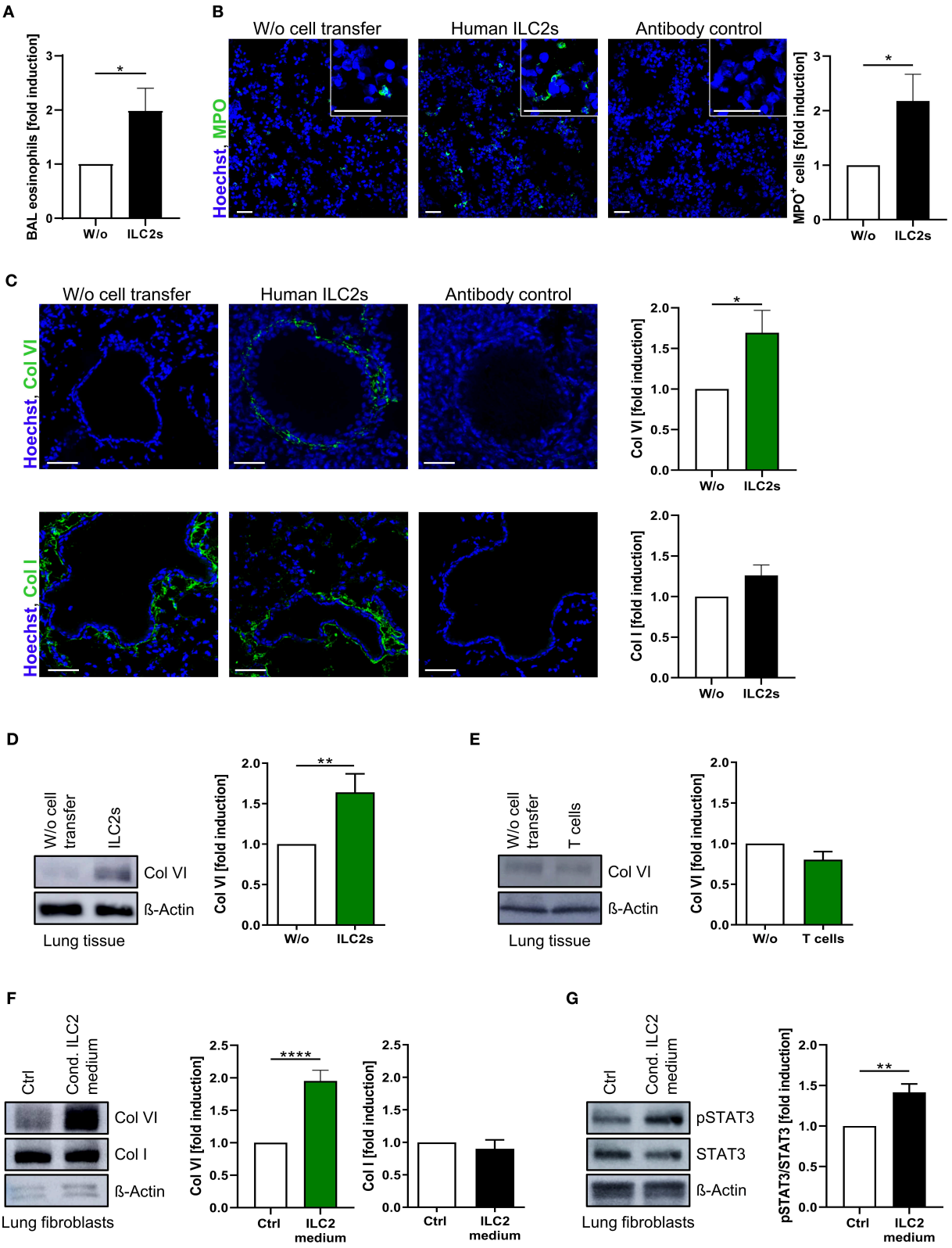

FIGURE 4 | Induction of pulmonary Col VI expression by pb-derived ILC2s *in vivo* and *in vitro*. **(A)** Relative induction of murine BAL eosinophils (flow cytometrically determined as CD11c^{neg} SiglecF^{+} granulocytes) after *i.v.* injection of expanded human ILC2s in papain-treated mice (ctrl and CF ILC2s pooled, $n = 13–21$). **(B)**

(Continued)

FIGURE 4 | Representative images of murine lung tissue stained for MPO 24 h after intravenous ILC2 transfer (scale bars: 50 μm) and corresponding quantification of MPO^+ cells (ctrl and CF ILC2s pooled, $n = 11–15$). **(C)** Representative images of murine lung tissue stained for Col VI ($n = 14–21$) and Col I ($n = 18–24$) 24 h after intravenous transfer of ctrl or CF ILC2s (scale bars: 50 μm) and corresponding quantifications of the peribronchial collagen/Hoechst signal intensities. **(D,E)** Western blot analysis of Col VI expression in lung tissue 24 h after *i.v* transfer of human ILC2s (D, ctrl and CF ILC2s pooled, $n = 19–30$) or $CD4^+$ T cells (E, ctrl $CD4^+$ T cells, $n = 4–7$); representative blots and corresponding quantifications. **(F,G)** Western blot analysis of Col VI ($n = 20–26$), Col I ($n = 8–12$) (F) and pSTAT3 (G; $n = 8–11$) expression in human lung fibroblasts treated for 48 h with 1:5 diluted ILC2-conditioned supernatants derived from *ex vivo* expanding human ctrl ILC2s; representative blots and corresponding quantifications. Fibroblasts stimulated with cytokines used for ILC2 expansion (IL-2, IL-33, IL-25, PHA) served as control. The one-sample *t*-test was applied. $^*p < 0.05$, $^{**}p < 0.01$, $^{****}p < 0.0001$.

(**Figure 4F**). Overall, these findings support the concept that lung-entering ILC2s do not only orchestrate type-2 immune responses, but also secrete soluble mediators that activate Col VI production by pulmonary fibroblasts and induce subsequent tissue remodeling.

Since the immune response underlying CF pathology has been suggested to be intrinsically affected by the inherited *CFTR* mutation (20), growing attention has been payed to the role of immune cells in CF. Therefore, we examined the function of circulating blood ILC2s in CF patients compared to healthy controls. In general, CF ILC2s showed a normal activation status and an unaltered capacity for expansion and lung migration after *ex vivo* stimulation (**Figures 5A–D**). Furthermore, all analyzed type-2 cytokines could clearly be detected in comparable levels in supernatants of restimulated CF and control ILC2s (**Figure 5E**), indicating an unchanged, but potent capacity of CF ILC2s for inflammatory cytokine production. In line with this, ILC2 conditioned supernatants derived from CF patients strongly induced Col VI expression in human lung fibroblasts to a similar extent as supernatants derived from simultaneously stimulated control ILC2s (**Figure 5F**). Thus, the inherited *CFTR* mutation in CF patients did not seem to influence ILC2 activity, leaving them functionally competent and with unaltered effector actions compared to ILC2s derived from healthy subjects.

Additive Effects of ILC2-Derived IL-4 and IL-13 Induce Col VI Production in Fibroblasts

As the observed Col VI-inducing capacity of ILC2s appeared to be driven by their secretome (**Figures 4F**, **5F**), we compared ILC2-conditioned supernatants derived from different ILC2 donors with regard to the concentrations of specific type-2 cytokines and their Col VI-inducing capacity. The performed studies indicated that ILC2-conditioned medium, which potently induced Col VI expression in lung fibroblasts, contained significantly increased levels of IL-4 and IL-13 compared to medium, which failed to induce Col VI expression (**Figure 6A**). In contrast, IL-5 and IL-9 concentrations did not show a similar association with induced levels of Col VI (**Figure 6A**). In accordance with these findings, exposure of lung fibroblasts to recombinant IL-4 or IL-13, in concentrations comparable to those detected in the supernatants of stimulated ILC2s, resulted in a significant induction of Col VI expression (**Figures 6B,C**). Moreover, conditioned ILC2 media substantially induced STAT6 phosphorylation in fibroblasts (**Figure 6D**), which is known to be exclusively activated in response to IL-4Rα signaling (67). Since both, the IL-4 and IL-13 receptor share the IL-4Rα subunit, this finding further indicated that ILC2-mediated Col VI induction is conveyed via IL-4 and IL-13 receptor signaling. Indeed, the extent of STAT6 activation significantly correlated with the intensity of Col VI induction (**Figure 6D**). Finally, the functional involvement of IL-4 and IL-13 in the postulated ILC2 – fibroblast – Col VI axis could be confirmed by the observation that combined antibody-mediated blockade of both cytokines was able to significantly dampen the Col VI-inducing capacity of the ILC2 secretome on pulmonary fibroblasts (**Figure 6E**). In the same experimental setting, selective blockade of either IL-4 or IL-13 alone only resulted in mild and non-significant effects on Col VI expression (**Figure 6E**). Hence, these analyses strongly suggested that additive effects of secreted cytokines, such as IL-4 and IL-13, on local fibroblast activation and Col VI production crucially mediate the tissue modulating function of pulmonary ILC2s.

DISCUSSION

Pulmonary fibrosis and persistent inflammation represent the key drivers of morbidity and mortality among CF patients. So far, the molecular mechanisms of CF lung injury are, however, only incompletely understood. In the present study, using a new humanized mouse model, we uncovered the capacity of circulating human ILC2s to follow a CCL20 gradient, accumulate in inflamed lung tissue and drive local pulmonary Col VI deposition. Moreover, ILC2-derived cytokines and in particular additive effects of IL-4 and IL-13 were identified as mediators of Col VI production by lung fibroblasts. Based on the correlation of reduced numbers of $CCR6^+$ ILC2s in the blood circulation of CF patients with enhanced lung inflammation and the previously described presence of pathologically increased CCL20 levels in CF BAL (15), we postulate the CCR6 - CCL20-driven ILC2 lung homing mechanism to be important in driving CF lung pathology.

In addition to the preferential accumulation of ILC2s at mucosal surfaces, like in the lung, gut and skin (68), it is also well-established that ILC precursors and even mature ILC2s are present in the blood stream of healthy individuals and patients with inflammatory diseases (22, 69–71). However, the question about the role of these circulating ILCs is still insufficiently answered, even though local pulmonary inflammation is well-established to be reflected in altered ILC2 numbers in the peripheral blood circulation (72–74). So far, there have been only very few studies on a functional involvement of human pb ILC2s in systemic immune responses or their capacity to home to specific tissue sites in order to increase the local pool

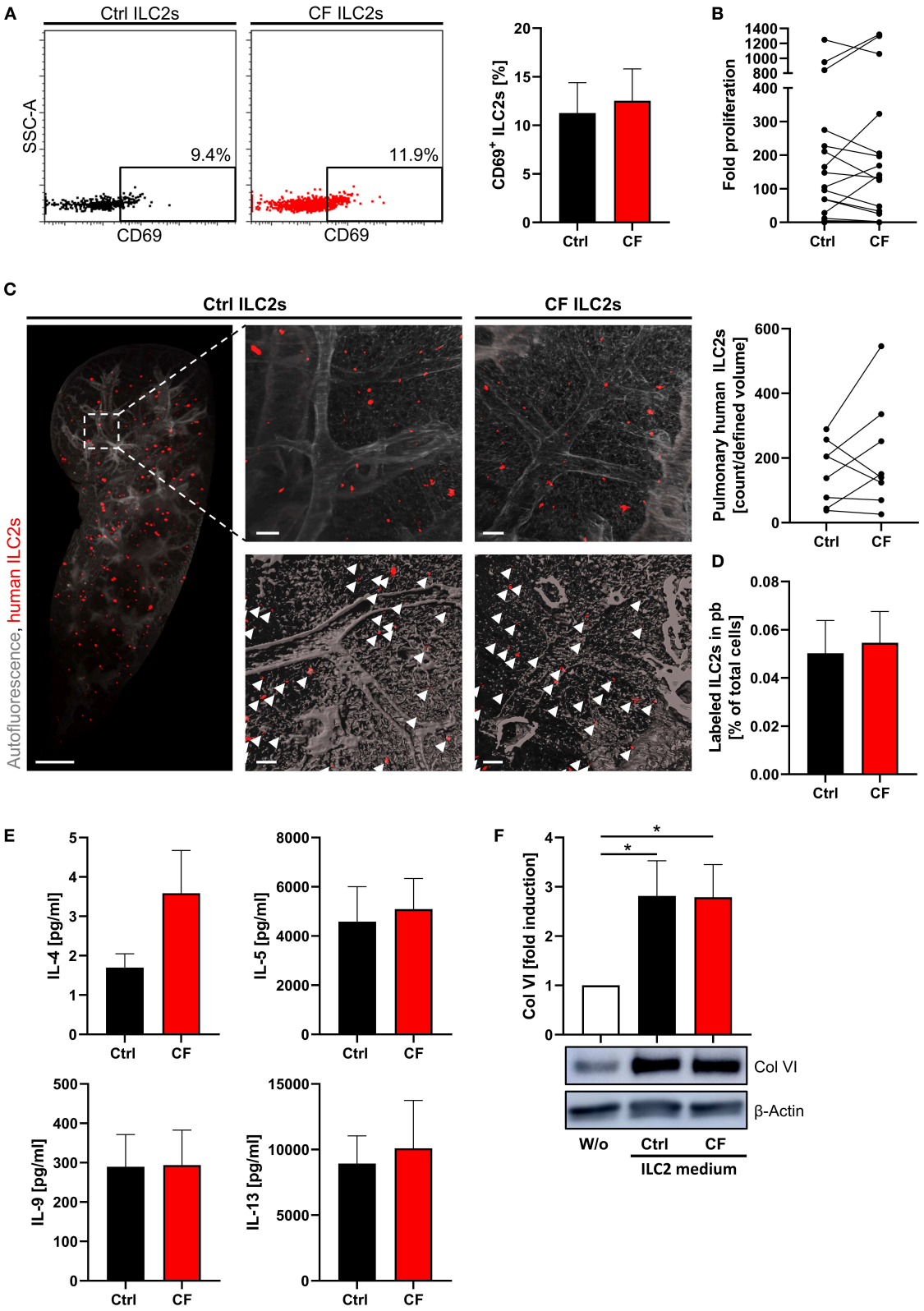

FIGURE 5 | Unaltered potent *ex vivo* expansion, cytokine production and lung homing capacity of human CF ILC2s. **(A)** Percentage of CD69$^+$ pb ILC2s in ctrl and CF subjects (n = 8–9) determined by flow cytometry; representative dot plots and corresponding quantification. **(B)** Fold proliferation of

(Continued)

FIGURE 5 | human pb-derived CF and ctrl ILC2s after 13–15 days of stimulation with PHA, IL-2, IL-33, and IL-25 in the presence of feeder cells ($n = 17$). **(C)** Representative LSFM images (3D reconstruction) of murine lung tissue with papain-induced inflammation 24 h after transfer of expanded labeled human CF or ctrl ILC2s and corresponding quantification of lung accumulated labeled human ILC2s ($n = 8$). Scale bars represent 1,000 μm for the overview image (MIP) and 100 μm for detailed images (top: MIP, bottom: surface mode). Labeled human ILC2s are displayed in red (indicated by arrows). **(D)** Corresponding quantification of labeled ILC2s in murine blood 24 h after *i.v.* transfer ($n = 7$). **(E)** Secreted cytokine levels by CF and ctrl ILC2s upon *ex vivo* stimulation ($n = 8$–16). Expanded and rested human ILC2s (adjusted cell numbers) were restimulated for 3 days with IL-2, IL-33, and IL-25; afterwards supernatants were collected for quantification of indicated cytokines via ELISA. Single outliers were detected by the Grubbs' test. **(F)** Western blot analysis of Col VI expression in human lung fibroblasts treated for 48 h with 1:5 diluted ILC2-conditioned supernatant derived from ctrl subjects and CF patients. Supernatants were harvested after 3 days of restimulating adjusted cell numbers of expanded human ILC2s; representative blot and corresponding quantification ($n = 5$–7). Fibroblasts stimulated with cytokines used for ILC2 restimulation (IL-2, IL-33, IL-25) served as control. The one sample *t*-test was applied. $^*p < 0.05$.

of resident ILC2s (75). Based on the here presented data, we postulate that in CF, $CCR6^+$ ILC2s are chemotactically attracted from the peripheral blood into inflamed pulmonary tissue sites, where they influence local disease progression. Using parabiotic mouse models, murine ILC2s have initially been described to be mainly tissue-resident under acute inflammatory states, whereas their homing capacity has already been indicated under chronic inflammatory conditions (76). The latter seems to be consistent with the recently described infection- or inflammation-triggered inter-organ migration of gut resident ILC2s via S1P-mediated chemotaxis and the arising idea of a milieu-dependent local recruitment and tissue-specific ILC-poiesis (51, 69, 75). In addition to S1P-driven chemotaxis, the CRTH2 ligand PGD2, the CCR4 ligand CCL22 and IL-33 have been described as potent mediators of chemotactic ILC2 attraction (31, 60, 77, 78). Our *in vitro* and *in vivo* data now additionally identified the chemotactic potential of CCL20 on human ILC2s. As IL-33 and CCL20 are both upregulated in the lung of CF patients (15, 44, 79), these findings suggest a joint chemotactic ILC2 recruitment into the inflamed lung in states of exacerbated CF. Taking into account that CCL20 expression can also be upregulated in other organs under inflammatory conditions (80, 81) it cannot be completely excluded that $CCR6^+$ ILC2s might partly also migrate to other CF-affected organs besides the lung. However, as the described 90-fold induction of CCL20 protein levels in the BAL of CF patients compared to healthy volunteers nearly doubled a 47-fold upregulation of CCL20 mRNA expression in the gut of patients suffering from ulcerative colitis, (15, 80) this indicates a particular relevance of the CCL20 - CCR6 axis for lung homing in CF. Moreover, a significant association between reduced blood $CCR6^+$ ILC2 counts and increased disease activity was observed in CF patients but in none of the other analyzed fibro-inflammatory diseases affecting the gut or joints, further strengthening an organ- and CF-specific role of $CCR6^+$ ILC2s. Besides the increased presence of chemotactic triggers in CF airways, the intrinsic lung homing capacity of CF ILC2s appeared to be independent of the inherited *CFTR* mutation. Based on the here identified chemotactic potential of CCL20 on human ILC2s, we suggest that decreased numbers of $CCR6^+$ ILC2s in the peripheral blood of CF patients reflect the enhanced attraction of these cells to the site of inflammation. Of course, the experimental validation of this concept in humans was limited to some extend by the fact that we were unable to directly compare and correlate results from blood-derived circulating ILC2s with the number and activation profile of ILC2s in lung tissue of the same patients due to the lack of corresponding lung tissue or BAL samples. However, in the context of aspirin-exacerbated respiratory disease as well as *Mycobacterium tuberculosis*-infected lungs, published data indicated that the local accumulation of ILC2s in mucosal tissue was associated with a parallel reduction of blood ILC2 percentages (72, 82). A similar impact of tissue-migrating immune cells on the number of their circulating counterparts has also been postulated for T cells in the context of IBD (83). Moreover, the *in vivo* ability of human blood ILC2s to accumulate in the inflamed lung tissue upon CCL20-mediated chemoattraction was proven in a newly established humanized mouse model. In the light of described inter-species differences between murine and human ILC2s (70, 84, 85) this humanized model of lung inflammation represented a clear advantage over classic mouse models and allowed us to directly analyze patient-derived primary human ILC2s under inflammatory *in vivo* conditions. Of particular relevance for the here described findings, there exist, to our knowledge, no published data on a potential CCR6 expression of circulating murine ILC2s, while in tissue-infiltrating murine helper ILCs, CCR6 expression seemed to be mainly restricted to ILC3s (86). Together with the observation that human and murine ILC2s differ in the expression profile of the prostaglandin D2 receptor CRTH2 (84), this potentially implicates that the migratory behavior of ILC2s is differentially regulated between both species. Collectively, the results acquired in the humanized *in vivo* model together with our human association data pointed to a relevant CCL20-triggered lung recruitment of systemic human ILC2s under the distinct pathologic conditions of CF.

Generally, neutrophilia and an IL-17 signature have been described as common hallmarks of CF-underlying pathomechanisms (58), although several studied also pointed to a relevant, but less acknowledged, skewing of immune responses towards type-2 mediated effects (87). Of particular interest in this context, a recently published study postulated the preferential transdifferentiation of ILC2s into IL-17 secreting ILC3-like cells in nasal polyps of CF patients (53). However, our own *in vivo* data demonstrated the retention of important type-2 functions of pb-derived ILC2s in inflamed lung tissue, indicated by a potent induction of lung eosinophilia, although we cannot exclude that transdifferentiation into ILC3-like cells might potentially occur at a later time point. Regarding the involvement of tissue-infiltrating neutrophils in the pathogenesis of CF lung disease, our observation that intravenously transferred human ILC2s resulted in increased pulmonary neutrophil accumulation in the

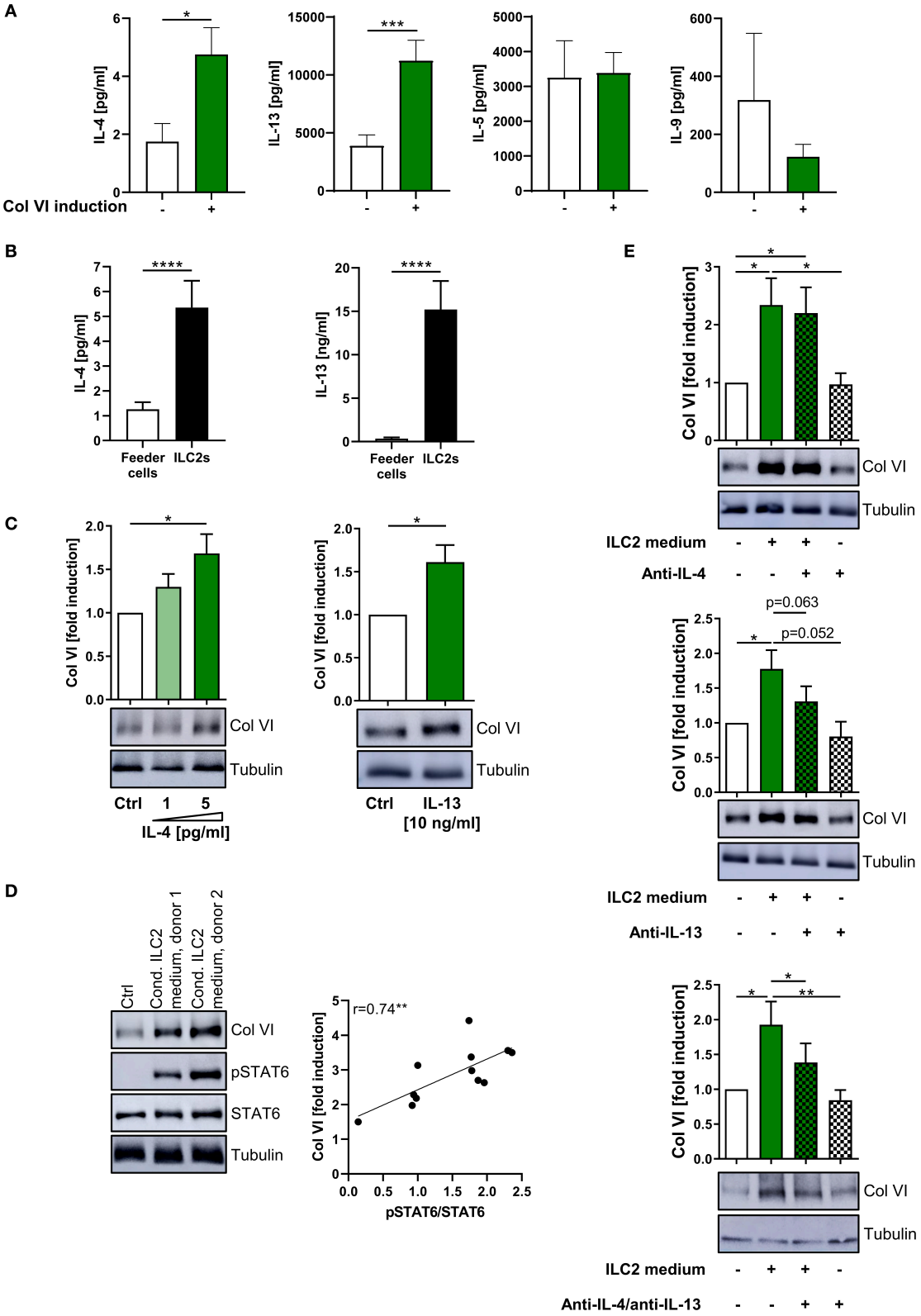

FIGURE 6 | Additive effect of ILC2-derived IL-4 and IL-13 on pulmonary Col VI induction. **(A)** ILC2 conditioned supernatants were grouped according to their potency to induce Col VI expression in human lung fibroblasts (based on Western blot analyses) and were analyzed for concentrations of IL-4 ($n = 5$–32), IL-13 ($n = 6$–30), IL-5

(Continued)

FIGURE 6 | ($n = 6$–31), and IL-9 ($n = 4$–21) via ELISA. The included raw data were partly also used in **Figures 4F**, **5E**. Single outliers were detected by the Grubbs' test. The unpaired Student's *t*-test with Welch correction was performed. **(B)** IL-4 ($n = 12$–33) and IL-13 ($n = 7$–25) levels secreted by *ex vivo* expanding human ILC2s as determined by ELISA. The Mann-Whitney test was applied. **(C)** Representative Western blot analysis of Col VI expression in human lung fibroblasts stimulated with rh IL-4 ($n = 5$) and rh IL-13 ($n = 10$) and corresponding quantifications. The one-sample *t*-test was performed. **(D)** Western blot analysis of Col VI and pSTAT6 expression in human lung fibroblasts stimulated for 48 h with 1:5 diluted conditioned ILC2 supernatants collected from *ex vivo* expanding human ILC2s (d11–d13) (representative for $n = 12$). Fibroblasts stimulated with IL-2, IL-33, IL-25, and PHA in 1:5 diluted Yssel's medium served as control. Corresponding correlation of quantified pSTAT6/STAT6 signals and fold Col VI induction. The Pearson correlation coefficient was calculated. **(E)** Representative Western blot analysis of Col VI expression in human lung fibroblasts stimulated with conditioned ILC2 supernatants as well as anti-IL-4 (10 ng/ml) and anti-IL-13 (20 ng/ml) as indicated ($n = 6$–9) and corresponding quantifications. The paired two-tailed Student's *t*-test was applied. $^{*}p < 0.05$, $^{**}p < 0.01$, $^{***}p < 0.001$, $^{****}p < 0.0001$.

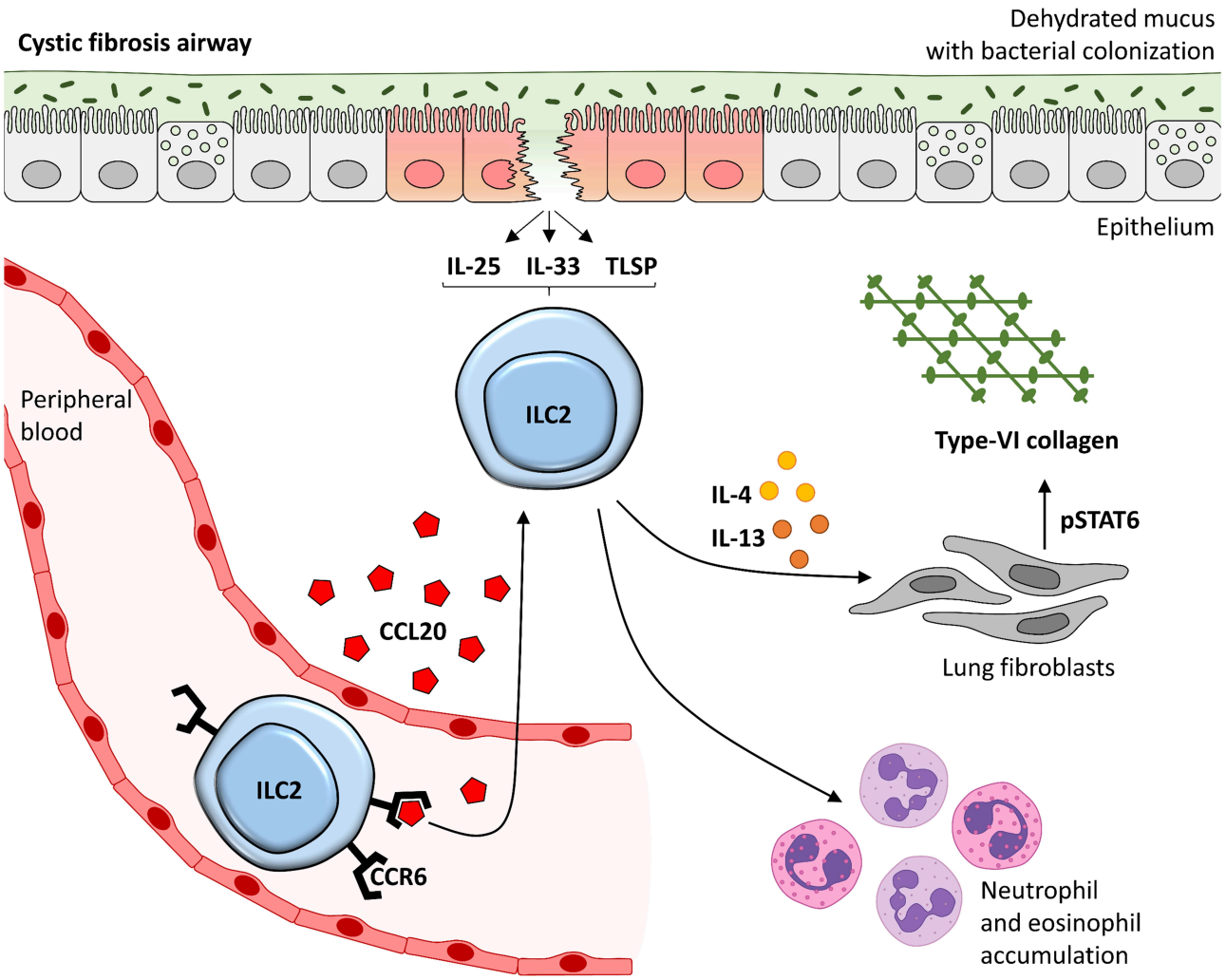

FIGURE 7 | Suggested model of the CCL20 - ILC2 – IL-4/IL-13 – Col VI axis in lung disease of CF patients. CCR6 expressing ILC2s in the peripheral blood stream are chemoattracted into the inflamed lung tissue of CF patients in a CCL20-dependent manner. Locally accumulated and activated pb-derived ILC2s likely induce type-2 mediated lung inflammation, including neutrophils and eosinophil accumulation, but also pulmonary Col VI expression in lung fibroblasts. This is mediated via the secreted mediators IL-4 and IL-13 in particular which signal via STAT6. This might finally lead to local tissue remodeling potentially driving disease progression in CF patients. TSLP, thymic stromal lymphopoietin.

humanized mouse model, might suggest an active contribution of ILC2s to the CF-related neutrophil recruitment into chronically inflamed pulmonary tissues sites. Thus, future studies are needed to further elucidate the molecular mechanisms underlying the ILC2-mediated numeric regulation of pulmonary neutrophils and their potential interference with the classically described IL-17-driven chemotaxis of neutrophils in CF patients (88).

Again by using the novel humanized mouse model of ILC2 homing to the inflamed lung, we noted that the pulmonary accumulation of human ILC2s drives Col VI production *in*

vivo. Indeed, pulmonary ILC2s are preferentially located in collagen-rich areas close to the airway epithelium (27, 29) immediately subjacent to Col VI (63, 89, 90) that functions as an important anchoring element linked to the basement membrane. Moreover, expression of Col VI is known to be increased during lung fibrosis (63), and subepithelial fibrosis and thickening of the reticular basement membrane have been described as important morphological alterations in CF lungs (91, 92). These findings support the pathogenic relevance of the described interplay between accumulated ILC2s, fibroblasts and Col VI for pulmonary tissue remodeling in chronic lung manifestations of CF. In line with the general concept that the pro-fibrotic function of activated ILC2s is driven by their capacity to release high amounts of type-2 cytokines (35, 42), it has recently been postulated that ILC2-derived IL-9 might support pulmonary inflammation in CF patients via activation of mast cells and subsequent release of TGF-β (14). However, we did not observe a significant association of increased IL-9 secretion and the capacity of human ILC2s to induce Col VI expression in human lung fibroblasts. Thus, our findings strongly suggest that other cytokines or mediators also contribute to the ILC2-mediated pathologic lung tissue remodeling in CF patients. Accordingly, we identified the two closely related cytokines IL-4 and IL-13, that both signal via downstream activation of STAT6 and STAT3 (67, 93), as key mediators of the ILC2-induced Col VI production. Notably, the here postulated functional relation between ILC2-triggered pulmonary tissue remodeling and the quality of CF lung disease is in accordance with the observation that increased type-2 cytokine levels in the BAL of CF patients significantly correlated with pathologic lung tissue alterations as assessed by high-resolution computed tomography (46). Overall, our data thus provide evidence for a crucial involvement of pb-derived human ILC2s in the pathogenesis of CF (**Figure 7**). In addition, the here described ILC2 – IL-4/IL-13 – Col VI axis elucidates a new aspect of their tissue modulating capacity, while our findings on CCL20-driven ILC2 chemotaxis highlight the relevance of the systemic ILC2 pool for the clinical course of CF. Although future studies are needed to confirm the strict CCR6-dependency of CCL20-triggered ILC2 lung homing under CF-relevant *in vivo* conditions, our results open new therapeutic avenues for the treatment of CF or other fibro-inflammatory lung diseases, potentially allowing a numeric regulation of local ILC2 pools in the inflamed lung tissue.

DATA AVAILABILITY STATEMENT

The datasets generated and analyzed during the current study are available from the corresponding author on reasonable request.

ETHICS STATEMENT

The studies involving human participants were reviewed and approved by Local ethical committee and the institutional review board of the University of Erlangen-Nuremberg, Germany. The patients/participants provided their written informed consent to participate in this study. The animal study was reviewed and approved by Government of Lower Franconia, Germany.

AUTHOR CONTRIBUTIONS

AS-K, VG, MD, and LK performed the experiments. AS-K, KH, RA, SZi, FF, SZu, RL-P, CN, AR, AK, AG, ES, SW, MN, and IA provided clinical samples, protocols, reagents, or designed experiments. AS-K, MN, and IA analyzed and interpreted the data, and drafted the manuscript. All authors critically revised the manuscript for important intellectual content.

FUNDING

The here described study was supported by grants from the DFG; German Research Foundation (TRR241: A07; CRC1181: A08, B02, Z02).

ACKNOWLEDGMENTS

The authors thank Stefan Jungbauer, Dirk Schramm, Simon Grewendorf and Volker Melichar for their support in the acquisition of blood samples. Moreover, the authors are thankful for excellent support by the FACS Core Unit and the Optical Imaging Center (OICE) of the University Hospital of Erlangen.

SUPPLEMENTARY MATERIAL

The Supplementary Material for this article can be found online at: https://www.frontiersin.org/articles/10.3389/fimmu.2020.00691/full#supplementary-material

REFERENCES

1. Salvatore D, Buzzetti R, Mastella G. Update of literature from cystic fibrosis registries 2012-2015. Part. 6: Epidemiology, nutrition and complications. *Pediatr Pulmonol.* (2017) 52:390–98. doi: 10.1002/ppul.23611
2. Bhagirath AY, Li Y, Somayajula D, Dadashi M, Badr S, Duan K. Cystic fibrosis lung environment and Pseudomonas aeruginosa infection. *BMC Pulm Med.* (2016) 16:174. doi: 10.1186/s12890-016-0339-5
3. Cohen TS, Prince A. Cystic fibrosis: a mucosal immunodeficiency syndrome. *Nat Med.* (2012) 18:509–19. doi: 10.1038/nm.2715
4. Elborn JS. Cystic fibrosis. *Lancet.* (2016) 388:2519–31. doi: 10.1016/S0140-6736(16)00576-6
5. Lima AN, Faria AC, Lopes AJ, Jansen JM, Melo PL. Forced oscillations and respiratory system modeling in adults with cystic fibrosis. *Biomed Eng Online.* (2015) 14:11. doi: 10.1186/s12938-015-0007-7
6. Sly PD, Wainwright CE. Diagnosis and early life risk factors for bronchiectasis in cystic fibrosis: a review. *Expert Rev Respir Med.* (2016) 10:1003–10. doi: 10.1080/17476348.2016.1204915
7. Harris WT, Kelly DR, Zhou Y, Wang D, MacEwen M, Hagood JS, et al. Myofibroblast differentiation and enhanced TGF-B signaling in cystic fibrosis lung disease. *PLoS ONE.* (2013) 8:e70196. doi: 10.1371/journal.pone.0070196

8. Boyton RJ, Altmann DM. Bronchiectasis: current concepts in pathogenesis, immunology, and microbiology. *Annu Rev Pathol*. (2016) 11:523–54. doi: 10.1146/annurev-pathol-012615-044344
9. Tan HL, Regamey N, Brown S, Bush A, Lloyd CM, Davies JC. The Th17 pathway in cystic fibrosis lung disease. *Am J Respir Crit Care Med*. (2011) 184:252–8. doi: 10.1164/rccm.201102-0236OC
10. Cockx M, Gouwy M, Van Damme J, Struyf S. Chemoattractants and cytokines in primary ciliary dyskinesia and cystic fibrosis: key players in chronic respiratory diseases. *Cell Mol Immunol*. (2018) 15:312–23. doi: 10.1038/cmi.2017.118
11. Bruscia EM, Bonfield TL. Innate and adaptive immunity in cystic fibrosis. *Clin Chest Med*. (2018) 37:17–29. doi: 10.1016/j.ccm.2015.11.010
12. Roesch EA, Nichols DP, Chmiel JF. Inflammation in cystic fibrosis: an update. *Pediatr Pulmonol*. (2018) 53:S30–50. doi: 10.1002/ppul.24129
13. Tiringer K, Treis A, Kanolzer S, Witt C, Ghanim B, Gruber S, et al. Differential expression of IL-33 and HMGB1 in the lungs of stable cystic fibrosis patients. *Eur Respir J*. (2014) 44:802–5. doi: 10.1183/09031936.00046614
14. Moretti S, Renga G, Oikonomou V, Galosi C, Pariano M, Iannitti RG, et al. A mast cell-ILC2-Th9 pathway promotes lung inflammation in cystic fibrosis. *Nat Commun*. (2017) 8:14017. doi: 10.1038/ncomms14017
15. Starner TD, Barker CK, Jia HP, Kang Y, McCray PB Jr. CCL20 is an inducible product of human airway epithelia with innate immune properties. *Am J Respir Cell Mol Biol*. (2003) 29:627–33. doi: 10.1165/rcmb.2002-0272OC
16. Brodlie M, McKean MC, Johnson GE, Anderson AE, Hilkens CM, Fisher AJ, et al. Raised interleukin-17 is immunolocalised to neutrophils in cystic fibrosis lung disease. *Eur Respir J*. (2011) 37:1378–85. doi: 10.1183/09031936.00067110
17. Garratt LW, Sutanto EN, Ling KM, Looi K, Iosifidis T, Martinovich KM, et al. Matrix metalloproteinase activation by free neutrophil elastase contributes to bronchiectasis progression in early cystic fibrosis. *Eur Respir J*. (2015) 46:384–94. doi: 10.1183/09031936.00212114
18. Sepper R, Konttinen YT, Ding Y, Takagi M, Sorsa T. Human neutrophil collagenase (MMP-8), identified in bronchiectasis BAL fluid, correlates with severity of disease. *Chest*. (1995) 107:1641–7. doi: 10.1378/chest.107.6.1641
19. Sly PD, Gangell CL, Chen L, Ware RS, Ranganathan S, Mott LS, M, et al. Risk factors for bronchiectasis in children with cystic fibrosis. *N Engl J Med*. (2015) 368:1963–70. doi: 10.1056/NEJMoa1301725
20. Rao S, Grigg J. New insights into pulmonary inflammation in cystic fibrosis. *Arch Dis Child*. (2006) 91:786–8. doi: 10.1136/adc.2004.069419
21. Diefenbach A, Colonna M, Koyasu S. Development, differentiation, and diversity of innate lymphoid cells. *Immunity*. (2014) 41:354–65. doi: 10.1016/j.immuni.2014.09.005
22. Wohlfahrt T, Usherenko S, Englbrecht M, Dees C, Weber S, Beyer C, et al. Type. 2 innate lymphoid cell counts are increased in patients with systemic sclerosis and correlate with the extent of fibrosis. *Ann Rheum Dis*. (2016) 75:623–6. doi: 10.1136/annrheumdis-2015-207388
23. Soare A, Weber S, Maul L, Rauber S, Gheorghiu AM, Luber M, et al. Cutting edge: homeostasis of innate lymphoid cells is imbalanced in psoriatic arthritis. *J Immunol*. (2015) 200:1249–54. doi: 10.4049/jimmunol.1700596
24. Donovan C, Starkey MR, Kim RY, Rana BMJ, Barlow JL, Jones B, et al. Roles for T/B lymphocytes and ILC2s in experimental chronic obstructive pulmonary disease. *J Leukoc Biol*. (2019) 105:143–50. doi: 10.1002/JLB.3AB0518-178R
25. Wojno ED, Monticelli LA, Tran SV, Alenghat T, Osborne LC, Thome JJ, et al. The prostaglandin D(2) receptor CRTH2 regulates accumulation of group. 2 innate lymphoid cells in the inflamed lung. *Mucosal Immunol*. (2015) 8:1313–23. doi: 10.1038/mi.2015.21
26. Hoyler T, Klose CS, Souabni A, Turqueti-Neves A, Pfeifer D, Rawlins EL, et al. The transcription factor GATA-3 controls cell fate and maintenance of type. 2 innate lymphoid cells. *Immunity*. (2012) 37:634–48. doi: 10.1016/j.immuni.2012.06.020
27. Mindt BC, Fritz JH, Duerr CU. Group 2 innate lymphoid cells in pulmonary immunity and tissue homeostasis. *Front Immunol*. (2015) 9:840. doi: 10.3389/fimmu.2018.00840
28. De Grove KC, Provoost S, Verhamme FM, Bracke KR, Joos GF, Maes T, et al. Characterization and quantification of innate lymphoid cell subsets in human lung. *PLoS ONE*. (2016) 11:e0145961. doi: 10.1371/journal.pone.0145961
29. van der Ploeg EK, Carreras Mascaro A, Huylebroeck D, Hendriks RW, Stadhouders R. Group 2 innate lymphoid cells in human respiratory disorders. *J Innate Immun*. (2020) 12:47–62. doi: 10.1159/000496212
30. Bal SM, Bernink JH, Nagasawa M, Groot J, Shikhagaie MM, Golebski K, et al. IL-1β, IL-4 and IL-12 control the fate of group. 2 innate lymphoid cells in human airway inflammation in the lungs. *Nat Immunol*. (2016) 17:636–45. doi: 10.1038/ni.3444
31. Xue L Salimi M, Panse I, Mjösberg JM, McKenzie ANJ, Spits H, et al. Prostaglandin D2 activates group. 2 innate lymphoid cells through chemoattractant receptor-homologous molecule expressed on TH2 cells. *J Allergy Clin Immunol*. (2014) 133:1184–94. doi: 10.1016/j.jaci.2013.10.056
32. Drake LY, Kita H. IL-33: biological properties, functions, and roles in airway disease. *Immunol Rev*. (2017) 278:173–84. doi: 10.1111/imr.12552
33. Ricardo-Gonzalez RR, Van Dyken SJ, Schneider C, Lee J, Nussbaum JC, Liang HE, et al. Tissue signals imprint ILC2 identity with anticipatory function. *Nat Immunol*. (2018) 19:1093–99 doi: 10.1038/s41590-018-0201-4
34. Maric J, Ravindran A, Mazzurana L, Van Acker A, Rao A, Kokkinou E, et al. Cytokine-induced endogenous production of prostaglandin D2 is essential for human group. 2 innate lymphoid cell activation. *J Allergy Clin Immunol*. (2019) 143:2202–14.e5 doi: 10.1016/j.jaci.2018.10.069
35. Hams E, Armstrong ME, Barlow JL, Saunders SP, Schwartz C, Cooke G, et al. IL-25 and type. 2 innate lymphoid cells induce pulmonary fibrosis. *Proc Natl Acad Sci USA*. (2014) 111:367–72. doi: 10.1073/pnas.1315854111
36. Stehle C, Hernandez DC, Romagnani C. Innate lymphoid cells in lung infection and immunity. *Immunol Rev*. (2018) 286:102–19. doi: 10.1111/imr.12712
37. Starkey MR, McKenzie AN, Belz GT, Hansbro PM. Pulmonary group 2 innate lymphoid cells: surprises and challenges. *Mucosal Immunol*. (2019) 12:299–11 doi: 10.1038/s41385-018-0130-4
38. Monticelli LA, Sonnenberg GF, Abt MC, Alenghat T, Ziegler CG, Doering TA, et al. Innate lymphoid cells promote lung-tissue homeostasis after infection with influenza virus. *Nat Immunol*. (2011) 12:1045–54. doi: 10.1038/ni.2131
39. Halim TYF, Rana BMJ, Walker JA, Kerscher B, Knolle MD, Jolin HE, et al. Tissue-restricted adaptive type. 2 immunity is orchestrated by expression of the costimulatory molecule OX40L on group 2 innate lymphoid cells. *Immunity*. (2018) 48:1195–207. e1196. doi: 10.1016/j.immuni.2018.05.003
40. Pelly VS, Kannan Y, Coomes SM, Entwistle LJ, Rückerl D, Seddon B, et al. IL-4-producing ILC2s are required for the differentiation of TH2 cells following Heligmosomoides polygyrus infection. *Mucosal Immunol*. (2016) 9:1407–17. doi: 10.1038/mi.2016.4
41. Mikami Y, Takada Y, Hagihara Y, Kanai T. Innate lymphoid cells in organ fibrosis. *Cytokine Growth Factor Rev*. (2018) 42:27–36. doi: 10.1016/j.cytogfr.2018.07.002
42. Kindermann M, Knipfer L, Atreya I, Wirtz S. ILC2s in infectious diseases and organ-specific fibrosis. *Semin Immunopathol*. (2018) 40:379–92. doi: 10.1007/s00281-018-0677-x
43. Chen K, Campfield BT, Wenzel SE, McAleer JP, Kreindler JL, Kurland G, et al. Antiinflammatory effects of bromodomain and extraterminal domain inhibition in cystic fibrosis lung inflammation. *JCI Insight*. (2016) 1:e87168. doi: 10.1172/jci.insight.87168
44. Roussel L, Farias R, Rousseau S. IL-33 is expressed in epithelia from patients with cystic fibrosis and potentiates neutrophil recruitment. *J Allergy Clin Immunol*. (2013) 131:913–16. doi: 10.1016/j.jaci.2012.10.019
45. Moser C, Jensen PO, Kobayashi O, Hougen HP, Song Z, Rygaard J, et al. The immune response to chronic Pseudomonas aeruginosa lung infection in cystic fibrosis patients is predominantly of the Th2 type. *APMIS*. (2002) 108:329–35. doi: 10.1034/j.1600-0463.2000.d01-64.x
46. Tiringer K, Treis A, Fucik P, Gona M, Gruber S, Renner S, et al. A Th17- and Th2-skewed cytokine profile in cystic fibrosis lungs represents a potential risk factor for Pseudomonas aeruginosa infection. *Am J Respir Crit Care Med*. (2013) 187:621–9. doi: 10.1164/rccm.201206-1150OC
47. Kim HY, Umetsu DT, Dekruyff RH. Innate lymphoid cells in asthma: will they take your breath away? *Eur J Immunol*. (2016) 46:795–806. doi: 10.1002/eji.201444557
48. Nielsen AO, Qayum S, Bouchelouche PN, Laursen LC, Dahl R, Dahl M, et al. Risk of asthma in heterozygous carriers for cystic fibrosis: a meta-analysis. *J Cyst Fibros*. (2016) 15:563–7. doi: 10.1016/j.jcf.2016.06.001

49. Schulz-Kuhnt A, Zundler S, Grüneboom A, Neufert C, Wirtz S, Neurath MF, et al. Advanced imaging of lung homing human lymphocytes in an experimental *in vivo* model of allergic inflammation based on light-sheet microscopy. *J Vis Exp JoVE*. (2019) 146:e59043. doi: 10.3791/59043
50. Klingberg A, Hasenberg A, Ludwig-Portugall I, Medyukhina A, Männ L, Brenzel A, et al. Fully automated evaluation of total glomerular number and capillary tuft size in nephritic kidneys using lightsheet microscopy. *J Am Soc Nephrol: JASN*. (2017) 28:452–9. doi: 10.1681/ASN.2016020232
51. Huang Y, Mao K, Chen X, Sun MA, Kawabe T, Li W, et al. S1P-dependent interorgan trafficking of group. 2 innate lymphoid cells supports host defense. *Science*. (2018) 359:114–19. doi: 10.1126/science.aam5809
52. Germain RN, Huang Y. ILC2s - resident lymphocytes pre-adapted to a specific tissue or migratory effectors that adapt to where they move? *Curr Opin Immunol*. (2018) 56:76–81. doi: 10.1016/j.coi.2018.11.001
53. Golebski K, Ros XR, Nagasawa M, van Tol S, Heesters BA, Aglmous H, et al. IL-1β, IL-23, and TGF-beta drive plasticity of human ILC2s towards IL-17-producing ILCs in nasal inflammation. *Nat Commun*. (2019) 10:2162. doi: 10.1038/s41467-019-09883-7
54. Mikhak Z, Strassner JP, Luster AD. Lung dendritic cells imprint T cell lung homing and promote lung immunity through the chemokine receptor CCR4. *J Exp Med*. (2013) 210:1855–69. doi: 10.1084/jem.20130091
55. Mavigner M, Cazabat M, Dubois M, L'Faqihi FE, Requena M, Pasquier C, et al. Gut-associated lymphoid tissue-primed CD4+ T cells display CCR9-dependent and -independent homing to the small intestine. *Blood*. (2012) 107:3447–54. doi: 10.1182/blood-2005-07-2860
56. Roan F, Stoklasek TA, Whalen E, Molitor JA, Bluestone JA, Buckner JH, et al. CD4+ Group. 1 innate lymphoid cells (ILC) form a functionally distinct ILC subset that is increased in systemic sclerosis. *J Immunol*. (2016) 196:2051–62. doi: 10.4049/jimmunol.1501491
57. Cephus JY, Stier MT, Fuseini H, Yung JA, Toki S, Bloodworth MH, et al. Testosterone attenuates group. 2 innate lymphoid cell-mediated airway inflammation. *Cell Rep*. (2017) 21:2487–99. doi: 10.1016/j.celrep.2017.10.110
58. Dubin PJ, McAllister F, Kolls JK. Is cystic fibrosis a TH17 disease? *Inflamm Res*. (2007) 56:221–7. doi: 10.1007/s00011-007-6187-2
59. Yamazaki T, Yang XO, Chung Y, Fukunaga A, Nurieva R, Pappu B, et al. CCR6 regulates the migration of inflammatory and regulatory T cells. *J Immunol*. (2008) 181:8391–401. doi: 10.4049/jimmunol.181.12.8391
60. Puttur F, Denney L, Gregory LG, Vuononvirta J, Oliver R, Entwistle LJ, et al. Pulmonary environmental cues drive group. 2 innate lymphoid cell dynamics in mice and humans. *Sci Immunol*. (2019) 4:eaav7638. doi: 10.1126/sciimmunol.aav7638
61. Morita H, Arae K, Unno H, Miyauchi K, Toyama S, Nambu A, et al. An interleukin-33-mast cell-interleukin-2 axis suppresses papain-induced allergic inflammation by promoting regulatory T cell numbers. *Immunity*. (2015) 43:175–86. doi: 10.1016/j.immuni.2015.06.021
62. Koller DY, Gotz M, Eichler I, Urbanek R. Eosinophilic activation in cystic fibrosis. *Thorax*. (1994) 49:496–9. doi: 10.1136/thx.49.5.496
63. Specks U, Nerlich A, Colby TV, Wiest I, Timpl R. Increased expression of type VI collagen in lung fibrosis. *Am J Respir Crit Care Med*. (1995) 151:1956–64. doi: 10.1164/ajrccm.151.6.7767545
64. Dassah M, Almeida D, Hahn R, Bonaldo P, Worgall S, Hajjar KA, et al. Annexin A2 mediates secretion of collagen VI, pulmonary elasticity and apoptosis of bronchial epithelial cells. *J Cell Sci*. (2014) 127:828–44. doi: 10.1242/jcs.137802
65. Goldstein RH. Control of type I collagen formation in the lung. *Am J Physiol*. (1991) 261:L29–40. doi: 10.1152/ajplung.1991.261.2.L29
66. Chakraborty D, Šumová B, Mallano T, Chen CW, Distler A, Bergmann C, et al. Activation of STAT3 integrates common profibrotic pathways to promote fibroblast activation and tissue fibrosis. *Nat Commun*. (2017) 8:1130. doi: 10.1038/s41467-017-01236-6
67. Nelms K, Keegan AD, Zamorano J, Ryan JJ, Paul WE. The IL-4 receptor: signaling mechanisms and biologic functions. *Annu Rev Immunol*. (1999) 17:701–38. doi: 10.1146/annurev.immunol.17.1.701
68. Mjosberg J, Eidsmo L. Update on innate lymphoid cells in atopic and non-atopic inflammation in the airways and skin. *Clin Exp Allergy*. (2014) 44:1033–43. doi: 10.1111/cea.12353
69. Lim AI, Li Y, Lopez-Lastra S, Stadhouders R, Paul F, Casrouge A, et al. Systemic human ILC precursors provide a substrate for tissue ILC differentiation. *Cell*. (2017) 168:1086–100.e1010. doi: 10.1016/j.cell.2017.02.021
70. Hochdorfer T, Winkler C, Pardali K, Mjosberg J. Expression of c-Kit discriminates between two functionally distinct subsets of human type 2 innate lymphoid cells. *Eur J Immunol*. (2019) 49:884–93 doi: 10.1002/eji.201848006
71. Gwela A, Siddhanathi P, Chapman RW, Travis S, Powrie F, Arancibia-Cárcamo CV, et al. Th1 and innate lymphoid cells accumulate in primary sclerosing cholangitis-associated inflammatory bowel disease. *J Crohn's Colitis*. (2017) 11:1124–34. doi: 10.1093/ecco-jcc/jjx050
72. Eastman JJ, Cavagnero KJ, Deconde AS, Kim AS, Karta MR, Broide DH, et al. Group. 2 innate lymphoid cells are recruited to the nasal mucosa in patients with aspirin-exacerbated respiratory disease. *J Allergy Clin Immunol*. (2017) 140:101–8.e103. doi: 10.1016/j.jaci.2016.11.023
73. Smith SG, Chen R, Kjarsgaard M, Huang C, Oliveria JP, O'Byrne PM, et al. Increased numbers of activated group. 2 innate lymphoid cells in the airways of patients with severe asthma and persistent airway eosinophilia. *J Allergy Clin Immunol*. (2016) 137:75–86.e78. doi: 10.1016/j.jaci.2015.05.037
74. Bartemes KR, Kephart GM, Fox SJ, Kita H. Enhanced innate type 2 immune response in peripheral blood from patients with asthma. *J Allergy Clin Immunol*. (2014) 134:671–8.e674. doi: 10.1016/j.jaci.2014.06.024
75. Lim AI, Di Santo JP. ILC-poiesis: ensuring tissue ILC differentiation at the right place and time. *Eur J Immunol*. (2019) 49:11–18. doi: 10.1002/eji.201747294
76. Gasteiger G, Fan X, Dikiy S, Lee SY, Rudensky AY. Tissue residency of innate lymphoid cells in lymphoid and nonlymphoid organs. *Science*. (2015) 350:981–5. doi: 10.1126/science.aac9593
77. Salimi M, Barlow JL, Saunders SP, Xue L, Gutowska-Owsiak D, Wang X, et al. A role for IL-25 and IL-33-driven type-2 innate lymphoid cells in atopic dermatitis. *J Exp Med*. (2013) 210:2939–50. doi: 10.1084/jem.20130351
78. Knipfer L, Schulz-Kuhnt A, Kindermann M, Greif V, Symowski C, Voehringer D, et al. A CCL1/CCR8-dependent feed-forward mechanism drives ILC2 functions in type 2-mediated inflammation. *J Exp Med*. (2019) 216:2763–77. doi: 10.1084/jem.20182111
79. Junttila IS. Tuning the cytokine responses: an update on interleukin (IL)-4 and IL-13 receptor complexes. *Front Immunol*. (2018) 9:888. doi: 10.3389/fimmu.2018.00888
80. Puleston J, Cooper M, Murch S, Bid K, Makh S, Ashwood P, et al. A distinct subset of chemokines dominates the mucosal chemokine response in inflammatory bowel disease. *Aliment Pharmacol Ther*. (2005) 21:109–120. doi: 10.1111/j.1365-2036.2004.02262.x
81. Abu El-Asrar AM, Berghmans N, Al-Obeidan SA, Gikandi PW, Opdenakker G, Van Damme J, et al. The CC chemokines CCL8, CCL13 and CCL20 are local inflammatory biomarkers of HLA-B27-associated uveitis. *Acta Ophthalmol*. (2019) 97:e122–e128. doi: 10.1111/aos.13835
82. Ardain A, Domingo-Gonzalez R, Das S, Kazer SW, Howard NC, Singh A, et al. Group. 3 innate lymphoid cells mediate early protective immunity against tuberculosis. *Nature*. (2019) 570:528–32. doi: 10.1038/s41586-019-1276-2
83. Connor SJ, Paraskevopoulos N, Newman R, Cuan N, Hampartzoumian T, Lloyd AR, et al. CCR2 expressing CD4+ T lymphocytes are preferentially recruited to the ileum in Crohn's disease. *Gut*. (2004) 53:1287–94. doi: 10.1136/gut.2003.028225
84. Sonnenberg GF, Mjosberg J, Spits H, Artis D. SnapShot: innate lymphoid cells. *Immunity*. (2016) 39:622.e621. doi: 10.1016/j.immuni.2013.08.021
85. Bernink JH, Ohne Y, Teunissen MBM, Wang J, Wu J, Krabbendam L, et al. c-Kit-positive ILC2s exhibit an ILC3-like signature that may contribute to IL-17-mediated pathologies. *Nat Immunol*. (2015) 20:992–1003. doi: 10.1038/s41590-019-0423-0
86. Allan DS, Kirkham CL, Aguilar OA, Qu LC, Chen P, Fine JH, et al. An *in vitro* model of innate lymphoid cell function and differentiation. *Mucosal Immunol*. (2015) 8:340–51. doi: 10.1038/mi.2014.71
87. Ratner D, Mueller C. Immune responses in cystic fibrosis: are they intrinsically defective? *Am J Respir Cell*

Mol Biol. (2012) 46:715–22. doi: 10.1165/rcmb.2011-0399RT
88. Tan HL, Rosenthal M. IL-17 in lung disease: friend or foe? *Thorax*. (2013) 68:788–90. doi: 10.1136/thoraxjnl-2013-203307
89. Mereness JA, Bhattacharya S, Wang Q, Ren Y, Pryhuber GS, Mariani TJ. Type VI collagen promotes lung epithelial cell spreading and wound-closure. *PLoS ONE*. 13:e0209095. doi: 10.1371/journal.pone.0209095
90. Groulx JF, Gagné D, Benoit YD, Martel D, Basora N, Beaulieu JF. Collagen VI is a basement membrane component that regulates epithelial cell-fibronectin interactions. *Matrix Biol*. (2011) 30:195–206. doi: 10.1016/j.matbio.2011.03.002
91. Liesker JJ, Ten Hacken NH, Zeinstra-Smith M, Rutgers SR, Postma DS, Timens W. Reticular basement membrane in asthma and COPD: similar thickness, yet different composition. *Int J Chron Obstruct Pulmon Dis*. (2009) 4:127–35. doi: 10.2147/COPD.S4639
92. Durieu I, Peyrol S, Gindre D, Bellon G, Durand DV, Pacheco Y. Subepithelial fibrosis and degradation of the bronchial extracellular matrix in cystic fibrosis. *Am J Respir Crit Care Med*. (1998) 158:580–8. doi: 10.1164/ajrccm.158.2.9707126
93. Bhattacharjee A, Shukla M, Yakubenko VP, Mulya A, Kundu S, Cathcart MK, et al. IL-4 and IL-13 employ discrete signaling pathways for target gene expression in alternatively activated monocytes/macrophages. *Free Radic Biol Med*. (2013) 54:1–16. doi: 10.1016/j.freeradbiomed.2012.10.553

Conflict of Interest: MN has served as an advisor for Pentax, Giuliani, MSD, Abbvie, Janssen, Takeda and Boehringer.

The remaining authors declare that the research was conducted in the absence of any commercial or financial relationships that could be construed as a potential conflict of interest.

frontiers in Immunology

ORIGINAL RESEARCH
published: 09 June 2020
doi: 10.3389/fimmu.2020.01121

Unveiling the Crucial Role of Type IV Secretion System and Motility of *Helicobacter pylori* in IL-1β Production via NLRP3 Inflammasome Activation in Neutrophils

Ah-Ra Jang[1], Min-Jung Kang[1], Jeong-Ih Shin[2], Soon-Wook Kwon[2], Ji-Yeon Park[1], Jae-Hun Ahn[1], Tae-Sung Lee[1], Dong-Yeon Kim[1], Bo-Gwon Choi[1], Myoung-Won Seo[1], Soo-Jin Yang[3], Min-Kyoung Shin[2] and Jong-Hwan Park[1]**

[1] Laboratory Animal Medicine, College of Veterinary Medicine and Animal Medical Institute, Chonnam National University, Gwangju, South Korea, [2] Department of Microbiology, School of Medicine, Gyeongsang National University, Jinju-si, South Korea, [3] School of Bioresources and Bioscience, Chung-Ang University, Anseong, South Korea

OPEN ACCESS

Edited by:
Maria Leite-de-Moraes, Université Paris Descartes, France

Reviewed by:
Christophe Paget, Institut National de la Santé et de la Recherche Médicale (INSERM), France
Payel Sil, National Institute of Environmental Health Sciences (NIEHS), United States

***Correspondence:**
Min-Kyoung Shin
mkshin@gnu.ac.kr
Jong-Hwan Park
jonpark@jnu.ac.kr

Specialty section:
This article was submitted to Molecular Innate Immunity, a section of the journal Frontiers in Immunology

Received: *07 November 2019*
Accepted: *07 May 2020*
Published: *09 June 2020*

Citation:
Jang A-R, Kang M-J, Shin J-I, Kwon S-W, Park J-Y, Ahn J-H, Lee T-S, Kim D-Y, Choi B-G, Seo M-W, Yang S-J, Shin M-K and Park J-H (2020) Unveiling the Crucial Role of Type IV Secretion System and Motility of Helicobacter pylori in IL-1β Production via NLRP3 Inflammasome Activation in Neutrophils. Front. Immunol. 11:1121. doi: 10.3389/fimmu.2020.01121

Helicobacter pylori is a gram-negative, microaerophilic, and spiral-shaped bacterium and causes gastrointestinal diseases in human. IL-1β is a representative cytokine produced in innate immune cells and is considered to be a key factor in the development of gastrointestinal malignancies. However, the mechanism of IL-1β production by neutrophils during *H. pylori* infection is still unknown. We designed this study to identify host and bacterial factors involved in regulation of *H. pylori*-induced IL-1β production in neutrophils. We found that *H. pylori*-induced IL-1β production is abolished in NLRP3-, ASC-, and caspase-1/11-deficient neutrophils, suggesting essential role for NLRP3 inflammasome in IL-1β response against *H. pylori*. Host TLR2, but not TLR4 and Nod2, was also required for transcription of NLRP3 and IL-1β as well as secretion of IL-1β. *H. pylori* lacking *cagL*, a key component of the type IV secretion system (T4SS), induced less IL-1β production in neutrophils than did its isogenic WT strain, whereas *vacA* and *ureA* were dispensable. Moreover, T4SS was involved in caspase-1 activation and IL-1β maturation in *H. pylori*-infected neutrophils. We also found that FlaA is essential for *H. pylori*-mediated IL-1β production in neutrophils, but not dendritic cells. TLR5 and NLRC4 were not required for *H. pylori*-induced IL-1β production in neutrophils. Instead, bacterial motility is essential for the production of IL-1β in response to *H. pylori*. In conclusion, our study shows that host TLR2 and NLRP3 inflammasome and bacterial T4SS and motility are essential factors for IL-1β production by neutrophils in response to *H. pylori*.

Keywords: bacterial motility, *Helicobacter pylori*, IL-1β, neutrophils, type IV secretion system (T4SS)

INTRODUCTION

Helicobacter pylori (*H. pylori*) is a gram-negative, microaerophilic, and spiral bacterium that colonizes the human gastric mucosa. More than 50% of the world's population are infected with the bacteria and the infection lasts a lifetime. *H. pylori* is the etiologic agent of gastrointestinal disorders that cause chronic gastritis, peptic ulcer, gastric adenocarcinoma, and

gastric mucosa-associated lymphoid tissue (MALT) lymphoma (1). For this reason, it was classified by the World Health Organization as a class I carcinogen in 1994 (2).

Interleukin 1β (IL-1β) is considered to be a key factor correlated with development of gastric malignancies (3). Recently, polymorphisms of the *IL-1B* gene and IL-1 receptor antagonist (IL-1RN) have been revealed to be associated with *H. pylori*-related gastric cancer in the Chinese, Italian, and Indian population (4–6). Moreover, when infected with *H. felis*, IL-β-overexpressed transgenic mice display accelerated gastric inflammation development, metaplasia, and carcinoma (7). Huang et al. also showed that *H. pylori*-induced gastric inflammation and DNA methylation were reduced in IL-1R-deficient mice or by administration of IL-1 receptor antagonist (IL-1ra) (8). In addition, infiltration of innate immune cells, such as neutrophils and macrophages, and a multiplicity of gastric cancer induced by *H. pylori* infection were significantly reduced in IL-1β-deficient mice (9). Increased expression of IL-8, IL-1β, and COX-2 genes was also observed in patients with chronic gastritis infected with *H. pylori* compared with *H. pylori* negative patients (10). These findings suggest that IL-1β may play a crucial role in the development of *H. pylori*-induced gastric inflammation and cancer.

As a cytosolic multiprotein complex, NLRP3 inflammasome is a major inflammatory pathway that is activated in response to a variety of signals, including microbial infection and tissue damage (11). Activation of NLRP3 inflammasome is composed of two-step signals. First, the priming step is initiated by transcription of pro-IL-1β and NLRP3 through the activation of NF-κB and AP-1 by pattern-recognition receptors (PRRs) in response to microbial stimuli (12, 13). The second step involves NLRP3 inflammasome oligomerization, caspase-1 activation, cleavage of pro-IL-1β by caspase-1, and then secretion of the mature IL-1β. This step is induced by various molecules, such as ATP, reactive oxygen species (ROS), and monosodium urate (MSU) (14). Several studies have demonstrated that *H. pylori* activates the NLRP3 inflammasome in innate immune cells, including dendritic cells (DCs) and neutrophils (15–18).

Neutrophils play an important role in host defense against bacterial and fungal pathogens (19, 20). Despite the crucial role in innate immune response, several studies have reported that neutrophils might be involved in gastric-cancer development (21, 22). This concept has been supported by the observation that there was more neutrophils recruitment in gastric-cancer tissue than in the tissues surrounding gastric cancer (23). Furthermore, the higher number of neutrophils in gastric cancer is correlated with increased levels of IL-8 (23). In addition to the potential role of neutrophils in gastric-cancer development, a recent study has also shown that *H. pylori* T4SS induced production of IL-1β in human neutrophils in a NLRP3 inflammasome-dependent manner (17). However, the exact molecular mechanisms by which *H. pylori* bacterial factors regulate production of IL-1β in host neutrophils are not well-defined. Thus, in this study, we sought to identify both bacterial and host factors associated with IL-1β production in neutrophils in response to *H. pylori* infection.

MATERIALS AND METHODS

Mice

We purchased wild type (WT), TLR2-, TLR4-, and NOD2-deficient mice on C57BL/6 background from the Jackson Laboratory (Bar Harbor, ME, USA). NLRP3-, Capase-1/11-, ASC-, and NLRC4- deficient mice were kindly provided by Prof. Gabriel Núñez (University of Michigan, USA). TLR5-deficient mice were gifts from Prof. Joon Haeng Rhee (Chonnam National University, Hwasun, Korea). We conducted all animal studies using protocols approved by the Institutional Animal Care and Use Committee of Chonnam National University (Approval No. CNU IACUC-YB-2018-85).

Bacterial Strains and Culture Conditions

Helicobacter pylori P1WT and its isogenic mutants P1Δ*CagL*, P1Δ*FlaA*, P1Δ*UreA*, and P1Δ*VacA* have been described previously (24). Another mutant with FlaA deficiency was generated by allelic exchange in *H. pylori* 26695 strain, and details are provided in the **Supplementary Material**. The following clinical isolates from child patients were provided from Gyeongsang National University Hospital (GNUH), as the Branch of National Culture Collection for Pathogens (NCCP, Jinju, Korea): three motile strains, *H. pylori* 5356AC, *H. pylori* 4930AC, *H. pylori* 5049AC; two non-motile strains, *H. pylori* 4940A, *H. pylori* 4980AC. *H. pylori* 52WT (non-motile) and its mouse-adapted strain *H. pylori* 52P6 (six time-passaged) were also provided from Gyeongsang National University Hospital. We cultured all *H. pylori* strains on Brucella broth containing 10% fetal bovine serum (FBS; Corning costar, Corning NY, USA), 1 μg/ml nystatin (Sigma-Aldrich, St. Louis, MO, USA, Cat No. N3503), 5 μg/ml trimethoprim (Sigma-Aldrich, Cat No. T7883), and 10 μg/ml vancomycin (Sigma-Aldrich, catalog no. V2002) at 37°C under microaerobic conditions.

Cell Culture and Bacterial Infection

We isolated thioglycollate-induced peritoneal neutrophils as previously described (25). Briefly, mouse peritoneal neutrophils were harvested after intraperitoneal injection of 2 ml of 4% thioglycollate broth (Sigma-Aldrich, Cat No. 70157). Four hours later, mice were injected intraperitoneally with 5 ml of PBS and peritoneal lavage was obtained twice. Red blood cells (RBCs) were lysed with cell lysis buffer. These collected peritoneal neutrophils were cultured in RPMI 1640 (Welgene, Gyeongsan, Gyeongsangbuk-do, Korea) containing 10% FBS in a 5% CO_2 incubator at 37°C. To obtain of neutrophils derived from bone marrow, we isolated cells from femurs and tibias using density gradient cell separation protocol. Total bone marrow cells were overlaid on a two-layer gradient of HISTOPAQUE-1119 (density: 1.119 g/ml; Sigma-Aldrich, Cat No. 11191) and HISTOPAQUE-1077 (density: 1.077 g/ml; Sigma-Aldrich, Cat No. 10771) and centrifuged (2,000 rpm, 30 min) without braking. The collected cells in the interface were used. Bone-marrow neutrophils (BMNs) were resuspended in RPMI 1640 (Welgene) containing 10% FBS in a 5% CO_2 incubator at 37°C. Purity of isolated neutrophils was confirmed by flow cytometry (Miltenyi Biotec, Bergisch Gladbach, Germany). Cells showing

$CD11b^+$ (FITC-conjugated anti-CD11b, BD Biosciences, San Jose, CA, USA, Cat No. 552850) and $Gr\text{-}1^+$ (APC-conjugated anti-Gr-1, BD Biosciences, Cat No. 553129) were > 90% (**Supplementary Figures 1A,B**). Human leukemia cell line HL-60 was cultured in RPMI 1640 medium (Welgene) containing 10% FBS, 1% Penicillin/Streptomycin (P/S; Gibco, Grand Island, NY, USA), 2 mM L-glutamine (Gibco), and 25 mM HEPES (Gibco). To differentiate into neutrophil-like cells, we stimulated cells with 1.25% DMSO for 7 days in a 5% CO_2 incubator at 37°C. These cells were seeded into 6-well or 48-well plates at a density of 2×10^6 cells or 2×10^5 cells, respectively, and incubated in a 5% CO_2 incubator at 37°C. Subsequently, cells were infected with *H. pylori* at the indicated dose and time points.

Evaluation of Cytokine Secretion by Bacteria Motility

To determine whether bacteria motility affected the secretion of IL-1β in peritoneal neutrophils, mild centrifugation (1,000 rpm, 10 min) was performed immediately after *H. pylori* P1WT and P1Δ*FlaA* (MOI 100) infection. At 24 h after infection, cell supernatant was collected for cytokine measurement.

Reagent and Inhibitor Assay

To activate the NLRP3 inflammasome, peritoneal neutrophils and BMNs were treated with 100 ng/ml LPS (InvivoGen, San Diego, CA, USA, Cat No. tlrl-eblps) for 3 h followed by treatment with 5 mM adenosine 5′-triphosphate disodium salt hydrate (ATP, Sigma-Aldrich, Cat No. A2383) for 45 min. For inhibitor assay, HL-60 cells were infected with *H. pylori* P1WT (MOI 100) for 24 h with or without pretreatment with glyburide (Sigma-Aldrich, Cat No. G2539) and Ac-YVAD-CMK (Calbiochem, La. Jolla, CA, USA, Cat No. 400012) for 2 h at indicated concentrations.

Measurement of Cytokines

We measured the concentrations of IL-1β (Cat No. DY401) and tumor necrosis factor alpha (TNF-α, Cat No. DY410) in culture supernatants of *H. pylori*-infected cells by using a commercial ELISA kit (R&D Systems, Minneapolis, MN, USA). To measure the levels of IL-18 in culture supernatant from *H. pylori*-infected peritoneal neutrophils, anti-mouse IL-18 antibody (MBL International, MA, USA, Cat No. D047-3) was coated on 384-well plate overnight at room temperature. The coated plate was washed three times with PBS containing 0.05% tween 20 (Sigma-Aldrich). After washed, the plate was incubated with 1% BSA for blocking for 1 h at room temperature. With three times washing between each step, the plate was further incubated with samples of culture supernatants for 2 h, the biotinylated-anti-mouse-IL-18 (MBL International, Cat No. D048-6) for 2 h, and the Streptavidin-HRP (R&D Systems) for 20 min at room temperature. Finally, the plate was washed and treated with the substrate solution (R&D Systems, Cat No. DY999). After the addition of stop solution, the optical density was measured at 450 nm.

Immunoblotting

Peritoneal neutrophils and BMNs were seeded at density of 2×10^6 cells/well in sterile 35 mm dishes and incubated overnight. These cells were infected with *H. pylori* (MOI 100) for 6 h. Culture supernatants and remaining cells were lysed by 1% Triton-X 100 (Sigma-Aldrich, Cat No. T9284) and a complete protease inhibitor cocktail (Roche, Mannheim, Germany, Cat No. 11-839-170-001). After centrifugation at 3,000 rpm for 5 min, we mixed the supernatant with SDS-PAGE sample loading buffer (5×). To detect target proteins, samples were separated by 15% SDS-PAGE and transferred to nitrocellulose (NC) membranes (GE Healthcare, Chicago, IL, USA, Cat No. 10600003). We probed membranes with primary antibodies against caspase-1 (AdipoGen Life Sciences, San Diego, CA, USA, Cat No. AG-20B-0042), IL-1β (R&D Systems, Cat No. AF-401-NA), and β-actin (Santa Cruz Biotechnology, Dallas, TX, USA, Cat No. sc-47778). After immunoblotting with goat anti-mouse IgG (H+L) secondary antibody, HRP (Thermo Fisher Scientific, MA, USA, Cat No. 31430) or goat anti-rabbit IgG (H+L) secondary antibody, HRP (Thermo Fisher Scientific, Cat No. 31460), we detected proteins using Clarity™ Western ECL Substrate (Bio-Rad, Hercules, CA, USA, Cat No. BR170-5061).

Real-Time Quantitative PCR (qPCR)

RNAs from *H. pylori* infected cells were extracted using easy-BLUE™ Total RNA Extraction Kit (Intron Biotechnology, Seongnam, Korea) and cDNA synthesis was done using ReverTra Ace® qPCR RT Master Mix (TOYOBO Bio-Technology, Osaka, Japan) according to the manufacturer's instructions. qPCR was performed by the CFX Connect™ Real-time PCR Detection System (Bio-Rad, Hercules, CA, USA) using 2x PCRBIO SyGreen Blue Mix Lo-ROS according to the manufacturer's instructions (Bio-D Co., Ltd., Hull, UK). GAPDH was used for normalization. The primers used for qPCR were as follows:

mNLRP3 forward: 5′-ATGGTATGCCAGGAGGACAG-3′;
mNLRP3 reverse: 5′-ATGCTCCTTGACCAGTTGGA-3′;
mIL-1β forward: 5′-GATCCACACTCTCCAGCTGCA-3′;
mIL-1β reverse: 5′-CAACCAACAAGTGATATTCTC CATG-3′;
mGAPDHforward: 5′-CGACTTCAACAGCAACTCCCA CTCTTCC-3′;
mGAPDH reverse: 5′-TGGGTGGTCCAGGGTTTCTTACT CCTT-3′.

Statistical Analysis

Statistical significance of differences among groups was found by using two-tailed Student's *t*-test or the one- or two-way analysis of variance (ANOVA) followed by Bonferroni post-tests. We calculated all statistics using GraphPad Prism version 5.01 (GraphPad Software, San Diego, CA, USA). Values of $P < 0.05$ were considered statistically significant.

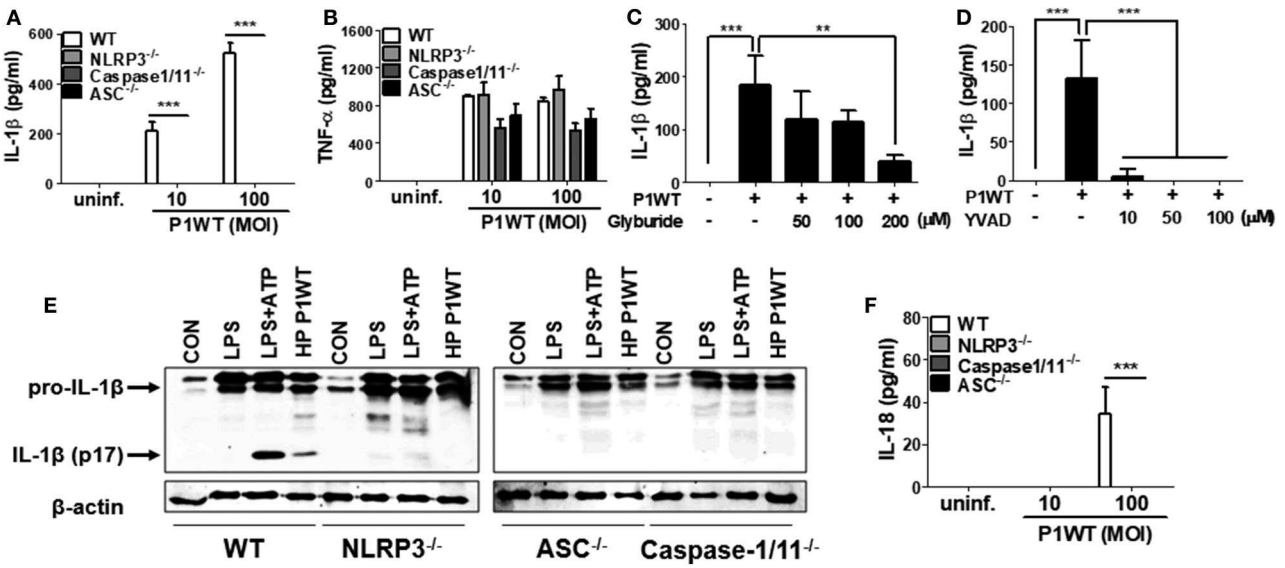

FIGURE 1 | *H. pylori* mediates production of IL-1β in NLRP3 inflammasome-dependent manner in neutrophils. WT, and NLRP3-, Caspase1/11-, and ASC-deficient mouse peritoneal neutrophils were infected with *H. pylori* P1WT (MOI 100) for 24 h **(A,B,F)**. The concentration of IL-1β, TNF-α, and IL-18 in supernatant was measured by ELISA. HL-60 cells were pretreated without or with glyburide **(C)** or Ac-YVAD-CMK **(D)** at the indicated concentrations for 2 h and subsequently infected with *H. pylori* P1WT (MOI 100) for 24 h. The concentration of IL-1β in supernatant was measured by ELISA. We infected peritoneal neutrophils from WT and NLRP3-, ASC-, and Caspase1/11-deficient mice with *H. pylori* P1WT (MOI 100) for 6 h **(E)**. We used culture supernatants and cell lysates to detect immature and cleaved forms of IL-1β by Immunoblotting. Antibody against β-actin was used as a loading control. Results are presented as mean ± SD. $^{**}P < 0.01$ and $^{***}P < 0.001$.

RESULTS

H. pylori Induces IL-1β Production in Neutrophils by Activating NLRP3 Inflammasome by Stimulating Various Danger Signals

NLRP3 inflammasome has been known to be required for caspase-1 activation and IL-1β maturation in DCs in response to *H. pylori* (15, 16, 18). Therefore, we first investigated whether NLRP3 inflammasome is also involved in *H. pylori*-induced IL-1β maturation in neutrophils. As shown in **Figure 1A**, *H. pylori* P1WT induced IL-1β secretion in peritoneal neutrophils isolated from WT mice, whereas the production of IL-1β was abolished in NLRP3-, caspase-1/11-, and ASC-deficient neutrophils. Unlike the induction of IL-1β, *H. pylori*-induced TNF-α production was not affected by the same genetic deficiencies (**Figure 1B**). To confirm these data in a human-cell system, HL-60 cells, a human promyelocytic leukemia cell line, was differentiated to neutrophil-like cells at the presence of DMSO as previously described (26). As expected, *H. pylori* P1WT could induce IL-1β production in the differentiated HL-60 cells, which was reduced by the presence of glyburide (a NLRP3 inflammasome inhibitor) or Ac-YVAD-CMK (a caspase-1 inhibitor) in a dose-dependent manner (**Figures 1C,D**). Next, we did Western-blot analysis to detect cleaved IL-1β as a mature form. *H. pylori* P1WT led to cleavage of IL-1β in WT neutrophils, but not in cells from NLRP3-, caspase-1/11-, and ASC-deficient mice (**Figure 1E**, **Supplementary Figure 2**). These findings suggest that the NLRP3/ASC/caspase-1 axis is essential for *H. pylori*-induced IL-1β production in neutrophils. Furthermore, we observed that the NLRP3, caspase-1, and ASC were also required for IL-18 production in response to *H. pylori* in neutrophils (**Figure 1F**).

Various signals, such as extracellular ATP, K^+ efflux, reactive oxygen species (ROS) generation, and cathepsin B release from lysosomes, mediates activation of NLRP3 inflammasome (14). To find out whether these stimuli are involved in *H. pylori*-induced IL-1β production in neutrophils, we carried out inhibitor assays. Oxidized ATP (oxATP) (a P2X7R antagonist) and extracellular addition of KCl reduced IL-1β production in *H. pylori* P1WT-infected neutrophils in a dose-dependent manner, and the cytokine production was completely abolished at a high concentration of those inhibitors, whereas TNF-α level was slightly influenced (**Supplementary Figures 3A–D**). We also observed that the detectable level of LDH was released even in untreated control cells (**Supplementary Figure 4**). The LDH release was increased by *H. pylori* infection, which was decreased by oxATP (**Supplementary Figure 4**), suggesting that dying or dead cells can be a source of extracellular ATP. A ROS inhibitor NAC reduced both IL-1β and TNF-α at 20 mM concentration (**Supplementary Figures 3E,F**). The IL-1β production was significantly inhibited by CA074Me, a cathepsin B inhibitor, even at a low concentration of 5 μM, which did not influence TNF-α level (**Supplementary Figures 3G,H**). These findings suggest that various extracellular signals, such as ATP/P2X7R, potassium efflux, ROS generation, and cathepsin

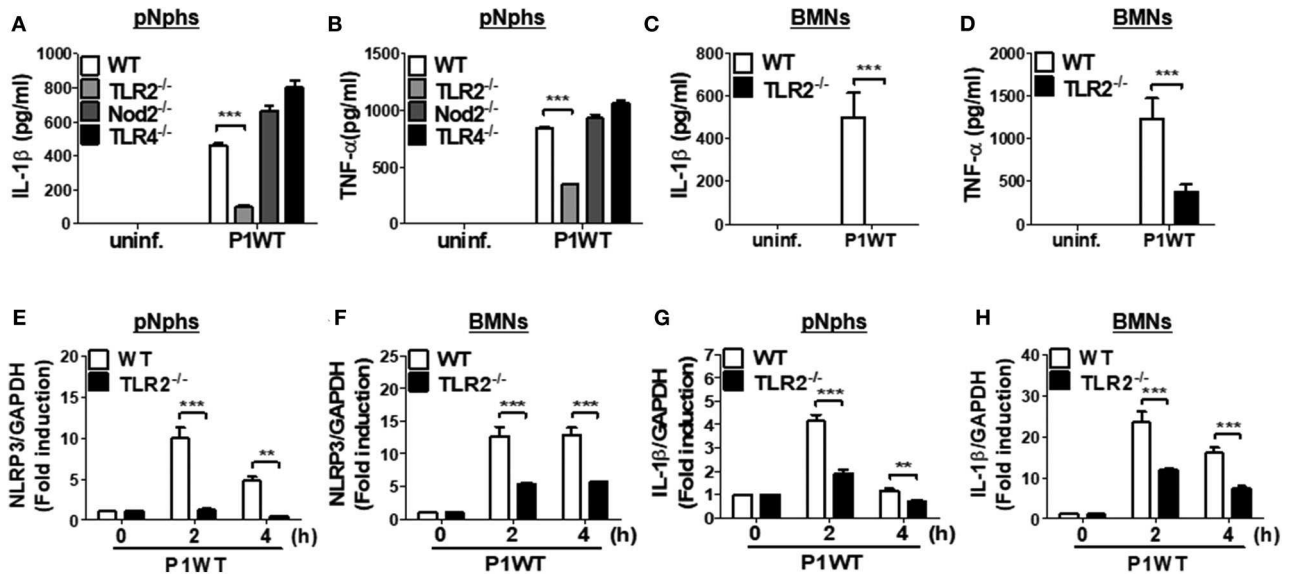

FIGURE 2 | TLR2, but not NOD2 and TLR4, is involved in *H. pylori* recognition in mouse neutrophils. WT and TLR2-, NOD2-, and TLR4-deficient peritoneal neutrophils **(A,B)** and BMNs **(C,D)** from WT and TLR2-deficient mice were infected with P1WT (MOI 100) for 24 h. The concentration of IL-1β **(A,C)** and TNF-α **(B,D)** in the supernatant was measured by ELISA. We infected WT and TLR2-deficient peritoneal neutrophils or BMNs with *H. pylori* P1WT (MOI 100) at indicated times **(E–H)**. Gene expressions of NLRP3 **(E,F)** and IL-1β **(G,H)** were evaluated by real-time PCR. Results are presented as mean ± SD. $^{**}P < 0.01$ and $^{***}P < 0.001$.

B, may contribute to *H. pylori*-induced activation of the NLRP3 inflammasome pathway in neutrophils.

TLR2, but Not Nod2 and TLR4, Is Required for Expression of IL-1β Gene and Secretion of IL-1β in *H. pylori*-Infected Neutrophils

Previously, TLR2 and Nod2 have been shown to be involved in *H. pylori*-mediated gene expression of NLRP3 and IL-1β in DCs (15). Moreover, *H. pylori* upregulates TLR4 expression in human gastric epithelial cells (27). We therefore explored whether such patterns of recognition mediate IL-1β production in neutrophils in response to *H. pylori* infection. TLR2 deficiency led to impaired production of both TNF-α and IL-1β in *H. pylori* P1WT-infected peritoneal neutrophils derived from mice (**Figures 2A,B**). In contrast, Nod2 and TLR4-deficient cells produced a comparable level of IL-1β and TNF-α (**Figures 2A,B**). Consistently, *H. pylori*-induced production of IL-1β and TNF-α was impaired in TLR2-deficient bone marrow-derived neutrophils (BMNs) (**Figures 2C,D**), while the deficiency of Nod2 and TLR4 did not affect the two cytokines production (**Supplementary Figures 5A,B**). To find out whether TLR2 contributes to priming of NLRP3 and IL-1β (signal 1), we evaluated their gene expression by RT-PCR. As shown by the results in **Figures 2E–H**, we observed increased expression of genes for NLRP3 and IL-1β in WT peritoneal neutrophils and BMNs, whereas we observed significantly lower levels of NLRP3 and IL-1β gene transcription in TLR2-deficient cells (**Figures 2E–H**). Collectively, these data indicate that TLR2 is a central innate receptor for regulating NLRP3 inflammasome priming (signal) in *H. pylori*-infected neutrophils.

H. pylori Type IV Secretion System Is Required for IL-1β Secretion Through Caspase-1 Activation and IL-1β Processing in Neutrophils

A previous report suggested that *H. pylori* uses a type IV secretion system (T4SS) to induce pro-IL-1β expression in DCs (15). In contrast, a recent study indicated that the *H. pylori* T4SS is dispensable for IL-1β production in human neutrophils (17). To assess the role of T4SS in production of IL-1β, we infected peritoneal neutrophils, BMNs, and the differentiated HL-60 cells with *H. pylori* P1WT and its isogenic mutant P1Δ*cagL*, in which T4SS is non-functional (28). As expected, we observed impaired production of IL-1β and IL-18 production in peritoneal neutrophils infected with P1Δ*cagL* (**Figure 3A**, **Supplementary Figure 6**). Consistently, *cagL* deficiency reduced the production of IL-1β in both BMNs and human neutrophil-like HL-60 cells (**Figures 3B,C**). In contrast to the production of IL-1β, the *cagL* mutant induced a comparable level of TNF-α in each cell type to its isogenic WT strain (**Figures 3D–F**). Western blot analysis revealed that cleavage of caspase-1 and IL-1β was reduced in P1Δ*cagL*-treated neutrophils more than in cells infected with P1WT (**Figures 3G,H**, **Supplementary Figures 7A,B**). There was no difference in expression level of the pro-form of IL-1β and casapse-1 between P1WT- and Δ*cagL*-infected neutrophils (**Supplementary Figure 8**). In addition, cagL deficiency did not influence the gene expression of NLRP3 and IL-1β in either peritoneal neutrophils or BMNs (**Supplementary Figures 9A–D**). These findings demonstrated that bacterial T4SS is involved in regulation of NLRP3

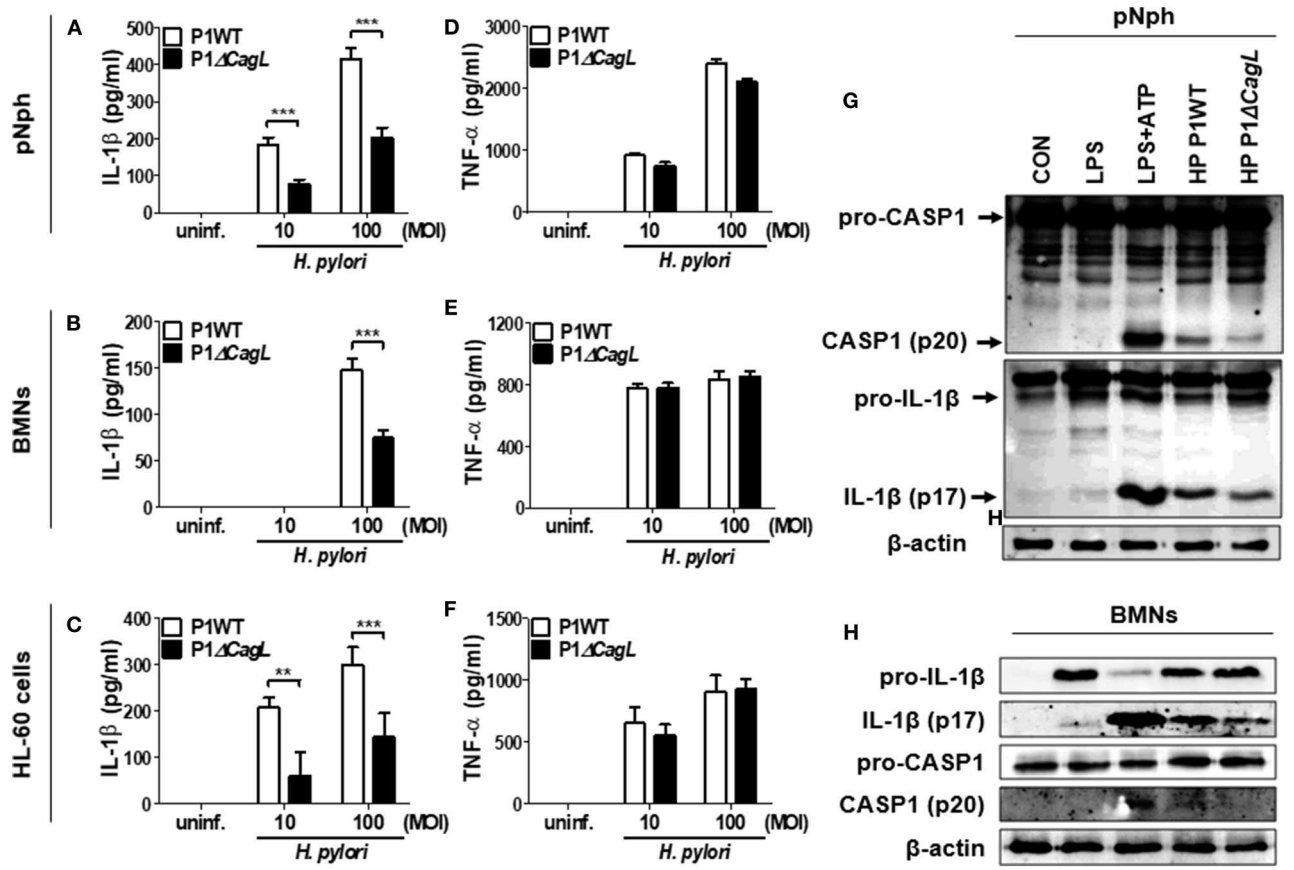

FIGURE 3 | *H. pylori* T4SS induces production of IL-1β in neutrophils. Peritoneal neutrophils **(A,D)**, BMNs **(B,E)**, and HL-60 cells **(C,F)** were infected with *H. pylori* P1WT and isogenic mutant deficient in cagL (MOI 10 and 100) for 24 h. The concentration of IL-1β **(A–C)** and TNF-α **(D–F)** in supernatant was measured by ELISA. Results are presented as mean ± SD. $^{**}P < 0.01$ and $^{***}P < 0.001$. Peritoneal neutrophils **(G)** and BMNs **(H)** were infected with P1WT and Δ*cagL* (MOI 100) for 6 h. We used culture supernatants and cell lysates to detect immature and cleaved forms of caspase-1 and IL-1β by Immunoblotting **(G,H)**. Antibody against β-actin was used as a loading control.

inflammasome activation (signal 2) rather than priming (signal 1) in host neutrophils in response to *H. pylori* infection.

Deficiency of FlaA, but Not of UreA and VacA, Distinctly Leads to Impaired IL-1β Secretion in *H. pylori*-Infected Neutrophils

It has been reported that the *H. pylori* virulence factors, such as VacA and UreA, are involved in IL-1β production and NLRP3 inflammasome activation in DCs (16, 18). Bacterial flagellin has also been proposed to be involved in IL-1β processing via NLRC4 inflammasome activation (29). Therefore, we investigated whether such bacterial factors are required for *H. pylori*-induced IL-1β production in neutrophils. As shown in **Figures 4A,B**, both UreA and VacA mutant strains exhibited a similar level of IL-1β to the isogenic WT strain in peritoneal neutrophils, whereas TNF-α induction was slightly decreased in the two mutant strains (**Figures 4A,B**). Unexpectedly, IL-1β production was significantly lower in P1Δ*FlaA*-treated neutrophils than in cells infected with the P1WT strain, whereas levels of TNF-α were comparable between the two strains (**Figures 4A,B**). In BMNs, the FlaA deficiency also impaired the production of IL-1β, but not TNF-α (**Figures 4C,D**). Neither UreA nor VacA affected IL-1β and TNF-α production in BMNs in response to *H. pylori* (**Figures 4C,D**). Production of IL-18 was also impaired in both peritoneal neutrophils and BMNs infected with FlaA mutant (P1Δ*FlaA*) as compared with P1WT strain (**Figures 4E,F**). To confirm these data in a different *H. pylori* genetic background strain, we infected peritoneal neutrophils with *H. pylori* 26695WT and its isogenic mutant 26695Δ*FlaA*. In agreement with the data generated with the P1WT strain, IL-1β level was significantly lower in 26695Δ*FlaA*-treated cells than in ones treated with the 26695WT strain, whereas the TNF-α level was not affected by deletion of the FlaA gene (**Figures 4G,H**). To find out whether FlaA is required for IL-1β production in DCs, as DCs are previously known to be able to produce IL-1β in response to *H. pylori* (15), we infected BMDCs with *H. pylori* P1WT and P1Δ*FlaA*. As shown in **Supplementary Figure 10**, the P1WT and P1Δ*FlaA* strains displayed comparable levels of IL-1β secretion in DCs. These results indicated that *H. pylori* FlaA distinctly contributes to production of IL-1β in neutrophils, but not in DCs.

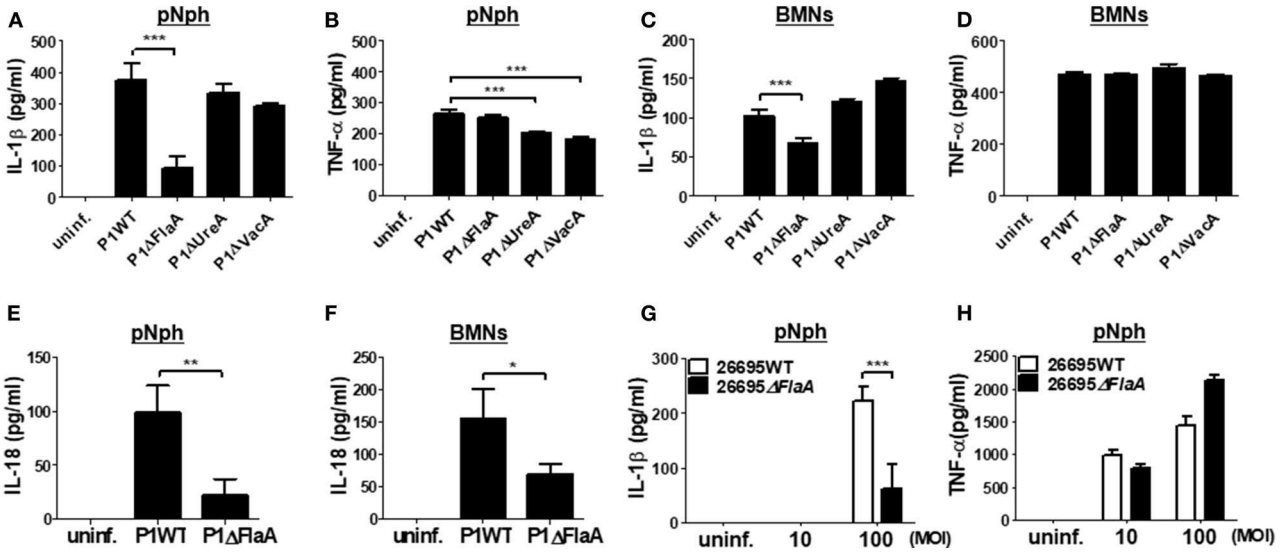

FIGURE 4 | *H. pylori* flagellin is important for IL-1β production in mouse neutrophils. Peritoneal neutrophils **(A,B,E,G,H)** and BMNs **(C,D,F)** were infected with indicated bacteria (MOI 100 in A-F) for 24 h. We measured the concentration of IL-1β **(A,C,G)**, TNF-α **(B,D,H)**, and IL-18 **(E,F)** in the supernatant by ELISA. Results are presented as mean ± SD. $^{*}P < 0.05$; $^{**}P < 0.01$; and $^{***}P < 0.001$.

FlaA Contributes to Both Priming and Inflammasome Activation of NLRP3 in Neutrophils in Response to *H. pylori*

We next explored whether FlaA-induced production of IL-1β is mediated via activation of NLRP3 inflammasome in neutrophils. *H. pylori* P1WT induced strong expression of pro-IL-1β protein, which was slightly reduced in the cells treated with P1Δ*FlaA* (**Figures 5A,C**, **Supplementary Figures 11A, 12A,C**). P1WT-infected BMNs also released a significantly higher level of cleaved IL-1β and caspase-1 (mature form) than did BMNs infected with the P1Δ*FlaA* strain (**Figure 5A**, **Supplementary Figure 11A**). These results were also confirmed in the experiment using peritoneal neutrophils (**Supplementary Figures 12A,C**). Similar to the P1Δ*FlaA* strain, FlaA deficiency in the 26695 background also led to reduced cleavage of IL-1β and caspase-1 and less pro IL-1β expression (**Figures 5B,D**, **Supplementary Figures 11B, 12B,D**). In addition, expression of NLRP3 and IL-1β genes was significantly lower in P1Δ*FlaA*-treated BMNs P1WT-treated cells (**Figures 5E,F**). Consistently, NLRP3 gene expression was reduced in BMNs in response to FlaA deficiency in the *H. pylori* 26695 strain (**Figure 5G**). Moreover, gene expression of IL-1β was also decreased in 26695Δ*FlaA*-treated cells at 2 h after infection (**Figure 5H**). These data indicate that *H. pylori* flagellin is involved in regulation of both priming and activation of NLRP3 inflammasome in neutrophils.

Bacterial Motility, but Not Host TLR5 and NLRC4, Is Required for *H. pylori*-Mediated IL-1β Production in Neutrophils

TLR5 and NLRC4 are dual sensors for bacterial flagellin at the cell surface and cytosol in host cells (28). Flagellin recognition by TLR5 leads to NF-κB activation, whereas NLRC4 is responsible for inflammasome activation. Since *H. pylori* FlaA was essential for IL-1β gene expression and maturation in neutrophils, we tried to find out whether TLR5 and NLRC4 are involved in *H. pylori*-mediated IL-1β production. As shown by the results in **Figures 6A,B**, WT neutrophils and neutrophils deficient of TLR5 or NLRC4 produced a comparable level of IL-1β and TNF-α in response to *H. pylori*, suggesting that *H. pylori* FlaA regulates IL-1β production in neutrophils in a TLR5- and NLRC4-independent manner. Because bacterial flagella are essential for motility, we next explored whether motility is essential for *H. pylori*-induced IL-1β production in neutrophils. In our *in vitro* system, we cultured neutrophils in a floating state. Therefore, we centrifuged the cells after bacterial infection to increase the contact between *H. pylori* and neutrophils. As shown in **Figure 6C**, the centrifuging increased IL-1β production and abolished the difference of IL-1β production by WT and Δ*FlaA* mutant, suggesting that motility may be involved in *H. pylori*-induced IL-1β production in neutrophils. We further investigated whether different levels of motility in clinical isolates of *H. pylori* correlate with the amount of IL-1β production in neutrophils. Five clinical isolates of *H. pylori* were divided into two groups based on the results from a bacterial motility assay (**Supplementary Figure 13**): a low motility group of two strains (4940A and 4980AC) and a high motility group with three strains (4930AC, 5049AC, and 5356AC). *H. pylori* strains with high motility induced increased levels of IL-1β in neutrophils vs. the strains with low motility (**Figure 6D**), whereas TNF-α level was not different between the two groups of strains (**Figure 6E**). When 5049AC and 4940A strains were used as a representative one for motile and non-motile strain, the difference of IL-1β production was also abolished by the centrifugation (**Figure 6F**).

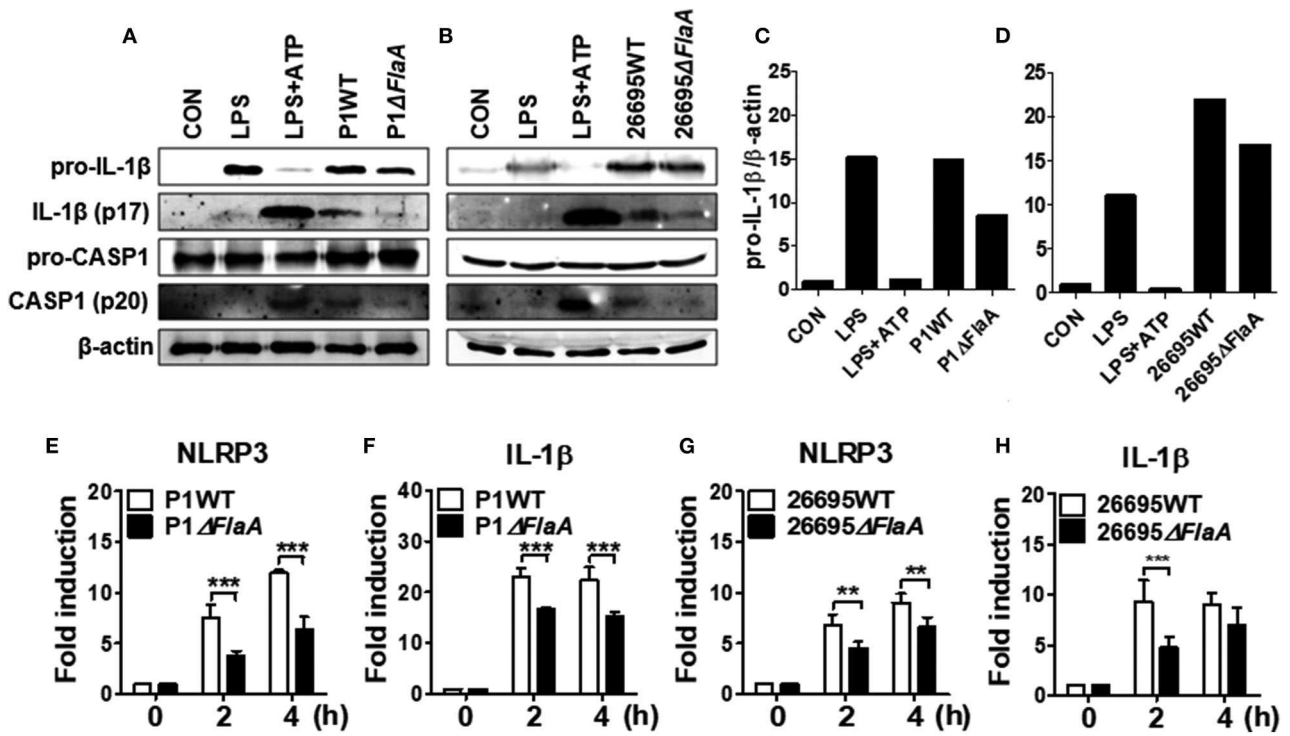

FIGURE 5 | *H. pylori* flagellin induces activation of IL-1β and caspase-1 in response to *H. pylori* in mouse neutrophils. BMNs were infected with *H. pylori* P1WT and Δ*flaA* **(A,C)** or 26695WT and Δ*flaA* **(B,D)** (MOI 100) for 6 h. We used culture supernatants and cell lysates to detect immature and cleaved forms of caspase-1 and IL-1β by Immunoblotting **(A–D)**. Antibody against β-actin was used as a loading control. Peritoneal neutrophils **(E,F)** and BMNs **(G,H)** were infected with *H. pylori* P1WT (MOI 100) at indicated time. We evaluated gene expression of NLRP3 **(E,G)** and IL-1β **(F,H)** by real-time PCR. Results are presented as mean ± SD. $^{**}P < 0.01$ and $^{***}P < 0.001$.

Furthermore, *H. pylori* 52 strain originally displayed a low motility phenotype, but it obtained high motility phenotype (HP 52 P6) after six passages in mice (data not shown). Interestingly, the passaged *H. pylori* strain induced a significantly higher level of IL-1β in neutrophils than did the original strain with low motility (**Figure 6G**). The two strains produced comparable level of TNF-α (**Figure 6H**). At last, we tried to confirm the involvement of cagL and FlaA in the production of IL-1β using neutrophils purified from human blood. Purity of the isolated neutrophils were confirmed by Flow cytometry and cytospin (**Supplementary Figures 14A,B**). Consistently, cagL and FlaA deficiencies resulted in lower production of IL-1β, but not TNF-α, in human neutrophils (**Supplementary Figures 14C,D**).

DISCUSSION

IL-1β is considered to be a central factor for gastric malignancy, as is supported by evidence that *IL-1B* gene polymorphism increases the risk of gastric cancer (30, 31) and overexpression of IL-1β leads to gastric inflammation and cancers in mice (7, 9). It has been known that *H. pylori* leads to IL-1β production in DCs through an NLRP3-dependent pathway, although there were controversies about *in vivo* role of NLRP3 in the bacterial clearance in the stomach of mice (15, 16, 18). Neutrophils are key innate immune cells that are involved in *H. pylori*-mediated gastric inflammation (32). Therefore, it is conceivable that both bacterial and host factors may play crucial roles in the production of IL-1β in neutrophils. However, only limited information is available on the precise molecular mechanisms involved in *H. pylori*-induced IL-1β production in neutrophils.

Recently, Perez-Figueroa et al. reported that *H. pylori* induces IL-1β production in human neutrophils in TLR2- and TLR4-independent manner (17). They also demonstrated that *H. pylori* increases the expression of NLRP3 inflammasome components and inhibitors for NLRP3 and caspase-1 reduces the production of IL-1β (17). Moreover, in contrast to the important role of T4SS in DCs, T4SS was dispensable for *H. pylori*-induced IL-1β production in human neutrophils (17). However, some aspects are inconsistent with our current study. In this study, we identified that NLRP3 inflammasome is a key host factor in neutrophils for production of IL-1β in response to *H. pylori* by showing that secretion and cleavage of IL-1β were abolished in NLRP3-, caspase-1/11-, and ASC-deficient neutrophils. However, unlike the previous report by Perez-Figueroa et al. (17), our data suggested that TLR2 is required for *H. pylori*-induced IL-1β production in both peritoneal neutrophils and BMNs. Expression of NLRP3 and IL-1β genes was also reduced in TLR2-deficient neutrophils. In *H. pylori*-infected DCs, TLR2 has been known to mediate IL-1β production

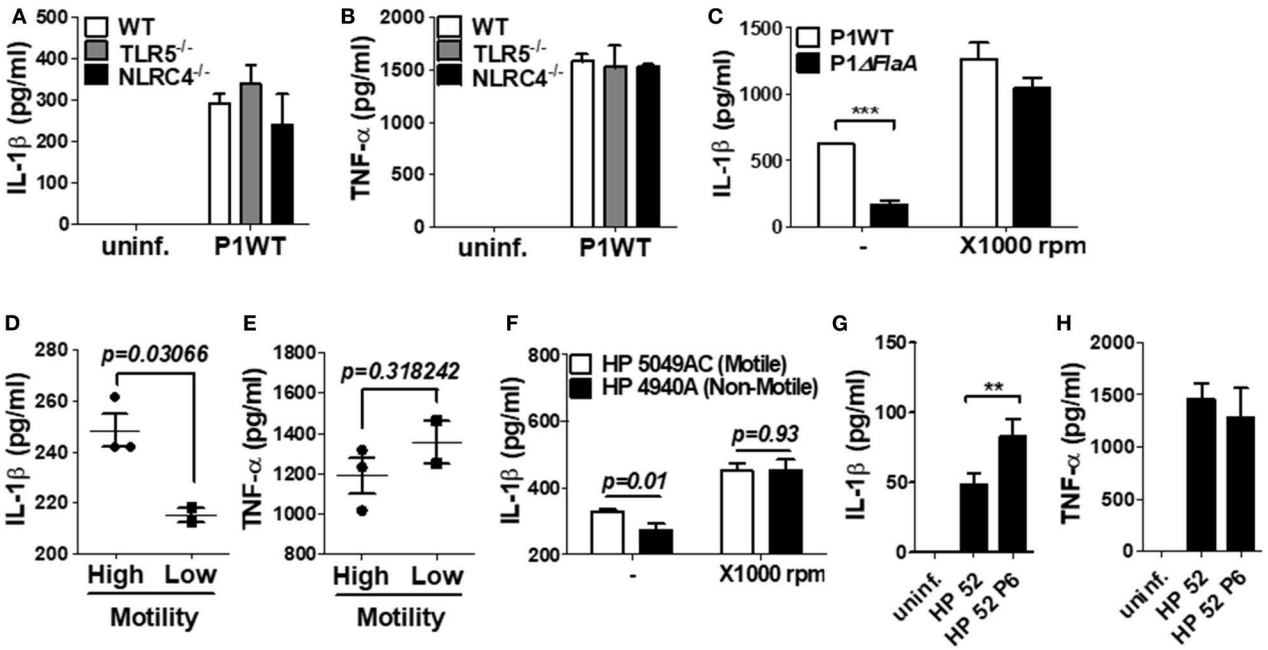

FIGURE 6 | The production of IL-1β is regulated by *H. pylori* motility of flagellin, but not TLR5 and NLRC4 in mouse neutrophils. WT and TLR5-, and NLRC4-deficient peritoneal neutrophils were infected with *H. pylori* P1WT (MOI 100) for 24 h **(A,B)**. To promote the contact between cells and *H. pylori*, we used mild centrifuging (1,000 rpm, 10 min) **(C,F)**. Clinical isolates of *H. pylori* with or without motility were infected in peritoneal neutrophils **(D–F)**. *H. pylori* 52 and mouse-adapted bacteria (passage 6) were infected in peritoneal neutrophils **(G,H)**. The concentration of IL-1β **(A,C,D,F,G)** and TNF-α **(B,E,H)** in supernatant was measured by ELISA. Results are presented as mean ± SD. $^{**}P < 0.01$ and $^{***}P < 0.001$, two-tailed Student's *t*-test.

by regulating NLRP3 and pro IL-1β expression (signal 1) (15, 16). Furthermore, TLR2 contributes to NF-κB activation and chemokine expression in gastric epithelial cells in response to *H. pylori* (33). Nevertheless, a TLR2-independent pathway should be considered, as detectable levels of IL-1β and TNF-α were secreted in TLR2-deficient neutrophils. Although TNF-α is also responsible for a TLR-independent priming of NLRP3 inflammasome (34), its role in TLR2-independent production of IL-1β is likely limited, since there was already a significant difference in the gene expression of NLRP3 and IL-1β between WT and TLR2-deficient neutrophils within 2 h of *H. pylori* infection. Signaling of other pattern recognition receptors may lead to the priming of NLRP3 inflammasome in response to *H. pylori* in neutrophils. In addition, it seems to be necessary to measure the induction levels of NLRP3 or IL-1β expression in the human neutrophils prepared in the reports by Perez-Figueroa et al., because TLR2 may be dispensable if the cells are primed sufficiently.

Several bacterial factors including T4SS, vacuolating toxin, and urease contribute to IL-1β production in response to *H. pylori* in BMDCs (15, 16, 18). Isogenic mutants lacking both *ureA* and *ureB* genes failed to activate caspase-1, whereas transcription of IL-1β was unaffected (16). The *vacA* mutant also led to less production of IL-1β and impaired caspase-1 activation in LPS-primed BMDCs (18). There is still a controversy on the precise role of T4SS in regulation of IL-1β production in DCs. Kim et al. reported that the cagL mutant produced level of IL-1β similar to that of the isogenic WT strain in LPS-primed DCs, in which NLRP3 and IL-1β are sufficiently induced, whereas mRNA expression of IL-1β and its secretion were reduced in cagL mutant-treated cells in the unprimed condition (15), suggesting that T4SS is essential for the priming step. In contrast, Semper et al. showed that a mutant lacking cagE produced less IL-1β in LPS-primed DCs (18). In the present study, we demonstrated that T4SS, but not VacA and UreA, is required for *H. pylori*-induced IL-1β production in neutrophils. In *H. pylori*-infected neutrophils, T4SS seems to regulate signal 2 of inflammasome activation rather than priming of NLRP3 and pro IL-1β, because cagL deficiency did not influence protein expression of pro IL-1β or gene expression of NLRP3 and IL-1β. Our current results are inconsistent with the previous report that suggested a dispensable role of T4SS in *H. pylori*-induced production of IL-1β (17). In the previous study, the experimental design apparently was flawed by using the *H. pylori* 26695 strain as the WT strain and the virD4 mutant originating from a different genetic background, *H. pylori* G27 strain (17). G27 and 26695 strains differ in many aspects including salt sensitivity, the expression level of Lewis antigens, and resistance to acyl-lysyl oligomers (35–37). Because the ability to produce IL-1β can also differ among bacterial strains, this should be confirmed by using isogenic set of *H. pylori* strains. Furthermore, differences in origin of used cells should be considered. In most experiments, we used thioglycollate-elicited neutrophils, BMNs, and HL-60 cells, while in a study by Perez-Figueroa et al. (17), neutrophils purified from healthy donor

blood were used. Cellular responses are likely to be different among these types of cells and, since cells purified from mice or humans are not entirely pure neutrophils, different compositions of contaminated cells can also affect results.

It is remarkable that the FlaA mutant led to less production of IL-1β in response to *H. pylori* in neutrophils, as was confirmed by using two sets of *H. pylori* strains, P1 and 26695. This seems to be specific in neutrophils, because FlaA deficiency did not influence IL-1β production in BMDCs. In addition, we showed that FlaA was required for gene transcription of NLRP3 and IL-1β and cleavage of caspase-1. TLR5 and NLRC4 are two central host receptors for the recognition of bacterial flagellin. TLR5 sensing of flagellin triggers NF-κB activation, followed by the production of pro-inflammatory cytokines (38). Bacterial flagellin can induce IL-1β production in innate immune cells through a NAIP-NLRC4-dependent pathway (39). However, in this study, both TLR5- and NLRC4-deficient neutrophils could produce a comparable level of IL-1β in response to *H. pylori*. In fact, it is known that *H. pylori* FlaA leads to weak activation of TLR5, and its purified flagellin fails to induce IL-8 production and p38 MAPK activation in gastric epithelial cells (40). Moreover, in contrast to *Salmonella typhimurium*, *H. pylori* flagellin could not induce activation of caspase-1 and production of IL-18 and LDH in macrophages, although it induced NLRC4 Ser533 phosphorylation (41). These findings indicate that *H. pylori* flagellin may contribute to production of IL-1β in neutrophils via a TLR5- and NLRC4-independent pathway. Instead, our results suggested that bacterial motility is essential for the production of IL-1β in response to *H. pylori*, as is supported by evidence that centrifuging that enhances bacteria to cell contact abolished the difference of IL-1β level produced by *H. pylori* P1WT and isogenic FlaA mutants and that clinical isolates with high motility produced more IL-1β than those with low motility. Since this phenomenon was seen only in neutrophils, but not BMDCs, a further study should be done to clarify the cell-type specific role of *H. pylori* flagellin in production of IL-1β. Additionally, our results showed that the bacterial motility in neutrophils is involved in both priming and activating NLRP3. It can be suggested as a mechanism, that *H. pylori* motility facilitates cell-to-cell contact, which may enhance NLRP3 priming by activating TLR2 and promote T4SS-mediated NLRP3 activation.

In conclusion, we shows here that *H. pylori* T4SS and flagellin are essential for IL-1β production in neutrophils. TLR2 and NLRP3 inflammasome are central host factors to regulate neutrophil production of IL-1β in response to *H. pylori*. Although not tested in this study, further consideration should be given to other pathways which regulate IL-1β processing in neutrophils. A cytosolic DNA sensor AIM2 is highly expressed in human neutrophils, in addition to NLRP3, and DNA treatment enhances the production of IL-1β in neutrophils (42). *H. pylori* DNA induces activation of TLR9 and secretion of cytokines in DCs (43). Accordingly, it is necessary to clarify whether AIM2 contributes to *H. pylori*-induced IL-1β production in neutrophils, even though it was dispensable in response to *H. pylori* in DCs for IL-1β secretion and caspase-1 processing (16). It should also be considered the involvement of extracellular neutrophil proteases, as they can lead to IL-1β processing in neutrophils through a caspase-1-independent pathway (44).

DATA AVAILABILITY STATEMENT

The raw data supporting the conclusions of this article will be made available by the authors, without undue reservation, to any qualified researcher.

ETHICS STATEMENT

This animal study was reviewed and approved by the Institutional Animal Care and Use Committee of Chonnam National University.

AUTHOR'S NOTE

This manuscript has been released as a Pre-Print at Jang et al. (45).

AUTHOR CONTRIBUTIONS

A-RJ acquired, analyzed, and interpreted data as well as developed study concept and wrote manuscript. M-JK, J-IS, S-WK, J-YP, J-HA, T-SL, D-YK, B-GC, and M-WS contributed to part of the experiments. S-JY and M-KS wrote manuscript. J-HP developed the study concept, obtained funding and ethics, interpreted data, and wrote manuscript. All authors read and approved the final manuscript.

FUNDING

This research was supported by Mid-Career Researcher Program (Grant No. 2018R1A2B3004143) of the National Research Foundation of Korea (NRF) funded by Ministry of Science and ICT (Information and Communication Technologies).

SUPPLEMENTARY MATERIAL

The Supplementary Material for this article can be found online at: https://www.frontiersin.org/articles/10.3389/fimmu.2020.01121/full#supplementary-material

REFERENCES

1. Kusters JG, van Vliet AH, Kuipers EJ. Pathogenesis of *Helicobacter pylori* infection. *Clin Microbiol Rev.* (2006) 19:449–90. doi: 10.1128/cmr.00054-05

2. Schistosomes, liver flukes and *Helicobacter pylori*. IARC working group on the evaluation of carcinogenic risks to humans. Lyon, 7-14 June 1994. *IARC Monogr Eval Carcinog Risks Hum.* (1994) 61:1–241.

3. El-Omar EM, Carrington M, Chow WH, McColl KE, Bream JH, Young HA, et al. Interleukin-1 polymorphisms associated with increased risk of gastric cancer. *Nature.* (2000) 404:398–402. doi: 10.1038/35006081
4. Yang J, Hu Z, Xu Y, Shen J, Niu J, Hu X, et al. Interleukin-1B gene promoter variants are associated with an increased risk of gastric cancer in a Chinese population. *Cancer Lett.* (2004) 215:191–8. doi: 10.1016/j.canlet.2004.07.012
5. Palli D, Saieva C, Luzzi I, Masala G, Topa S, Sera F, et al. Interleukin-1 gene polymorphisms and gastric cancer risk in a high-risk Italian population. *Am J Gastroenterol.* (2005) 100:1941–8. doi: 10.1111/j.1572-0241.2005.50084.x
6. Kumar S, Kumar A, Dixit VK. Evidences showing association of interleukin-1B polymorphisms with increased risk of gastric cancer in an Indian population. *Biochem Biophys Res Commun.* (2009) 387:456–60. doi: 10.1016/j.bbrc.2009.07.033
7. Tu S, Bhagat G, Cui G, Takaishi S, Kurt-Jones EA, Rickman B, et al. Overexpression of interleukin-1beta induces gastric inflammation and cancer and mobilizes myeloid-derived suppressor cells in mice. *Cancer Cell.* (2008) 14:408–19. doi: 10.1016/j.ccr.2008.10.011
8. Huang FY, Chan AO, Lo RC, Rashid A, Wong DK, Cho CH, et al. Characterization of interleukin-1beta in *Helicobacter pylori*-induced gastric inflammation and DNA methylation in interleukin-1 receptor type 1 knockout [IL-1R1(-/-)] mice. *Eur J Cancer.* (2013) 49:2760–70. doi: 10.1016/j.ejca.2013.03.031
9. Shigematsu Y, Niwa T, Rehnberg E, Toyoda T, Yoshida S, Mori A, et al. Interleukin-1beta induced by *Helicobacter pylori* infection enhances mouse gastric carcinogenesis. *Cancer Lett.* (2013) 340:141–7. doi: 10.1016/j.canlet.2013.07.034
10. Bartchewsky W Jr., Martini MR, Masiero M, Squassoni AC, Alvarez MC, Ladeira MS, et al. Effect of *Helicobacter pylori* infection on IL-8, IL-1beta and COX-2 expression in patients with chronic gastritis and gastric cancer. *Scand J Gastroenterol.* (2009) 44:153–61. doi: 10.1080/00365520802530853
11. Man SM, Kanneganti TD. Regulation of inflammasome activation. *Immunol Rev.* (2015) 265:6–21. doi: 10.1111/imr.12296
12. Roman J, Ritzenthaler JD, Fenton MJ, Roser S, Schuyler W. Transcriptional regulation of the human interleukin 1beta gene by fibronectin: role of protein kinase C and activator protein 1 (AP-1). *Cytokine.* (2000) 12:1581–96. doi: 10.1006/cyto.2000.0759
13. He Y, Hara H, Nunez G. Mechanism and regulation of NLRP3 inflammasome activation. *Trends Biochem Sci.* (2016) 41:1012–21. doi: 10.1016/j.tibs.2016.09.002
14. Franchi L, Eigenbrod T, Munoz-Planillo R, Nunez G. The inflammasome: a caspase-1-activation platform that regulates immune responses and disease pathogenesis. *Nat Immunol.* (2009) 10:241–7. doi: 10.1038/ni.1703
15. Kim DJ, Park JH, Franchi L, Backert S, Nunez G. The Cag pathogenicity island and interaction between TLR2/NOD2 and NLRP3 regulate IL-1beta production in *Helicobacter pylori* infected dendritic cells. *Eur J Immunol.* (2013) 43:2650–8. doi: 10.1002/eji.201243281
16. Koch KN, Hartung ML, Urban S, Kyburz A, Bahlmann AS, Lind J, et al. *Helicobacter* urease-induced activation of the TLR2/NLRP3/IL-18 axis protects against asthma. *J Clin Invest.* (2015) 125:3297–302. doi: 10.1172/JCI79337
17. Perez-Figueroa E, Torres J, Sanchez-Zauco N, Contreras-Ramos A, Alvarez-Arellano L, Maldonado-Bernal C. Activation of NLRP3 inflammasome in human neutrophils by *Helicobacter pylori* infection. *Innate Immun.* (2016) 22:103–12. doi: 10.1177/1753425915619475
18. Semper RP, Mejias-Luque R, Gross C, Anderl F, Muller A, Vieth M, et al. *Helicobacter pylori*-induced IL-1beta secretion in innate immune cells is regulated by the NLRP3 inflammasome and requires the cag pathogenicity island. *J Immunol.* (2014) 193:3566–76. doi: 10.4049/jimmunol.1400362
19. Freitas M, Lima JL, Fernandes E. Optical probes for detection and quantification of neutrophils' oxidative burst. A review. *Anal Chim Acta.* (2009) 649:8–23. doi: 10.1016/j.aca.2009.06.063
20. Malech HL, Deleo FR, Quinn MT. The role of neutrophils in the immune system: an overview. *Methods Mol Biol.* (2014) 1124:3–10. doi: 10.1007/978-1-62703-845-4_1
21. Zhao JJ, Pan K, Wang W, Chen JG, Wu YH, Lv L, et al. The prognostic value of tumor-infiltrating neutrophils in gastric adenocarcinoma after resection. *PLoS ONE.* (2012) 7:e33655. doi: 10.1371/journal.pone.0033655
22. Caruso RA, Bellocco R, Pagano M, Bertoli G, Rigoli L, Inferrera C. Prognostic value of intratumoral neutrophils in advanced gastric carcinoma in a high-risk area in northern Italy. *Mod Pathol.* (2002) 15:831–7. doi: 10.1097/01.mp.0000020391.98998.6b
23. Fu H, Ma Y, Yang M, Zhang C, Huang H, Xia Y, et al. Persisting and increasing neutrophil infiltration associates with gastric carcinogenesis and E-cadherin downregulation. *Sci Rep.* (2016) 6:29762. doi: 10.1038/srep29762
24. Kwok T, Zabler D, Urman S, Rohde M, Hartig R, Wessler S, et al. *Helicobacter* exploits integrin for type IV secretion and kinase activation. *Nature.* (2007) 449:862–6. doi: 10.1038/nature06187
25. Forlow SB, Ley K. Selectin-independent leukocyte rolling and adhesion in mice deficient in E-, P-, and L-selectin and ICAM-1. *Am J Physiol Heart Circ Physiol.* (2001) 280:H634–41. doi: 10.1152/ajpheart.2001.280.2.H634
26. Chang HH, Oh PY, Ingber DE, Huang S. Multistable and multistep dynamics in neutrophil differentiation. *BMC Cell Biol.* (2006) 7:11. doi: 10.1186/1471-2121-7-11
27. Su B, Ceponis PJ, Lebel S, Huynh H, Sherman PM. *Helicobacter pylori* activates Toll-like receptor 4 expression in gastrointestinal epithelial cells. *Infect Immun.* (2003) 71:3496–502. doi: 10.1128/iai.71.6.3496-3502.2003
28. Backert S, Selbach M. Role of type IV secretion in *Helicobacter pylori* pathogenesis. *Cell Microbiol.* (2008) 10:1573–81. doi: 10.1111/j.1462-5822.2008.01156.x
29. Franchi L, Amer A, Body-Malapel M, Kanneganti TD, Ozoren N, Jagirdar R, et al. Cytosolic flagellin requires Ipaf for activation of caspase-1 and interleukin 1beta in *salmonella*-infected macrophages. *Nat Immunol.* (2006) 7:576–82. doi: 10.1038/ni1346
30. El-Omar EM, Carrington M, Chow WH, McColl KE, Bream JH, Young HA, et al. The role of interleukin-1 polymorphisms in the pathogenesis of gastric cancer. *Nature.* (2001) 412:99. doi: 10.1038/35083631
31. Figueiredo C, Machado JC, Pharoah P, Seruca R, Sousa S, Carvalho R, et al. *Helicobacter pylori* and interleukin 1 genotyping: an opportunity to identify high-risk individuals for gastric carcinoma. *J Natl Cancer Inst.* (2002) 94:1680–7. doi: 10.1093/jnci/94.22.1680
32. Peek RM, Jr., Fiske C, Wilson KT. Role of innate immunity in *Helicobacter pylori*-induced gastric malignancy. *Physiol Rev.* (2010) 90:831–58. doi: 10.1152/physrev.00039.2009
33. Smith MF Jr., Mitchell A, Li G, Ding S, Fitzmaurice AM, Ryan K, et al. Toll-like receptor (TLR) 2 and TLR5, but not TLR4, are required for *Helicobacter pylori*-induced NF-kappa B activation and chemokine expression by epithelial cells. *J Biol Chem.* (2003) 278:32552–60. doi: 10.1074/jbc.M305536200
34. Bauernfeind F, Niepmann S, Knolle PA, Hornung V. Aging-associated TNF production primes inflammasome activation and nlrp3-related metabolic disturbances. *J Immunol.* (2016) 197:2900–8. doi: 10.4049/jimmunol.1501336
35. Makobongo MO, Kovachi T, Gancz H, Mor A, Merrell DS. *In vitro* antibacterial activity of acyl-lysyl oligomers against *Helicobacter pylori*. *Antimicrob Agents Chemother.* (2009) 53:4231–9. doi: 10.1128/AAC.00510-09
36. Hildebrandt E, McGee DJ. *Helicobacter pylori* lipopolysaccharide modification, Lewis antigen expression, and gastric colonization are cholesterol-dependent. *BMC Microbiol.* (2009) 9:258. doi: 10.1186/1471-2180-9-258
37. Gancz H, Jones KR, Merrell DS. Sodium chloride affects *Helicobacter pylori* growth and gene expression. *J Bacteriol.* (2008) 190:4100–5. doi: 10.1128/JB.01728-07
38. Miao EA, Andersen-Nissen E, Warren SE, Aderem A. TLR5 and Ipaf: dual sensors of bacterial flagellin in the innate immune system. *Semin Immunopathol.* (2007) 29:275–88. doi: 10.1007/s00281-007-0078-z
39. Zhao Y, Shao F. The NAIP-NLRC4 inflammasome in innate immune detection of bacterial flagellin and type III secretion apparatus. *Immunol Rev.* (2015) 265:85–102. doi: 10.1111/imr.12293
40. Gewirtz AT, Yu Y, Krishna US, Israel DA, Lyons SL, Peek RM Jr. *Helicobacter pylori* flagellin evades toll-like receptor 5-mediated innate immunity. *J Infect Dis.* (2004) 189:1914–20. doi: 10.1086/386289
41. Matusiak M, Van Opdenbosch N, Vande Walle L, Sirard JC, Kanneganti TD, Lamkanfi M. Flagellin-induced NLRC4 phosphorylation primes the inflammasome for activation by NAIP5. *Proc Natl Acad Sci USA.* (2015) 112:1541–6. doi: 10.1073/pnas.1417945112

42. Bakele M, Joos M, Burdi S, Allgaier N, Poschel S, Fehrenbacher B. Localization and functionality of the inflammasome in neutrophils. *J Biol Chem.* (2014) 289:5320–9. doi: 10.1074/jbc.M113.505636
43. Rad R, Ballhorn W, Voland P, Eisenacher K, Mages J, Rad L, et al. Extracellular and intracellular pattern recognition receptors cooperate in the recognition of *Helicobacter pylori*. *Gastroenterology.* (2009) 136:2247–57. doi: 10.1053/j.gastro.2009.02.066
44. Clancy DM, Sullivan GP, Moran HBT, Henry CM, Reeves EP, McElvaney NG, et al. Extracellular neutrophil proteases are efficient regulators of IL-1, IL-33, and IL-36 cytokine activity but poor effectors of microbial killing. *Cell Rep.* (2018) 22:2937–50. doi: 10.1016/j.celrep.2018.02.062
45. Jang AR, Kang MJ, Shin JI, Kwon SW, Park JY, Ahn JH, et al. Unveiling the crucial role of type IV secretion system and motility of *Helicobacter pylori* in IL-1β production via NLRP3 inflammasome activation in neutrophils. *bioRXiv [Preprint].* doi: 10.1101/733790

Conflict of Interest: The authors declare that the research was conducted in the absence of any commercial or financial relationships that could be construed as a potential conflict of interest.

frontiers in Immunology

ORIGINAL RESEARCH
published: 30 June 2020
doi: 10.3389/fimmu.2020.01361

A Novel Cecropin-LL37 Hybrid Peptide Protects Mice Against EHEC Infection-Mediated Changes in Gut Microbiota, Intestinal Inflammation, and Impairment of Mucosal Barrier Functions

Xubiao Wei[1], *Lulu Zhang*[1], *Rijun Zhang*[1]*, *Matthew Koci*[2], *Dayong Si*[1], *Baseer Ahmad*[1], *Junhao Cheng*[1], *Junyong Wang*[1], *Maierhaba Aihemaiti*[1] *and Manyi Zhang*[1]

[1] *Laboratory of Feed Biotechnology, State Key Laboratory of Animal Nutrition, College of Animal Science and Technology, China Agricultural University, Beijing, China,* [2] *Prestage Department of Poultry Science, College of Agriculture and Life Sciences, North Carolina State University, Raleigh, NC, United States*

OPEN ACCESS

Edited by:
Elba Mónica Vermeulen, Academia Nacional de Medicina CABA, Argentina

Reviewed by:
Philip Sherman, University of Toronto, Canada
Rashika El Ridi, Cairo University, Egypt

***Correspondence:**
Rijun Zhang
rjzhang@cau.edu.cn

Specialty section:
This article was submitted to Mucosal Immunity, a section of the journal Frontiers in Immunology

Received: *18 November 2019*
Accepted: *28 May 2020*
Published: *30 June 2020*

Citation:
Wei X, Zhang L, Zhang R, Koci M, Si D, Ahmad B, Cheng J, Wang J, Aihemaiti M and Zhang M (2020) A Novel Cecropin-LL37 Hybrid Peptide Protects Mice Against EHEC Infection-Mediated Changes in Gut Microbiota, Intestinal Inflammation, and Impairment of Mucosal Barrier Functions. Front. Immunol. 11:1361. doi: 10.3389/fimmu.2020.01361

Intestinal inflammation can cause impaired epithelial barrier function and disrupt immune homeostasis, which increases the risks of developing many highly fatal diseases. Enterohemorrhagic *Escherichia coli* (EHEC) O157:H7 causes intestinal infections worldwide and is a major pathogen that induces intestinal inflammation. Various antibacterial peptides have been described as having the potential to suppress and treat pathogen-induced intestinal inflammation. Cecropin A (1–8)-LL37 (17–30) (C-L), a novel hybrid peptide designed in our laboratory that combines the active center of C with the core functional region of L, shows superior antibacterial properties and minimized cytotoxicity compared to its parental peptides. Herein, to examine whether C-L could inhibit pathogen-induced intestinal inflammation, we investigated the anti-inflammatory effects of C-L in EHEC O157:H7-infected mice. C-L treatment improved the microbiota composition and microbial community balance in mouse intestines. The hybrid peptide exhibited improved anti-inflammatory effects than did the antibiotic, enrofloxacin. Hybrid peptide treated infected mice demonstrated reduced clinical signs of inflammation, reduced weight loss, reduced expression of pro-inflammatory cytokines [tumor necrosis factor-alpha (TNF-α), interleukin-6 (IL-6), and interferon-gamma (IFN-γ)], reduced apoptosis, and reduced markers of jejunal epithelial barrier function. The peptide also affected the MyD88–nuclear factor κB signaling pathway, thereby modulating inflammatory responses upon EHEC stimulation. Collectively, these findings suggest that the novel hybrid peptide C-L could be developed into a new anti-inflammatory agent for use in animals or humans.

Keywords: enrofloxacin, *Escherichia coli*, hybrid peptide, inflammation, microflora, mucosal barrier, O157:H7

INTRODUCTION

Commensal microflora in the intestinal mucosal can promote intestinal stability and prevent pathogens from invading the intestine. However, when the balance of intestinal microbiota is disturbed, the intestinal defense function and immunoregulatory functions dramatically decrease, which can cause intestinal inflammation (1–5). Intestinal inflammation is a defensive response to stimulation of the host by microbiological toxins or pathogens (1–4). Although a controlled inflammatory response is beneficial, it can become detrimental if the response fails to eliminate the pathogen or the inflammatory process persists for an extended period of time (6).

Within the intestinal epithelium, the mucosal barrier plays an important role in maintaining physiological homeostasis by physically blocking the passage of harmful foreign antigens, microbes, and their toxins into the host (5, 7). When this barrier function breaks down the intestinal contents and bacteria can diffuse past the mucosal layer, which can initiate host responses that lead to further break down of the epithelia barrier resulting in activation of the intestinal inflammatory response (5, 7). While not all bacteria induce inflammatory diseases, intestinal pathogens like enterohemorrhagic *E. coli* (EHEC) O157:H7 induce a particularly acute and potentially fatal infection if left untreated (8, 9). Even with treatment EHEC O157:H7 infection can lead to hemolytic-uremic syndrome and permanent kidney damage, especially in young children (8, 9).

Short-term, appropriate application of antibiotics is an option to reduce the intestinal bacterial load and intestinal inflammatory disease severity caused by overgrowth of pathogenic bacteria (10–14). Historically, the broad-spectrum antibiotic enrofloxacin (Enro) has been used to treat diseases during previous decades (10–13). However, antibiotic resistance has become a serious global issue and is steadily increasing worldwide in almost every species treated with antibiotics (15, 16). Also of increasing concern, long-term antibiotic treatment can alter the microecosystem balance by causing compositional changes in the intestinal microbiota and may lead to a homeostatic imbalance by altering the expression of tight junction proteins, mucin, antimicrobial peptides, and cytokines in intestinal epithelial cells (17, 18). Thus, it is necessary to explore novel safe antibiotic alternatives for inflammation therapy.

Recent findings suggest that specific antibacterial peptides (AMPs) elicit certain anti-inflammatory effects (19–24); specifically, Cecropin A (C) (19) and LL37 (L) (20). Previously, we generated a hybrid peptide, Cecropin A (1–8)-LL37 (17–30) (C-L), by combining the N-terminal cationic hydrophobic fragment of C with the core functional region of L and examined its properties (25). As compared to the parental peptides (C and L), the hybrid C-L peptide exhibited excellent antibacterial properties and was more effective against gram-positive and gram-negative bacteria (25). These results demonstrate that the hybrid C-L peptide may serve as a potential antibacterial pharmaceutical agent. Hence an important question arises as to whether the C-L peptide can prevent or attenuate intestinal inflammation induced by harmful gut bacteria while killing them.

In this study, we investigated whether the C-L peptide could provide effective therapy against intestinal inflammation and impairment of epithelial barrier function induced by EHEC O157:H7 and explore the underlying mechanisms, using a mouse model of intestinal inflammation.

MATERIALS AND METHODS

Peptide Synthesis

The C-L peptide (KWKLFKKIFKRIVQRIKDFLRN) was chemically synthesized (95% purity) by KangLong Biochemistry (Jiangsu, China). The molecular weight of the C-L peptide was confirmed using a Thermo Finnigan LCQ ion-trap mass spectrometer (Thermo Finnigan, CA, USA). The peptide was then suspended in endotoxin-free water and stored at −80°C.

Animal Model

Seventy-two C57/BL6 female mice (4 weeks of age) were purchased from Charles River Laboratories (Beijing, China) and maintained under standard conditions. The animal experiments were conducted with the approval of the China Agricultural University Animal Care and Use Committee (Beijing, China).

All animals had free access to feed and fresh water during the experimental period. EHEC O157:H7 (ATCC43889) strain was purchased from China Veterinary Culture Collection Center (Beijing, China) and cultured in Luria–Bertani (LB) broth. Mice were randomly divided into the following six groups ($n = 12$): the control, EHEC, EHEC+Enro, EHEC+C-LL (EHEC+low dose of C-L), EHEC+C-LM (EHEC+moderate dose of C-L), and EHEC+C-LH (EHEC+high dose of C-L) groups. The control group was orally administered 100 μL sterile phosphate-buffered saline (PBS); the EHEC group was orally administered 100 μL sterile PBS containing 1×10^8 colony-forming units (CFUs) EHEC O157:H7; the EHEC+Enro group was orally administered 100 μL sterile PBS containing 1×10^8 CFUs EHEC O157:H7 and then treated by intraperitoneal (i.p.) injection with 8 mg/kg Enro once/day for 3 days; the EHEC+C-LL, EHEC+C-LM, and EHEC+C-LH groups were administered 100 μL sterile PBS containing 1×10^8 CFUs EHEC O157:H7 and then treated by i.p. injection with 4, 8, and 16 mg/kg C-L, respectively, once/day for 3 days. After 3 days, the mice were euthanized, and tissues were collected for analysis. The method used in this section is similar to that previously presented by Zhang et al. (26) and Wang et al. (27). Before and after the study, the body weights of mice were confirmed and recorded.

Microbial Composition Analysis

Total bacterial DNA was extracted using cecal samples collected from the control, EHEC, EHEC+Enro, and EHEC+C-LM groups with the EZNA Stool DNA Kit (Omega Bio-tek, Norcross, GA, United States) according to the manufacturer's protocols. The DNA purity and yield were quantified using a NanoDrop 8000 spectrophotometer (Thermo Fisher Scientific, Scoresby, Australia). The V4 region of the bacterial 16S rRNA gene was amplified from the genome of cecal samples using the 515F (5′-GTGCCAGCMGCCGCGGTAA-3′) and 806R (5′-XXXXXXGGACTACHVGGGTWTCTAAT-3′) primer pair.

All samples were sequenced on the Illumina MiSeq platform, according to standard protocols. Paired-end reads from the original DNA fragments were analyzed using fast-length adjustment of short reads (FLASH) software, version 1.2.8 (http://ccb.jhu.edu/software/FLASH). Operational taxonomic units (OTUs) were clustered using UPARSE (version 7.1, https://drive5.com/uparse/) at a 97% similarity level. Ribosomal Database Project (RDP) classifiers were applied to distribute 16S rRNA gene sequences into distinct taxonomic categories by aligning representative sequences with taxonomically annotated sequences.

Induction of Intestinal Inflammation and Assessment of the Disease Activity Index (DAI)

EHEC-induced intestinal inflammation was assessed by determining the DAI, as described previously (23, 28). The DAI was determined as the sum of scores assigned for the body weight, stool consistency, and occult blood in the stool. Regarding body weights, the following scores were assigned: 0 for mice showing no weight loss, 1 for mice with 1–5% weight loss, 2 for mice with for 5–10% weight loss, 3 for mice with 10–20% weight loss, and four for mice with more than 20% weight loss. Stool consistency was scored as follows: 0, well-formed pellets; 2, pasty and semi-formed stools that did not adhere to the anus; and 4, liquid stools that adhered to the anus. For occult blood, a score of 0 was assigned for no blood, 2 was assigned for occult blood, and 4 was assigned for gross bleeding. For each mouse, the sum of these scores was divided by three, resulting in DAIs ranging from 0 (healthy) to 4 (maximal intestinal inflammation).

Histopathology and Immunohistochemistry

Full-thickness sections of the middle jejunum were excised, dissected longitudinally, fixed immediately in 4% paraformaldehyde solution, and embedded in paraffin (26, 27). Samples were cut into 5-μm-thick sections, mounted on slides, and stained with hematoxylin and eosin (H&E). The epithelial morphological characteristics were observed microscopically (RM2235, Leica, Wetzlar, Germany). Chiu's scores were determined under blinded conditions using a histologic injury scale, as previously described (29, 30).

To prevent nonspecific binding during immunohistochemical analysis of CD177 expression, samples were blocked with PBS for 1 h containing 1% w/v bovine serum albumin (BSA) and incubated overnight at 4°C with anti-CD177 antibodies (Santa Cruz Biotechnology, CA, USA) at a dilution of 1:100. After washing three times with PBS, the samples were treated with horseradish peroxidase (HRP)-conjugated rabbit anti-goat IgG (Santa Cruz Biotechnology) at a ratio of 1:100. The samples were incubated at 4°C for 1 h and washed three times with PBS. Subsequently, the sections were treated with 3,3′-diaminobenzidine (DAB) substrate (50–100 μL; DAKO, Carpinteria, CA, USA) and stained with Harris hematoxylin. Finally, the samples were dehydrated with an alcohol gradient (70–100%), and xylene was used to increase the transparency of the slides. A neutral balsam was applied for mounting.

The apoptotic cells in the jejunal sections were detected via the terminal deoxynucleotidyl transferase dUTP nick-end labeling (TUNEL) method using a TUNEL staining kit (Roche, Indianapolis, IN, USA) according to the manufacturer's instructions. The sections were co-stained with the 4′,6-diamidino-2-phenylindole (DAPI; Servicebio, Wuhan, China), and the number of apoptotic cells was counted in 4–6 randomly selected fields at 200× magnification.

Cytokine and Myeloperoxidase (MPO)-Activity Assay

Interleukin-6 (IL-6), interferon-gamma (IFN-γ), and tumor necrosis factor (TNF-α) levels were qualified in the jejunum, using commercial enzyme-linked immunosorbent assay (ELISA) kits (eBioscience, San Diego, CA, USA). The MPO activities in the jejunum were determined using an ELISA kit (Boster, Wuhan, China). Samples were assessed according to the manufacturers' instructions.

Western Blotting

Jejunum tissues were ground and lysed using a Total Protein Extract Kit (KeyGEN Biotech, Nanjing, China) according to manufacturer's instructions. Proteins in each supernatant were separated by 10% sodium dodecyl sulfate-polyacrylamide gel electrophoresis and transferred onto a nitrocellulose membrane. Next, the membranes were blocked with 5% (w/v) skim dried milk proteins in 0.05% (w/v) TBST and immunoblotted overnight with primary antibodies against nuclear factor-κ-gene binding (NF-κB; p65), phospho-NF-κB (p-NF-κB; p-p65), inhibitory subunit of NF-κB (IκB)-α, phosphor-IκB-α (p-IκB-α), inhibitor of NF-κB kinase (IKK)-β, phosphor-IKK-β (p-IKK-β), ZO-1, occluding, or β-actin (Santa Cruz, CA, USA) at 4°C. After washing with TBST, the proteins of interest were labeled with HRP-conjugated secondary antibodies (HuaAn, Hangzhou, China) for 1 h. Bands were detected using the SuperSignal West Femto maximum sensitivity substrate (Pierce Biotechnology, Rockford, Illinois, USA).

Electrophysiology Measurements

The transepithelial-electrical resistance (TEER) values of intestinal membranes were evaluated using an *in vitro*-diffusion chamber method and stripped mice jejunal membranes. After removing the underlying muscularis of the intestinal membranes, the intestinal segments were mounted in a diffusion chamber (World Precision Instruments; Narco Scientific, Mississauga, Ontario, Canada) equipped with two pairs of Ag/AgCl electrodes connected to the chambers via 3 M KCl/3.5% agar bridges. This method was used to identify and quantify the potential difference (PD), short-circuit current (Isc), and total electrical resistance (RT). Electrical resistance was calculated according to Ohm's law (Equation 1) (31):

$$RT = \mathrm{PD}/\mathrm{Isc} \quad (1)$$

Immunofluorescence Analysis of Tight Junction (TJ) Proteins

The expression level of the intercellular TJ protein zonula occludens-1 (ZO-1) was detected. Nonspecific binding sites were blocked with PBS containing 1% w/v BSA for 30 min at 25°C. The samples were incubated with an anti-ZO-1 antibody (Santa Cruz Biotechnology) overnight at 4°C. The slices were washed several times with PBS, followed by incubation with a tetramethylrhodamine isothiocyanate-conjugated secondary antibody (Santa Cruz Biotechnology) at a ratio of 1:100 for 1 h at 25°C in the dark. Nuclei were stained with DAPI. For the mounting of the samples onto slides, Glycerol was used. Images were acquired with a fluorescence microscope (BZ-800; Keyence, Osaka, Japan).

Transmission Electron Microscopy (TEM)

Epithelial cell junctions and microvilli were characterized by TEM. For TEM processing, jejunum tissues were fixed with 2.5% glutaraldehyde. After washing, the samples were treated with 2% osmium tetroxide buffer and then placed in 0.5% aqueous uranyl acetate. The tissue sections were washed with 50% alcohol and then dehydrated using a graded ethanol series. Samples were embedded in eponate. Serial ultrathin sections were cut and imaged on a TEM (H-7650, Hitachi, Japan).

Bacterial Transfer During EHEC Infection

After the mice were treated as described in section Animal Model above, 10 mice each from the control, EHEC, EHEC+Enro, and EHEC+C-LM groups were randomly selected. The mice were euthanized, and their livers and spleens were collected and homogenized in cold PBS. The amount of CFUs were quantified by plating serial dilutions on Luria–Bertani agar plates.

Statistics

The data are presented as mean ± standard deviation from a minimum of three independent experiments. Statistical comparisons were carried out using Student's *t*-tests and one-way analysis of variance using GraphPad Prism v6 software (La Jolla, California). A $P \leq 0.05$ was considered as significant. NS: $P > 0.05$, $^{*}P \leq 0.05$, $^{**}P \leq 0.01$, $^{***}P \leq 0.001$, $^{****}P \leq 0.0001$.

RESULTS

C-L Treatment Improved the Microbiota Composition and Microbial Community Balance in Mouse Intestines

We examined the effects of EHEC infection, with and without C-L and Enro treatment on the microbiota composition in mouse ceca by Illumina sequencing of the 16S rRNA V4 region. A Venn diagram was constructed to show the numbers of common and unique OTUs (**Figure 1A**) (32). The unique OTUs in the control, EHEC, EHEC+Enro, and EHEC+C-LM groups were 42, 23, 19, and 34, respectively; the total number of OTUs in each sample was 523, 489, 423, and 498, respectively. Thus, the ratios of unique to total OTUs were 8, 4.7, 4.4, and 6.8%, respectively (**Figure 1A**). Firmicutes, Bacteroidetes, Verrucomicrobia, and Proteobacteria were the four most abundance bacterial phyla among all groups, and both C-L and Enro reduced EHEC-dependent Proteobacteria induction and overcame EHEC-induced Firmicutes and Bacteroidetes downregulation (**Figure 1B**). At the genus level, 35 genera were identified (**Figure 1C**). *Lactobacillus*, *Prevotellaceae*, and *Akkermansia* species were the most prominent in the control, EHEC+Enro, and EHEC+C-LM groups. EHEC infection lead to a significant increase of *Peptoclostridium*, *Escherichia-Shigella*, *Klebsiella*, *Lachnoclostridium*, *Coprobacillus*, *Blautia*, and *Lachnospiraceae* species, C-L and Enro administration significantly downregulated these species, and C-L showed stronger downregulation than Enro (**Figure 1C**). Additionally, using nonmetric multidimensional scaling analysis, we found that samples of the EHEC+Enro group formed a unique cluster and separated from the other groups (**Figure 1D**), suggesting that Enro may adversely affect the microbial composition.

Effect of C-L on the Body Weight and DAI

Based on the body weight and DAI data, we concluded that the mouse intestinal inflammation model was successfully established (**Figure 2**). As expected, Mice in the EHEC-treated group had significantly more weight loss than did those in the control group, whereas mice in other groups had less weight loss compared with mice in the EHEC-treated group (**Figure 2A**). Notably, mice in the C-L plus EHEC groups demonstrated less weight loss as compared to the EHEC group, in the case of C-LM and C-LH less weight loss than the Enro control. In addition to body weight loss, EHEC infection induced several other gross clinical changes. All of these clinical signs (weight loss, blood in the perianal region, and the presence of diarrhea) were scored and the scores combined into a DAI to holistically assess the impact C-L treatment had on EHEC induced disease. In contrast with the EHEC-treated group, which showed a significantly higher DAI value than the control group, mice in the EHEC+C-LM group apparently recovered, as reflected by the reduced DAI value. Furthermore, the DAI value of the EHEC+C-LM group was markedly lower than that of the EHEC+Enro group (**Figure 2B**).

The Protective Effects of C-L Against EHEC-Induced Damage in Intestinal Tissue

EHEC infection lead to damage to the jejunal epithelium and intestinal inflammation (**Figure 3**). H&E staining of jejunum tissue revealed EHEC infection caused considerable villi blunting, thicker serosa, infiltration of lymphocytes, and edema (**Figure 3A**). In contrast, tissues sections from mice treated with peptide or antibiotic were observed to have reduced signs of damage to the epithelium (**Figure 3A**).

As shown in **Figure 3B**, the villus height/crypt depth ratio (V/C) in the EHEC-infected group decreased markedly as compared to the control group. In contrast, mice in the EHEC+Enro, EHEC+C-LM, and EHEC+C-LH groups had significantly higher V/C values than mice in the EHEC group. Moreover, the C-L peptide more potently improved the V/C ratio than did Enro at the same concentration. Additionally, no differences were detected between the EHEC-infected group and the EHEC+C-LL group (**Figure 3B**). Chiu's score in the

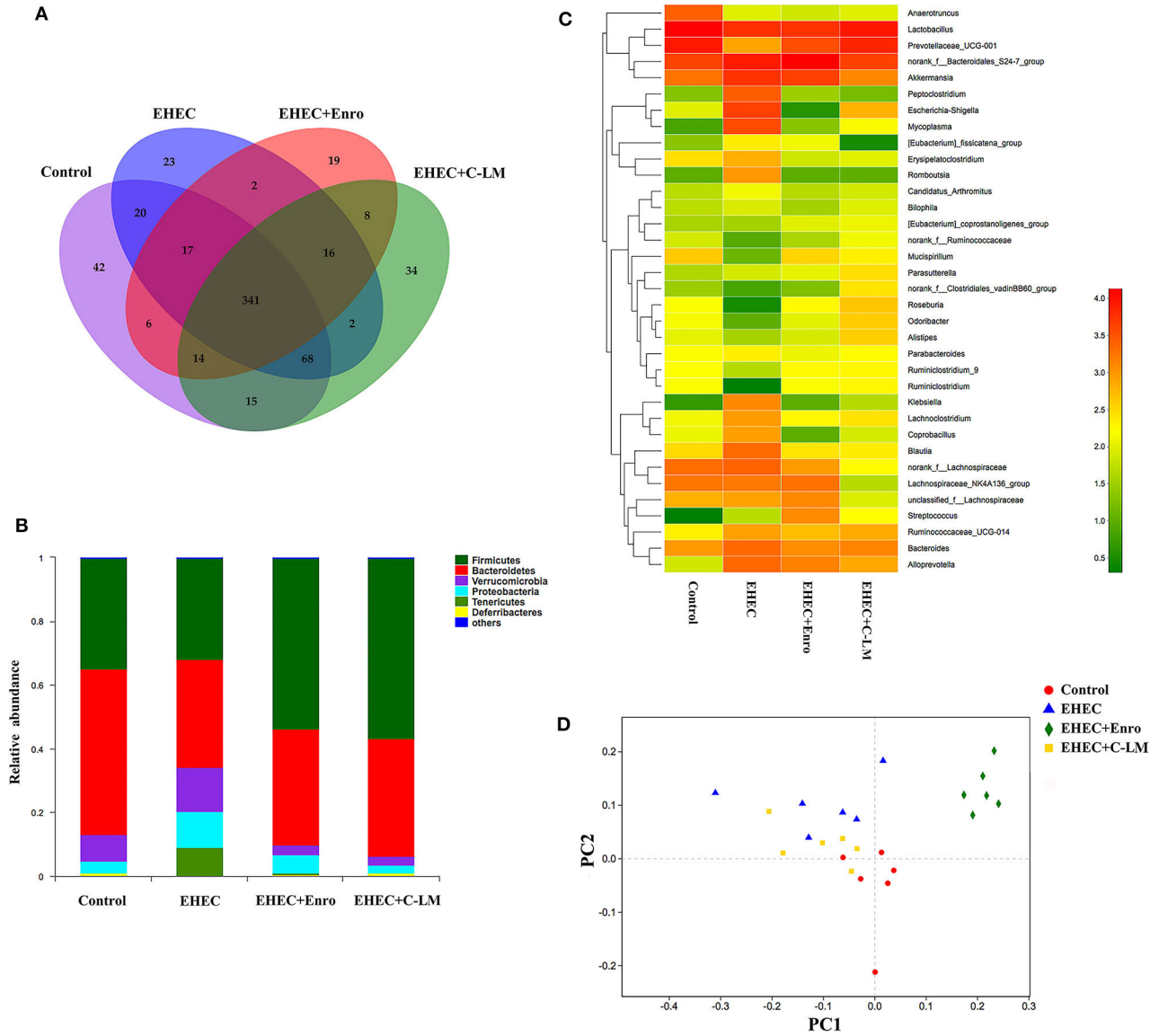

FIGURE 1 | C-L improved the microbiota composition and microbial community balance in mouse intestines. The cecal microbial communities in mice were investigated by 16S rRNA gene sequencing, using the Illumina platform ($n = 6$). **(A)** Venn diagram showing the unique and common OTUs in the mouse intestine. **(B)** Relative abundance of the most abundant bacterial phyla. **(C)** Heat map constructed with the top 35 genera. **(D)** Nonmetric multidimensional scaling based on the OTU levels. The control group was orally administered 100 μL sterile PBS; the EHEC group was orally administered 100 μL sterile PBS containing 1×10^8 CFUs EHEC O157:H7; the EHEC+Enro and EHEC+C-LM groups were administered 100 μL sterile PBS containing 1×10^8 CFUs EHEC O157:H7 and then treated by i.p. injection with 8 mg/kg Enro and C-L, respectively, once/day for 3 days.

C-LM-treated group was also markedly lower than that in the antibiotic-treated group. Overall, our data indicated that C-L treatment significantly attenuated EHEC-induced intestinal damage (**Figure 3C**).

To evaluate the inhibitory effects of C-L and Enro on the EHEC-induced inflammatory response, the expression levels of the pro-inflammatory cytokines TNF-α (**Figure 4A**), IL-6 (**Figure 4B**), and IFN-γ (**Figure 4C**) in mice jejunum tissues were measured by ELISA. As shown in **Figures 4A–C**, the TNF-α, IL-6, and IFN-γ levels in the EHEC+C-LM and EHEC+Enro groups were significantly lower than those in the EHEC-infected group. In addition, mice that were infected with EHEC in the presence of 8 mg/kg C-L (C-LM) showed markedly lower TNF-α, IL-6, and IFN-γ expression than Enro-treated mice.

Immunohistochemical analysis demonstrated that mice treated with C-L (8 or 16 mg/kg) or Enro, the EHEC-infected group had significantly lower neutrophil infiltration than the group infected with EHEC alone (**Figure 4D**). These qualitative observations were then verified using a quantitative MPO ELISA to assay for MPO levels in the jejunum. These results

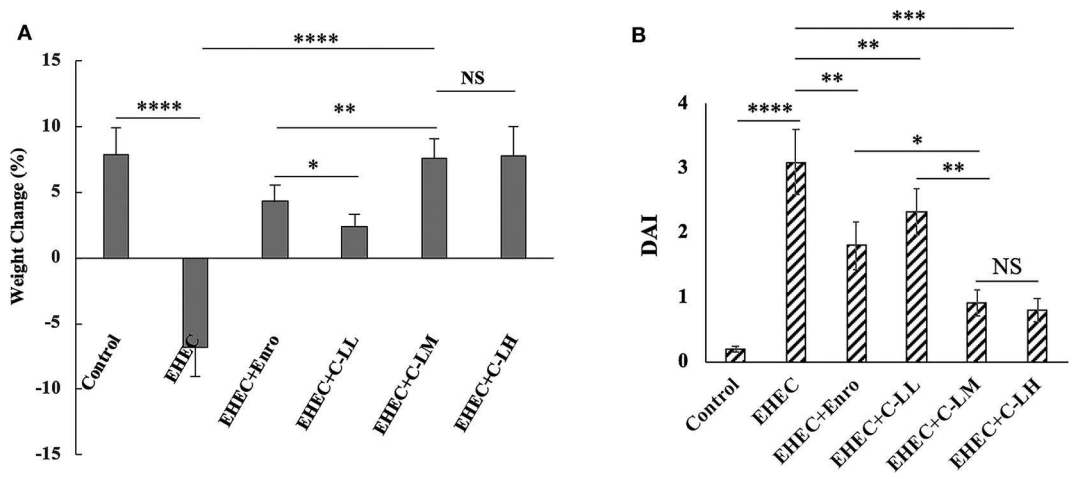

FIGURE 2 | Effect of C-L on the body weight **(A)** and DAI **(B)**. The EHEC+C-LL, EHEC+C-LM, EHEC+C-LH, and EHEC+Enro groups were orally administered 100 μL sterile PBS containing 1×10^8 CFUs EHEC O157:H7 and then treated by i.p. injection with 4, 8 mg/kg, or 16 mg C-L/kg body weight C-L, or 8 mg Enro/kg body weight, respectively, once/day for 3 days. The control and EHEC groups were orally administered 100 μL sterile PBS or 100 μL sterile PBS containing 1×10^8 CFUs EHEC O157:H7, respectively, without any follow-up treatments. The DAI value was derived from scores relating to weight loss, stool consistency, and occult blood. The data are shown as the mean ± standard deviation ($n = 12$). NS, $P > 0.05$; *$P \leq 0.05$; **$P \leq 0.01$; ***$P \leq 0.001$; ****$P \leq 0.0001$.

demonstrate a clear increased in MPO in EHEC-infected mice as compared with control mice, with reduced levels of MPO in conjunction with C-L or Enro treatment, most notably in the EHEC+C-LM and EHEC+C-LH groups (**Figure 4E**).

Jejunum tissue sections were analyzed by TUNEL staining to assay for changes in EHEC induced apoptosis (**Figure 5**). These results demonstrate a significant increase in apoptosis (green signals) in the EHEC-infected group as compared to the control group (**Figure 5**). Compared with the EHEC-infected group, C-L or Enro treated mice had significantly lower apoptotic indices (**Figure 5B**). Notably, the apoptosis index in mice treated with C-LM was similar to that in mice treated with C-LH, which was significantly lower than those for the mice in the Enro- and C-LL-treated groups (**Figure 5B**).

The Effects of C-L on The MyD88–NF-κB Signaling Pathway in EHEC-Infected Mice

To investigate the mechanism of C-L in modulating intestinal inflammation in mice stimulated with EHEC, the MyD88–NF-kB-signaling was examined (**Figure 6**). MyD88 levels and IKK-β, NF-κB (p65), and IκB-α phosphorylation in the jejunum increased significantly after infection with EHEC (**Figures 6A,B**). In contrast, the results showed that MyD88 expression and IKK-β, NF-κB, and IκB-α phosphorylation were suppressed in the jejunum following C-L treatment.

C-L Prevented EHEC-Induced Disruption of The Intestinal TJ Structure and Function

To characterize the effects of C-L on the functional integrity of the mouse intestinal epithelium, TEER values were evaluated over a 60 min period (**Figure 7A**). EHEC infection reduced the TEER values remarkably, indicating that permeability had increased. In contrast, tissues from C-LM or C-LH treated mice demonstrated TEER values ∼80% of the control, confirming the role of C-L activation in minimizing EHEC-induced intestinal epithelial damage (**Figure 7A**). Tissues from Enro treated mice also demonstrated higher TEER values than the EHEC alone group, but its effect was significantly less than C-LM.

The expressions of specific TJ marker proteins (e.g., occluding and ZO-1) were analyzed by western blotting to further assess the impact of EHEC-induced damage to epithelial barrier function, and to what extent C-L treatment might ameliorate that damage (**Figure 7B**). TJ marker expression levels were downregulated in mice infected with EHEC alone, compared with control animals. Notably, treatment with C-LM and C-LH appeared to prevent the ZO-1 and occludin change in expression following EHEC-infection, whereas the expression levels of these TJ markers in the EHEC+Enro group was significantly lower than the EHEC+C-LM group (**Figure 7B**). These protective effects were further verified by immunofluorescent examination of the jejunum tissue (**Figure 7C**). EHEC infection significantly decreased occludin expression compared with the control group, whereas C-L treatment (8 mg/kg in particular) markedly increased occludin protein expression (**Figure 7C**).

Consistently, the tight junctions between the intestinal epithelial cells were verified by TEM, and these results confirmed that C-L protected against EHEC-induced damage in jejunum tissues (**Figure 7D**).

C-L Decreased EHEC-Induced Bacterial Transfer

EHEC infection significantly increased the transfer of bacteria to the spleen and liver compared to the control group, which was effectively attenuated by Enro or C-L treatment (**Figure 8**). In addition, C-L was more effective than Enro at the same concentration.

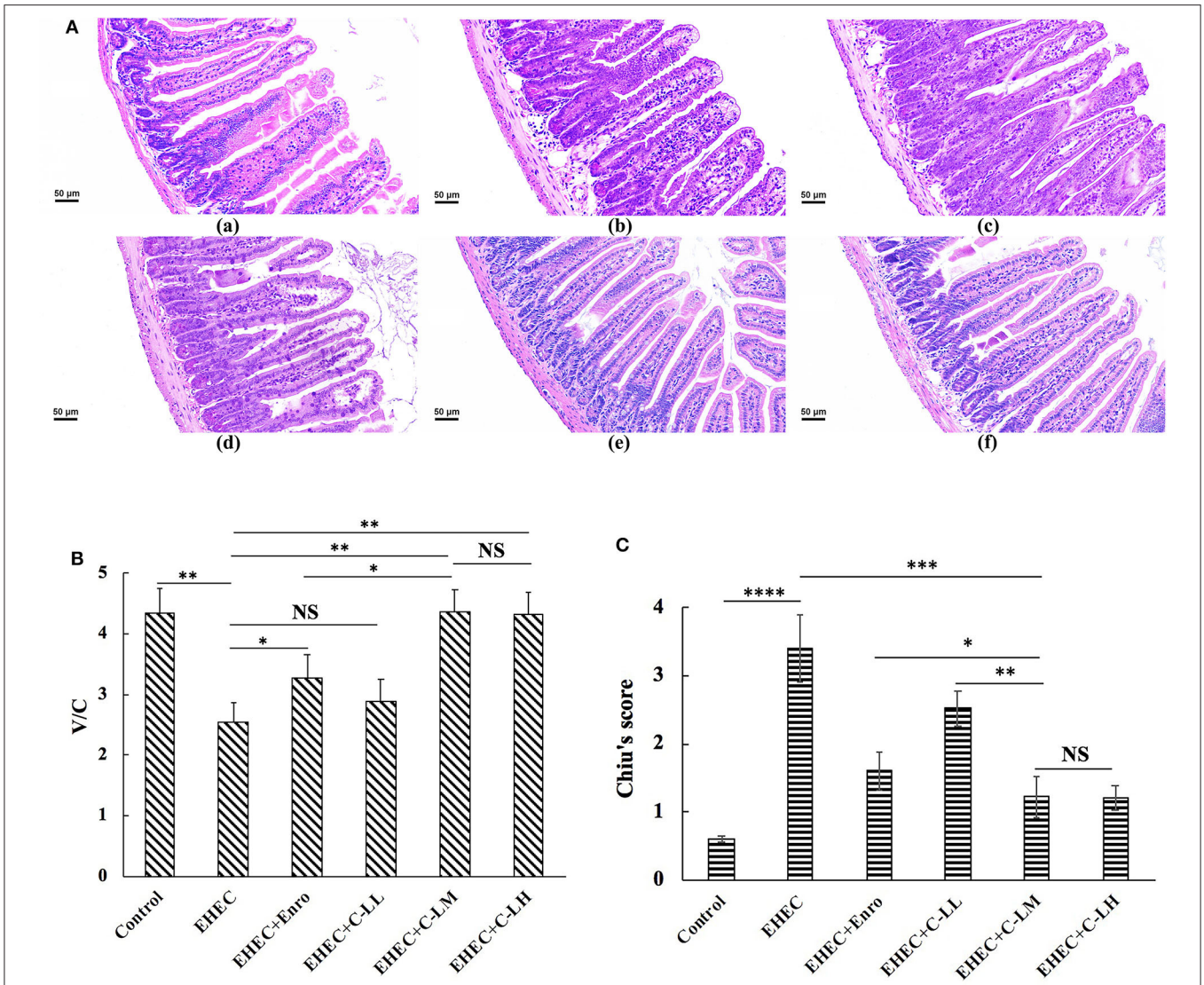

FIGURE 3 | The protective effects of C-L against EHEC-induced clinical symptoms in the mouse jejunum. Representative H&E-stained sections from mice in the (**A**-a) control, (**A**-b) EHEC, (**A**-c) EHEC+Enro, (**A**-d) EHEC+C-LL, (**A**-e) EHEC+C-LM, and (**A**-f) EHEC+C-LH groups. Scale bar, 50 μm. **(B)** The effect of C-L on the jejunum V/C ratio. **(C)** The effect of C-L on Chiu's score. The control group was orally administered 100 μL sterile PBS; the EHEC group was orally administered 100 μL sterile PBS containing 1×10^8 CFUs EHEC O157:H7; the EHEC+Enro group was orally administered 100 μL sterile PBS containing 1×10^8 CFUs EHEC O157:H7 and then treated by i.p. injection with 8 mg/kg Enro once/day for 3 days; the EHEC+C-LL, EHEC+C-LM, and EHEC+C-LH groups were administered 100 μL sterile PBS containing 1×10^8 CFUs EHEC O157:H7 and then treated by i.p. injection with 4, 8, and 16 mg/kg C-L, respectively, once/day for 3 days. The data are shown as the mean ± standard deviation ($n = 8$). NS, $P > 0.05$; *$P \leq 0.05$; **$P \leq 0.01$; ***$P \leq 0.001$; ****$P \leq 0.0001$.

DISCUSSION

Bacterial infection is responsible for many serious and fatal diseases. Bacteria can elicit mucosal immune responses, and if unresolved can lead to a breakdown in mucosal homeostasis and inflammation (2). Microbial pathogens, such as EHEC, could induce severe intestinal inflammation leading to severe systemic complications (3, 8, 9). Antibiotics, such as Enro (10–13), have been commonly used to treat inflammation, based on their antibacterial activities (33). However, as the incidence of antibiotic-resistant increases worldwide (34, 35), the need to develop new classes of anti-inflammatory compounds to fight tissue inflammation also increases.

Previously, it was reported that specific AMPs elicit anti-inflammatory effects (19–23), such as C (19) and L (20). These AMPs merit consideration as clinical alternatives against the rising threat of inflammation. Hybridization is a novel method for designing new peptides to combine the advantages of different native peptides. The novel hybrid peptide C-L, designed in our laboratory, showed significantly increased antimicrobial activity and minimized cytotoxicity, compared to the parental peptides (C and L), suggesting that it has tremendous potential for use as a novel anti-inflammatory agent (25).

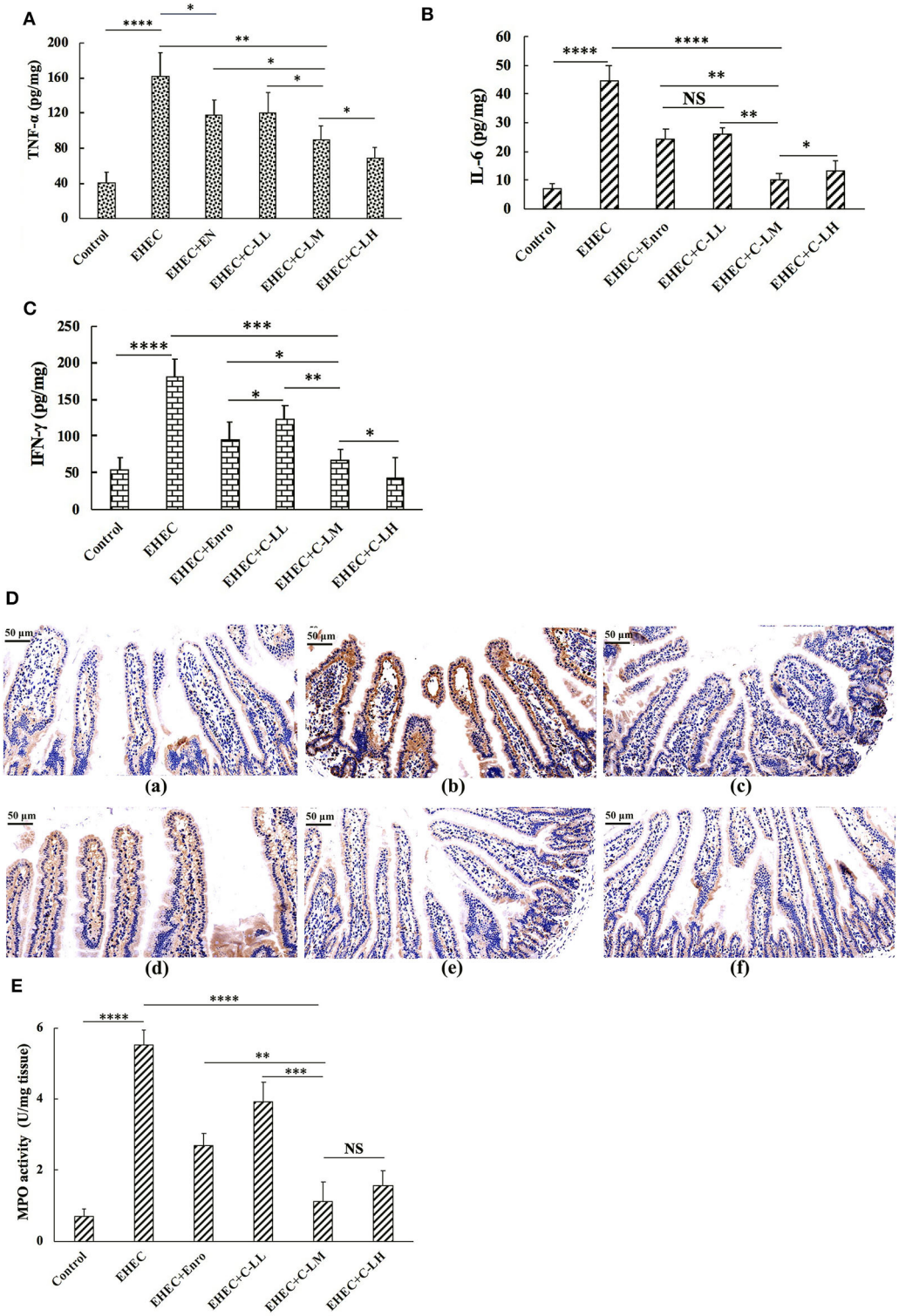

FIGURE 4 | The protective effects of C-L on inflammatory response. The expression levels of TNF-α **(A)**, IL-6 **(B)**, and IFN-γ **(C)** in mouse jejunum tissues were measured by ELISA. **(D)** Representative images of CD177^{+} cells in the (**D**-a) control, (**D**-b) EHEC, (**D**-c) EHEC+Enro, (**D**-d) EHEC+C-LL, (**D**-e) EHEC+C-LM, and (**D**-f) EHEC+C-LH groups. Scale bar, 50 μm. Enzymatic activities of MPO were measured **(E)**. The control group was orally administered 100 μL sterile PBS; the EHEC group was orally administered 100 μL sterile PBS containing 1 × 10^8 CFUs EHEC O157:H7; the EHEC+Enro group was orally administered 100 μL sterile PBS containing 1 × 10^8 CFUs EHEC O157:H7 and then treated by i.p. injection with 8 mg/kg Enro once/day for 3 days; the EHEC+C-LL, EHEC+C-LM, and EHEC+C-LH groups were administered 100 μL sterile PBS containing 1 × 10^8 CFUs EHEC O157:H7 and then treated by i.p. injection with 4, 8, and 16 mg/kg C-L, respectively, once/day for 3 days. The data are shown as the mean ± standard deviation ($n = 8$). NS, $P > 0.05$; *$P \leq 0.05$; **$P \leq 0.01$; ***$P \leq 0.001$; ****$P \leq 0.0001$.

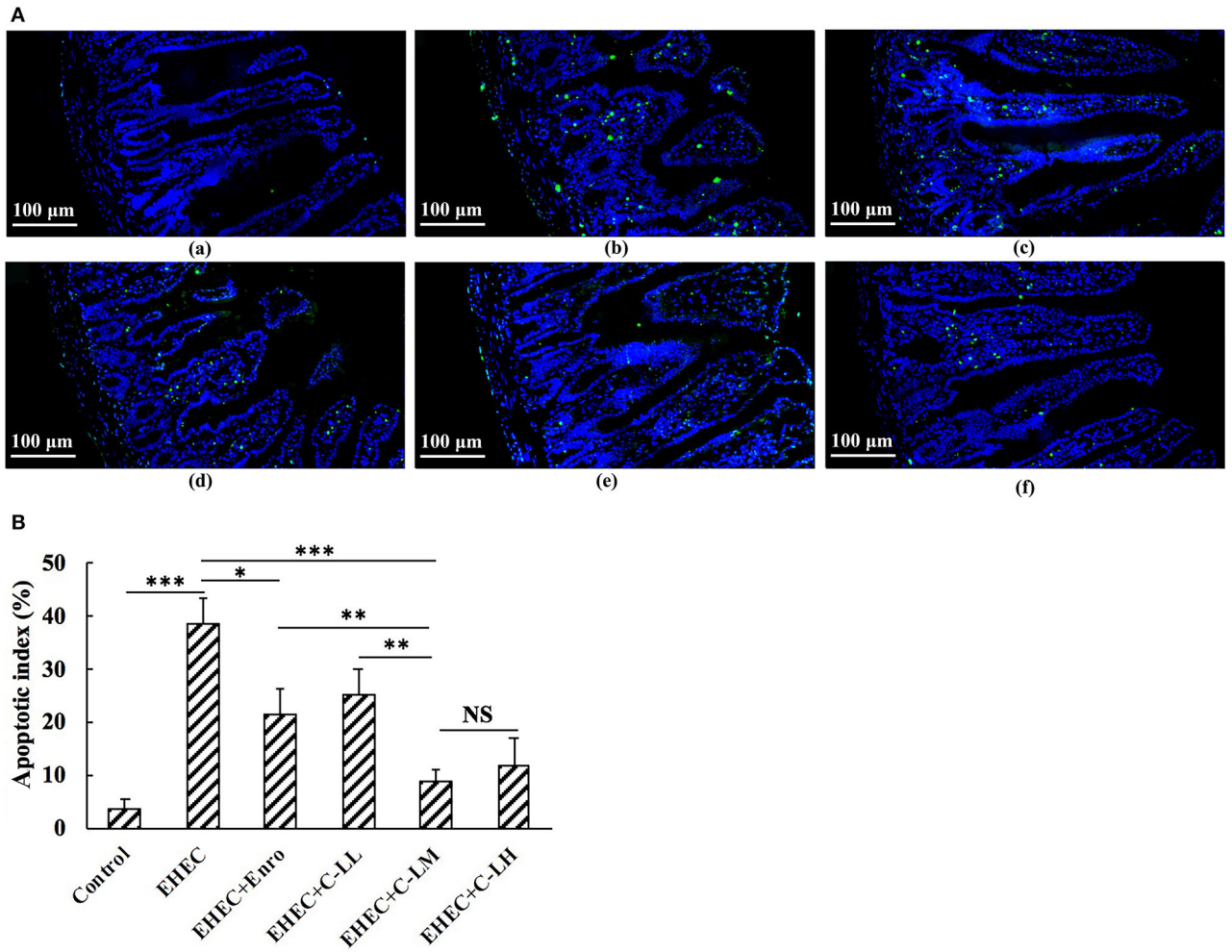

FIGURE 5 | TUNEL staining of jejunum tissues from the panel (**A**-a) control, (**A**-b) EHEC, (**A**-c) EHEC+Enro, (**A**-d) EHEC+C-LL, (**A**-e) EHEC+C-LM, and (**A**-f) EHEC+C-LH groups. **(B)** The numbers of apoptotic cells were counted based on the average number of positive (green) cells. Bar, 100 μm. The control group was orally administered 100 μL sterile PBS; the EHEC group was orally administered 100 μL sterile PBS containing 1×10^8 CFUs EHEC O157:H7; the EHEC+Enro group was orally administered 100 μL sterile PBS containing 1×10^8 CFUs EHEC O157:H7 and then treated by i.p. injection with 8 mg/kg Enro once/day for 3 days; the EHEC+C-LL, EHEC+C-LM, and EHEC+C-LH groups were administered 100 μL sterile PBS containing 1×10^8 CFUs EHEC O157:H7 and then treated by i.p. injection with 4, 8, and 16 mg/kg C-L, respectively, once/day for 3 days. The data are shown as the mean ± standard deviation ($n = 8$). NS, $P > 0.05$; $^*P \leq 0.05$; $^{**}P \leq 0.01$; $^{***}P \leq 0.001$.

Murine models of intestinal inflammation have been extensively used to investigate the regulatory mechanisms that relieve inflammation and maintain intestinal homeostasis (36). In this study, we established an EHEC-induced mouse model to investigate the anti-inflammatory activity of C-L and its potential as a new therapeutic to replace or supplement antibiotics.

Intestinal microbes form a symbiotic ecosystem that helps maintain the homeostatic balance in the gut, and is indispensable for human and animal health (37). It was reported that alterations in the bacterial flora of the intestine can cause intestinal inflammation (38, 39). With Illumina sequencing of the 16S rRNA gene, we found that the microbial diversity differed significantly between EHEC-infected mice and non-infected controls. The microbiota of EHEC-infected mice displayed reduced levels of two phyla of bacteria, *Firmicutes* and *Bacteriodetes*, compared with non-infected controls. The ability to increase the levels of *Firmicutes* and *Bacteriodetes* in the gut might enable C-L and Enro to develop anti-inflammatory activity. This possibility was supported by the study of Scanlan et al. (40) who speculated that the decrease in *Firmicutes* and *Bacteriodetes* may be related to the occurrence of intestinal inflammation. A substantial body of evidence has demonstrated that *Peptoclostridium* (41, 42), *Escherichia-Shigella* (41), *Klebsiella* (43), *Lachnoclostridium* (44), *Blautia* (45, 46), and *Lachnospiraceae* (46, 47) species are important drivers of intestinal inflammation. In this study, treatment with C-L and Enro effectively inhibited the increase of *Peptoclostridium*, *Escherichia-Shigella*, *Klebsiella*, *Lachnoclostridium*, *Blautia*, and

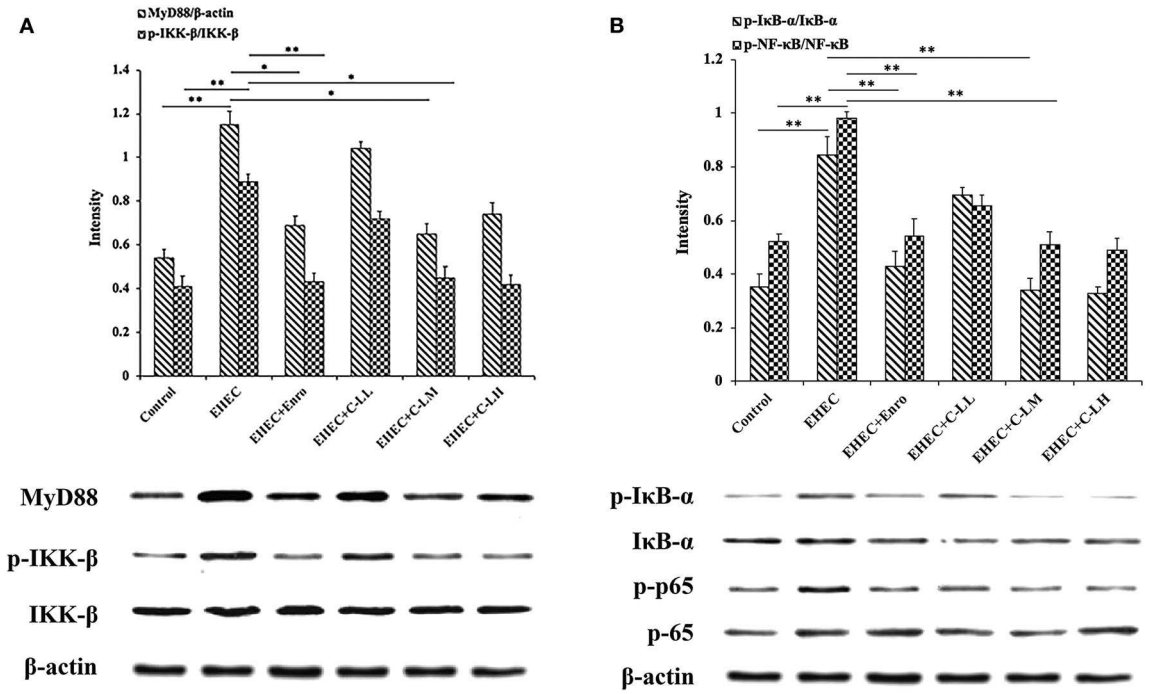

FIGURE 6 | C-L inhibited the NF-κB (p65)-signaling pathway in mouse jejunum tissues. The same control image is used in the left **(A)** and right **(B)** columns. The control group was orally administered 100 μL sterile PBS; the EHEC group was orally administered 100 μL sterile PBS containing 1×10^8 CFUs EHEC O157:H7; the EHEC+Enro group was orally administered 100 μL sterile PBS containing 1×10^8 CFUs EHEC O157:H7 and then treated by i.p. injection with 8 mg/kg Enro once/day for 3 days; the EHEC+C-LL, EHEC+C-LM, and EHEC+C-LH groups were administered 100 μL sterile PBS containing 1×10^8 CFUs EHEC O157:H7 and then treated by i.p. injection with 4, 8, and 16 mg/kg C-L, respectively, once/day for 3 days. Data are given as the mean ± standard deviation ($n = 5$). $^*P \leq 0.05$; $^{**}P \leq 0.01$.

Lachnospiraceae species induced by EHEC infection, suggesting that C-L has the potential to inhibit EHEC-induced enteritis by inhibiting the growth of inflammatory pathogens in the intestine. In addition, the EHEC+Enro and control groups had significantly different OTU values, and compared to the EHEC+C-LM group, the OTU values of the group treated with C-L were better and closer to that of the control group than the group treated with Enro. Further, after Enro treatment, the bacterial intestinal flora formed unique clusters that separated from the other groups, suggesting that antibiotic treatment may have distinct negative effects on the microbial composition.

We further examined the anti-inflammatory activity of C-L. We found that both Enro and C-L treatments could result in efficient protection against EHEC-induced damage, as assessed by the DAI values, Chiu's scores, and histological damage to the intestines. The villus height:crypt depth ratios, which were closely associated with the hosts' growth performance and intestinal absorption, were significantly improved by C-L administration to EHEC-induced mice. Additionally, administering C-L or Enro ameliorated EHEC-induced intestinal inflammation and effectively decreased the infiltration of activated neutrophils, which can produce superoxide anions and other reactive species, leading to the formation of highly reactive hydroxyl radicals that may contribute significantly to tissue necrosis and mucosal dysfunction (48–50). The MPO activity level is directly proportional to the concentration of neutrophils in inflamed tissues and is, thus, an index of inflammation and neutrophil infiltration (51). Consistently, our findings showed that treatment with C-L or Enro significantly reduced MPO activity in jejunum tissues in EHEC-infected mice.

Intestinal inflammation is regulated by release of pro-inflammatory cytokines, such as TNF-α, IL-6, and IFN-γ (52, 53). In our study, the expression of these pro-inflammatory cytokines was significantly suppressed by Enro and C-L. Notably, C-L inhibited inflammatory cytokine production more potently than Enro at the same concentration.

Numerous studies have identified important functions for necroptosis in inflammation and have suggested that it could be implicated in the pathogenesis of many inflammatory diseases (54). It was reported apoptosis is one of the ulcerogenic processes associated with intestinal inflammation (53). In addition, apoptosis is active in hosts with inflammatory bowel disease (IBD) and heightens intestinal inflammation (54–56). In this study, TUNEL staining showed that EHEC stimulation robustly increased apoptosis in mouse intestinal cells. C-L dose-dependently inhibited apoptosis in EHEC-infected mice. Enro-treated mice showed less potent inhibition of EHEC-induced apoptosis at the same concentrations.

It was reported that the NF-κB signaling is a principal pathway that regulates cytokines, such as IL-1β, IL-6, and TNF-α, and cells that participate in inflammatory process (57). Activation of the MyD88-dependent pathway leads to IKK and NF-κB

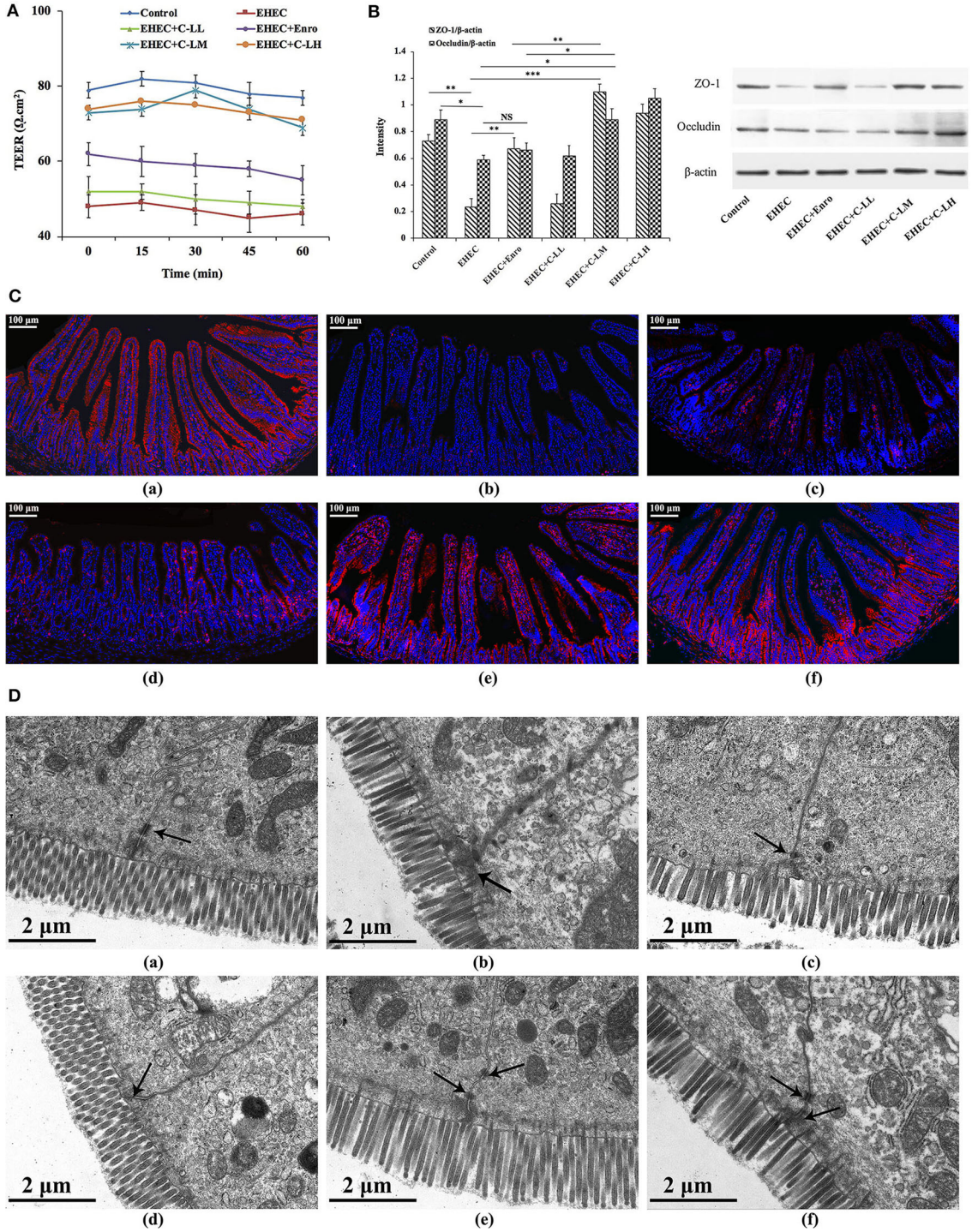

FIGURE 7 | The protective effects of C-L on the intestinal barrier. **(A)** TEER values in mouse jejunum epithelium were detected using a Ussing chamber. **(B)** Expression levels of epithelial barrier function-related proteins (occluding and ZO-1) were determined by western blotting. **(C)** For immunofluorescence staining of occludin (red color) in jejunum tissue, stained slides with the (**C**-a) Control, (**C**-b) EHEC, (**C**-c) EHEC+Enro, (**C**-d) EHEC+C-LL, (**C**-e) EHEC+C-LM, (**C**-f) EHEC+C-LH groups were observed under a fluorescence microscope. Scale bar, 100 μm. **(D)** The protective effects of C-L on intestinal tight junction structures were examined by TEM for the (**D**-a) Control, (**D**-b) EHEC, (**D**-c) EHEC+Enro, (**D**-d) EHEC+C-LL, (**D**-e) EHEC+C-LM, (**D**-f) EHEC+C-LH groups. Narrower intervals and clearer desmosomes (black arrows) between the intestinal epithelial cells were found in C-L-treated mice. Scale bar, 2 μm. The control group was orally administered 100 μL sterile PBS; the EHEC group was orally administered 100 μL sterile PBS containing 1×10^8 CFUs EHEC O157:H7; the EHEC+Enro group was orally administered 100 μL sterile PBS containing 1×10^8 CFUs EHEC O157:H7 and then treated by i.p. injection with 8 mg/kg Enro once/day for 3 days; the EHEC+C-LL, EHEC+C-LM, and EHEC+C-LH groups were administered 100 μL sterile PBS containing 1×10^8 CFUs EHEC O157:H7 and then treated by i.p. injection with 4, 8, and 16 mg/kg C-L, respectively, once/day for 3 days. The data are shown as the mean ± standard deviation ($n = 5$). NS, $P > 0.05$; $^*P \leq 0.05$; $^{**}P \leq 0.01$; $^{***}P \leq 0.001$.

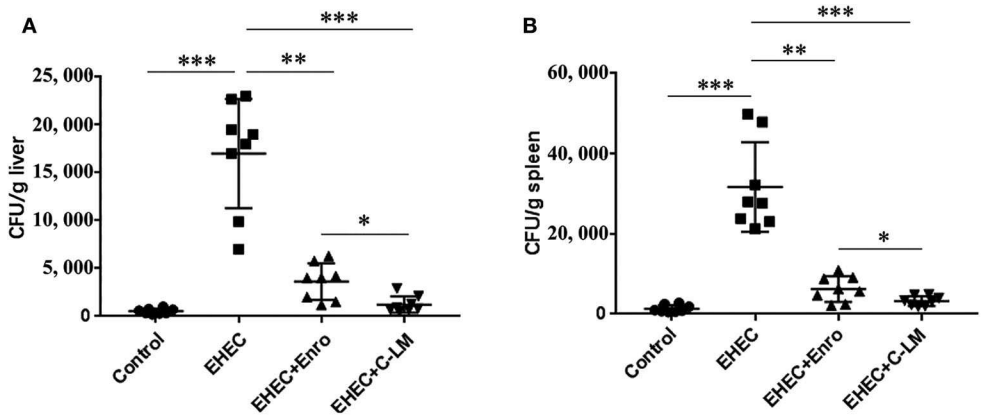

FIGURE 8 | Improvement of host defense against EHEC infection by C-L. The number of bacterial CFUs transferred to the liver **(A)** and spleen **(B)** on day 3 after infection are shown. The control group was orally administered 100 μL sterile PBS; the EHEC group was orally administered 100 μL sterile PBS containing 1×10^8 CFUs EHEC O157:H7; the EHEC+Enro and EHEC+C-LM groups were administered 100 μL sterile PBS containing 1×10^8 CFUs EHEC O157:H7 and then treated by i.p. injection with 8 mg/kg Enro and C-L, respectively, once/day for 3 days. The data are shown as the mean ± standard deviation ($n = 5$). NS, $P > 0.05$; $^*P \leq 0.05$; $^{**}P \leq 0.01$; $^{***}P \leq 0.001$.

phosphorylation, eventually contributing to pro-inflammatory cytokine expression (58). Given this background, we decided to assess the phosphorylation levels of key factors involved in the NF-κB-signaling pathway. The results showed that IKK-β, IκB-α, and p65 phosphorylation was typically increased in the small intestines of mice after EHEC infection, whereas EHEC+C-L treatment effectively downregulated the phosphorylation level of these proteins. In addition, C-L treatment decreased MyD88 expression in the jejunum. Collectively, these findings indicated that C-L could prevent EHEC-induced intestinal inflammation by inhibiting the MyD88–NF-κB-signaling pathway.

The gastrointestinal epithelial cells act as a physical barrier regulating the passive movement of ions, solutes, macromolecules, and microbes into the host (59). Intestinal permeability and barrier function are regulated by the expression of TJ proteins including occludin, claudin, and ZO-1 (59). Gut inflammation, such as IBD (60), coeliac disease (61), and ulcerative jejunitis (62) may lead to impaired gut-epithelial barrier function, thus causing the diffusion of pathogens, toxins, and allergens from the lumen into the circulatory system. In this study, we assayed for changes in TEER of the mouse jejunal epithelium, as an indicator of intestinal epithelial integrity and permeability (63). Both C-L and Enro were able to reverse EHEC-dependent changes in TEER, however, Enro had less of an effect on TEER values than C-L. Our western blot data revealed that EHEC infection decreased occludin and ZO-1 protein expression in the jejunum of mice. C-L effectively attenuated the EHEC-induced disruption of occludin and ZO-1 expression in the jejunum, whereas Enro only attenuated the disruption of ZO-1 expression. Collectively, C-L showed a stronger protective effect on the intestinal epithelial barrier function than Enro, which may be attributed to the better anti-inflammatory activity of C-L. In addition, immunofluorescence analysis revealed that C-L enhanced the abundance of TJ proteins and promoted ZO-1 localization to the intestinal epithelium. Consistent with these findings, TEM results also supported the protective effect of C-L against EHEC-induced impairment in jejunum tissues. Collectively, these data show that C-L protected barrier integrity by maintaining the expression of TJ proteins and reducing the severity of gut inflammation. Given the differential effects of C-L and Enro on the functions of the intestinal epithelial barrier and microbiota, we also investigated the defense of Enro- or C-L-treated mice against EHEC infection. Consistently, more bacteria were present in the spleen and liver of Enro-treated group than those of C-L-treated mice, suggesting that C-L-treated mice mounted a better defense against bacterial infection than antibiotic-treated mice.

CONCLUSION

The present findings indicate that a novel hybrid peptide, C-L, designed in our laboratory effectively attenuated intestinal inflammation in EHEC O157:H7-infected mice. C-L treatment improved the microbiota composition and microbial community balance in mouse intestines. The hybrid peptide exhibited improved anti-inflammatory properties compared to Enro at the same concentration. Hybrid peptide treated infected mice demonstrated reduced clinical signs of inflammation, reduced weight loss, reduced expression of pro-inflammatory cytokines TNF-α, IL-6, and IFN-γ, reduced apoptosis, and reduced markers of jejunal epithelial barrier function. Our data suggest that the appropriate level of C-L treatment in animals may be 8–16 mg/kg. The anti-inflammatory potential of C-L could be exploited in technological and clinical applications, i.e., as antibacterial agents, healthcare formulas, or therapeutic anti-inflammatory drugs for animals or even humans.

DATA AVAILABILITY STATEMENT

All datasets generated for this study are included in the article/supplementary material.

ETHICS STATEMENT

The animal study was reviewed and approved by Institutional Animal Care and Use Committee of China Agricultural University.

AUTHOR CONTRIBUTIONS

XW, LZ, RZ, MK, DS, and BA conceived and designed the experiments. XW, LZ, BA, JC, JW, MA, and MZ performed experiments and evaluated the data. XW prepared the manuscript and MK revised the manuscript. All authors assisted in the preparation of the manuscript and approved the final version.

FUNDING

This research was funded by the National Key R&D Program of China (grant number 2018YFD0500600) and National Natural Science Foundation of China (grant numbers 31572442 and 31272476).

REFERENCES

1. Stromberg ZR, Van Goor A, Redweik GAJ, Brand MJW, Wannemuehler MJ, Mellata M. Pathogenic and non-pathogenic *Escherichia coli* colonization and host inflammatory response in a defined microbiota mouse model. *Dis Model Mech.* (2018) 11:dmm035063. doi: 10.1242/dmm.035063
2. Sartor RB, Wu GD. Roles for intestinal bacteria, viruses, and fungi in pathogenesis of inflammatory bowel diseases and therapeutic approaches. *Gastroenterology.* (2017) 152:327–39.e4. doi: 10.1053/j.gastro.2016.10.012
3. Sartor RB. Microbial influences in inflammatory bowel diseases. *Gastroenterology.* (2008) 134:577–94. doi: 10.1053/j.gastro.2007.11.059
4. Sartor RB. Mechanisms of disease: pathogenesis of Crohn's disease and ulcerative colitis. *Nat Clin Pract Gastr.* (2006) 3:390–407. doi: 10.1038/ncpgasthep0528
5. Shen ZH, Zhu CX, Quan YS, Yang ZY, Wu S, Luo WW, et al. Relationship between intestinal microbiota and ulcerative colitis: mechanisms and clinical application of probiotics and fecal microbiota transplantation. *World J Gastroentero.* (2018) 24:5–14. doi: 10.3748/wjg.v24.i1.5
6. Medzhitov R. Origin and physiological roles of inflammation. *Nature.* (2008) 454:428–35. doi: 10.1038/nature07201
7. Mukherjee S, Joardar N, Sengupta S, Babu SPS. Gut microbes as future therapeutics in treating inflammatory and infectious diseases: lessons from recent findings. *J Nutr Biochem.* (2018) 61:111–28. doi: 10.1016/j.jnutbio.2018.07.010
8. Tarr PI, Gordon CA, Chandler WL. Shiga-toxin-producing *Escherichia coli* and haemolytic uraemic syndrome. *Lancet.* (2005) 365:1073–86. doi: 10.1016/S0140-6736(05)74232-X
9. Johnson-Henry KC, Donato KA, Shen-Tu G, Gordanpour A, Sherman PA. *Lactobacillus rhamnosus* strain GG prevents enterohemorrhagic *Escherichia coli* O157:H7-Induced changes in epithelial barrier function. *Infect Immun.* (2008) 76:1340–8. doi: 10.1128/IAI.00778-07
10. Klaudia C, Alina W. The influence of enrofloxacin, florfenicol, ceftiofur and *E. coli* LPS interaction on T and B cells subset in chicks. *Vet Res Commun.* (2015) 39:53–60. doi: 10.1007/s11259-015-9632-7
11. Pomorska-Mol M, Czyzewska-Dors E, Kwit K, Pejsak Z. Enrofloxacin in therapeutic doses alters cytokine production by porcine PBMCs induced by lipopolysaccharide. *Drug Chem Toxicol.* (2017) 40:295–9. doi: 10.1080/01480545.2016.1223093
12. Pomorska-Mol M, Czyzewska-Dors E, Kwit K, Pejsak Z. Enrofloxacin decreases IL-6 and TNF-alpha production by lipopolysaccharide-stimulated porcine peripheral blood mononuclear cells. *J Vet Res.* (2016) 60:189–93. doi: 10.1515/jvetres-2016-0028
13. Dosogne H, Meyer E, Sturk A, van Loon J, Massart-Leen AM, Burvenich C. Effect of enrofloxacin treatment on plasma endotoxin during bovine Escherichia coli mastitis. *Inflamm Res.* (2002) 51:201–5. doi: 10.1007/PL00000293
14. Sales-Campos H, Basso PJ, Alves VBF, Fonseca MTC, Bonfa G, Nardini V, et al. Classical and recent advances in the treatment of inflammatory bowel diseases. *Braz J Med Biol Res.* (2015) 48:96–107. doi: 10.1590/1414-431x20143774
15. Xu LJ, Wang H, Yang XL, Lu LQ. Integrated pharmacokinetics/pharmaco dynamics parameters-based dosing guidelines of enrofloxacin in grass carp *Ctenopharyngodon idella* to minimize selection of drug resistance. *Bmc Vet Res.* (2013) 9:126. doi: 10.1186/1746-6148-9-126
16. Avendano-Herrera R, Nunez S, Barja JL, Toranzo AE. Evolution of drug resistance and minimum inhibitory concentration to enrofloxacin in *Tenacibaculum maritimum* strains isolated in fish farms. *Aquacult Int.* (2008) 16:1–11. doi: 10.1007/s10499-007-9117-y
17. Wlodarska M, Finlay BB. Host immune response to antibiotic perturbation of the microbiota. *Mucosal Immunol.* (2010) 3:100–3. doi: 10.1038/mi.2009.135
18. Morgun A, Dzutsev A, Dong XX, Greer RL, Sexton DJ, Ravel J, et al. Uncovering effects of antibiotics on the host and microbiota using transkingdom gene networks. *Gut.* (2015) 64:1732–43. doi: 10.1136/gutjnl-2014-308820
19. Lee E, Shin A, Kim Y. Anti-inflammatory activities of cecropin a and its mechanism of action. *Arch Insect Biochem.* (2015) 88:31–44. doi: 10.1002/arch.21193
20. Ishida W, Harada Y, Fukuda K, Fukushima A. Inhibition by the antimicrobial peptide LL37 of lipopolysaccharide-induced innate immune responses in human corneal fibroblasts. *Invest Ophth Vis Sci.* (2016) 57:30–9.
21. Ahmad B, Hanif Q, Wei XB, Zhang LL, Shahid M, Si DY, et al. Expression and purification of hybrid LL-37T alpha 1 peptide in *Pichia pastoris* and evaluation of its immunomodulatory and anti-inflammatory activities by LPS neutralization. *Front Immunol.* (2019) 10:1365. doi: 10.3389/fimmu.2019.01365
22. Zhang LL, Wei XB, Zhang RJ, Petitte J, Si DY, Li ZX, et al. Design and development of a novel peptide for treating intestinal inflammation. *Front Immunol.* (2019) 10:1841. doi: 10.3389/fimmu.2019.01841
23. Zhang L, Wei X, Zhang R, Si D, Petitte JN, Ahmad B, et al. A novel peptide ameliorates LPS-induced intestinal inflammation and mucosal barrier damage via its antioxidant and antiendotoxin effects. *Int J Mol Sci.* (2019) 20:3974. doi: 10.3390/ijms20163974
24. Heinbockel L, Sanchez-Gomez S, de Tejada GM, Domming S, Brandenburg J, Kaconis Y, et al. Preclinical investigations reveal the broad-spectrum neutralizing activity of peptide Pep19-2.5 on bacterial pathogenicity factors. *Antimicrob Agents Ch.* (2013) 57:1480–7. doi: 10.1128/AAC.02066-12
25. Wei XB, Wu RJ, Si DY, Liao XD, Zhang LL, Zhang RJ. Novel hybrid peptide cecropin A (1-8)-LL37 (17-30) with potential antibacterial activity. *Int J Mol Sci.* (2016) 17:983. doi: 10.3390/ijms17070983
26. Zhang HW, Hua R, Zhang BX, Guan QF, Wang BB, Zeng JF, et al. Cathelicidin-derived PR39 protects enterohemorrhagic *Escherichia coli* O157:H7 challenged mice by improving epithelial function and balancing the microbiota in the intestine. *Sci Rep.* (2019) 9:9456. doi: 10.1038/s41598-019-45913-6
27. Wang J, Lu JX, Xie XW, Xiong J, Huang NN, Wei HK, et al. Blend of organic acids and medium chain fatty acids prevents the inflammatory response and intestinal barrier dysfunction in mice challenged with enterohemorrhagic *Escherichia coli* O157:H7. *Int Immunopharmacol.* (2018) 58:64–71. doi: 10.1016/j.intimp.2018.03.014
28. da Silva VC, de Araujo AA, Araujo DFD, Lima MCJS, Vasconcelos RC, de Araujo RF, et al. Intestinal anti-inflammatory activity of the aqueous extract from *Ipomoea asarifolia* in DNBS-induced colitis in rats. *Int J Mol Sci.* (2018) 19:4016. doi: 10.3390/ijms19124016

29. Jang SE, Hyam SR, Jeong JJ, Han MJ, Kim DH. Penta-O-galloyl-beta-D-glucose ameliorates inflammation by inhibiting MyD88/NF-kappa B and MyD88/MAPK signalling pathways. *Br J Pharmacol.* (2013) 170:1078–91. doi: 10.1111/bph.12333
30. Chiu CJ, Scott HJ, Gurd FN. Intestinal mucosal lesion in low-flow states. 2. Protective effect of intraluminal glucose as energy substrate. *Arch Surg.* (1970) 101:484–8. doi: 10.1001/archsurg.1970.01340280036010
31. Chen H, Hu YH, Fang Y, Djukic Z, Yamamoto M, Shaheen NJ, et al. Nrf2 deficiency impairs the barrier function of mouse oesophageal epithelium. *Gut.* (2014) 63:711–9. doi: 10.1136/gutjnl-2012-303731
32. Cheng Z, Hu X, Sun ZR. Microbial community distribution and dominant bacterial species analysis in the bio-electrochemical system treating low concentration cefuroxime. *Chem Eng J.* (2016) 303:137–44. doi: 10.1016/j.cej.2016.05.131
33. Sun Y, Shang DJ. Inhibitory effects of antimicrobial peptides on lipopolysaccharide-induced inflammation. *Mediat Inflamm.* (2015) 2015:167572. doi: 10.1155/2015/167572
34. Burgess DJ. Microbial genetics amplified origins of antibiotic resistance. *Nat Rev Genet.* (2014) 15:362. doi: 10.1038/nrg3740
35. Lewis K. Platforms for antibiotic discovery. *Nat Rev Drug Discov.* (2013) 12:371–87. doi: 10.1038/nrd3975
36. Brown SJ, Mayer L. The immune response in inflammatory bowel disease. *Am J Gastroenterol.* (2007) 102:2058–69. doi: 10.1111/j.1572-0241.2007.01343.x
37. Preidis GA, Ajami NJ, Wong MC, Bessard BC, Conner ME, Petrosino JF. Composition and function of the undernourished neonatal mouse intestinal microbiome. *J Nutr Biochem.* (2015) 26:1050–7. doi: 10.1016/j.jnutbio.2015.04.010
38. Khalif IL, Quigley EMM, Konovitch EA, Maximova ID. Alterations in the colonic flora and intestinal permeability and evidence of immune activation in chronic constipation. *Digest Liver Dis.* (2005) 37:838–49. doi: 10.1016/j.dld.2005.06.008
39. Mima K, Ogino S, Nakagawa S, Sawayama H, Kinoshita K, Krashima R, et al. The role of intestinal bacteria in the development and progression of gastrointestinal tract neoplasms. *Surg Oncol.* (2017) 26:368–76. doi: 10.1016/j.suronc.2017.07.011
40. Scanlan PD, Shanahan F, O'Mahony C, Marchesi JR. Culture-independent analyses of temporal variation of the dominant fecal microbiota and targeted bacterial subgroups in Crohn's disease. *J Clin Microbiol.* (2006) 44:3980–8. doi: 10.1128/JCM.00312-06
41. Vindigni SM, Zisman TL, Suskind DL, Damman CJ. The intestinal microbiome, barrier function, and immune system in inflammatory bowel disease: a tripartite pathophysiological circuit with implications for new therapeutic directions. *Ther Adv Gastroenter.* (2016) 9:606–25. doi: 10.1177/1756283X16644242
42. Cojocariu C, Stanciu C, Stoica O, Singeap AM, Sfarti C, Girleanu I, et al. Clostridium difficile infection and inflammatory bowel disease. *Turk J Gastroenterol.* (2014) 25:603–10. doi: 10.5152/tjg.2014.14054
43. Lee IA, Kim DH. *Klebsiella pneumoniae* increases the risk of inflammation and colitis in a murine model of intestinal bowel disease. *Scand J Gastroenterol.* (2011) 46:684–93. doi: 10.3109/00365521.2011.560678
44. Meehan CJ, Beiko RG. A phylogenomic view of ecological specialization in the *Lachnospiraceae*, a family of digestive tract-associated bacteria. *Genome Biol Evol.* (2014) 6:703–13. doi: 10.1093/gbe/evu050
45. Yilmaz B, Juillerat P, Oyas O, Ramon C, Bravo FD, Franc Y, et al. Microbial network disturbances in relapsing refractory Crohn's disease. *Nat Med.* (2019) 25:323–36. doi: 10.1038/s41591-018-0308-z
46. Schirmer M, Garner A, Vlamakis H, Xavier RJ. Microbial genes and pathways in inflammatory bowel disease. *Nat Rev Microbiol.* (2019) 17:497–511. doi: 10.1038/s41579-019-0213-6
47. Vila AV, Imhann F, Collij V, Jankipersadsing SA, Gurry T, Mujagic Z, et al. Gut microbiota composition and functional changes in inflammatory bowel disease and irritable bowel syndrome. *Sci Transl Med.* (2018) 10:eaap8914. doi: 10.1126/scitranslmed.aap8914
48. Vieira ELM, Leonel AJ, Sad AP, Beltrao NRM, Costa TF, Ferreira TMR, et al. Oral administration of sodium butyrate attenuates inflammation and mucosal lesion in experimental acute ulcerative colitis. *J Nutr Biochem.* (2012) 23:430–6. doi: 10.1016/j.jnutbio.2011.01.007
49. Talero E, Sanchez-Fidalgo S, de la Lastra CA, Illanes M, Calvo JR, Motilva V. Acute and chronic responses associated with adrenomedullin administration in experimental colitis. *Peptides.* (2008) 29:2001–12. doi: 10.1016/j.peptides.2008.07.013
50. Buell MG, Berin MC. Neutrophil-independence of the initiation of colonic injury - comparison of results from 3 models of experimental colitis in the rat. *Digest Dis Sci.* (1994) 39:2575–88. doi: 10.1007/BF02087693
51. Choudhary S, Keshavarzian A, Yong S, Wade M, Bocckino S, Day BJ, et al. Novel antioxidants Zolimid and AEOL11201 ameliorate colitis in rats. *Digest Dis Sci.* (2001) 46:2222–30. doi: 10.1023/A:1011975218006
52. Raetz CRH, Whitfield C. Lipopolysaccharide endotoxins. *Annu Rev Biochem.* (2002) 71:635–700. doi: 10.1146/annurev.biochem.71.110601.135414
53. Han FF, Zhang HW, Xia X, Xiong HT, Song DG, Zong X, et al. Porcine β-defensin 2 attenuates inflammation and mucosal lesions in dextran sodium sulfate-induced colitis. *J Immunol.* (2015) 194:1882–93. doi: 10.4049/jimmunol.1402300
54. Pasparakis M, Vandenabeele P. Necroptosis and its role in inflammation. *Nature.* (2015) 517:311–20. doi: 10.1038/nature14191
55. Pierdomenico M, Negroni A, Stronati L, Vitali R, Prete E, Bertin J, et al. Necroptosis is active in children with inflammatory bowel disease and contributes to heighten intestinal inflammation. *Am J Gastroenterol.* (2014) 109:279–87. doi: 10.1038/ajg.2013.403
56. Atreya R, Mudter J, Finotto S, Mullberg J, Jostock T, Wirtz S, et al. Blockade of interleukin 6 trans signaling suppresses T-cell resistance against apoptosis in chronic intestinal inflammation: evidence in Crohn disease and experimental colitis in vivo (vol 6, pg 583, 2000). *Nat Med.* (2010) 16:1341. doi: 10.1038/nm1110-1341
57. Zhang D, Cheng L, Huang X, Shi W, Xiang J, Gan H. Tetrandrine ameliorates dextran-sulfate-sodium-induced colitis in mice through inhibition of nuclear factor-kappaB activation. *Int J Colorectal Dis.* (2009) 24:5–12. doi: 10.1007/s00384-008-0544-7
58. Kawai T, Adachi O, Ogawa T, Takeda K, Akira S. Unresponsiveness of MyD88-deficient mice to endotoxin. *Immunity.* (1999) 11:115–22. doi: 10.1016/S1074-7613(00)80086-2
59. Park EJ, Thomson ABR, Clandinin MT. Protection of intestinal occludin tight junction protein by dietary gangliosides in lipopolysaccharide-induced acute inflammation. *J Pediatr Gastr Nutr.* (2010) 50:321–8. doi: 10.1097/MPG.0b013e3181ae2ba0
60. Hering NA, Schulzke JD. Therapeutic options to modulate barrier defects in inflammatory bowel disease. *Digest Dis.* (2009) 27:450–4. doi: 10.1159/000233283
61. Liu H, Brais R, Lavergne-Slove A, Jeng Q, Payne K, Ye H, et al. Continual monitoring of intraepithelial lymphocyte immunophenotype and clonality is more important than snapshot analysis in the surveillance of refractory coeliac disease. *Gut.* (2010) 59:452–60. doi: 10.1136/gut.2009.186007
62. Sigman T, Nguyen VH, Costea F, Sant'Anna A, Seidman EG. Ulcerative jejunitis in a child with celiac disease. *BMC Gastroenterol.* (2014) 14:29. doi: 10.1186/1471-230X-14-29
63. Li W, Sun K, Ji Y, Wu Z, Wang W, Dai Z, et al. Glycine regulates expression and distribution of claudin-7 and ZO-3 proteins in intestinal porcine epithelial cells. *J Nutr.* (2016) 146:964–9. doi: 10.3945/jn.115.228312

Conflict of Interest: The authors declare that the research was conducted in the absence of any commercial or financial relationships that could be construed as a potential conflict of interest.

Advantages of publishing in Frontiers

OPEN ACCESS
Articles are free to read for greatest visibility and readership

FAST PUBLICATION
Around 90 days from submission to decision

HIGH QUALITY PEER-REVIEW
Rigorous, collaborative, and constructive peer-review

TRANSPARENT PEER-REVIEW
Editors and reviewers acknowledged by name on published articles

Frontiers
Avenue du Tribunal-Fédéral 34
1005 Lausanne | Switzerland

Visit us: www.frontiersin.org
Contact us: info@frontiersin.org | +41 21 510 17 00

REPRODUCIBILITY OF RESEARCH
Support open data and methods to enhance research reproducibility

DIGITAL PUBLISHING
Articles designed for optimal readership across devices

FOLLOW US
@frontiersin

IMPACT METRICS
Advanced article metrics track visibility across digital media

EXTENSIVE PROMOTION
Marketing and promotion of impactful research

LOOP RESEARCH NETWORK
Our network increases your article's readership